Building Long-Term Seismo-Acoustic Catalogues to Assess Open-Vent Activity at Guatemalan Volcanoes

Thesis submitted in accordance with the requirements of the University of Liverpool for the degree of Doctor in Philosophy

by

William Samuel Carter

November 2021

Declaration of Authorship

I, William Samuel Carter, declare that this thesis titled, "Building Long-Term Seismo-Acoustic Catalogues to Assess Open-Vent Activity at Guatemalan Volcanoes" and the work presented in it are my own. I confirm that:

- This thesis was completed as part of a research degree at the University of Liverpool.
- The material contained in this thesis has not been presented, nor is currently being presented, either wholly or in parts, for any other degree or qualifications.
- Where I have consulted published studies, this have been clearly referenced.
- Where the work was part of a collaborative effort, I have made clear what others have done and what I have contributed myself.
- Parts of this thesis have been published or in preparation for publication as:
    - **William S. Carter**, Andreas Rietbrock, Yan Lavallée, Ellen Gottschämmer, Alejandro Díaz Moreno, Gustavo Chigna, Silvio De Angelis. (Submitted to *Nature Data* and peer reviewed). **Catalogued explosions at Volcán Santiaguito (Guatemala) from seismic network recordings between 2014 and 2018.**
    - **William S. Carter**, Andreas Rietbrock, Yan Lavallée, Ellen Gottschämmer, Alejandro Díaz Moreno, Jackie E. Kendrick, Oliver D. Lamb, Paul A. Wallace, Gustavo Chigna, Silvio De Angelis. (Published in *Journal of Volcanology and Geothermal Research*). **Statistical evidence of transitioning open-vent activity towards a paroxysmal period at Volcán Santiaguito (Guatemala) during 2014–2018.**
    - **William S. Carter**, Yan Lavallée, Andreas Rietbrock, Amilcar Roca, Silvio De Angelis. (In Preparation). **Characterisation of open-vent activity at Volcán de Fuego from seismo-acoustic network observations and energy partitioning.**

Signed:

William Samuel Carter

November 2021

Abstract

Open-vent volcanoes produce activity spanning a wide range of magnitudes over prolonged periods. Volcán de Fuego and the Santiaguito lava dome complex are two such volcanoes situated in Guatemala, Central America. The hazards associated with paroxysmal phases at these volcanoes have caused devastation to the local communities and regional disruption. To better understand these volcanic systems, I have undertaken analysis of long-term (several years) recordings of seismic and acoustic signals with networks of sensors deployed around the flanks of the volcanoes. Long-term geophysical datasets are important for enabling the comparison of geophysical observations to other long-term datasets, and informing interpretations about deeper processes, which operate over longer time periods. To process the large datasets, I developed automatic detection and classification algorithms to catalogue the explosions and tremor (both seismic and acoustic). These algorithms relied on amplitude and frequency attributes, as well as template matching tools to separate events from the background noise and other volcanic and regional tectonic signals. The algorithms produced highly complete catalogues, useful for analytical techniques, which aid and compliment manual analytics. However, due to the uniqueness of the data from each volcano, the automatic detection and classification of volcanic events requires similarly unique algorithms. The catalogues produced in this thesis were the first of their kind in Guatemala, with 18,896 explosions recorded at Santiaguito, and 99,618 explosions, 6,048 seismic tremor events and 2,200 acoustic tremor events recorded at Fuego. I statistically analysed the patterns in the catalogues, including the energy released, frequency content, occurrence rates and the comparison of occurrence between different event types to infer information on the source processes. Further, I related the field observations to models which describe the paroxysms. At both Santiaguito and Fuego, I found that the activity could be split into phases which displayed distinct characteristics. At Santiaguito, I found that the magnitude-frequency relationship for explosions is described by a power-law, with changes to the *b*-value occurring between phases due to changes in rupture mechanisms, likely controlled by variable magma properties. The repose times at Santiaguito are described by a Poissonian distribution, which also changed between phases due to changing source properties, limiting the potential for long-term assessments of future activity. At Fuego, I found that the explosions during background activity have two statistically distinct endmembers: gas-rich and ash-rich. I showed how the volcanic acoustic-seismic ratio can be used to identify phases in the activity, and along with crater fill observations, rates of explosion and tremor occurrence, and energy radiated both seismically and acoustically, I produced a conceptual model of the evolution of the activity.

Contents

List of Figures

Chapter 1

Chapter 2

Chapter 3

Chapter 4

Appendix 1

Acknowledgements

It has definitely been a journey over the last four years, and I would not have got to this point if it were not for several important people who have helped me throughout it all. First and foremost, I would like to say a huge thank you to Silvio who has gone above and beyond as my supervisor, both in academia and the "real world". Without your consistent support and guidance this thesis would not have been possible (and I may still be stuck in Italy!). I would also like to say a big thank you to both Andreas and Yan for their supervision throughout the PhD. Andreas, with whom this journey started, thank you for introducing me to such a fascinating research topic and helping me become the researcher I am today. Yan, you have always been able to give me confidence and encouragement when I needed it most, your enthusiasm and curiosity for research is infectious and I am so happy for all that rubbed off on me! I would also like to thank Alejandro, an unofficial supervisor, but someone I could always turn to for help and who's discussions always sharpened my ideas.

Over the past few years, I have had the privilege of working in the most beautiful places, collaborating with some amazing people. Firstly, Armando, I will always remember fondly the times I have spent in Guatemala, all of which I shared with you and enjoyed so much. Your help was invaluable. I must also thank the wonderful people at INSIVUMEH, especially Amilcar and Gustavo, your insights were key to everything I accomplished. I have also had the pleasure to collaborate with Ellen and Alicia from KIT. Working with you both on Santiaguito really helped me see the bigger picture of the research efforts in Guatemala and you made the trips there even more enjoyable.

I must also thank the Natural Environmental Research Council for funding this PhD as part of the EAO Doctoral Training Partnership. Your support is gratefully acknowledged.

Of course, my PhD experience would not have been the same if it were not for all the friends I made along the way, both in and out of the office (in particular, Hannah, Elliott, Josh and Amy), and for everyone at the Ultimate Frisbee team (especially Alex, Alex and Kayleigh). I have made so many great memories with you all that I will remember for a long time to come.

And lastly, but by no means least, I want to give a massive thanks to my family and my amazing girlfriend Lauren for all the support you have given me along the way. Having you all by my side no matter what has made this journey so much smoother. I can't fully put into words how much you all mean to me. Thankyou!

Chapter 1. Introduction

1.1. Thesis Motivation

Open-vent volcanoes are volcanic systems which are in a prolonged state of unrest, producing a recurring pattern of activity (Vergnolle and Métrich, 2021). These volcanic systems are characterized by a low-level, nearly continuous, background activity which, depending on the nature of the magma, can include lava flows, permanent plumes, gas emissions, and explosion events (Vergnolle and Métrich, 2021). Background activity at some open-vent volcanoes can be interrupted by shorter periods of heightened activity, called paroxysms (Vergnolle and Métrich, 2021). These paroxysms produce hazards which threaten local communities and can cause widespread disruption to air-travel and destroy infrastructure, leading to socio-economic stresses. Although highly hazardous, these open-vent volcanoes provide an opportunity to investigate the internal mechanisms and plumbing systems of volcanoes, as well as the range in style of eruptive behaviour, via the study of the activity through geophysical methods.

Volcanoes which transition from quiet periods with little-to-no activity to large eruptions, such as the 2018 eruption of Anak Krakatau following 15 months of quiet (GVP, 2018a; Rose and Matoza, 2021), often give clear signals before the large events occur. The signals which occur during the change from a quiet period to large activity can allow for forecasting methods to be applied and warnings given for evacuations (Sparks, 2003), which help mitigate the hazards and reduce the impact of the events, saving lives and minimising the socio-economic impacts. However, for open-vent volcanoes, there is often a constant level of background activity between the large paroxysms which can make the identification of precursor activity harder to understand or even identify. This can lead to there being less or no warning being given to the local populations living by these volcanoes, ultimately resulting in loss of life, livestock, and increased socio-economic stresses as a result of the events. Being able to better understand the background level activity, to investigate the mechanisms controlling the activity, and also to identify trends and key signals in the data, which can be used to improve the forecasting of large events is a critical question to investigate at these open-vent systems.

Many of the worlds active volcanoes are situated on the Pacific Ring of Fire due to the tectonic plate boundaries around the Pacific Ocean. Guatemala, located in Central

Introduction

America forms part of the Pacific Ring of Fire, sits on top of the North American and Caribbean tectonic plates, where the Cocos plate subducts beneath them at the middle America trench, producing arc-volcanism along the spine of the country as part of the Central American Volcanic Arc (Stoiber and Carr, 1973). Currently, 3 of the 37 volcanoes in the country are producing vent activity, and with populated areas nearby these volcanoes, allowing for ease of access to study their activity, Guatemala provides an ideal setting to investigate open-vent volcanoes. These open-vent volcanoes are Volcán de Fuego, the Santiaguito lava dome complex, and Pacaya (Figure 1.1). In this study I focus on Fuego and Santiaguito.

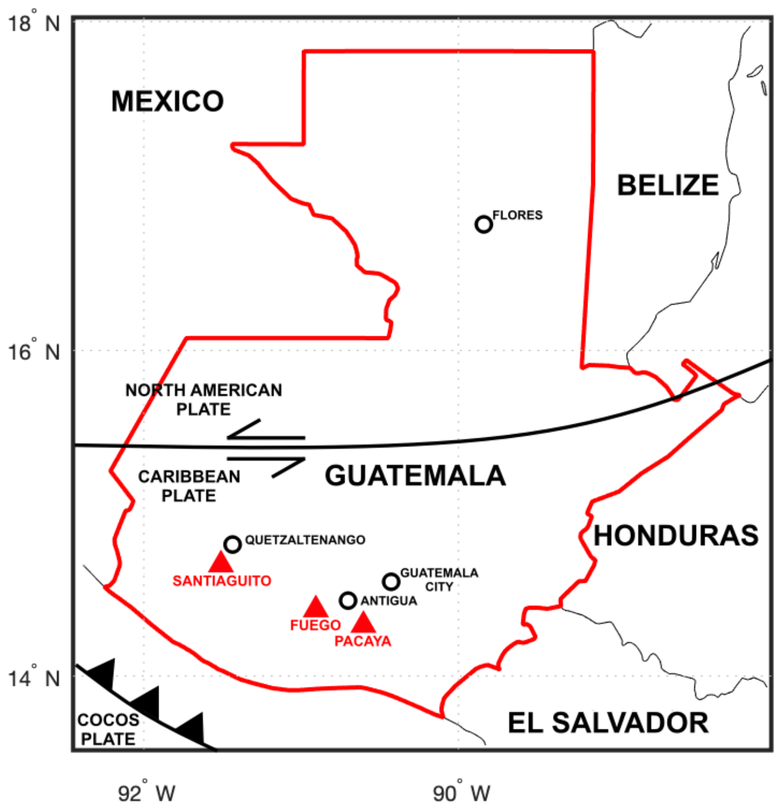

Figure 1.1. *Map of Guatemala and surrounding countries. Included are the locations of the three volcanoes displaying vent activity of Santiaguito, Fuego and Pacaya (red triangles). Major cities in Guatemala (black circles) and the tectonic plate boundaries in the region are also highlighted.*

The local communities to The Santiaguito lava dome complex and Volcán de Fuego volcanoes are heavily reliant upon the agriculture on and around the flanks of the volcanoes for their living, as these are idealistic areas for crops such as coffee and nuts due to the climate and fertile soils which the volcanoes provide. However, due to the activity at these volcanoes, these rural communities are at risk of losing their homes, farmland and livestock, as well as their lives to the volcanic activity which has historically caused much devastation (e.g., Rose, 1973; De Angelis et al., 2019; Naismith et al., 2019). Not only are the local rural communities at risk from the volcanic hazards, but the growing urban population living in both Guatemala City (40 km East from Fuego) and Quetzaltenango (11km to the north of Santiaguito) would be greatly affected by the largest possible eruption events at these volcanoes, with air travel disruption, reduction in air quality, destruction of crops for food supply, and even damage to infrastructure likely to occur from heavy ash dispersal. In living memory, Guatemala has been affected by many large eruptions of these volcanoes, with villages such as El Palmar and San Miguel Los Lotes either completely destroyed or devastated by volcanic activity. More recently in June 2018, at least 169 people lost their lives, 256 people remain missing, and 13,000 people were displaced from their homes when Fuego erupted (GVP, 2018b). Mitigation of the impacts of these hazards is therefore vitally important for the health of the socio-economic stability of the country, and protection of the people who live there.

There has been an increased interest and range of studies that have taken place at both the Santiaguito lava dome complex and Volcán de Fuego in the past two decades. Largely these have been in response to some of these high-impact events, however as many studies have been on short timescales (e.g., Sanderson et al., 2010; Lyons and Waite, 2011; Nadeau et al., 2011; Johnson et al., 2014; Scharff et al., 2014; Aldeghi et al., 2019), questions still remain about how the activity changes over longer timescales. Long timescale studies are required to obtain a more complete understanding of how the internal mechanisms work over prolonged time periods, how the different styles of activity are linked to physical parameters, and how to forecast large hazardous events in the medium to long temporal range to mitigate the impact the large events have on the local communities.

Seismo-acoustic networks are commonly being deployed at volcanoes worldwide to investigate the activity and infer details about the processes which cause them (e.g., De Angelis et al., 2012; Fee et al., 2020), some of which occur over longer periods of time than the duration of many geophysical campaigns, highlighting the need for long-term investigations. With the ever-improving technologies to record and wirelessly transmit seismic and acoustic data at volcanoes, investigations at open-vent volcanoes are becoming ever easier to carry out. It has been stated that the investigation of background activity is important for improving medium-term forecasts (Tilling et al., 2008; Brill et al., 2018), allowing for comparisons of new and past activity to indicate how the activity will change in the future, which may be possible for both Fuego and Santiaguito. Long-term investigations of volcanoes and the use of networks of seismic and acoustic stations creates large datasets of the activity. Handling of these large datasets to obtain high quality catalogues of volcanic events is key to unravel long-term changes in different signals (e.g., signals associated with magmatic recharge, other magmatic processes, as well as with the priming and evolution of volcanic activity), and as such, there has been an effort to move away from time consuming manual assessments of the data to instead use automatic systems to process the raw data recorded (e.g., Stephens and Chouet, 2001; Scarpetta et al., 2005; Green and Neuberg, 2006; Langer et al., 2006; Umakoshi et al., 2008; Hammer et al., 2012; Hammer et al., 2013). It is important to answer the question as to whether automatic detection and classification schemes can be applied to the volcanic systems at Santiaguito and Fuego to reliably and robustly catalogue the events for later analysis and investigations into the mechanisms and internal properties. The production of catalogues is especially important as recent developments of powerful computational solutions now allows us to robustly analyse such large datasets via machine-learning-based algorithms to identify previously unrecognised patterns and resolve volcanic activity in new ways in order to improve hazard mitigation strategies. These systems require large catalogues of known events for their training, and so obtaining these catalogues from automatically detected events from long-term recordings is an essential first step to reach this goal.

Understanding the internal mechanisms of volcanic systems through direct measurements is not possible. Therefore, indirect measurements must be used with inversions and comparisons to models to make evidence-based inferences to their cause. As an example, we cannot directly image/measure the size or style of faulting within a conduit, so the measurements of seismic waves produced by the faulting is investigated to obtain information on the faulting event. In this way, I am to use long-term observations of the activity at Santiaguito and Fuego to build up evidence which will allow for interpretations of their internal properties and mechanisms. These can in turn be compared to the physical models used to describe the behaviour of the systems, allowing for an assessment of the likely drivers of the activity observed. In this thesis, I will investigate the use of networks of seismic and acoustic sensors deployed around the flanks of the open vent volcanoes Volcán de Fuego and Santiaguito, as a way to obtain this record of activity from low baseline levels to paroxysmal eruptions. I will develop algorithms that can process the large volumes of data that will be recorded from these long-term networks to obtain catalogues of activity and determine how appropriate these algorithms are as a tool to produce datasets for investigations into the phases of activity and source mechanisms. The catalogues produced will be the first at these locations, allowing for long-term investigations to be carried out. Finally, I will investigate the uses of long-term catalogues of activity as a way to infer further information about the mechanisms governing the behaviour of these open-vent systems, suggest how changes to the activity can be used to model changes to the physical parameters within the magma system and to recognise patterns and trends in the activity to determine if these datasets can offer assistance to forecasting efforts.

1.2. Volcanic Signals and Monitoring

Across the globe open-vent volcanoes have been monitored and investigated using a range of geophysical and geochemical methods. These methods aim to monitor activity (e.g. Johnson, 2018; Giudicepietro et al., 2019; De Angelis et al., 2019; Ilanko et al., 2019; Coppola et al., 2019; Hanagan et al., 2020), understand the mechanisms and magma processes causing the ongoing activity (e.g. Chouet, 1996; Giudicepietro et al., 2019; Barrière et al., 2019; Woitischek et al., 2020), characterise the different styles of activity and different event types (e.g. Gaudin et al., 2017; Brill et al., 2018; Lamb et al., 2019; Diaz-Moreno et al., 2020), aid forecasting efforts to mitigate future hazards (e.g. Chouet, 1996; Garcés et al., 1999; Aki and Ferrazzini, 2000; Ortiz et al., 2003; Ripepe et al., 2017; Brill et al., 2018; Johnson et al., 2018), or to investigate the internal structure of the volcano from the deeper magma chambers in the lower crust up to the conduit and vent systems near the surface (e.g. Lyons and Waite, 2011; Scott et al., 2012; Turner et al., 2013; Greenfield et al., 2016). Methods commonly used include seismics (e.g. Hagerty et al., 2000; Lyons et al., 2010; Rivet et al., 2014; Richardson et al., 2014; Greenfield et al., 2016; Giudicepietro et al., 2019), acoustic infrasound (e.g. Hagerty et al., 2000; Richardson et al., 2014; De Angelis et al., 2016; Johnson et al., 2018; Lamb et al., 2019; Diaz-Moreno et al., 2020), ground deformation and tilt (e.g. Voight et al., 1998; Poland et al., 2006; Lyons et al., 2012; Johnson et al., 2014; Parker et al., 2014; Rivet et al., 2014; Chen et al., 2017), gas measurements (e.g. Symonds et al., 1996; Chiodini et al., 2010; Coppola et al., 2019; Ilanko et al., 2019), petrology (e.g. Beard and Borgia, 1989; Scott et al., 2012; Reubi et al., 2019; Liu et al., 2020), and thermal imagery (e.g. Wooster, 2001; Sahetapy-Engel et al., 2008; Coppola et al., 2019). In the studies presented in this thesis, I use seismic and acoustic recordings of the activity at Fuego and Santiaguito to investigate the volcanic systems.

1.2.1. Volcanic Seismology

The use of seismology is common in volcano studies and has been used to investigate many questions surrounding the different events produced at open-vent volcanoes, including the source hypocentres (e.g. Nugraha et al., 2019; Basuki et al., 2019; Gottschämmer et al., 2021), source mechanisms (e.g. Kim et al., 2014; Chouet, 2005; Neuberg et al., 2006; Rohnacher et al., 2021), source properties (e.g. Zobin and Sudo, 2017), classes of events (e.g. Scarpetta et al. 2005; Green and Neuberg, 2006), mapping the subsurface structures of the volcano (e.g. Lyons and Waite 2011; Walker et al., 2021), and time delays between seismic onsets and plume emergence (e.g. Sahetapy-Engel et al., 2008).

Seismic waves are radiated from a host of different volcanic sources and can be recorded remotely at safe distances (several km) from hazardous vent activity. Continuous recording at sites around the vent can be undertaken with minimal upkeep, making seismic recording an ideal tool to monitor the activity at volcanoes. Volcanoes can cause seismicity through subsurface movement of high-frequency volcano-tectonic (VT) earthquakes (Roman and Cashman, 2006; McNutt and Roman, 2015), low-frequency (or sometimes referred to as 'long-period') events (Chouet, 1996; McNutt and Roman, 2015), explosions (Nishimura, 1998; McNutt and Roman, 2015), tremor (Chouet, 1988; Julian, 1994; McNutt and Roman, 2015), and surface impact from rockfalls, lahars, landslides and pyroclastic flows (McNutt and Roman, 2015). The mechanisms of the subsurface seismic sources are debated in the literature. The mechanisms that are suggested often vary from volcano to volcano, and multiple mechanisms can be proposed at an individual volcano. Separation of the different event types through classification based on different properties (both in the time and frequency domain) can allow for analysis on the source mechanisms and be used to assess the state of the activity (e.g., Green and Neuberg, 2006). As well as volcanic events, seismic recordings at volcanoes detect regional and local earthquakes caused by tectonic activity. Due to their increased distance from the volcano, these events can be identified and filtered out from the volcanic records. In this thesis, the primary focus will be on explosions and tremor events, however it is important to understand the different signals present in the data (Figure 1.2).

Volcanic explosions occur when large quantities of gases (e.g., water, CO_2 and other volatiles), and pyroclasts in the upper conduits are rapidly expelled into the atmosphere. The expulsive ejection of gas and pyroclastic material occurs after a build-up of pressure, due to buoyancy, which ultimately leads to the opening of a pathway for the escape of the gas and any fractured material at the surface. The causation of the fracturing that occurs to open up the pathways during an explosion may contrast, where in some models fracture occurs within the plug after gas build-up (Johnson et al., 1998) and in other models it occurs via shear fracturing at the conduit walls as the plug rises (Bluth and Rose, 2004; Green and Neuberg, 2006). Explosions have also been modelled by the bursting of gas bubbles reaching a free surface (Blackburn et al., 1976), and by an implosive volume causing a single vertical force (Kanamori et al., 1984). The source of the seismicity from explosions at open-vent volcanoes can be non-destructive and repeatable in nature (e.g., Arciniega-Ceballos et al., 1999; Chouet et al., 1999). These events are typically low-frequency and can have an impulsive onset, with durations under a minute (Figure 1.2A).

VT events are caused by the rupture of rocks due to local and regional stresses, as well as due to magma as it forces its way through rocks during ascent to the Earth's surface (Rubin and Gillard, 1998; McNutt and Roman, 2015). It is not known though if the intrusion of magma initiates faulting, or if the faulting causes the intrusion of magma to occur (Oliva et al., 2019). These events can range in their source depth and commonly occur in swarms rather than as isolated events (McNutt, 2005). VT events have a much higher frequency content compared to many other volcanic events, and each individual event is often short-lived (Figure 1.2B).

Low-frequency events, as their name suggests, are long-period events with relatively low-frequency content compared to other volcanic events (Figure 1.2C). They are commonly observed before and during eruptions. These events are generally thought to be caused by a fluid (e.g. McNutt, 2005; Lipovsky and Dunham, 2015; McNutt and Roman, 2015; Greenfield et al., 2019), although there have been several models proposed to explain their occurrence at volcanoes worldwide such as brittle magma failure (Neuberg et al., 2006; Lavallée et al., 2008; De Angelis and Henton, 2011; Oikawa et al., 2019), gas flux (e.g. Cruz and Chouet, 1997), and incremental plug ascent (Iverson et al., 2006; Johnson et al., 2008; Bell et al., 2017; Neuberg et al., 2018). These models are invoked by the knowledge that buoyant magma will move from depth towards the surface through the magmatic plumbing system of the volcano (McNutt and Roman, 2015).

Seismic tremor is broadly defined by the occurrence of long-lasting high amplitude ground movement (Figure 1.2D). At volcanoes this is generally caused by the movement of fluids through cracks which cause resonance of the surrounding material (Chouet, 1988; 1996) although it has also been suggested that it can be caused by the coalescence of bubbles in shallow magma with relatively low viscosity (Ripepe and Gordeev, 1999). Tremor can be harmonic or non-harmonic, which is defined by the frequency signature of the event. Harmonic tremor has peaks in the frequency spectra at a fundamental frequency, and overtones at integer multiples of the fundamental, while non-harmonic tremor is broadband in nature.

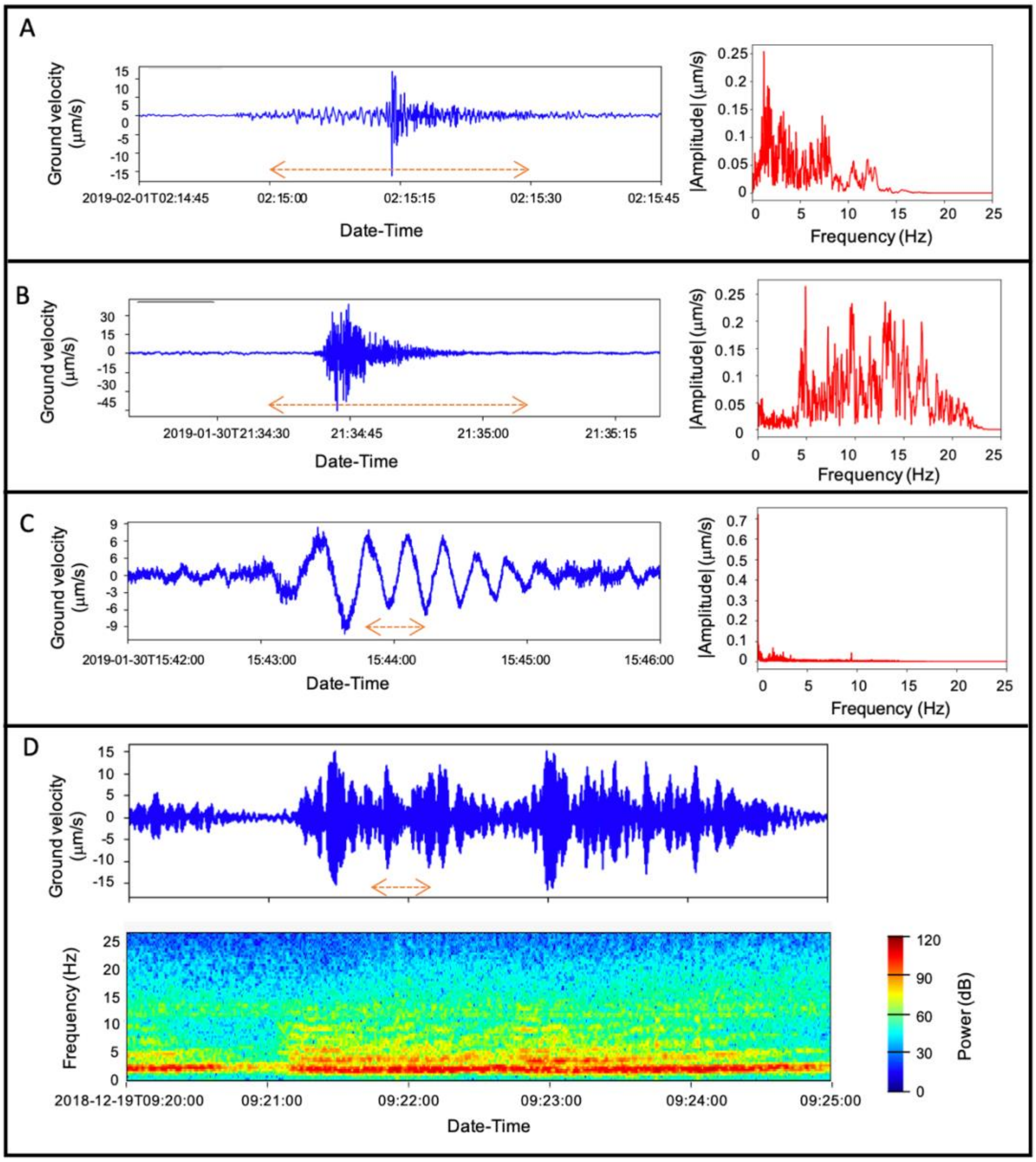

Figure 1.2. *Example seismic waveforms. All examples have been taken from station FG12 at Volcán de Fuego A) Explosion waveform and its frequency spectrum showing the low-frequency content of the explosion. B) Volcano-tectonic earthquake from and its frequency spectrum which shows the contribution of high frequencies. C) Low-frequency event and its frequency spectrum, showing the low frequency peak at 0.06 Hz associated with it. D) Tremor and its spectrogram. This tremor event was harmonic in nature as shown by the banding of energy at regular frequency intervals. Arrows have been added to the waveforms of each example to indicate 30 seconds of recording. Frequencies have been given from 0 Hz to 25 Hz, which for this station is the Nyquist frequency.*

1.2.2. Acoustic Infrasound at Volcanoes

Acoustic infrasound is a tool used to monitor activity at open-vent volcanoes through the recording of air pressure changes caused by compressional waves propagating from an oscillating source, as produced during vigorous gas emissions and explosive volcanism. (Fee and Matoza, 2013). Acoustic sources can be described as being either monopoles, dipoles or quadrupoles (Woulff and McGretchin, 1976; Pierce and Smith, 1981; Russell et al., 1999), where monopole sources are created by volumetric changes, dipole sources are caused by solid-fluid interactions, and quadrupole sources are caused by fluid-fluid interactions (Woulff and McGretchin, 1976). When modelling acoustic signals and calculating source properties, the assumption is often made that events such as explosions can be represented by volumetric sources, and can therefore be treated as a monopole, to simplify the problems and obtain basic estimations (e.g., Johnson and Aster, 2005). Through the analysis of volcanic infrasound, studies have detected hidden explosions from distant eruptions (e.g., De Angelis et al., 2012), mapped vent emissions (e.g., Jones and Johnson, 2011), characterised eruptive activity (e.g., Johnson et al., 2011), inferred details on eruption source parameters (e.g., Ripepe et al., 2013), and calculated properties of the plumes, including the ejection velocity, volume, density, height and radiation (e.g., Ripepe et al., 2013; Lamb et al., 2015). The acoustic signals can also be compared with seismic signals of the same events for investigations of their sources (e.g., Johnson and Aster, 2005; Palacios et al., 2016).

Volcanoes emit acoustic signals from a wide variety of eruptive activity ranging from Hawaiian to Plinian eruptions (Fee and Matoza, 2013). In a similar manner to seismic recording, acoustic microphones can be deployed at safe distances from the vent, record continually with minimal maintenance, and are sensitive to many vent-centred events which produce atmospheric disturbances, making acoustic infrasound another ideal tool to monitor and study active volcanoes. Volcanic infrasound sources can be impulsive, short-lasting events, such as from explosions, or longer lasting tremor events from continual degassing (Johnson and Ripepe, 2011; Fee and Matoza, 2013). Surface events such as lahars, rockfalls, landslides and pyroclastic flows also cause compressional acoustic waves as they punch through the atmosphere (Fee and Matoza, 2013).

Explosions cause atmospheric perturbations when the gas and ash mixture is ejected into the atmosphere. Despite being a part of the same overall sequence of events as the fracturing which causes seismic wave propagation, the source of the acoustic wave propagation is at the surface of the vent, where the ejected material first comes into contact with the atmosphere (Johnson and Ripepe, 2011). Explosions typically cause impulsive acoustic signals as the ejected material punches its way into the atmosphere (Figure 1.3A). Shockwaves are common with larger explosions and the signals typically last for the duration of plume emission.

Acoustic tremor, much like seismic tremor, is defined as elongated periods of high amplitude fluctuations in air pressure (Figure 1.3B), caused by a prolonged source. These events, much like their seismic counterparts can also show harmonic and non-harmonic frequency spectra (Johnson and Ripepe, 2011). Acoustic tremor has received much less attention than seismics, mostly due to the more recent development of acoustic techniques compared to the more established use of seismics but has been considered a key precursor to eruptions (Fee and Garcés, 2007).

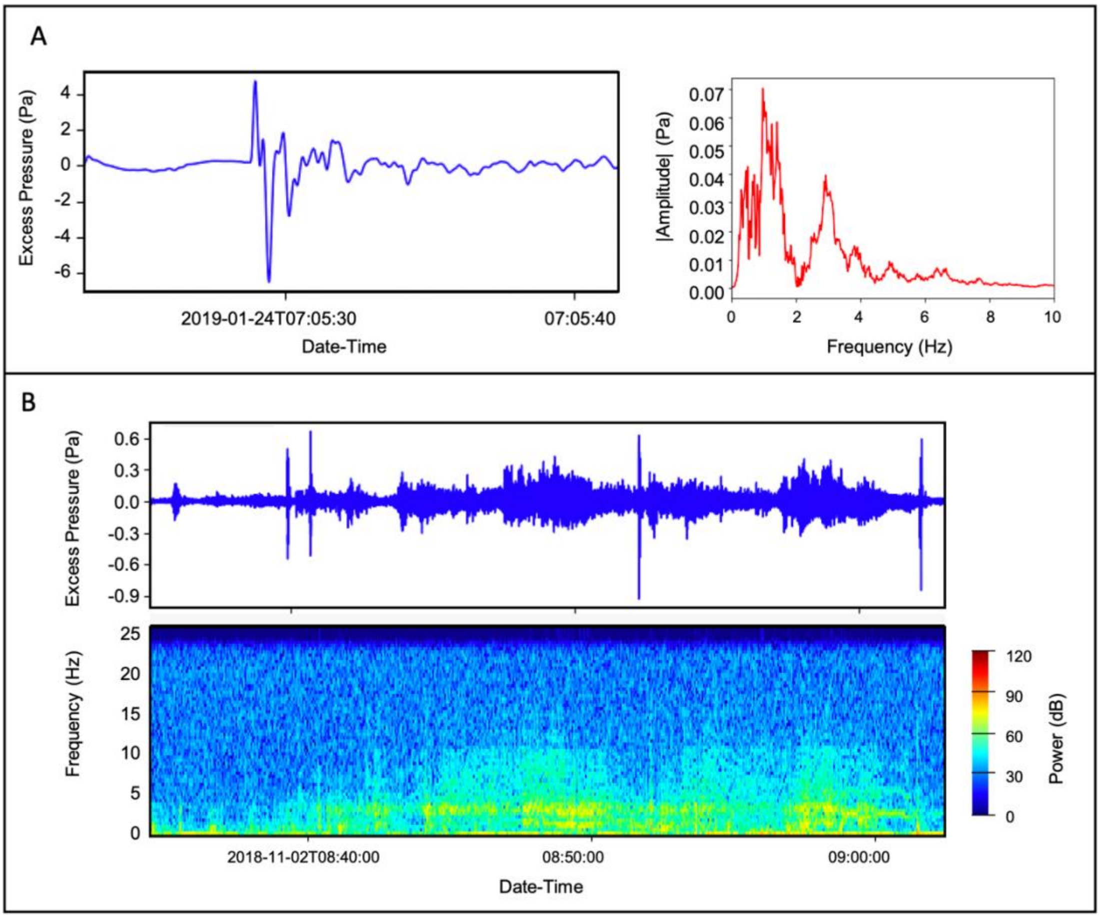

Figure 1.3. *Example acoustic waveforms recorded at Fuego Volcano at station FG12. A) An explosion waveform along with its frequency spectrum. B) Acoustic tremor and its spectrogram. The tremor event is harmonic, shown by the banding of energy at regular frequency intervals.*

1.2.3. Seismo-Acoustic Networks

Volcanic activity produces either seismic or acoustic waves, or both, which has led to seismic and acoustic recording to commonly be used together in order to gain a more complete account of activity at the volcano (e.g., Hagerty e al., 2000; De Angelis et al., 2012; Fee et al., 2020).

Seismic and acoustic monitoring is increasingly being adopted with multiple stations, rather than a single station, which can either be deployed as localised arrays or as larger networks around the volcano (e.g., De luca et al., 1997; Neuberg et al., 1998; Chouet, 2005; Prejean and Brodsky, 2011; Kim et al., 2014; De Angelis et al., 2016; Lamb et al., 2019). Networks allow for increased coverage of activity, the reduction of interference with noise, and identification of non-volcanic sources of energy. Arrays and networks can be used to locate event sources (e.g. Braun and Ripepe, 1993; Jones and Johnson, 2011; Soubestre et al., 2019), classify eruptive activity (e.g. Fehler and Chouet, 1982; Yamaoka et al., 1991; Sherburn et al., 1998; Neuberg et al., 1998; Scarpetta et al., 2005; Langer et al., 2006; Fee et al., 2010; Johnson et al., 2011; Cannata et al., 2013; Coombs et al., 2018), investigate the source mechanisms (e.g. Neuberg et al., 1998; Sherburn et al., 1998; Nakano et al., 2003; Chouet et al., 2005; Kim et al., 2014; Lanza and Waite, 2018), assess the eruption outputs (e.g. Fee et al., 2017; Iezzi et al., 2019; Diaz-Moreno et al., 2019), map the subsurface structure of the volcano (e.g. Brengruier et al., 2014; Jeddi et al., 2016; Lanza and Waite, 2018; Obermann et al., 2019), link of subsurface activity and surface observations (e.g. Neuberg et al., 1998; Chouet et al., 2005), detect events (e.g. De Angelis et al., 2012; Cannata et al., 2013; Coombs et al., 2018; Power et al., 2020), model eruption plumes (e.g. Prejean and Brodsky, 2011; De Angelis et al., 2016), and track the movement of hazards (e.g. Kumagai et al., 2009; Marchetti et al., 2019; Sanderson et al., 2021).

1.3. Volcanic Setting and Impacts

1.3.1. Volcán de Fuego

Location, Setting and Formation

Volcán de Fuego (hereafter referred to as Fuego), located at 14.47°N, 90.88°W in the central highlands of Guatemala, is an active composite stratovolcano with a summit 3,763 m above sea level (Figure 1.4). Fuego sits in a complex tectonic setting, close to the triple junction of the North American, Cocos, and Caribbean tectonic plates, and is placed in the second most northern of eight different volcanic sections of the Central American volcanic arc (Stoiber and Carr, 1973). Fuego is the youngest and most southern vent in the 230,000-year-old Fuego-Acatenango massif composed of the vents of Yepocapa, Acatenango, Meseta and Fuego (Chesner and Rose, 1984). Most of the growth of the complex has been attributed to the past 84,000 years (Vallance et al., 2001), with the activity at Fuego being calculated to have started with a minimum age of between 8,500 years ago through extrapolation of the time of effusion from a lava sequence on the flank of Meseta (Chesner and Rose, 1984), or 13,000 years ago through the extrapolation of the eruption rate of the past 450 years by Martin and Rose (1981). The maximum age of the activity at Fuego is given as 30,000 years by Vallance et al. (2001). The early formation of Fuego is thought to have occurred following a flank collapse of Meseta's eastern flank, which occurred between 30,000 and 8,500 years ago (Vallance et al., 1995), which ended the period of activity centred at Meseta (Martin and Rose, 1981; Vallance et al., 2001).

Through time, the eruptive products from Fuego have transitioned towards being more mafic, from being initially basaltic, to basaltic andesites, to andesitic (Chesner and Rose, 1984). The lavas produced have mostly been basaltic-andesitic in composition, and since 1974, the products from Fuego have been mainly high-Al basalt which are volatile rich (2.1–6.1 wt % H_2O), whereas the previous eruptive centres produced mostly andesitic lavas (Sisson and Layne, 1993; Roggensack, 2001). The high volatile content of the magma is thought to highly influence the eruptive behaviour at Fuego (Lyons et al., 2010)

Figure 1.4. *Volcán de Fuego. Viewed from the summit of Acatenango.*

Historic Activity

Historically, there have been over 50 eruptions with Volcanic Explosivity Index (VEI) ≥ 2, including five sub-Plinian events (VEI ≥ 4) recorded at Fuego since 1524 (Rose et al., 2008; Hutchison et al., 2016), the year of the Spanish conquest of Guatemala, making it one of the most active vents in the Central American volcanic arc. These large eruptive events are separated by low-level open-vent activity with durations of months to decades, which in-turn are separated by periods of repose which last up to several decades (Martin and Rose, 1981). The periods of open-vent activity are defined by volcanic events which range over several orders of magnitude including frequent Strombolian eruptions (Waite et al., 2013; Naismith et al., 2019; Diaz-Moreno et al., 2020), lava flow effusion (Martin and Rose, 1981; Brill et al., 2018; Naismith et al., 2019), seismic and acoustic tremor (Lyons and Waite, 2011; Lyons et al., 2013; Brill et al., 2018; Diaz-Moreno et al., 2020), continuous gas release (Brill et al., 2018; De Angelis et al., 2019; Naismith et al., 2019; Diaz-Moreno et al., 2020), and larger paroxysmal eruptions which occur less often, commonly with several months between each event (Naismith et al., 2019). It has been estimated that 75% of the historic activity (since 1524) has been constrained to just four of these periods, lasting between 20 and 70 years each (Hutchison et al., 2016).

The most recent sub-Plinian eruption occurred in October 1974, towards the end of an open-vent phase that spanned much of the 1970s. The eruption consisted of a series of 4 eruptions between the 10th and 23rd of October, and produced pyroclastic flows, lava flows and high amounts of ashfall, subsequently causing lahars, all which had a large impact on the local communities (Rose at al., 1978). The eruption expelled 0.2 km^3 of basaltic tephra that was deposited up to 200 km to the west of the vent (Rose et al., 2008). This eruption is the largest at Fuego since a large event that occurred in 1932, which caused seismicity to be felt as far as Honduras and El Salvador, as well as emitting large volumes of tephra which was deposited throughout Guatemala. After the 1974 eruption, there were smaller paroxysmal eruptions until 1978, when the vent went into another period of repose (Rose et al., 1978). After 20 years of quiescence, with only small isolated strombolian eruptions occurring in 1987 and 1988 (Andres et al., 1993), activity resumed once more on the 21st of May 1999 with a VEI 2 eruption which restarted typical open-vent activity which has been occurring until the present day (Naismith et al., 2019) with blocky lava flows, Strombolian eruptions, ash-rich explosions, and degassing events (Lyons et al., 2010; Lyons and Waite, 2011). The occurrence of paroxysmal eruptions also resumed, breaking up the background activity (Lyons and Waite, 2011). These paroxysms have not occurred regularly, but there have been phases in which there have been several paroxysms per year, and years absent of paroxysms (Naismith et al., 2019).

It is thought that there was no magma recharge between the 1974 sub-Plinian eruption and the new eruptive phase in 1999 (Liu et al., 2020), as the magma composition is seen to be geochemically related, with higher variability of volatiles and an increase in differentiation from the newer 1999 eruption (Berlo et al., 2012). The crystal and volatile rich magma has been linked to the eruption style being similar to that of magmas with a higher silica content (Lyons and Waite, 2011). The initial activity of the current eruptive phase in 1999 has been said to represent a clearing of this residual magma that was not erupted in the 1974 event, and the current activity has been theorised to be caused by an intrusion of new magma deep within the system (Berlo et al., 2012).

Recent Activity

Since the start of the current period of activity there have been several phases which can be defined by the occurrence rate of paroxysmal activity. Between 1999 and 2006, paroxysms usually occurred between one and two times per year, this increased in 2007 with at least 5 large events before the occurrence of paroxysms stopped between 2008 and 2012 (Naismith et al., 2019). During this repose in paroxysmal activity, background extrusion and low energy explosions still remained an ongoing feature of activity. The effusion rate was noticed to have picked up in 2011 before the paroxysms resumed again in September 2012, and in 2015 the rate of paroxysms increased sharply with between 12 and 15 events occurring per year (Naismith et al., 2019). In June 2018, a large paroxysmal event occurred, with a smaller paroxysm following in November of the same year. Since then, there has been no further paroxysms, but similarly to the time period between 2008 and 2012, there has been a continuation of the low-level background activity. Since the beginning of the current eruptive phase in 1999 there have been 11 events of VEI ≥ 2 (Naismith e al., 2019; Figure 1.5A), with 42 paroxysms alone since 2015 (Figure 1.5B).

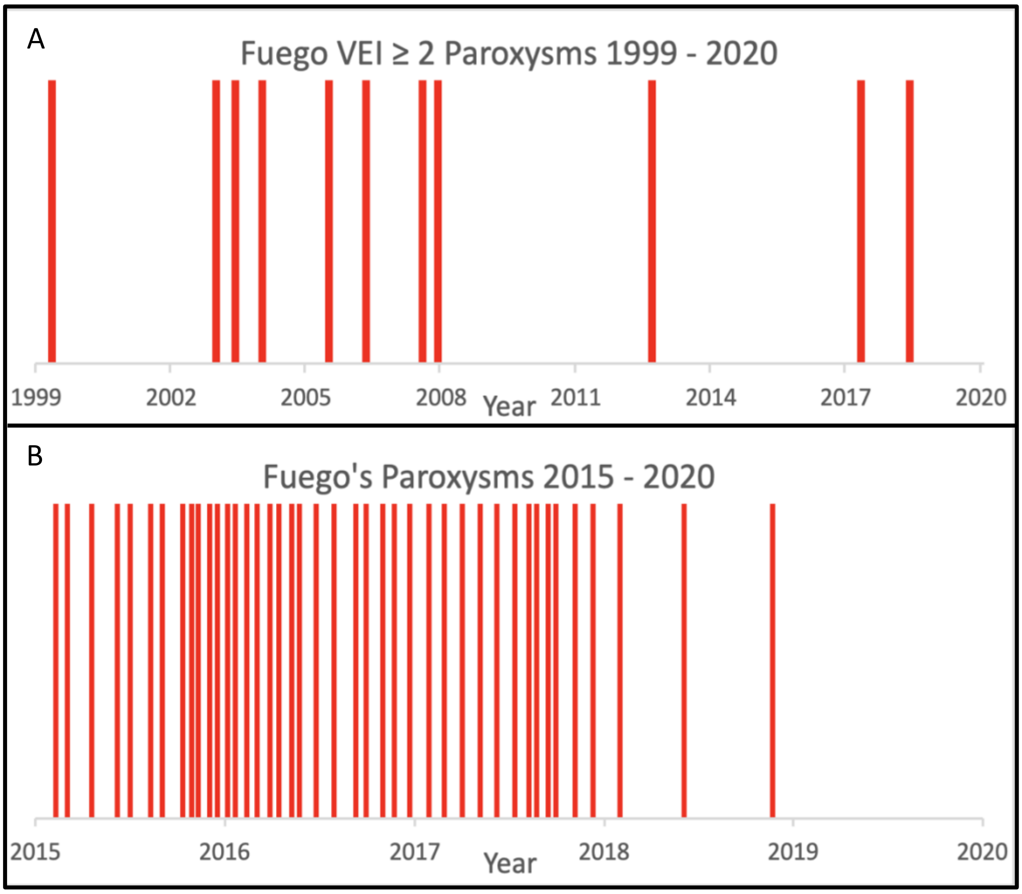

Figure 1.5. *Timing of paroxysms at Volcán de Fuego. A. Significant (VEI ≥ 2) paroxysms since the start of the current period of activity in 1999. B. All paroxysms since 2015, a period of elevated paroxysmal activity (Naismith et al., 2019).*

Hazards and Impact

The large eruptions that have occurred at Fuego have caused damage, disruptions and in the most severe cases, death in the local communities which surround the vent, through both direct and secondary hazards. Historic records from the 1717 eruption show that mud flows originating from Fuego, as well as nearby Agua Volcano severely impacted the communities of Mixtan and Masagua on the Río Guacalate (Hutchison et al., 2016). Over a century and a half after 1717, an eruption in 1880 caused the communities in Mazatenango and Retalhuleu to use artificial light during the day due to the darkness caused by thick continuous ash fallout (Feldman, 1993), which are 67.5 km and 85.9 km from the vent at Fuego, respectively. In recent history, the 1971 eruption was noted to have produced large pyroclastic flows to the East, and heavy ash-fall (up to 30 cm depth) to the West which caved in 20% of the roofs in San Pedro Yepocapa (Bonis and Salazar, 1973). The large 1974 eruption also caused roofs to collapse in San Pedro Yepocapa, and deposited ash as far as Guatemala City, 40km to the East of the vent (Vallance et al., 2001). The sub-Plinian eruption produced large pyroclastic flows which travelled over 8 km from the vent summit (Rose, 1978). During the current eruptive episode beginning in 1999, there have been several eruptions which have caused evacuations and heavy destruction. In January 2003, a paroxysmal eruption caused several communities to be evacuated (Webley et al., 2008), and in September 2012 a paroxysm caused the alert level to quickly escalate to require immediate evacuation as pyroclastic density currents began to flow down the southern flanks (GVP, 2012). The most recent major event occurred on the 3rd of June 2018, which has been more destructive in terms of casualties than any other event within the 20th-21st centuries (Witham, 2005) causing at least 169 fatalities, and leaving 256 people missing, as well as displacing nearly 13,000 people from their homes (GVP, 2018b). The eruption was the most intense during the current eruptive period (Naismith et al., 2019). The eruption began similarly to most paroxysms (Pardini et al., 2019), but underwent an increase in intensity around 6 hours into the eruption, causing ash plumes to rise 9 km above sea level (GVP, 2018b), and pyroclastic flows to descend 11 km from the vent, upon the local community of San Miguel Los Lotes to the southeast, destroying several bridges and causing devastation to the local people who could not evacuate (GVP, 2018b). Currently, it is estimated that around 60,000 people in surrounding communities are at risk to the hazards posed by large eruptions at Fuego (Naismith et al., 2019), and the risk of a partial edifice collapse of the southern flank could be catastrophic (Vallance et al., 1995; 2001).

Previous Studies

Thanks to the ease of access to the flanks of Fuego and the viewpoint from the peak of Acatenango, there have been several studies on the volcanic activity at Fuego, mostly since the start of the current eruptive phase. These studies have used a range of methods including seismics (e.g., Lyons and Waite, 2011; Nadeau et al., 2011; Brill et al., 2018), acoustic infrasound (e.g., Lyons et al., 2013; Diaz-Moreno et al., 2020), petrology (Berlo et al., 2012; Liu et al., 2020), thermal imaging (e.g., Lyons et al., 2010), gas measurements (e.g., Nadeau et al., 2011), as well as tilt and ground deformation (Lyons et al., 2012). These studies have focused on determining the internal geometry of the magma plumbing system (e.g., Lyons and Waite, 2011), external morphology (e.g., Aldeghi et al., 2019), source mechanisms (e.g., Pardini et al., 2019; Liu et al., 2020), monitoring and classifying the events (e.g., Brill et al., 2018; Diaz-Moreno et al., 2020), and understanding the patterns in the eruptions (e.g., Martin and Rose, 1981; Lyons et al., 2010; Naismith et al., 2019).

The studies have found that there are commonly two vents at the summit of Fuego, producing distinct activity, one predominantly produces ash-rich explosions, while the other emits gas-rich explosions (Lyons and Waite, 2011; Diaz-Moreno et al., 2020). Aerial photos by Lyons and Waite (2011) found the crater to have a diameter between 100-150 m, while each vent was approximately 50-75 m apart from one another. These were labelled as a central and western vent, with the central vent acting as the main centre of the explosions, with the western vent emitting mostly weak gas-and-ash emissions as well as passive degassing.

Beneath the surface vent, the conduit and shallow magma storage have been modelled to be an inclined sill at 300 m depth below the summit vents, and centred 300m to the west, fed by a deeper magma supply (Lyons and Waite, 2011). The sill sits below a pipe-like upper conduit system to the summit vents (Waite and Lanza, 2016). This sill undergoes a cycle of pressurisation when a volume builds within it, depressurisation when the tensile strength of the capping magma plug has been overcome to release the pressure through the expulsion of the volume via an explosion, and then a consequent repressurisation of the sill when the fractures have closed over and resealed the plug (Lyons and Waite, 2011).

The explosions associated with this cycle of sill pressurisation cause both seismic and acoustic wave propagation. The acoustic signals of these explosions typically show an impulsive onset with an extended coda which represents the initial release of pressure, and then the fragmentation of the foam within the conduit (Johnson et al., 2004). The explosions have also been observed to trigger high amplitude seismic tremor events, which can last for several minutes to hours, and can be both harmonic or non-harmonic (Lyons and Waite, 2011). Seismic tremor is not always caused by an explosion at Fuego, often occurring without any initial impulsive onset, and has been observed by several studies (e.g., Lyons et al., 2010; Lyons and Waite, 2011; Nadeau et al., 2011; Brill et al., 2018). As well as seismic tremor, acoustic tremor has also been observed to occur at Fuego, also with both harmonic and non-harmonic events recorded (e.g., Lyons et al., 2013; Diaz-Moreno et al., 2020).

Introduction

There has been a strong link between different observations at Fuego, such that a recording of one feature can be used as an indicator to another. One of these is the association of gas emission and seismicity, such that non-harmonic tremor is often recorded at the same time that gases are emitted non-explosively (Nadeau et al., 2011). The different explosions from the vents have also been observed to cause differences in the seismic (Waite et al., 2013) and acoustic signals (Diaz-Moreno et al., 2020). Before an explosion, tilt data shows that there is an inflation of the summit starting 20-30 minutes prior, due to the pressurisation within the sill (Lyons et al., 2012). Thermal emission and lava effusion have both typically increased alongside the increase in activity, as seen in 2003, 2007 and between 2015 and 2018, which has indicated that there has been magma closer to the surface in the conduit (Naismith et al., 2019).

As the most dangerous common event at Fuego, the paroxysms have had studies dedicated to understanding their triggering mechanisms. It has been identified that there are times during the active periods when there is a cyclicity to the behaviour of the volcano (Lyons et al., 2010). Lyons et al. (2010) described the cycles of paroxysmal eruptions as having three phases: an initial phase of increased frequency and energy in Strombolian explosions and the observation of gas chugging; a main phase of explosive activity with lava flows and a maintained eruptive column due to continuous explosions of ash and gas, causing pyroclastic flows; and a final reduction in activity back to background levels. This observation was later backed up by the more recent study by Naismith et al., (2019). Lyons at al., (2010) observed this cycle 5 times during their two-year investigation of the activity at Fuego through visual observations and thermal data from satellites, aided partially by seismic and infrasound recordings, where the paroxysmal phase lasts for 1-2 days between months of background level activity.

The triggers to the paroxysmal eruptions at Fuego have been debated and there are several models which have been proposed as likely candidates to explain them. The driving factors proposed are gas flux, magma recharge and depressurisation of the system (e.g. Jaupart and Vergniolle, 1998; Lyons et al., 2010; Naismith et al., 2019).

Fuego's paroxysms have been suggested to be gas-driven, based on the collapsing foam model (Jaupart and Vergniolle, 1998) due to the high degassing and chugging seen at the vent in the build-up to the paroxysms (Lyons et al., 2010). This model assumes an unstable layer of foam accumulates in the conduit, and after a critical thickness has been reached, it collapses into an underlying gas slug which drives the fountaining of the material in the high energy event (Jaupart and Vergniolle, 1998). Along with the time for the foam layer to form, the clearing of the conduit would then lead to a volume for later refill, giving a timing constraint on the cycles observed. For this model to be valid at Fuego and allow for cyclicity in the events, a sufficiently high viscosity magma, or high gas flux would be required. For the case of the large June 2018 paroxysm, Liu et al. (2020) have proposed that the gases may have accumulated below a low permeability plug in a process of gas-holdup, where the mass of the magma remains constant, while its volume increases, leading to the eventual failure of the plug. Further petrological monitoring of Fuego by Liu et al. (2020) has claimed that the majority of paroxysms have been gas-driven by exsolved gases from deep magmas within the plumbing system.

The paroxysms at Fuego have also been debated to be magma driven (e.g., Lyons et al., 2010; Naismith et al., 2019), with the rise-speed dependent model often put forward (Parfitt and Wilson, 1995), which claims that different styles of eruption are controlled by the rate of ascent of materials through the conduit. When the rise speeds are lower, bubbles can more easily coalesce before they reach the surface and burst in a Strombolian eruption, however, higher ascent rates reduce the amount of coalescence as there is a lower differential ascent rate between the magma and the bubbles (Parfitt and Wilson, 1995). As the bubbles are more spread-out within the magma, the 75% volume threshold for fragmentation to occur for run-away coalescence at depth, causing lava fountaining in a paroxysmal event (Parfitt and Wilson, 1995). Parfitt (2004) linked observations at Fuego to this model, showing how the increase in rise speed causes shorter repose between Strombolian explosions as well as increased energies in these events during the build-up to a paroxysm. In magma driven paroxysms, changes to the bulk composition of either the erupted material or the rims of major crystals is expected (e.g., Viccaro et al., 2014), and it was found that magma recharge had occurred prior to the 1974 sub-Plinian eruption (Berlo et al., 2012). Although Liu et al. (2020) argue for a gas-driven paroxysm trigger mechanism, they acknowledge that gas fluxing through the system could be due to deep, fresh, volatile rich magma degassing as it rises, thereby the paroxysms ultimately being caused by a magma-driven model.

Both the gas and magma driven models for paroxysm triggering are thought to be capable of producing a cyclicity comparable to those observed at Fuego, and that they are both likely able to stiffen the magma in the conduit and produce a plug, under which gases can accumulate for periodic release akin to that of background emissions observed at the vent (Diaz-Moreno et al., 2020).

A third model has been proposed by Naismith et al. (2019), which states that unloading via the shedding of material from the summit cone could cause sufficient depressurisation to drive a paroxysm. They acknowledge that this mechanism would not explain all paroxysms, as there have been several events which do not have observations of unloading occurring prior to eruption. Naismith et al. (2019) state that an ephemeral cone slowly builds during baseline activity due to the lava fountaining of the persistent Strombolian eruptions. This cone can be destroyed by avalanches from lava flows during crater overspill, removing enough volume to cause sufficient decompression of the magmatic system to cause a paroxysm. This is similar to the decompression model proposed for Stromboli (Ripepe et al., 2017), where decompression leads to a disequilibrium between shallow and deep magma reservoirs and causes the paroxysm as the magma exsolves gases. The decompression mechanism has been claimed to have been responsible for several eruptions in Fuego's history, including the 1974 paroxysm (Pardini et al., 2019), however the scale of the mass loss occurring before the paroxysms should be considered as a significant amount of loss is required for this to have an effect.

It is possible that the mechanisms described by these three models all contribute to eruptions at Fuego, either separately or in conjunction with one another, where several conditions must be satisfied for an eruption to occur.

1.3.2. Santiaguito Lava Dome Complex

Location, Setting and Formation

The Santiaguito lava dome complex, located at 14.76°N, 91.55°W in the Western Highlands of Guatemala and standing 2,520 m above sea level (Figure 1.6) is an active dacitic stratovolcano which is situated in the collapse scarp of the 1902 flank eruption of its parent volcano, Santa Maria, which was one of the largest Plinian eruptions in recorded history (Williams and Self, 1983). The dome complex is tectonically close to the triple junction of the North American, Cocos, and Caribbean tectonic plates, which drives the volcanism in the region (Stoiber and Carr, 1973). Santa Maria itself is an andesitic stratovolcano, with a summit at 3,745 m above sea level and has an estimated age of ~30,000 years (Rose, 1987). Argon dating of the oldest lava formations has suggested that Santa Maria formed between 100 and 25 thousand years ago (Escobar-Wolf et al., 2010). It is thought that an intrusion of basaltic andesite into a dacitic magma storage zone triggered the October 1902 flank eruption of Santa Maria (Rose, 1987), which lasted for 36 hours, expelling 20 km^3 of tephra and creating a 0.5 km^3 crater in the south-western flank of the once symmetrical cone volcano (Rose, 1973; Conway et al., 1994). After 20 years of repose following the 1902 Santa Maria eruption, the Santiaguito Lava dome complex first started erupting in the flank crater. The Santiaguito lava dome complex is made up of four separate domes: Caliente, La Mitad, El Monje and El Brujo, which sit on an East-West trending fracture. These four domes are calculated to total 1.1 – 2 km^3 in volume (Harris et al., 2003; Durst, 2008; Escobar-Wolf et al., 2010). Activity at Santiaguito is currently centred at the Caliente dome, and has been since 1975 (Harris et al., 2003). The summit structure of Caliente has a dacitic dome growing within the ~300 m wide vent rim, from which most of the activity originates (Bluth and Rose, 2004). The activity at the dome is controlled by a stiff magmatic plug in the conduit, with regular ash-and-gas explosions occuring, which resemble weak vulcanian eruptions, and block lava flows continually occurring (e.g. Bluth and Rose 2004; Johnson et al. 2004; Sahetapy-Engel, 2004; Johnson et al. 2008; Sahetapy-Engel et al., 2008, Lamb et al., 2019). The explosive activity is often seen to emanate from ring shaped fractures on the surface of the dome, which has suggested that the conduit system has a typical cylindrical shape, with possible conical widening at the top (Bluth and Rose, 2004).

Figure 1.6. *The Santiaguito lava dome complex. Santiaguito (left, exploding) sitting in the collapse scarp of Santa Maria (right)*

Historic Activity

Santiaguito has been continually active since it first erupted in 1922 until the present day. Before the mid 1960s, the activity at Santiaguito had been described as undergoing alternate phases of rapid dome extrusion and phases of block lava flow extrusion with lower levels of explosive activity (Harris et al., 2003). The domes of Santiaguito have been noted to have historically grown in six phases since it first erupted in 1922 (Rose, 1972; 1987), with the extrusion rate being shown to have been cyclical, with high extrusion during 3-to-6-year periods, interspersed between low extrusion periods lasting between 3 and 11 years (Harris et al., 2002). Harris et al. (2002) also found that the extrusion rate on average was reducing through time, while block-lava flow lengths had increased, suggesting a decrease in silica content and viscosity. Activity first began at the Caliente dome between 1922 and 1925 in the first cycle of growth and then again between 1929 and 1934 before migrating to the west to build La Mitad (1939-1942), El Monje (1949 – 1955), and El Brujo (1958-1963), before returning to the East when activity restarted at Caliente along-side activity at El Brujo (1972-1975) (Rose 1987). The building of the domes and general activity at Santiaguito initially was endogenous, with magma building within the dome below the ground surface, however after a transition period spanning 1929-1958, the activity has been dominated by exogenous growth, with lava extrusion from the summit vents causing dome growth (Harris et al., 2002). The early phases of lava effusion between 1922 and 1934 have been found to have extruded with the highest rates, building over 30 % of the dome structures which were present by the 1970s (Rose, 1973). In the following periods between 1935 and 1971, there was extrusion of at least 8 lava flows and almost continuous activity (Rose, 1973), and since the 1960s the activity has seen a rise in lava flows (Rose, 1972; Harris et al., 2003; Bluth and Rose, 2004), with increasing flow lengths which has been attributed to the decrease in silica content through time (Harris et al., 2003).

During the ~100 years of activity at Santiaguito, there have been several notable eruptions. One of the largest events was a dome collapse between the 2nd and 4th of November 1929, with an approximate of over 3 million m^3 of extruded material which extended over 11km from the dome where the block and ash flows were reported to have caused the deaths of at least 21 local villagers in El Palmar (Rose, 1987). Smaller collapses of the block-flow fronts have caused avalanches of material, such as in 1973 (Rose et al., 1977) and larger eruptions have caused large ash plumes and pyroclastic flow activity posing hazards to the local communities.

Recent Activity

Since 1975 the activity at Santiaguito has been centred at Caliente, with activity characterised by the effusion of block lava flows and gas-rich explosions (Harris et al., 2003; Sahetapy-Engel et al., 2008; Holland et al., 2011; Lamb et al., 2019; Gottschämmer et al., 2021; Rohnacher et al., 2021). Pyroclastic flows are also seen to be generated from some of the larger explosions (e.g., Holland et al., 2011), as well as the ejection of pyroclastic bombs which commonly land on the flanks of the dome (Bluth and Rose, 2004), although can be ejected further in larger blasts (e.g., GVP, 2016a). Since activity restarted at Caliente, explosions have been a constant behavioural feature (e.g., Sahetapy-Engel et al., 2008; Johnson et al., 2014; Lavallée et al., 2015; De Angelis et al., 2016). The explosions have been recorded to have repose intervals between 30 minutes (Rose, 1987; Scharff et al., 2014; Lavallée et al., 2015) and several hours (e.g., GVP, 2017a). These explosions can range between small, short-duration gas-rich explosions producing white plumes that rise ~0.5 - 1 km high, to more powerful, longer lasting ash-rich explosions with darker plumes rising 1.5 km above the vent. In shorter lasting periods of heightened activity, these explosions can generate plumes that rise up to 7 km in height (e.g., GVP, 2016a). As well as gas release during the explosions, almost continual release of SO_2 has been measured between the events (Holland et al., 2011). Passive emission of white steam has been visually observed (e.g., Bluth and Rose, 2004) in both elongated emission episodes, and smaller discrete puffs from several locations around the summit crater.

Due to an observed decline in extrusion rates and bulk SiO_2 observed, Harris et al. (2003) estimated that by 2014 to 2024 the activity at Santiaguito would come to an end. However, the eruption rates were later seen to increase since 2010, with a period of high activity in 2016 which has indicated there may have been a renewal of the magma system feeding activity (Rhodes et al., 2018; Lamb et al., 2019). In 2016 an increase in the level of explosive activity was observed, with explosions emitting plumes up to 7 km in height, excavating the conduit in the removal of the dacitic dome (Lamb et al., 2019). Wallace et al. (2020) showed through the characterisation of ash samples and ballistic bombs that the intensification of explosivity during this period was likely caused by an injection of a deep sourced (~17-24 km), higher temperature (~960-1020 ˚C) and volatile-rich magma into the shallower magmatic system at ~2 km depth. Since the short-lived increase in explosivity in 2016, the eruption style at Santiaguito has returned with the re-growth of the lava dome within the vent and remained at a low constant level which typifies the normal baseline behaviour of the volcano, with explosions occurring between 70 and 100 times a week (Gottschämmer et al., 2021), and lava effusion has further filled the crater of Caliente, building the dacitic dome within (Gottschämmer et al., 2021; Rohnacher et al., 2021). Gottschämmer et al. (2021) also identified the occurrence of tremor at Santiaguito in their study between 2018 and 2020, showing that between 10 and 50 events occur per week, with cumulative durations of 40-130 minutes per week, where the source is estimated to be at depths between 500-750 m below the summit of Caliente.

Hazards and Impact

As well as the loss of life caused by dome collapse events, pyroclastic flows and lahars, such as in the 1929 dome collapse, there has also been loss of livestock, farmland and crops, and property. Pyroclastic flows have been caused by both front collapses of the block lava flows and summit explosions (Harris et al., 2002; 2003), and are typically seen to occur on the southern and western flanks of the domes. The fluvial systems originating in the western highlands of Guatemala by Santiaguito flow to the Pacific Ocean, and due to the high volume of volcanic sediment, have made the region highly populated due to good farmland. The town of San Felipe, located within 7km to the south of Santiaguito, has a population of approximately 31,800, therefore, lahar and aggradation activity has high potential impacts on the people of this community, as well as others in the region (Harris et al., 2006). This therefore makes any large eruption or dome collapse a large risk to the communities who live near the volcano, in low lying areas likely to be destroyed if large pyroclastic flows are produced and flow down one of the 5 drainage channels which are all directed towards the south. The town of El Palmar for example, which suffered many losses over the years due to the activity of Santiaguito and the subsequent lahars from the remobilization of erupted material during the wet season, was eventually abandoned and later destroyed due to lahar activity (Harris et al., 2003). 11 km to the north of Santiaguito is Quetzaltenango, Guatemala's second city, which has a population of just over 180,000. Any large event with little warning could cause large-scale devastation due to the difficulty to evacuate such a population, and the destruction of infrastructure would also have large impacts socio-economically. Further afield, 110 km to the east is Guatemala City, which is a hub of transport for the country. Large ash clouds and ash-fall-out could greatly impact this, bringing the county to a halt. Although not a hazard to life, the slowly growing lava flows have been seen to encroach on farmland on the lower slopes, impacting the farming life of the local communities who live there.

Previous Studies

Thanks to the protracted eruption of Santiaguito, the advantage point offered by the summit of Santa Maria, as well as accessibility around the volcano due to the local towns, villages and farmed land, there have been many studies at Santiaguito using a wide range of techniques to better understand the ongoing processes. The studies at Santiaguito have used seismic (e.g. Sanderson et al., 2010; Johnson et al., 2014; Scharff et al., 2014; Lavallée et al., 2015; Lamb et al., 2019; Hornby et al., 2019), acoustic infrasound (e.g. Johnson and Lees, 2010; Jones and Johnson, 2011; Scharff et al., 2014; De Angelis et al., 2016; Lamb et al., 2019), ground deformation and tilt (e.g. Johnson et al., 2004; Johnson et al., 2014; Lavallée et al., 2015); visual observation (e.g. Bluth and Rose, 2004; Johnson et al., 2008), thermal observation (e.g. Sahetapy-Engel et al., 2008; Sahetapy-Engel and Harris, 2009; De Angelis et al., 2016; Lamb et al., 2019) doppler radar (e.g. Scharff et al., 2014), UV imaging (e.g. Holland et al., 2011; Esse et al., 2018), gas measurements (e.g. Yamamoto et al., 2008), and petrologic studies (e.g. Scott et al., 2012; Wallace et al., 2020).

Scott et al. (2012) used petrological analysis of lava samples to investigate the plumbing system below Santiaguito, between the surface and the lower mid-crust. They used amphibole and plagioclase phenocrysts to show that crystals in the magma formed at ~ 24 km and ~ 12 km beneath the surface, indicating likely storage zones. Amphibole breakdown rims indicated that magma may rise relatively quickly from ~ 12 km to the surface and become increasingly more viscous before eruption (Scott et al., 2012). The depths they found are similar to those suggested by Wallace et al. (2020) for the source of the fresh magma associated with the increased activity observed in 2016.

As the most common event type at Santiaguito, much of the work has been focused on the small-to-moderate gas-and-ash explosions. These explosions have been noted by Scharff et al. (2012) to either occur as a single pulse, or as a series of pulses, where 83 % of the 157 explosions in their study had more than one pulse. The explosion plumes have been shown to be mainly volatile rich and ash deficient (Yamamoto et al., 2008), where the explosion products have been assessed by De Angelis et al. (2016) who showed that the volume fraction of ash in the early momentum-driven phase of the explosion plume ejection to be between 2.3 – 4.5 $\cdot 10^{-5}$ when the density of ash is assumed to be 2,650 kg/m^3, and where the remaining fraction of the plume is composed of gas. The emission speed of the explosions has been measured to occur at around 10 ms^{-1}, although it has a range between 5 and 30 ms^{-1}, where the eruptive phase has a duration of 30-60 s, which is followed by gas fuming for several minutes (Bluth and Rose, 2004). The surface release of the explosions is not simple which has been reflected in the acoustic infrasound semblance study by Johnson et al. (2011). Johnson et al. (2011) found that the pulses occur from all over the dome summit, originating at different points of the ring fractures, and state that the acoustic signal can be created by the gas flux from the surface, or from the rise and fall of the dome surface as it inflates and deflates.

Many studies have tried to decipher the cyclic explosions at Santiaguito, to understand the trigger mechanisms and properties within the magmatic system. There have been three main models put forward to describe the mechanisms of these explosions:

1. Gas slug accumulation and disruption under a plug

The first mechanism proposed relies upon a pressure source of gas build-up in the magma column, leading to a cycle of deformation as the gas is periodically released before renewed build up (Johnson et al., 2008; Sanderson et al., 2010; Johnson et al., 2014). This has been proposed due to the observation that the strongest period of gas emission corresponds to the peak of the inflation cycle, as detected by tiltmeter observations (Johnson et al., 2014) and that the inflations cause between 0.2 and 0.5 m of vertical uplift to the plug at the moment of the explosion onset (Johnson et al., 2008). The inflation of the dome prior to an explosion and increased very long-period seismicity observed (Lavallée et al., 2015) could be explained by this pressure source within the shallow conduit. Johnson et al. (2008) gives the plug dimensions as 200 m in diameter and between 20 and 80 m thick. They also show how the uplift of the dome initially occurs at the centre of the dome and then radiates out at speeds of 30 – 50 ms^{-1}, causing high strain rates which cause brittle failure of the dome, allowing the escape of the accumulated gases in an explosive event which occurs in different regions of the dome throughout the course of a day, rather than from repeated fractures. The dome uplift was shown by Scharff et al. (2012) to occur 1.5 seconds before the plume was first ejected from the fractures. Sanderson et al. (2010) used pseudo-tilt measurements to locate a mogi-source at depths of 250 m below the vent, and 200 m to the west of the dome centre.

2. Shear zone fracturing at the conduit margins

Bluth and Rose (2004) suggested that the explosions at Caliente are triggered by a shear induced fragmentation of the dacitic magma near the margins of the conduit. The model is based on the theory that the upper magma column rises within the conduit, causing a shearing at the conduit walls (Goto, 1999; Papale, 1999), and is thought to be brought on by an increase in the magma flow velocity which leads to viscosity increases after degassing. The viscosity increase ultimately allows brittle deformation to occur under the high strain rate in the shallow conduit system (Holland et al., 2011), creating many small but connected cracks (Rhodes et al., 2018). As the margin of the conduit fractures, rapid gas release is triggered from the shallow conduit along these fractures in the magma, causing an explosion with a gas-and-ash plume (Harris et al., 2003; Johnson et al., 2008; Holland et al., 2011; Lavallée et al., 2013; Scharff et al., 2014). Following the explosions, the fractures shut and begin to heal, allowing the cycle to start over (Holland et al., 2011). The shear fracturing mechanism is supported by the observations of ring fractures on the surface of the dacitic dome at the onset of eruption, first noted by Gonnermann and Manga (2003) and later by Sahetapy-Engel & Harris (2009). Sahetapy-Engel & Harris (2009) also showed the occurrence of inner and outer ring fractures, textural disequilibrium from rapid frictional heating seen on emitted ash samples, and increased tilt signals and very long period seismicity. Bluth and Rose (2004) noted that the ring fractures occurred on ~50% of the eruptions they observed. Thermal and acoustic infrasound observations by Sahetapy-Engel et al. (2008) further supports the plug-flow extrusion model through stepwise flow with fractures and subsequent healing. They used the time delay of acoustic signals to show that the depth of fragmentation, and therefore the source of the explosions varied between 100 and 620 m depth, which they claim would not be observed if the source were at a fixed location as with gas build-up below a plug.

3. Magma–water interaction

The final mechanism that has been explored, although is now not considered a major factor in the triggering of explosions at Santiaguito, is the interaction of water with the magma system (Rose, 1987; Bennett et al., 1992). It has also been considered as a major factor in the occurrence of dome collapses (Ball et al., 2013). With the eruption crater acting to drain rainfall to the base of Santiaguito, Ball el at. (2013) claim that this water infiltrates into the system and drives activity. The presence of low temperature fumaroles has been noted to be affected by daily, as well as seasonal, rainfall (Stoiber and Rose, 1974), indicating that meteoric water can interact with the system.

Further to these three proposed mechanisms, Wallace et al. (2020) interpreted that the increased eruptive activity in 2016 deviated from the usual source mechanisms, with the injection of fresh magma causing a transition to a deep overpressure-driven fragmentation, which led to the excavation of the conduit. More recent work by Rohnacher et al. (2021) using a seismo-acoustic network showed a weak precursory seismic signal which occurred 2-6 s before an explosion, linked to the main eruption signal, and located at ~600m depth. They linked the precursory signal to the opening of tensile cracks which, through a bottom-up process, permeate upwards and open up pathways for rapid gas escape in the main explosion, which has been located at the shallower depth of ~200m.

1.4. Data and Methods

1.4.1. Data Collection

Seismic and acoustic instruments were deployed in networks at both Santiaguito and Fuego. These instruments required maintenance, and the data which were recorded by them needed to be collected, which both in turn required regular fieldwork campaigns. Both these networks were established before the research within this thesis began, however, during this research, to ensure the continued recording of the stations within the networks, and to elongate the records as far as possible, I visited Guatemala for month long trips in January 2018, 2019, and 2020. The Santiaguito network was deployed by the University of Liverpool in 2014, with its upkeep maintained as a collaboration between the University of Liverpool and the Karlsruhe Institute of Technology, along with the continued assistance of the Guatemalan Institute of Seismology, Volcanology, Meteorology and Hydrology or "Instituto Nacional de Sismologia, Vulcanologia, Meteorologia, e Hydrologia" in Spanish (referred to as INSIVUMEH). The Fuego network was principally deployed by INSIVUMEH, with the aid of several international collaborators, including the University of Liverpool, in response to the June 2018 eruption.

While in the field in Guatemala, I mostly worked at the Santiaguito network, working to maintain the network by re-installing stations that had previously gone offline, collected data from the data-loggers (DataCubes) which stored the data on-site, installed modems to allow for live transmission of data, removing the need for on-site data storage with the DataCubes, and updated the power to the stations, either with new batteries to provide power to the instruments, or by installing solar panels (Figure 1.7F). The set up for the stations was simple, with the sensor being powered by a battery (which in turn was re-charged by solar panels at some stations), the sensor was connected to a digitiser which would take the analogue signals from the sensor and make it digital, so that the digital signal could either be stored on site in a DataCube or transmitted via a modem to a central server.

At Santiaguito, different sites had different levels of accessibility, most sites were accessible by car, although 4x4 off-road vehicles were the often the only cars which were able to get to these sites due to their remote nature (e.g., Figure 1.7D). Other sites, which were more remote, required a full day hike in order to access them (e.g., Figure 1.7E), with all equipment needing carrying, making the possibilities at the sites limited, and improvements on the set up taking several visits. At the sites, it was necessary to ensure that the sensors were as well protected as possible, as well as ensuring that they would encounter minimal noise. For sensors at the permanent stations these were protected by the wind and rain, being inside concrete huts (e.g., Figure 1.7D) which had windows open to ensure the air pressure could still be accurately recorded, and seismic instruments were placed on concrete floors/blocks to ensure good coupling with the ground (e.g., Figure 1.7A). At the temporary and more remote stations, the infrastructure was not there, and so different methods to protect the sensors were made. One way for seismic stations to be deployed was by making a small concrete base, and placed inside a waterproof drum (e.g., Figure 1.7B) which were buried to keep safe, while acoustic microphones were placed in upturned boxes above the surface to protect them from the rain and elevated enough to ensure surface water did not damage them (e.g., Figure 1.7C). Initially, the network at Santiaguito was constructed with sensors recording and storing data on site in DataCubes. The regular trips were required to collect the data and wipe the systems before the storage hit capacity. During the campaigns, I replaced several DataCubes with modems which allowed for the sensors to be checked remotely to ensure they were still operational, limiting the number of trips needed, and allowing for instant analysis.

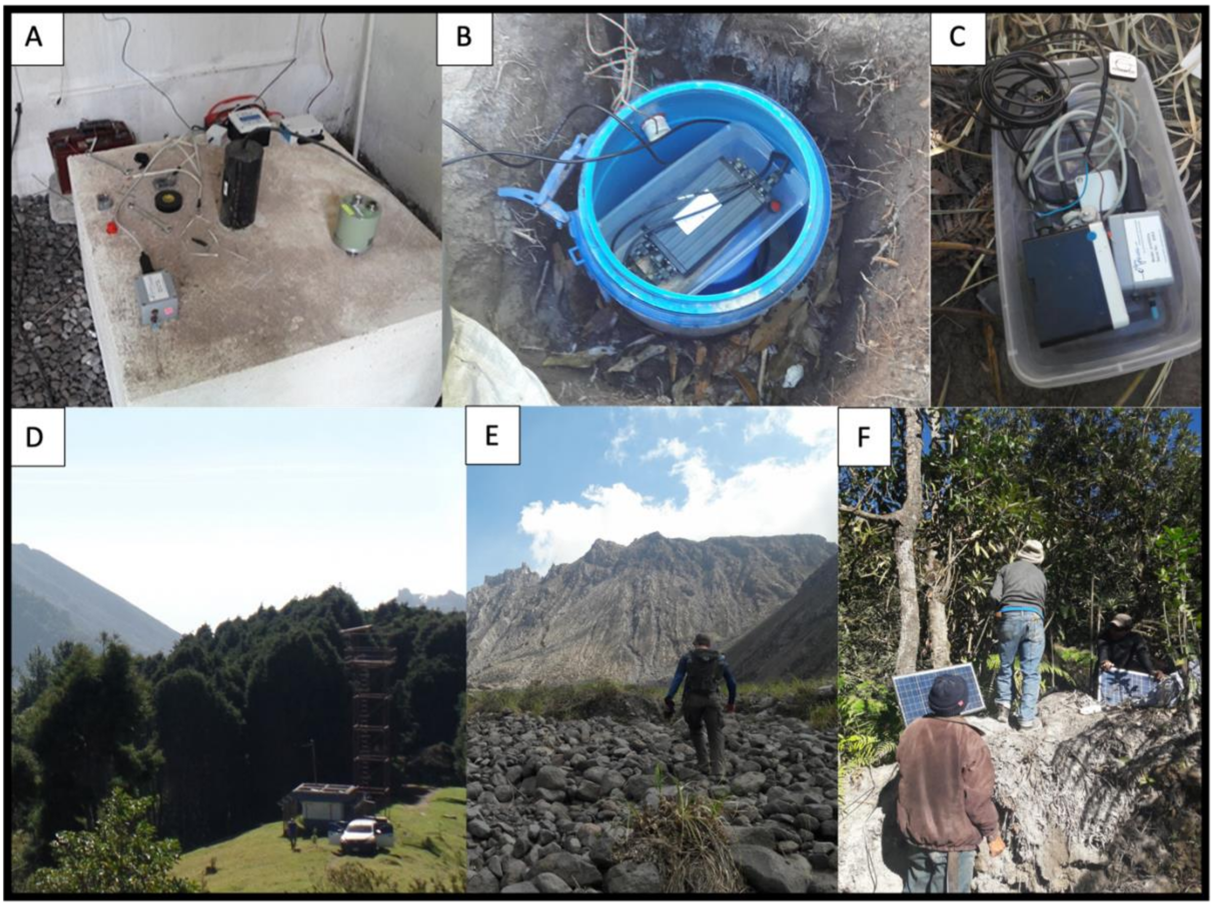

Figure 1.7. *Fieldwork in Guatemala. A) Seismic (green Nanometrics Trillium T120C broadband seismometer, right) and acoustic (grey iTem prs100 infrasound sensor, left), deployed in a permanent station at Santiaguito. B) Temporary seismic station at Santiaguito, buried in a barrel close to the active vent. C) Temporary acoustic station at Santiaguito, sensors deployed in an upturned box to keep them dry. D) Permanent station in the Santiaguito network (concrete hut) which is accessible by off-road car. E) Hiking at the Santiaguito lava dome complex in order to access remote, temporary stations. F) Installation of new solar panels at a station in the Santiaguito network.*

1.4.2. Automatic Detection and Classification Schemes

Real-world data from continuous geophysical datasets at open-vent volcanoes are complex. In volcanic environments the levels of noise are generally high and the magnitude of seismic events low, making event detection and classification a challenging task.

For small datasets, or for volcanoes with relatively low levels of activity, this can be done manually. However, for longer datasets, datasets with high rates of activity, for situations with time constraints such warning systems from 24/7 real-time analysis, manual detection and cataloguing of events may not the most appropriate method, while the use of automatic algorithms can be more suited for the rapid handling of large datasets. There are many different methods for automatic detection and classification of events. The methods used will depend upon several factors, such as the type and complexity of data being catalogued, the speed at which results are required, the accuracy in the results needed, the properties of the event signals which discriminate them from background noise, the size and representativeness of any training data set, and how many different event types need to be catalogued.

The methods used in automatic algorithms use either waveform attributes or frequency attributes to detect and/or classify events. Waveform attributes use the shape and amplitude of the waveforms, from methods such as amplitude thresholds, amplitude ratios, and template matching. A common amplitude ratio method is the short-term average to long-term average method (STA/LTA; Allen, 1982), which has been used in many detection schemes (e.g., Ibs-von Seht, 2008; Huang et al., 2012; Shinoharra et al., 2017). The STA/LTA method takes the average amplitude of a defined long window and compares it with a short window from within the larger window to produce a ratio. When the ratio exceeds a defined threshold, a detection is made, with the end of the detection being identified when the ratio drops down below a second threshold. Frequency attributes of the waveforms are also used (e.g., Power et al., 1994; Miller et al., 1998; Hammer et al., 2012; Hibert et al., 2017). These methods compare known attributes of waveforms that have been previously identified to the detected waveforms. This requires a test dataset to be used for preliminary parameterisation of the event types of interest so that parameters which are unique to each event type can be identified. These parameters can be as simple as the dominant frequency or bandwidth or can be more complicated with ratios of different frequency amplitudes to check the shape of the frequency spectra. Often, the raw data are pre-filtered as the waveforms from events only contain energy within specific energy bands, and so filtering is used to remove noise from the signal. Some studies also use cross correlations, or other template matching methods to identify event types of interest, which can be done in either the time or frequency domain (e.g. Cardaci et al., 1993; Stephens and Chouet, 2001; Green and Neuberg, 2006; Gibbons and

Ringdal, 2006; Umakoshi et al., 2008), which can be used either directly on the long-term data or as a second step after waveforms have been detected by methods such as the STA/LTA. Cross correlations are specific to an event type and can be made with either a reference waveform, stacked waveform or a synthetic waveform.

When building algorithms, trade-offs are often made between speed of an algorithm versus the number of steps and checks, as well as between the number of false positives and number of missed events. Typically, the more attributes used, both in the time and frequency domains, the higher the reliability of a positive detection is, although the higher chance of rejecting true events becomes, and the longer it takes to produce the catalogue. The trade-off between true event detection and false positives is a feature of all catalogues and is also dependent on the severity of thresholds chosen for the parameters used. Stricter thresholds will reduce the number of false positive detections, but omit several real events, whereas a more relaxed threshold will result in a catalogue which contains more of the events that have occurred but will be less clean with higher rates of false positives. The choices made with these trade-offs when building an algorithm depend on the requirements of the catalogue being produced.

More complex workflows, such as neural networks require large catalogues of events for training and development. These machine learning tools further remove manual assessments from the equation. One of the aims of creating catalogues through automatic algorithms in this thesis is to produce a large training set that can be used for the future deployment of neural networks which can assess live data streams and aid with the development of early warning systems and the forecasting of future activity.

1.4.3. Seismo-Acoustic Studies at Volcanoes

There are many different techniques that can be used to infer information about the volcanic activity, and its mechanisms. Different methods require different datasets ranging from a small number of high-quality, large amplitude events to many events which range across the spectrum of amplitudes possible to give a fair representation of the activity.

Several features of seismic and acoustic datasets which are often studied include the magnitude of events (e.g. Ripepe et al., 2001; Lamb et al., 2019), the signal attributes (e.g.

Chouet, 1988; Neuberg et al., 1998; Neuberg et al., 2006; Brill et al., 2018; Lamb et al., 2019; Diaz-Moreno et al., 2020), the repose time between events (e.g. Neuberg et al., 1998), the energy split between the ground and atmosphere (e.g. Johnson and Aster, 2005; Palacios et al., 2016), the change in the events through time (e.g. Johnson and Aster, 2005; Lyons et al., 2010; Waite et al., 2013; Naismith et al., 2019), time delay time between different signals (e.g. Sahetapy-Engel et al., 2008; Lamb et al., 2019), waveform inversion (e.g. Chouet et al., 2005; Lyons and Waite, 2011; Kim et al., 2014; Kim et al., 2015; De Angelis et al., 2019) and the relation between different signals and the surface expression (e.g. Neuberg et al., 1998, Nadeau et al., 2011), the moveout of the signal across the network (e.g. Johnson et al., 2011; De Angelis et al., 2012).

Studies on open-vent systems have been able to infer information regarding the location of events, (e.g. De Angelis et al., 2012), source location and depth (e.g. Sahetapy-Engel et al., 2008; Lyons and Waite, 2011; Jones and Johnson, 2011; Johnson et al., 2011; Brill et al., 2018), the source mechanisms triggering the events (e.g. Chouet, 1988; Neuberg et al., 1998; Ripepe et al., 2001; Chouet et al., 2005; Neuberg et al., 2006; Kim et al., 2014; Palacios et al., 2016; Naismith et al., 2019), define the baseline behaviour of the volcano (e.g. Lyons et al., 2010; Brill et al., 2018), estimate the propagation, volume and height of the plumes (e.g. Caplan-Auerbach et al., 2010; Lamb et al., 2015; Kim et al., 2015; De Angelis et al., 2019), understand the internal dynamics of the volcanic conduit (e.g. Johnson and Aster, 2005, Nadeau et al., 2011; Waite et al., 2013) and characterise the activity (e.g. Johnson et al., 2011; Brill et al., 2018 Lamb et al., 2019; Diaz-Moreno et al., 2020).

In this thesis, I will perform a statistical study of long-term catalogues to better understand the baseline behaviour of both Santiaguito and Fuego, investigate the paroxysms and the internal dynamics for both these large events and the smaller scale activity which occurs regularly from the vents. I will also analyse the long-term data to examine the longer-term processes that short-term geophysical studies are not sensitive to.

1.5. Status of Papers and Co-Author Contributions

Chapter 2

Manuscript Title:

Catalogued explosions at Volcán Santiaguito (Guatemala) from seismic network recordings between 2014 and 2018

Authors:

William Carter[a], Andreas Rietbrock[b], Yan Lavallée[a], Ellen Gottschämmer[b], Alejandro Díaz Moreno[c], Gustavo Chigna[d], Silvio De Angelis[a].

Affiliations:

[a]Department of Earth, Ocean and Ecological Sciences, University of Liverpool, Liverpool, UK

[b]Geophysical Institute, Karlsruhe Institute of Technology, Karlsruhe, Germany

[c]School of Geography, Politics and Sociology, Newcastle University, Newcastle upon Tyne, UK

[d]Instituto Nacional de Sismologia, Vulcanologia, Meteorologia, e Hydrologia (INSIVUMEH), Guatemala City, Guatemala

Journal:

Nature Data

Status:

Peer reviewed and accepted for publication, however, due to constraints on the public release of the datasets used, the publication is yet to go ahead. Once the data can be made public, the paper will be resubmitted.

Author Contributions:

William Carter: Conceptualization, Methodology, Investigation, Software, Formal analysis, Writing - original draft, Visualization.

Andreas Rietbrock: Supervision, Methodology, Investigation, Project administration, Writing - review & editing.

Yan Lavallée: Supervision, Writing - review & editing.

Ellen Gottschämmer: Investigation.

Alejandro Díaz Moreno: Supervision, Visualization.
Gustavo Chigna: Resources, Data curation, Investigation.
Silvio De Angelis: Supervision, Resources, Methodology, Investigation, Funding acquisition, Writing - review & editing.

Chapter 3

Manuscript Title:

Statistical evidence of transitioning open-vent activity towards a paroxysmal period at Volcán Santiaguito (Guatemala) during 2014–2018

Authors:

William Carter[a], Andreas Rietbrock[b], Yan Lavallée[a], Ellen Gottschämmer[b], Alejandro Díaz Moreno[a], Jackie E. Kendrick[a], Oliver D. Lamb[c], Paul A. Wallace[a], Gustavo Chigna[d], Silvio De Angelis[a]

Affiliations:

[a]Department of Earth, Ocean and Ecological Sciences, University of Liverpool, 4 Brownlow Street, Liverpool, L69 3GP, United Kingdom
[b]Geophysical Institute, Karlsruhe Institute of Technology, Karlsruhe, Germany
[c]Department of Geological Sciences, University of North Carolina at Chapel Hill, Chapel Hill, NC, United States
[d]Instituto Nacional de Sismologia, Vulcanologia, Meteorologia, e Hydrologia (INSIVUMEH), Guatemala City, Guatemala

Journal:

Journal of Volcanology and Geothermal Research

Status:

Published

DOI:

https://doi.org/10.1016/j.jvolgeores.2020.106891

Publication Date:

1st June 2020

Author Contributions:

William Carter: Conceptualization, Methodology, Investigation, Software, Formal analysis, Writing - original draft, Visualization.
Andreas Rietbrock: Supervision, Methodology, Investigation, Project administration, Writing - review & editing.
Yan Lavallée: Supervision, Writing - review & editing.
Ellen Gottschämmer: Investigation.
Alejandro Díaz Moreno: Supervision.
Jackie E. Kendrick: Writing – review & editing.
Oliver D. Lamb: Validation, Investigation.
Paul A. Wallace: Validation.
Gustavo Chigna: Resources, Data curation, Investigation.
Silvio De Angelis: Supervision, Resources, Methodology, Investigation, Funding acquisition, Writing - review & editing.

Chapter 4

Manuscript Title:

Characterisation of open-vent activity at Volcán de Fuego from seismo-acoustic network observations and energy partitioning.

Authors:

William Carter[a], Yan Lavallée[a], Andreas Rietbrock[b], Amilcar Roca[c], Silvio De Angelis[a]

Affiliations:

[a]Department of Earth, Ocean and Ecological Sciences, University of Liverpool, 4 Brownlow Street, Liverpool, L69 3GP, United Kingdom
[b]Geophysical Institute, Karlsruhe Institute of Technology, Karlsruhe, Germany
[c]Instituto Nacional de Sismologia, Vulcanologia, Meteorologia, e Hydrologia (INSIVUMEH), Guatemala City, Guatemala

Status:

In Preparation

Author Contributions:

William Carter: Conceptualization, Methodology, Investigation, Software, Formal analysis, Writing - original draft, Visualization.

Yan Lavallée: Supervision, Writing - review & editing.

Andreas Rietbrock: Supervision, Writing - review.

Amilcar Roca: Resources, Data curation, Investigation.

Silvio De Angelis: Supervision, Resources, Methodology, Project administration , Investigation, Funding acquisition, Writing - review & editing.

Chapter 2. Catalogued Explosions at The Santiaguito Lava Dome Complex

2.1. Summary

In this paper, entitled "Catalogued explosions at Volcán Santiaguito (Guatemala) from seismic network recordings between 2014 and 2018", we present the key methodology of designing, testing and applying an automatic algorithm to long term seismic data recorded at Santiaguito from the network that was deployed there between 2014 and 2018. The algorithm was designed to detect and catalogue explosions from the vent at Santiaguito, with the aim to have a high level of completeness, which is to say that as many true events as possible were detected above a low signal to noise ratio. The catalogue produced, totalling 18,896 explosions, is attached in the supplementary records to this thesis and gives the start time, seismic wave duration, seismically radiated energy and the energy magnitude of the explosions (Appendix A3.1).

The main steps in any algorithm used to build a catalogue are the detection phase, classification stage and then cleaning stage. In the paper we explain how each step was carried out for the case of Santiaguito, explaining the decisions which were made in order to produce the final catalogue. In the production of algorithms to sort through continuous data to classify specific event types, distinct features in the waveforms need to be identified to sort the true events of interest from other event types and background noise. This step is manually done in order to calibrate the thresholds used in the algorithm for each test done when a signal is detected. In producing a complete catalogue, the issue of false positive detections is introduced, so the post detection 'cleaning' of the catalogue has been discussed to show how to mitigate the issues which arise from aiming to have a complete catalogue. For both increasing the completeness of the catalogue and aiding in the cleaning steps, the use of a network of stations is shown to be highly useful, relying upon network coincidence to increase the reliability of the detections which are included in the catalogue.

We also carried out checks on the catalogue to show that the algorithm is robust, and to indicate any limitations to the methodology used to produce the catalogue. These checks show how remote data collection has its natural issues regarding the noise levels, and how the decisions made in the algorithm steps effectively deal with them to ensure that the final catalogue is clear of false detections.

In this paper we outline the production of the largest catalogue of events at Santiaguito spanning the longest continual recording undertaken at the volcano to date. The results of the catalogue will be useful in understanding the baseline activity, analysing the source mechanisms of explosions, and building towards a better understanding of current states of activity which ultimately could help with forecasting efforts.

Since the production of the catalogue of explosions at Santiaguito from the algorithm developed in this paper, a study at INSIVUMEH has been undertaken to deploy a neural network to assess real-time data for detections and build towards early warning systems. The catalogue I produced in this study is being used as a training dataset for the neural network to learn the key parameters that can be used to make these detections and assessments of the real-time data.

2.2. Abstract:

Long-term seismic catalogues (multiple years) of volcanic activity can enable the identification of both baseline and changing behaviour, allowing insights into source properties and forecasting, for example. Here, we construct a long-term catalogue of explosions at Santiaguito volcano (Guatemala) over the period November 2014 to December 2018 from a network of seismic stations deployed to monitor volcanic activity and hazards. At Santiaguito volcano, explosions are produced regularly by a repeating and restorative source with a high degree of self-similarity, which is reflected in the seismic record. We designed and applied an automatic detection and classification algorithm using frequency attributes and cross-correlations to extract explosion events from the monitored datasets. We provide the time, duration and magnitude of 18,896 explosions in a high-quality catalogue for the recorded period, as well as the waveforms for each event. This dataset of explosion waveforms is the largest at Santiaguito and is the first of its kind made public worldwide. The catalogue has the potential to aid future monitoring efforts at this hazardous volcano.

2.3. Background

The Santiaguito dome complex, Guatemala, began erupting in 1922 and has been continually active for almost 100 years (Harris et al., 2003). During this period, small-to-moderate explosions have been a common feature, with interval times between 30 minutes (Rose, 1987) and several hours (GVP, 2017a); although a period of heightened explosive activity in late 2015 - early 2016 saw the generation of very large explosions at irregular intervals of days to a few weeks (Lamb et al., 2019; Wallace et al., 2020; Carter et al., 2020). The Santiaguito complex consists of four lava domes: Caliente, La Mitad, El Monje, and El Brujo. Since 1975 activity has been centred at Caliente (Harris et al., 2003), with explosions occurring from the lava dome within the vent. Common seismic signals observed by the stations deployed at Santiaguito include explosions, rockfalls, tremor, lahars, regional earthquakes and, on rare occasions, volcano-tectonic swarm events (Lamb et al., 2019). There have been few seismological studies at Santiaguito investigating the explosive behaviour (Johnson et al., 2004; Sahetapy-Engel et al., 2008; Sanderson et al., 2010; Johnson et al., 2014; Scharff et al., 2014; Lavallée et al., 2015; Hornby et al., 2019; Lamb et al., 2019), many of which have recorded seismicity over short time periods on the order of days to a few weeks. The source of the explosion has been located to depths of between 100 m and 620 m by comparing the delay time between seismic and infrasound signal onsets (Sahetapy-Engel et al., 2008), and between 100 m and 600 m from analysis of rock samples in lava units (Scott et al., 2012). It has also been found that the long-period signals related to volcanic explosions at Santiaguito are self-similar and associated with depressurisation from within the source (Sanderson et al., 2010).

In open vent volcanic systems with continual unrest, long term datasets of emissions are key to understanding baseline activity and the forecasting of future activity change (Chiodini et al., 2010; Werner et al., 2014; Barrière et al., 2017; Papale, 2018). At Santiaguito, which has a large population nearby, the potential hazards associated with a paroxysmal event are large. Improved modelling of eruptive behaviour and increased monitoring and forecasting capabilities can help to mitigate these hazards. It is therefore critical that long term datasets are made available to aid in this pursuit.

Between November 2014 and December 2018, The University of Liverpool and The Karlsruhe Institute of Technology installed and maintained what, to date, remains the largest and longest operating network of seismometers to continuously record activity at Santiaguito. This dataset allowed identifying different eruptive phases at Santiaguito during 2014-2017, including a notable shift in the regime of eruption from mild effusion to major explosive activity between late 2015 and mid-2016 (Lamb et al., 2019; Wallace et al., 2020; Carter et al., 2020). In this paper we present the most complete catalogue of explosions to date for Santiaguito for the period 2014-2018. The catalogue is obtained from an automatic detection and classification algorithm that we implemented ad-hoc for Santiaguito. Over the four years of network deployment, we observed five different types of surface emissions from the active vent: small gas plumes, small-to-moderate gas-and-ash explosions, small gas plumes followed a few seconds later by ash emission, small explosions followed by prolonged gas emission, and large explosive eruptions. In this manuscript we catalogue all explosions into one class, while noting that different explosion types exist within the dataset. Further classification of identified events will form the basis of future studies.

Automatic detection and classification tools for seismic data at volcanoes are commonly used for datasets which would be impractical to manually assess, or to make real time detections (Stephens et al., 2001; Scarpetta et al., 2005; Langer et al., 2006; Green and Neuberg, 2006; Gibbons and Ringdal, 2006; Umakoshi et al., 2008; Hammer et al., 2013). The methods used to detect and classify events vary in approach depending on the needs of the user, computing power available, type of data under investigation, and accuracy level required. For investigations in volcanic settings where the seismic waveforms are repeatable, show a high degree of similarity, produced at a known location, and occur regularly enough to provide a large training set of events, detection and classification algorithms rely upon identification of characteristic frequency-domain attributes and cross correlations (Stephens et al., 2001; Green and Neuberg, 2006; Gibbons and Ringdal, 2006; Umakoshi et al., 2008). These algorithms can be relatively simple in design while capable of detecting and classifying events with a high degree of accuracy, attaining high detection performance while minimising false triggers, making them a valuable tool for cataloguing and extracting event waveforms from continuous datasets with minimal user time. In this manuscript we apply frequency-domain attribute matching and cross-correlation methods for the case of Santiaguito to produce a high-quality catalogue of explosions. The dataset of assembled waveforms is the first of its kind for a Guatemalan volcano, and the first publicly available long-term dataset of explosions worldwide.

2.4. Methods

2.4.1. Data Collection

The University of Liverpool and the Karlsruhe Institute of Technology maintained a network of seismic stations between November 2014 and December 2018 (Figure 2.1). The network included 12 station sites which ranged between 810m and 7700m from the active Caliente vent and were deployed at safe and accessible sites while optimizing azimuthal coverage. Site locations can be seen in Figure 2.1A. The seismic network comprised six Nanometrics Trillium T120C broadband (T=120s) seismometers and six Lennartz 3DLite short-period (T=1s) seismometers; data were recorded at all sites with a sampling frequency of 100Hz at a resolution of 24-bit. We undertook ten field campaigns over the four-year observation period to maintain the network and acquire complementary field observations and samples; these campaigns occurred in November 2014, April 2015, December 2015, January 2016, June 2016, February 2017, May 2017, January 2018, June 2018 and January 2019. Malfunctioning equipment and changes to location access caused gaps in data from individual stations within the network. With the exception of four data gaps when none of the stations were operating, the network provided a continuous record of seismic activity at Santiaguito throughout the four-year study (Figure 2.1B). In total, 315 of the 1499 days were missing data, with 246 of these in the large data gap between June 2017 and Jan 2018.

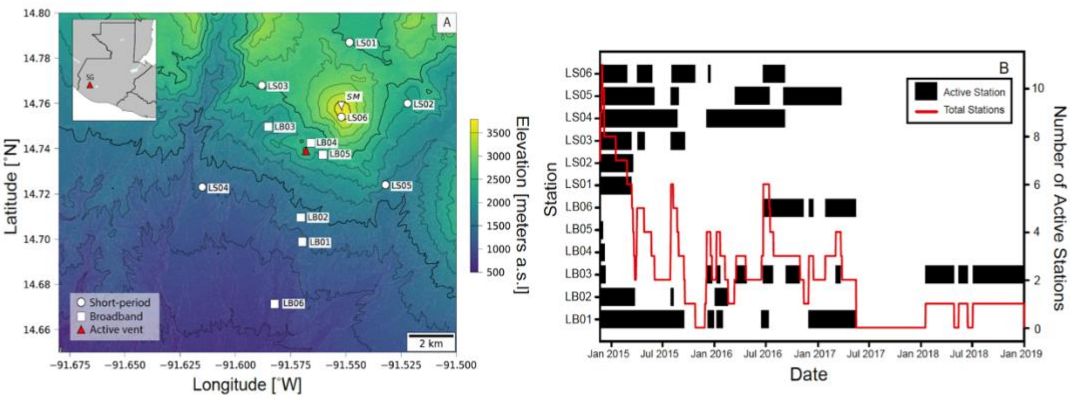

Figure 2.1. *Santiaguito seismic network. A) Station map of the Santiaguito Volcano network of seismic stations deployed between 2014 and 2018. Red triangle marks the active Caliente Vent; Santa Maria (SM) is marked with an inverted triangle; and thick and thin contour lines mark 500 and 100 m intervals in elevation from sea level, respectively. Inset: Map of Guatemala with the location of Santiaguito (SG, red triangle). B) Station activity through time. The activity for each station in the network is displayed with the horizontal broken bar chart. Red line shows the total number of active stations through time.*

2.4.2. Catalogue Production

We designed a detection and classification algorithm to extract and catalogue seismic signals associated with volcanic explosions, recorded by our network at Santiaguito. The main requirements of the algorithm were to be unsupervised and to maximise catalogue completeness, while reducing false triggers. Automation was essential to speed up reliable detection of tens of thousands of explosive events and to reject noise and other volcanic signals from the final catalogue. A complete, high-quality, catalogue, which is representative of the activity at the volcano over the recording period is the foundation for future work into understanding and forecasting the eruptive behaviour at Santiaguito and providing analogues for other similar volcanoes. As well as providing times of the explosions, the data presented here include their size in terms of seismic radiated energy (SRE) and energy magnitude (M_e).

Feature selection

A training set of manually selected waveforms was initially analysed to identify parameters to allow effective separation of explosion signals from noise and other seismic signals not directly linked to surface volcanic activity. Explosions and other common signals recorded by the Santiaguito network (e.g., rockfalls, regional earthquakes, tremor etc...) exhibit distinctive signatures and are easily separated based on waveform features measured in the frequency domain (Lamb et al., 2019). The training data set consisted of 50 explosions, recorded between the 22nd of November and the 1st of December 2014. The waveforms selected all had signal-to-noise ratios (SNR) above 5, where the noise level was taken as the maximum absolute amplitude during a section of data void of signals, and the signal level was taken as the peak amplitude of the explosion waveform. Analysis of the training data set relative to all other signals recorded by the network suggested that the frequency attributes that best identify and separate explosion from all other waveforms are: 1) the dominant frequency, defined as the frequency with the largest amplitude peak; 2) the central frequency, defined as the frequency where 50% of the area under the frequency spectra lies either side; and 3) the 50% bandwidth, defined as the width of the frequency spectra at 50% of the maximum amplitude. These frequency attributes are graphically represented in Figure 2.2. Typical values for these parameters that characterize explosions fall into the following ranges: between 0.2 Hz and 2.5 Hz for the dominant frequency, between 0.75 Hz and 2.75 Hz for the central frequency, and between 0.3 Hz and 2.5 Hz for the 50% bandwidth. To account for variations in the signals caused by site and path effects (Figure 2.2A), the critical parameter values used to separate explosions from all other signals were selected for each station individually. The frequency band of the waveforms was unaffected by explosion magnitude.

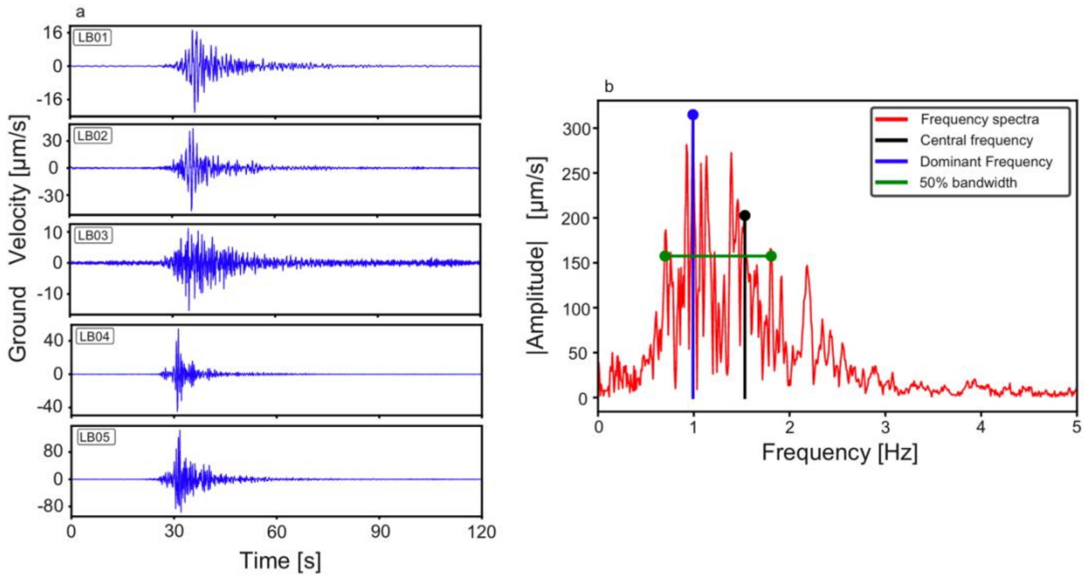

Figure 2.2. *Explosion seismic waveform attributes. A) Seismograms at stations LB01, LB02, LB03, LB04 and LB05 for a single explosion on the 4th of December 2014. Differences can be observed between the waveforms at each station, caused by the different source-receiver ray paths and site effects. B) Frequency attributes used in the automatic detection and classification algorithm. The dominant frequency is at the peak amplitude in the frequency spectra, the central frequency is at the point where 50 % of the energy occurs at frequencies above and below, and the 50 % bandwidth is the width of the frequency spectra at half of the peak amplitude. The differences observed in the time series are reflected by changes in the frequency spectra.*

As the explosions have a self-similarity (Sanderson et al., 2010), the waveforms all have features which fall within a constrained range. A typical explosion waveform lasts for between 15 to 35 seconds, with the peak amplitude commonly occurring within the first 5 seconds after the first arrival. After the peak amplitude is reached, the amplitude of the coda decays exponentially until it reaches background noise levels, waning at a slower rate than the initial waxing of amplitude. An example of a typical seismic waveform for an explosion is shown in Figure 2.3A. At the ends of the expected range of waveforms produced, events are seen to have more emergent or impulsive onsets than the mean waveform (Figure 2.3B and C, respectively). Furthermore, not all events are isolated from other volcanic events, with some large explosions causing pyroclastic density currents and/or tremor directly following the explosive event, which is attached to the explosion waveform (Figure 2.3D). Over the 4 years of recording, the explosions also showed a wide variety of amplitudes, due to the span of explosion magnitudes produced. Although a spectrum of waveform shapes is produced by the explosion source, there is a high coherency between events, and therefore a cross-correlation approach was employed for the classification process. Normalising the waveforms allowed comparisons across magnitudes. To ensure that the spread of waveforms was accounted for, a reference waveform was produced through stacking, using the training data set for candidate explosions to be compared with.

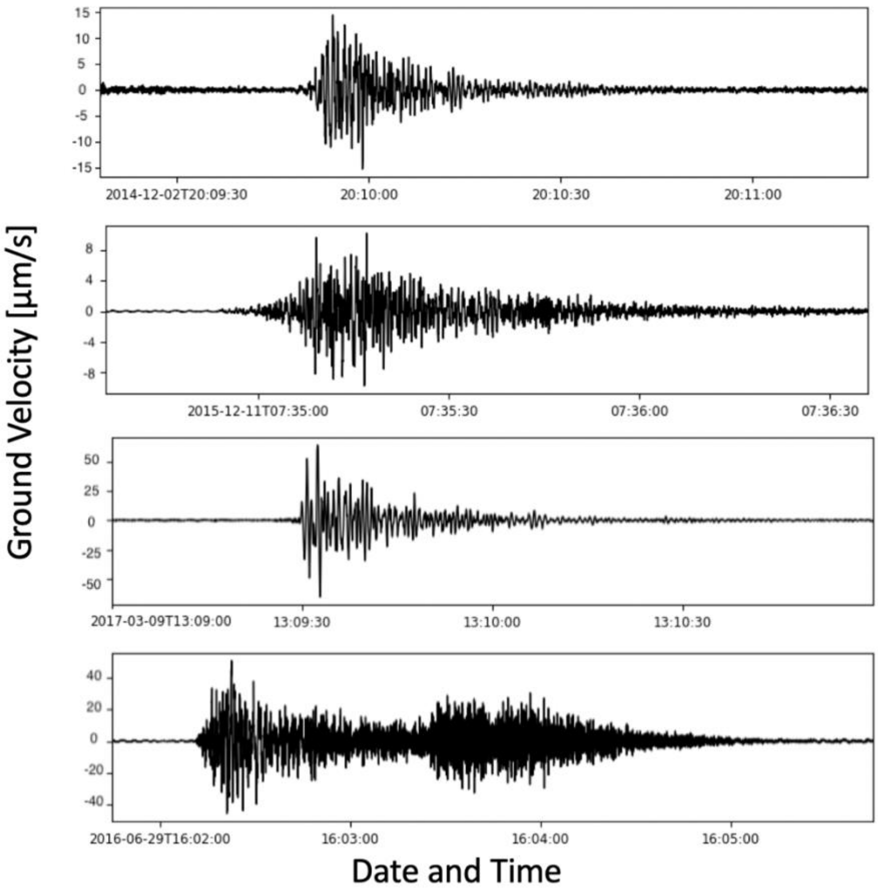

Figure 2.3. *Example explosion waveforms. All explosions were recorded at station LB03. A) Most common explosion waveform shape. B) Emergent waveform with longer coda. C) Explosion waveform with a more impulsive onset. D) Waveform of a large explosion that generated pyroclastic density currents for several minutes after the initial explosion.*

Algorithm steps

The automatic algorithm designed to detect explosion waveforms consisted of three main steps (Figure 2.4). 1) Extraction of waveforms with SNR above a given threshold from continuous data across the network; 2) Identification of candidate explosion waveforms based on frequency-domain parametrisation and cross-correlation with a template event; 3) Confirmation or rejection of candidate waveforms through network coincidence. Waveforms that passed all three steps successfully were catalogued as an explosion, those that did not were discarded.

An amplitude ratio approach was adopted for the detection of waveforms. The frequency band of the explosion waveforms was found to be between 0.5 and 3 Hz, therefore the data streams were initially filtered between 0.1 and 10 Hz to mitigate the effect of noise at both high and low frequencies. The streams were then segmented into consecutive 2-minute intervals to identify times with a waveform with an amplitude above the noise level. The noise level was selected from a section of the data stream void of any explosions or other earthquakes. As broadband seismometers are capable of detecting lower frequencies than the short-period seismometers, and therefore capture more of the typical frequency band of an explosion, the detection performance of these stations was higher than the short-period seismometers.

Analysis of high-SNR waveforms in the processing stage started with the comparison of frequency attributes with the critical bands determined from the training data. All waveforms that satisfied selection criteria based on the three frequency parameters had their envelopes cross-correlated with the envelope of a template explosion waveform. Cross-correlation was performed with the envelopes of the waveforms to suppress the maximum correlation coefficients from non-explosive signals and increase the coefficients from explosions. A critical correlation coefficient of 0.6 was set for a waveform to be tagged as a candidate explosion.

Explosions, with sufficient energy radiated in all directions, should be detected at multiple stations across the network, while local, non-volcanic sources of noise would be detected at a single station. Regional sources of noise (such as earthquakes) and many other volcanic events produce waveforms with conflicting frequency attributes and are thus removed in the processing of step 2. Candidate waveforms were therefore compared across the network to determine if they had been sufficiently detected to be classified as an explosion. The requirements for a sufficient detection were adapted to the changing network configuration throughout the recording period. As the broadband seismometers had a higher detection performance than short period seismometers, when multiple broadband stations were active, an explosion was required to be detected at a minimum of one broadband station and one other station (broadband or short-period); during times when only one broadband station was active an event had to be detected by that station, irrespective of the number of active short-period stations; when only multiple short-period stations were active, at least two detecting stations were needed to confirm the explosion; and at times when only a single short-period station was active, the algorithm would have no choice but to accept the candidate explosion to the catalogue.

To reflect the changes in confidence in each explosion's classification due to the changes in network configuration and subsequent classification criteria, a 'trust' value was assigned to each catalogued explosion. For events detected by two or more broadband seismometers, a trust value of 4 was assigned, irrespective of the number of short period seismometers also making the detection; if an event was detected by a single broadband seismometer, and one or more short period seismometers, a trust value of 3 was assigned; events which were only detected by a single broadband seismometer, or by multiple short period seismometers with no broadband seismometers, were assigned a trust value of 2; and a trust value of 1 was assigned to events which were detected by a single short period seismometer only.

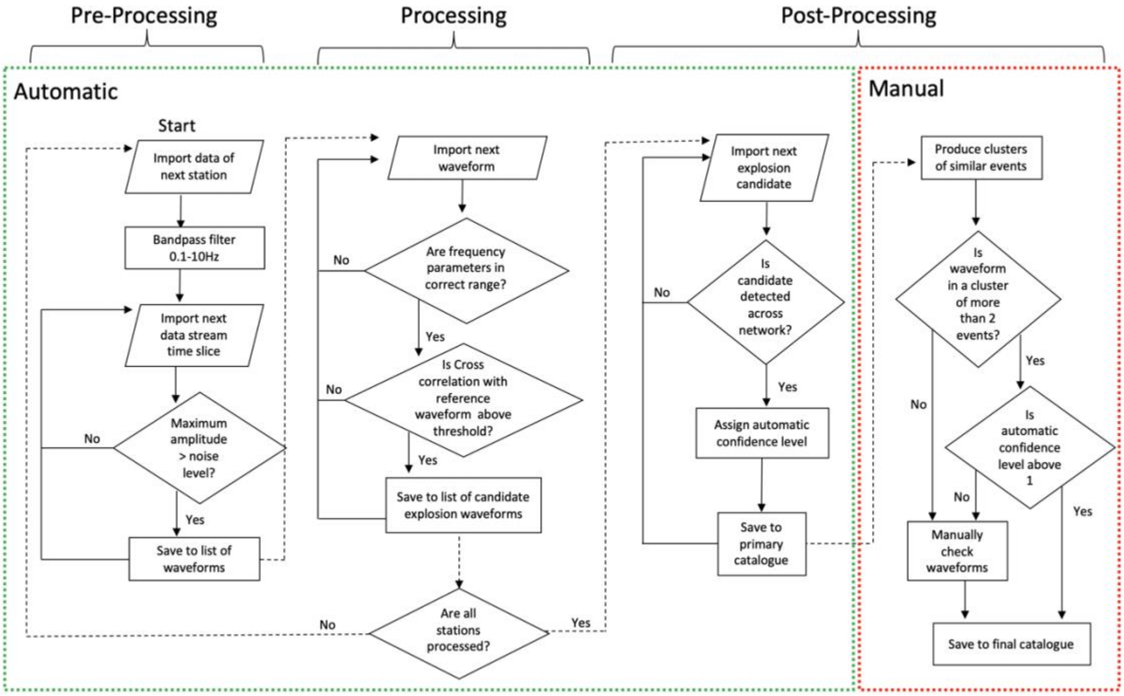

Figure 2.4: *Catalogue production flow chart. The automatic section of the flow chart (outlined in green) was undertaken by the detection and classification algorithm. Manual cleaning steps are outlined in red. Dashed arrows indicate the path taken when a loop has been exhausted or a phase has been completed.*

Benchmarking

The algorithm was initially benchmarked with a classified dataset of explosions recorded in the week between the 8th and 14th of December 2014. Manual checks were carried out on the detection performance and inclusion of false triggers to determine the quality of the algorithm results. Through a process of trial and improvement, the critical parameter values were updated to optimise the detection rate and reduce the number of false triggers included. Once optimised, the new parameter values were applied to the algorithm used on the full data set, which we then compared with previously unseen data in the validation step to check for bias and ensure performance is consistent across the long-term dataset.

Validation

The detection and classification algorithm produced an initial catalogue of 19,233 individual events. To validate the algorithm, we manually checked 4 weeks of data from across the recording period from January 2015, September 2015, February 2017 and September 2018 against the raw data to determine the detection success rate and number of false detections in the catalogue. Across these weeks, a manually labelled catalogue of 674 explosions was produced. We found that the automatic catalogue contained 90.5 % (610 out of 674) of manually detected events, with additional false triggers accounting for less than 2 % of detections. During these weeks, there were high levels of noise, and so we believe that the detection performance of the algorithm is well represented by the rates determined by the manually checked weeks.

Catalogue Cleaning

To further reduce the number of false detections (~2%) that are not associated with volcanic explosions, we applied a two-step procedure (manual post-processing steps in Figure 2.4). First, we grouped events into clusters based on waveform correlation (clustering was performed with routines available in the GISMO toolbox (Celso et al., 2018). Events would be added to the cluster which it best correlated with, provided the cross-correlation coefficient was above a minimum threshold, while events that did not correlate with a pre-existing cluster would form a new cluster for subsequent waveforms to be compared against. As expected, we found that the explosions produced clusters with large numbers of events, while noise would not cluster; all clusters with less than three events were manually inspected to determine if the events were false detections. All false triggers were removed from the catalogue. We also found that many explosion waveforms, which were corrupted by noise (mostly of instrumental origin and/or other event types) did not cluster with other events; these were kept in the catalogue. The second step to remove false triggers was a manual inspection of waveforms that were assigned an automatic trust level of 1 during post-processing. These events were only detected by a single short-period station, and so had no possible network coincidence. The two-step cleaning process led to the removal of 337 false events from the catalogue. After catalogue cleaning, the final catalogue contained 18,896 individual explosions.

2.5. Explosion Energy Magnitude

We also provide an estimate of the size of each explosion in the catalogue in terms of their seismically radiated energy (SRE) and M_e. The SRE of an explosion (E_s) is calculated as the elastic energy generated from an isotropic source at the surface of a homogeneous half space (Boatwright, 1980; Johnson and Aster, 2005):

$$E_s = 2\pi r^2 \rho_{earth} c_{earth} \frac{S^2}{A} \int U(t)^2 dt \qquad (2.1)$$

where ρ_{earth} is the density of the surrounding subsurface, C_{earth} is the wave velocity in the surrounding subsurface, *r* is the radial distance from source to receiver, *U* is the particle velocity at the receiver, *S* is the site response and *A* is the attenuation, which was set to unity (Johnson and Aster, 2005). Different source to receiver paths and site amplifications cause the calculated SRE to vary from station to station. To account for these variations, and to provide a consistent SRE calculation from the network irrespective of active stations, we estimated relative site correction factors for each station. We initially calculated the SRE at each station without site corrections or amplification factors; then, using station LB03 as the reference station, we calculated correction factors as the ratio between the SRE calculated at each station and LB03. The ratios vary between events and are normally distributed about a mean ratio, with variances of less than 10% the value of the mean. The mean site corrections were found for each station by averaging, with re-deployments being taken into account.

SRE can be translated into M_e (Choy and Boatwright, 1995) using the equation:

$$M_e = (2/3)\log_{10}(E_s) - 2.9 \qquad (2.2)$$

If we assume that the explosions at Santiaguito follow a distribution akin to the Gutenberg-Richter distribution, then we can expect the catalogue to be incomplete below a magnitude threshold due to low SNR. We find through cumulative magnitude distributions that the magnitude of completeness in this catalogue is at $M_e = 0.76$.

2.6. Explosion Duration

The duration of the explosion events was calculated using the cumulative energy of the seismic waveform, using 2-minute-long seismic traces containing the full event waveform. Explosions at Santiaguito commonly have relatively impulsive onsets, therefore the start of the events was picked at 2.5 % of the total energy of the seismic trace. Many explosions had coda which slowly returned to amplitudes comparable to the background noise. It was decided that for the explosions, the end of the explosion occurred at 90 % of the cumulative energy, once the signal had returned to background levels. These calculations found that explosion waveforms have a mean duration of 19.5s. In the few cases where the explosion signals have interference from other sources such as rockfalls, tremor or regional earthquakes, the onset and end of events may not necessarily be representative of the explosion duration, which may affect the accuracy of the calculated duration estimates. The durations calculated here are the signal duration, and not the duration of the source.

2.7. Technical Validation

Dependence on Station Activity

A robust algorithm should minimise the effects of data scarcity in times when network coverage is lowest, maintaining a high level of catalogue quality. By comparing the changes in network coverage and the rate of detections, we find that the detection rate of the catalogue has minimal dependence upon the activity of stations within the network. Although between the start of the recording in November 2014 and July 2015 we observe that the number of detections decreases along with the number of active stations, visual observations confirm that this correlation is incidental, owing to the actual decreased number of explosions occurring at the same time as stations ending their recording (GVP, 2016a; GVP, 2017a). After July 2015 changes in the station activity were not reflected in the number of explosion detections.

Diurnal Variations in Detection

Variable levels of background noise can be a significant issue for automatic detection and classification algorithms. Background noise from sources such as wind, animals or human activity can make detections of true events harder by reducing the signal to noise ratio, especially for weaker events. Due to human and animal activity, the level of background noise is typically higher during the daytime at stations close to roads, residential areas and farmland. Therefore, selection of station deployment location is important to obtain clean data with reduced noise. In practice, this must be managed alongside other factors such as site access and safety of field personnel and equipment. Observations of the recordings at individual stations over the course of multiple days shows the variety of diurnal changes within the network (Figure 2.5). Daytime hours are considered to be between 6am and 8pm local time (1200 to 0200^{+1} UTC) with the night-time from 8pm to 6am local time (0200 to 1200 UTC). The difference between night-time and day-time detection rates vary depending on the active stations within the network. We find periods when the night- and day-time detection rates are the same, and others when there are 19 % fewer detections made per hour in the daytime compared to the night-time. Many missed events are likely to be caused by the increased noise level being greater than the amplitudes of some of the smaller explosions, which has led to the magnitude of completeness at 0.76 M_e. We note, qualitatively, that if stations were deployed in more remote areas and closer to the active vent, it is likely that additional signals would have been detected and the magnitude of completeness would be lower.

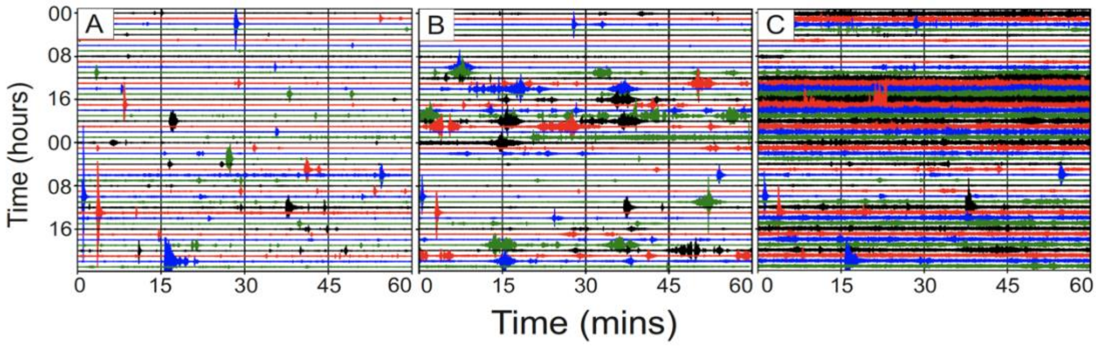

Figure 2.5. *Diurnal variations in noise level across the Santiaguito network. 48-hour seismic traces at: A) LB03: No visible diurnal variations, B) LB06: Extra waveforms caused by increased daytime noise, C) LS01: Background noise level significantly higher during the daytime than the night-time. All traces start at 2016-06-25T00:00:00 UTC.*

2.8. Data Records

We have made the catalogue and associated waveforms available for public use (University of Liverpool and Karlsruhe Institute of Technology, 2020) . Also available are instrument response files, calibration information and example python codes to read and plot the waveforms. The waveforms provided are unfiltered, calibrated to ground velocity (in m/s), and have not had the instrument response deconvolved. The codes provided to read and plot waveforms was written in python version 3.7.4 and uses obspy version 1.1.0. The catalogue is provided as a .csv file and waveforms as miniseed files. Waveforms for each event across the network are provided in a single multi-channel file. Response files are given as .txt files. The catalogue of explosions has also been added to appendix A3.1.

The continuous dataset, from which the catalogued explosions are a subset of, is also available for public use (University of Liverpool and Karlsruhe Institute of Technology, 2019).

Chapter 3. Statistical Evidence of Transitioning Open-Vent Activity at Santiaguito

3.1. Summary

This paper, entitled "Statistical evidence of transitioning open-vent activity towards a paroxysmal period at Volcán Santiaguito (Guatemala) during 2014–2018", describes the analytical techniques carried out on the catalogue that was produced in chapter 2, showing for the case of Santiaguito how these long recording datasets at volcanoes can be used to infer information about the state of the volcano and understand both the baseline behaviours and phases of increased activity.

Through the statistical assessment of inter-explosion repose times, cumulative energy release, and magnitude-frequency analysis, we showed how the activity at the volcano had evolved through time and how the activity at Santiaguito can be separated temporally into different phases. We show how the inspection of these phases, and the understanding of the signals is important for the assessment of future hazards through the assessment of key parameters such as the seismic *b*-value and make inferences on the controlling mechanisms triggering the explosions with assessment of the rate parameter. We further used these parameters to discuss the stability of the source of the explosions, as well as assessing the potential largest magnitude events during each phase.

These parameters require complete catalogues of events to obtain as well as long-term recording to ascertain a representative value for the state of the volcano. This highlighted the importance of having the catalogue of explosions to allow these techniques to be undertaken in order to get the results that we did.

As a side observation to the main results in this paper, we showed how the catalogue identified the presence of secondary explosions. This event type has never been studied in any previous work at Santiaguito. We showed how the event type is a common occurrence at the vent and discussed its implications for understanding how the explosion cycle works in regard to the post explosion healing of the system to restore the upper conduit to the same state as it was before the explosion occurred, producing a non-destructive cycle.

This paper shows how when one has a long-term, complete and clean catalogue of volcanic events, simple calculations can be made, and techniques can be applied to extract information which can deepen the knowledge of the open-vent volcano. With the results made here at Santiaguito, this paper demonstrates the possibility that similar algorithms and catalogues can be used at other volcanoes to study long-term trends in the background activity and periods of heightened activity to develop the understanding of how the systems work and assess the current and future hazards they pose.

3.2. Abstract

Long-term eruptive activity at the Santiaguito lava dome complex, Guatemala, is characterized by the regular occurrence of small-to-moderate size explosions from the active Caliente dome. Between November 2014 and December 2018, we deployed a seismo-acoustic network at the volcano, which recorded several changes in the style of eruption, including a period of elevated explosive activity in 2016. Here, we use a new catalogue of explosions to characterise changes in the eruptive regime during the study period. We identify four different phases of activity based on changes in the frequency and magnitude of explosions. At the two ends of the spectrum of repose times we find pairs of explosions with near-identical seismic and acoustic waveforms, recorded within 1-10 minutes of one another, and larger explosions with recurrence times on the order of days to weeks. The magnitude-frequency relationship for explosions at Santiaguito is well described by a power-law; we show that changes in *b*-value between eruptive regimes reflect temporal and spatial changes in rupture mechanisms, likely controlled by variable magma properties. We also demonstrate that the distribution of inter-explosion repose times between and within phases is well represented by a Poissonian process. The Poissonian distribution describing repose times changes between and within phases as the source dynamics evolve. We find that changes in source properties restrict the extrapolation of explosive behaviour to within a given eruptive phase, limiting the potential for long-term assessments of anticipated eruptive behaviour at Santiaguito.

3.3. Background

The Santiaguito lava dome complex, situated in the Western Highlands of Guatemala, has been continually active since 1922 (Harris et al., 2003). The complex consists of four domes, Caliente, La Mitad, El Monje and El Brujo, which formed along an East-West trending fracture at the southern foot of the collapse amphitheatre formed by the 1902 plinian eruption of Santa Maria Volcano (Rose, 1972). Since 1975 activity at Santiaguito has been centred at Caliente, mostly characterised by effusion of blocky lava flows and small-to-moderate gas-rich explosions (Harris et al., 2003). The Instituto Nacional de Sismologia, Vulcanologia, Meteorologia e Hidrologia (INSIVUMEH), responsible for monitoring the activity at Santiaguito, issues regular activity reports including information on the rates of occurrence of explosions and the height of the associated plumes. During 'normal' eruptive behaviour, as revealed by decades of monitoring, explosion plumes have been observed to reach heights between 0.5-1 km above the active vent (e.g., GVP, 1880; 1885; 1990; 1996; 2003; 2007; Bluth and Rose, 2004; Sahetapey-Engel et al., 2008; Johnson et al., 2014; GVP, 2015; Figure 3.1). The volume fractions of ash during the brief (seconds-long) initial momentum-driven phase of plume ejection at Santiaguito has been calculated at $\phi = 2.3$–$4.5\cdot10^{-5}$ (when ϱ_{ash}=2650 kg/m^3), with the remaining fraction of the plume, gas (De Angelis et al., 2016). In contrast, during the period of heightened activity in 2016, the majority of plumes rose approximately 1.5 km above the active vent, whilst some exceptional explosions generated plumes reaching up to 7 km (e.g., GVP, 2016a; 2016b; Figure 3.1A). 'Normal' gas-and-ash explosions have been documented to occur at intervals with repose times varying from periods as low as ~30 minutes (e.g., Rose, 1987; Scharff et al., 2014; Lavallée et al., 2015) to several hours (e.g., GVP, 2017a), with the period of heightened activity displayed more erratic recurrence patterns (e.g., Lamb et al., 2019; Wallace et al., 2020). We analyse this characteristic across the eruptive phase transitions herein.

Due to its protracted eruption, which has lasted for nearly 100 years, and the unique vantage point offered by the summit of Santa Maria overlooking the active caliente vent, the explosions at Santiaguito have been the focus of many multi-disciplinary investigations. Previous studies have included the use of optical imagery, thermographic cameras (e.g. Sahetapy-Engel et al., 2004; Johnson et al., 2004; Sahetapy-Engel, Harris and Marchetti, 2008; De Angelis et al., 2016; Lamb et al., 2019), tiltmeter (e.g. Johnson et al., 2004; Johnson et al., 2014; Lavallée et al., 2015), infrasound (e.g. Sahetapy-Engel, Harris and Marchetti, 2008; Jones and Johnson, 2011; Scharff et al., 2014; De Angelis et al., 2016; Lamb et al., 2019), seismic (e.g. Johnson et al., 2004; Sahetapy-Engel, Harris and Marchetti, 2008; Sanderson et al,. 2010; Johnson et al., 2014; Scharff et al., 2014; Lavallée et al., 2015; Lamb et al., 2019; Hornby et al., 2019), doppler radar (Scharff et al., 2014) and UV imaging (e.g., Holland et al., 2011; Esse et al., 2018). Bluth and Rose (2004) proposed that the primary mechanism of the small-to-moderate gas-and-ash explosions at Caliente is shear-induced fragmentation of dacitic magma near the margins of the conduit. This shearing is induced by the increased flow velocity brought on by closed system degassing as the ascending magma undergoes decompression, causing the magma viscosity to increase and prompting brittle deformation at the high strain rate experienced in the shallow conduit (Holland et al., 2011). The shearing events are thought to generate many small, connected cracks (Rhodes et al. 2018), which are held open during release of the gas-and-ash mixture (cf. Kendrick et al., 2016). After the explosion the fracture pathways shut and begin to heal, resetting the system, leading to the cyclic nature of the explosive activity observed at Santiaguito (Holland et al, 2011). This mechanism is supported by the observations that 1) volcanic ash and gas are released along active fractures which can be seen on the dome surface at the onset of the explosions, 2) volcanic ash associated with these small explosions shows textural disequilibrium resulting from rapid frictional heating (i.e., unhomogenised melt schlieren containing fresh vesicles) associated with faulting events, and 3) more pronounced tilt signals and very-long-period (VLP) seismicity occur as a result of increased shear traction when ash is generated (Lavallée et al., 2015). The explosion source has been constrained to depths between 100 and 620 m below the vent through the comparison of acoustic and seismic signal onsets (Sahetapy-Engel et al. 2008), between depths of 100 and 600 m though the analysis of rock samples taken from the lava flow units (Scott et al., 2012), and at about 300 m depth below the vent via Mogi source modelling of VLP signals (Johnson et al., 2014). Yet, these models proposed for the small-to-moderate gas-and-ash explosions do not apply to the large explosions during the period of heightened activity of 2016, which were sufficiently powerful to excavate the lava dome (Lamb et al., 2019).

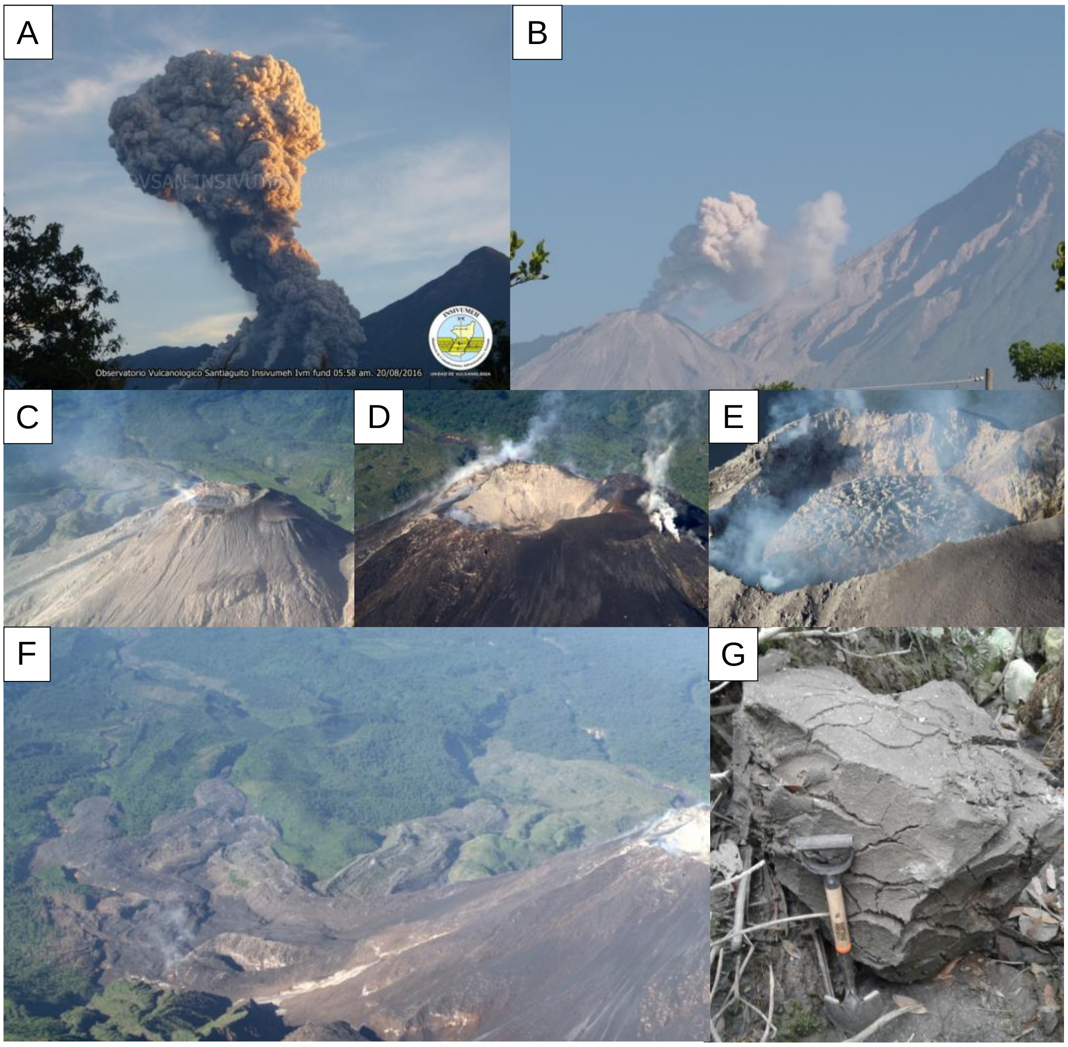

Figure 3.1. *Activity at Santiaguito over the four-year recording period. A) Explosion in August 2016, characteristic of the large explosions during this time. B) Explosion in January 2018, characteristic of the small-to-moderate explosions in the effusive regime. C) Lava dome in the vent of Caliente in November 2014. D) Excavated vent of Caliente in June 2016. E) New lava dome growing in the vent of Caliente in December 2016. F) Lava flows on the southeast flank of the Caliente dome. G) Large bomb ejected from Caliente during a large explosion in 2016, located 1.5 km from the vent. Image A was provided by INSIVUMEH. Images C, D and E are adapted from Lamb et al. (2019). Image G is provided courtesy of A. Pineda.*

Protracted volcano monitoring provides us with datasets, which may be scrutinised to understand eruptive behaviour with the aim to find ways to predict recurrence in activity (e.g., Papale, 2018). The monitored datasets of open-vent volcanic systems are different to those of volcanoes ending a period of quiescence, where unrest can indicate an impending eruption. For open-vent systems such as Santiaguito, where activity has persisted for nearly 100 years, changes in the eruption style may be signalled in a more subtle way (Sparks, 2003). Therefore, understanding the day-to-day 'baseline' behaviour and associated trends and statistical attributes of geophysical signals during different phases of eruption is crucial in efforts to provide accurate forecasting of paroxysmal activity, which pose great hazards to the surrounding areas. In systems that produce many self-similar events which display a range of magnitudes, magnitude-frequency analysis can be used to determine the relationship between small and large events via the so-called seismic *b*-value. Magnitude-frequency analysis, most commonly used in seismic studies (e.g. Schorlemmer et al., 2005; Chen et al., 2006; Tsukakoshi and Shimazaki, 2008; Farrell et al., 2009; El-Isa and Eaton, 2014; Huang and Beroza, 2015), often refers to the Gutenberg-Richter (GR) relationship (Gutenberg and Richter, 1944) and Ishimoto–Iida's formula (Ishimoto and Iida, 1939), but has also been applied to explosive volcanic eruptions (e.g. Deligne et al., 2010; Nishimura et al., 2016; Sheldrake and Caricchi, 2017; Rougier et al., 2018). These studies have characterised the magnitude-frequency relationships for global volcanism as well as for individual volcanoes and have shown how these distributions carry information on the explosion sources and eruption style. Repose time analysis has also become an important tool at open-vent systems (e.g. Connor et al., 2003; Watt et al., 2007; Lamb et al., 2014; Varley et al., 2018) in establishing relationships between source processes. Changes in the repose time between explosions have been used as an indicator of changes within volcanic systems, and differences in repose times between events has been used to show differences in the physics controlling eruptive processes (Varley et al., 2018).

Between November 2014 and December 2018, the University of Liverpool (UK) and the Karlsruhe Institute of Technology (Germany) deployed a permanent seismo-acoustic network around Santiaguito to continuously record the activity of the volcano. During this period multiple phases of activity were observed including effusive behaviour interspersed with small-to-moderate explosions, characteristic of the normal baseline behaviour as defined by Harris et al. (2003), and a period of heightened activity defined by large gas rich explosions during 2016 (Lamb et al., 2019; Wallace et al., 2020). In the initial 12 months following our installation at Santiaguito, activity consisted primarily of the extrusion of blocky lava flow from the summit of Caliente along with regular explosions emitting weak gas-and-ash plumes between 0.5 and 1.5 kilometres above the vent (GVP, 2016b; Lamb et al., 2019; Wallace et al., 2020). During late 2015 and 2016 however, the activity was observed to shift in style and magnitude, as we noted a gradual decline in the number of explosions from its peak occurrence rate in early 2015, with explosions producing larger plumes (Lamb et al., 2019; Wallace et al., 2020). The explosions occurred with greater repose times, with large explosions occurring at a rate of less than once per day, and weak to moderate explosions occurring up to 4 times per day (GVP, 2017a). The large explosions generated larger proportions of pyroclasts as plumes rose up to 7 km above the vent (Figure 3.1A). The largest explosions, which occurred in April-June 2016, excavated a large crater in the caliente dome structure (Figure 3.1D; GVP, 2016a). During this period of heightened explosive activity, there was no extrusion of lava flows (GVP, 2016a). The explosions instead triggered pyroclastic density currents from column collapse and ejected large bombs up to 3 m in diameter to distances of 3 km (Figure 3.1G; GVP, 2016a). During October 2016 the explosive regime came to an abrupt end, and the effusive regime resumed, accompanied with frequent smaller explosions at a rate of 25-35 per day (GVP, 2017a), similar to pre-2014 activity (Rose, 1987; Johnson et al., 2014). A lava dome emerged in the vent of Caliente in October 2016 (Figure 3.1E; GVP, 2017a). During 2017 new lava continued to fill the excavated crater inside Caliente, leading to over-spill that caused block-and-ash flows (GVP, 2017b). Similarly to 2014/15, gas-and-ash plumes rose to heights of up to 800 m above the active vent, at a rate between 9 and 36 times per day (GVP, 2017b). By the end of 2017 the lava dome had appeared to be fully re-established its original (pre-2016) shape and INSIVUMEH reported that there was little change in activity between November 2017 and April 2018 with plumes rising approximately 500 m above the vent of Caliente (GVP, 2018c). During this time, between 15 to 21 explosions were commonly recorded per day. This level of activity decreased slightly until the end of the year, with explosions occurring between 11 and 15 times per day, producing plume heights of 500-800 m above the vent (GVP, 2018d).

Early work conducted on the data collected by the seismo-acoustic network can be found in De Angelis et al. (2016), Lamb et al. (2019), Hornby et al. (2019), and Wallace et al. (2020). Lamb et al. (2019) analysed the seismic activity complemented by visual and thermal infrared observations to produce an early catalogue of 6,101 explosions between 2014 and 2017. They presented a description of the types of volcanic processes and associated signals and characterised the cumulative seismic energy which highlighted the increase in explosivity associated with the period of heightened activity recorded in 2016. A more recent study by Wallace et al. (2020) went further by constraining seismic energy, variable time delays between seismic and acoustic arrivals, thermal evolution and petrological changes associated with the increased explosivity. Characterisation of ash samples and ballistic bombs collected between 2014 and 2017 showed that changes in the chemical composition, mineralogy and groundmass texture throughout different eruptive phases occurred due to the fresh injection of a deep-sourced, volatile-rich magma into the shallow magmatic mush leftover from protracted activity in the last decades, causing mingling and intensification of the explosive activity in 2016 (Wallace et al., 2020).

We have aimed to refine the identification of explosive events which led to the generation of a catalogue of explosions with improved completeness with respect to that used in Lamb et al. (2019). Algorithms used in the catalogue production constrained the occurrence of 18,895 explosions for the period between November 2014 and December 2018 (see section 3.4.3). This dataset provides new insights into the volcanic and magmatic processes leading to shifts in eruptive style at Santiaguito. In this study we assess the seismic energy associated with individual explosions -a proxy for magnitude- and their variable occurrence rates; we exploit these measurements to investigate the magnitude-frequency relationship of explosions across different phases of eruptive behaviour with the aim of constraining four years of activity at Santiaguito.

3.4. Dataset and Analyses

3.4.1. Data Acquisition

Between November 2014 and December 2018, we deployed and maintained a network of seismic and infrasound stations at the Santiaguito lava dome complex. The seismic network consisted of six Nanometrics Trillium T120 compact broadband seismometers (T = 120s) and six Lennartz 3DLite short-period seismometers (T = 1s). All instruments recorded with a sampling frequency of 100 Hz at a resolution of 24-bit. The twelve stations in the network (Figure 3.2), were located between 810 and 7700 m from the active Caliente vent and were deployed to achieve the best possible azimuthal coverage. Seven iTem prs100 infrasound sensors were also deployed, co-located with all broadband seismometers, as well as with the short-period seismometer at station LS01. Over the four years between 2014 and 2018 we conducted ten field campaigns in November 2014, April 2015, December 2015, January 2016, June 2016, February 2017, May 2017, January 2018, June 2018 and January 2019. Due to variable access to specific locations, and equipment malfunctioning, the stations in the network did not always operate simultaneously;

however, with the exception of four data gaps, the network provided a quasi-continuous record of the activity over the four-year period (Figure 3.2B).

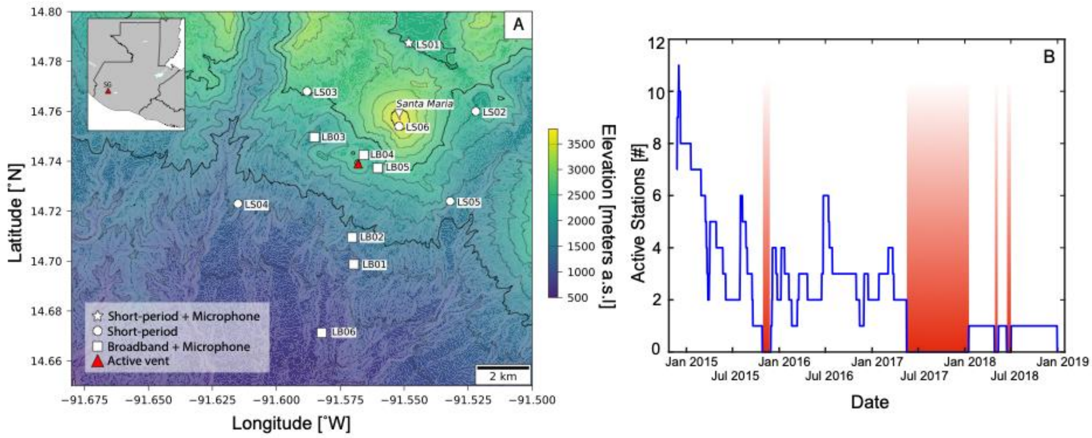

Figure 3.2. *Santiaguito seismo-acoustic network. A) Station map of the Santiaguito Volcano network of seismic and infrasound stations deployed between 2014 and 2018 with station names given. Red triangle marks the location of the active Caliente Vent, while Santa Maria is marked with an inverted triangle. Thick and thin contour lines mark 500 and 100 m intervals in elevation from sea level, respectively. Inset: Map of Guatemala with the location of Santiaguito (SG, red triangle). B) Network activity through time. The number of active stations in the network is displayed with the blue line, and the red bars indicate times where there were no stations active, causing data blackouts.*

3.4.2. Visual Observations

Throughout the network deployment visual observations were routinely conducted by INSIVUMEH staff based at the local Santiaguito Volcano Observatory (OVSAN). These are documented in the Smithsonian Institution Global Volcanism Programme's weekly reports and monthly bulletins (published at: http://volcano.si.edu/volcano.cfm?vn=342030; last accessed 23/12/2019). Visual observations are frequently hindered by cloud coverage, and at night-time the local observatory is not manned. Furthermore, it is sometimes difficult to visually distinguish between passive degassing and small explosions. The observations made by INSIVUMEH were complemented by regular visits of the volcano of the Liverpool and KIT teams during the past 5 years. Despite the irregular nature of visual observations, they provide important information to link geophysical data to the ongoing volcanic activity. Visual observations were made throughout the recording period, making note of explosion frequency, plume heights, plume descriptions, lava dome appearance, and the presence of active lava flows.

Direct links can be made between the visually observed explosions, and the seismic data (Figure 3.3), which demonstrate how it is possible for an understanding of the surface expression of the explosions from the seismic, given an initial observation to initially make these connections. Once several observations have been made, and linked to their corresponding signals, further observations of the same type of signal will have a strong confidence that the events have also produced the same surface expression from the same type of event. This allows for the catalogues to have high certainty that the classifications given to events are accurate.

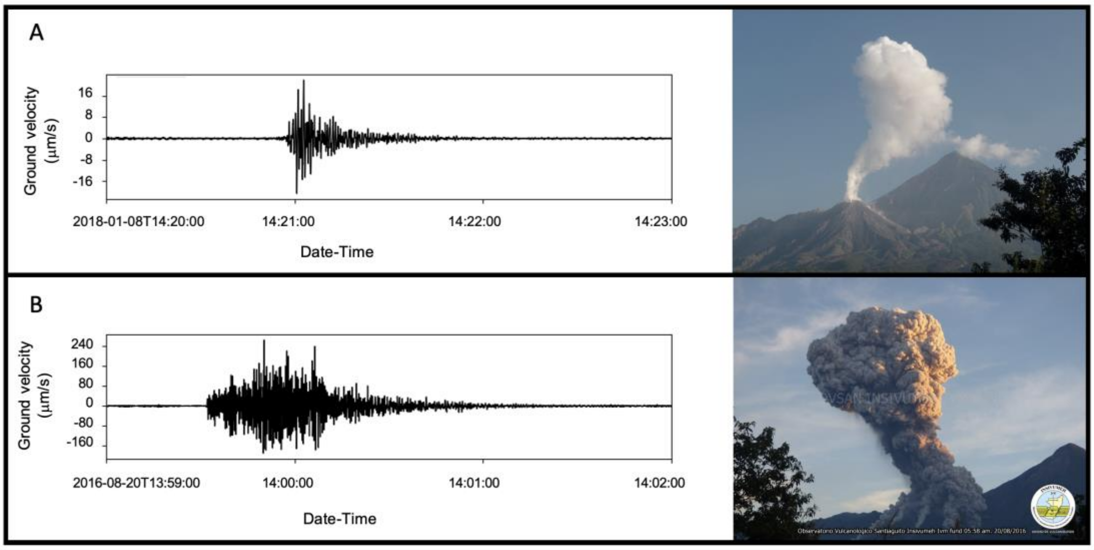

Figure 3.3. *Explosion seismic waveforms and visual observations. A) Small gas-rich explosion from January 2018. B) Large ash-rich explosion from the 2016 paroxysmal phase. Image in B was provided by INSIVUMEH.*

3.4.3. Explosion Catalogue

We designed and applied a detection and classification algorithm to extract and catalogue explosion signals from the continuous seismic data streams recorded across the network at Santiaguito between 2014 and 2018. The automatic algorithm consists of three main steps:

1) Pre-processing: Rapid signal detection at individual stations across the network based on signal to noise ratio (SNR) thresholding. To detect event waveforms in the continuous data streams, waveforms which had a SNR above 1.1 were extracted for the later

processing steps. We fixed the noise level at a manually selected time void of signals. Although slower than a traditional STA/LTA, this ensured waveforms in periods of high noise, induced by non-explosive signals such as human activity, were also detected. To assist the detection of only explosions, the raw data streams were initially filtered between 0.1 and 10 Hz to remove noise in different frequency bands than explosions.

2) Processing: Producing a list of candidate explosion signals based on pre-selected waveform attributes. The detected waveforms were first compared to a preset group of frequency attributes. These attributes included the central and dominant frequencies, as well as the bandwidth at 50% of the dominant frequency's amplitude in the frequency spectrum. The envelope of waveforms which met the frequency criteria were then cross correlated with an envelope of a template waveform, which consisted of a stack of manually detected waveforms. A cross-correlation coefficient threshold of 0.6 was set, with all waveforms correlating above the threshold labelled as candidate waveforms.

3) Post-processing: Using network association to determine if a candidate waveform can be catalogued as a true explosion. An explosion, originating within the network, should radiate seismic energy in all directions and be detected across the network by multiple stations. Noise, however, could either be local to one station, or sweep across the network from one side to the other. The only noise which would be expected to behave in the same way as explosions are other volcanically generated events such as rockfalls, VT events or tremor. These events contain different frequency information, and therefore were removed during the processing steps. Candidate waveform detection times were compared across the network to determine if it was sufficiently detected to be classified as an explosion. Due to the changing station configuration, the criteria for sufficient network association to classify an event as an explosion changed accordingly. As the more reliable instrument, when multiple broadband stations were active, an explosion had to be detected at a minimum of 2 broadband stations. If only one broadband station was available, a detection had to be made by this station. In cases where no broadband station was active, an explosion had to be detected by 2 or more short-period stations. In the most extreme case when only one short-period station was active, the algorithm accepted all detections. However, to account for the change in criteria for a detection to be classified as an explosion, a 'trust' value was automatically assigned to catalogued events based on the number and type of stations which detected the event. If only one short

period seismometer detected an event, a trust of 1 was assigned; if only one broadband or multiple short period seismometers detected an explosion, a trust value of 2 was assigned; a trust of 3 was assigned when one broadband seismometer and one or more short period seismometers detected an event; and a trust value of 4 was assigned when two or more broadband seismometers detected an explosion, with any number of short period seismometers.

Following this post-processing step, an initial catalogue was produced, which was further refined through manual checks of events with a trust value of 1 and event clustering using cross-correlations. Events which did not cluster with other explosions, were manually checked.

The resulting catalogue contained 18,895 explosion signals, expanding the previous record (Lamb et al., 2019) by a factor of approximately 3. The new catalogue includes a further 18 months of recording and separates explosions with smaller repose intervals, which were considered as one event in Lamb et al. (2019). For the range between November 2014 to May 2017, the two catalogues exhibit the same trends. Quality control on four weeks of our new catalogue of explosions was performed from January 2015, September 2015, February 2017 and September 2018 against the raw data streams and found the catalogue contained 90.5% of manually detectable events (610 out of 674), with fewer than 0.5% false detections in these periods. The four weeks contained high levels of noise, and with further checks on individual days throughout the recording period which maintained a comparable quality level, we believe the data checked in these weeks are representative of the most challenging conditions in the dataset. We checked for the influence of network configuration during a period of high-density station coverage in January 2015. We found that with a reduction of 50% of the available stations, and with the same criteria set for explosion detections, a drop of 15% in the detection rate is observed. Despite this drop we find that the trends in the data, and the results from the calculations made with this reduced data set vary minimally.

We calculated the size of all explosions in terms of their seismic radiated energy (SRE) and their associated energy magnitudes (M_e). The SRE and M_e will be used to investigate the variability of the source dynamics for the different eruptive phases in the recording period, determine diagnostic features for these phases, and constrain relationships for the inter-explosion repose times.

3.4.4. Explosion Energy Calculations

The SRE was calculated for each event, defined as the elastic energy generated from an isotropic source at the surface of a homogeneous half space (Boatwright, 1980; Johnson and Aster, 2005), using Equation 2.1. The integral is taken over a two-minute window which contains the full explosion waveform. Background noise included in the window is considered negligible to the calculation. Energy calculations vary from station to station due to unknown site effects, attenuation, and differences in the low-frequency content between the short-period and broadband sensors. Therefore, relative station corrections were determined to obtain a consistent energy calculation of SRE from the network, so that all stations would obtain the same results irrespective of these differences. Station specific correction factors were calculated by determining the amplitude ratios for each station with LB03, which was used as the reference station. This is similar to the method of Lamb et al. (2019), who used LB01 as the reference station. LB03 was chosen as the new reference site to ensure consistency throughout the whole observation period. With variability between events, mean amplitude ratios were used as the relative station corrections for each station, taking into account re-deployments over the observation time span. Station correction factors used are shown in supplementary tables (Appendix A2.1). To obtain robust energy values, SRE calculations were made using catalogued data from the station most active across the recording period to maintain consistency between calculations.

The energy magnitude for seismically observed volcanic explosions, based on ground motion velocity data, is a useful metric to assess the size of explosions at Santiaguito. Choy and Boatwright (1995) derived M_e as given in Equation 2.2. We have calculated the energy magnitude for all events. As in all seismic catalogues, the smallest events may suffer from incomplete detection rates due to low SNR. The magnitude of completeness of a catalogue is defined as the minimum magnitude above which all events are reliably recorded. Using cumulative magnitude distributions, we calculated the magnitude of completeness for the catalogue to be 0.76 M_e.

3.5. Evolution of Explosive Activity

Eruptive activity, and in particular the nature and characteristics of explosions, evolved significantly at Santiaguito throughout the monitoring period; analysis of the new catalogue allows for tracking of the evolution of explosive activity during 2014-2018.

Explosion rates

The new catalogue provides a robust quantitative description of the rate at which explosions occurred during the four-year period. The catalogue shows highly variable activity, with explosions occurring over 500 times per week in January 2015, and less than 5 times a week in May 2016. Between these two dates, the rate of explosions decreased almost linearly. This decrease coincided with a shift from frequent small-to-moderate explosions to erratic and violent, ash-rich events (GVP, 2016a). Following the return to a dominantly effusive regime in October 2016, our data indicate a rapid increase in the number of weekly explosions. By 2018 the rate of explosions became more consistent from week to week, with a steady level of detections recorded in the catalogue.

Secondary Explosions

Over extended periods of time (~days to weeks), the explosions at Santiaguito often display an expected repose interval, statistically constrained at ca. 30-300 min; however, certain explosions are rapidly followed by a second, separate pulse of momentum-driven gas-and-ash with identical acoustic signals within 10 minutes from the leading event (Figure 3.4). We term these pairs as 'primary' and 'secondary' explosions. Secondary explosions commonly release less energy than the associated primary event, with 85% radiating <25% of the energy relative to the primary explosion (Figure 3.3B). These paired explosions were commonly observed during 'normal' eruptive activity. Between 2014 and 2018, 4520 secondary explosions were found in the catalogue, making up 24% of all events. However, during the period of heightened explosivity in 2016, only 8% of the explosions were found to have repose times less than ten minutes. We also observe no major difference between the seismic waveforms of primary explosions and isolated explosions that are not followed by a secondary explosion, as they display a high degree of similarity (Fig. 3.4A).

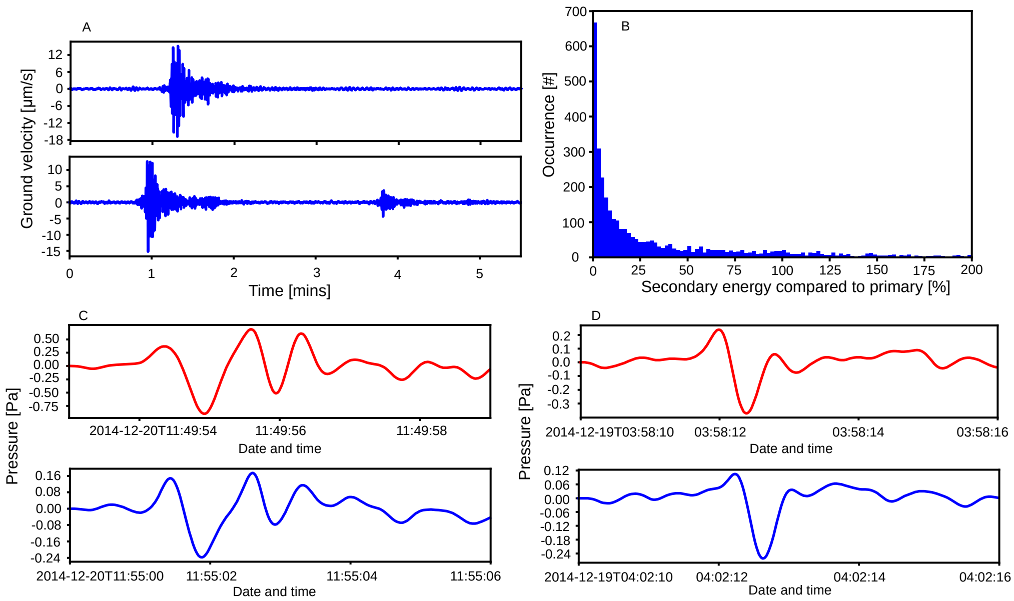

Figure 3.4: *Secondary explosions. A) Seismic record of explosion events. Top: Isolated Explosive event consisting of only one explosion. Bottom: Explosive event with a primary and secondary explosion. Both explosions are recorded at LB01 on 28th December 2014. B) Histogram of relative seismic energy release by a secondary explosion compared to its associated primary explosion. 85 % of secondaries release less than a quarter of the energy compared to its associated primary explosion. C) and D) Example pairs of primary and secondary infrasound waveforms, filtered between 0.2 and 2Hz. Primary explosions are shown in red, while secondary explosions are shown below in blue. The primary and secondary explosions have a significantly higher correlation than the correlation between two independent explosions.*

3.6. Catalogue Analysis

3.6.1. Energy Trends

We used the weekly cumulative SRE to characterise different eruptive phases at Santiaguito (Figure 3.5), calculated by summing the network SRE over consecutive 7-day periods. Although there may be bias introduced into the absolute values of SRE by the assumptions made in the site and path effects, our procedure ensures that relative changes are trustworthy. Changes in SRE, assisted by visual observations made during 2014-2018 indicate four distinct phases of eruptive behaviour. Phase 1 (November 2014 - September 2015) is characterised by a high number of small-to-moderate explosions during a dominantly effusive eruption regime, with an increase in the cumulative weekly explosion energy observed. Towards the end of phase 1 explosions became less frequent but larger. During phase 2 (September 2015 - October 2016), explosions are much less frequent and contain higher magnitude events which account for much of the weekly energy release. Phase 3 (October 2016 - March 2017), which initiated when effusion of lava resumed at Caliente to fill the summit crater, is accompanied by an increase in SRE, caused by high rates of occurrence of small-to-moderate explosions. Phase 4 (April 2017 - December 2018) is characterised by continued effusion after a lava dome had become established within the crater. SRE remained low and slowly decreased due to a low but consistent number of small-to-moderate explosions. Although phase 4 contains a large gap in seismic data, visual observations do not indicate any additional change in behaviour during this time period.

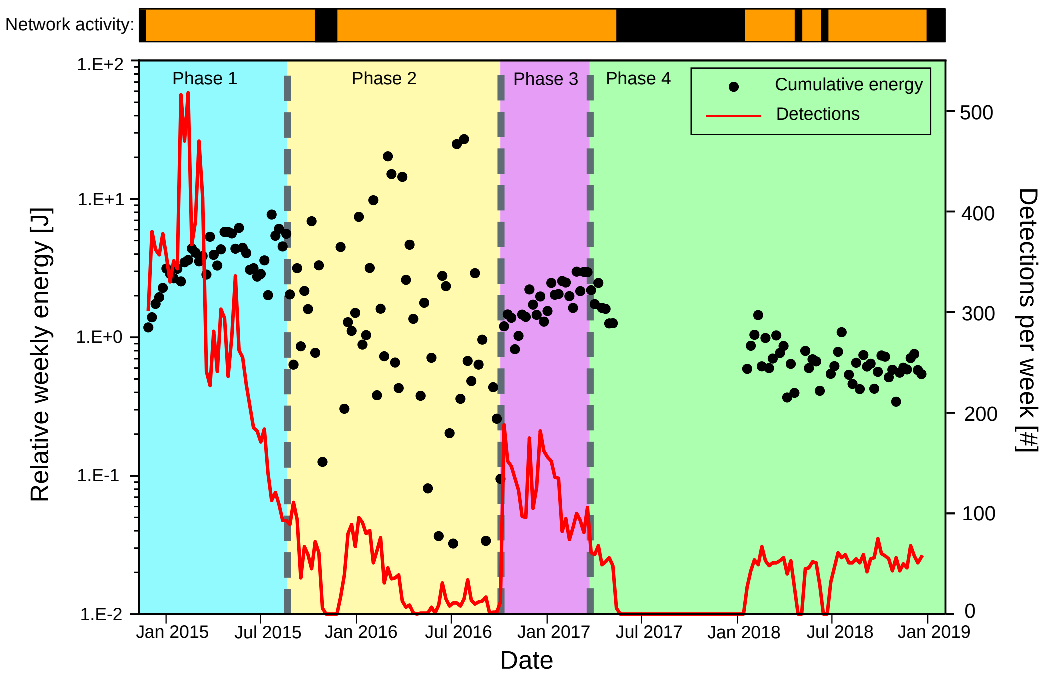

Figure 3.5: *Cumulative weekly seismic radiated energy and eruption phases. Coloured boxes represent phases of the volcanic energy release as described in the text. Blue = phase 1, Yellow = phase 2, Purple= phase 3, Green = phase 4. The boundaries between phases were determined through the combination of the SRE trends observed and the visual observations made on the eruptive behaviour. As transitions are not instantaneous, grey dashed bars separate the phases. The number of detections per week are shown by the red line. Network activity is shown by the orange and black bar, where black indicates data blackouts and orange indicates that the network has at least one active station.*

3.6.2. Magnitude-Frequency

Magnitude-frequency analysis is traditionally used to assess the ratio of small to large events within self-similar systems. Although most commonly used to analyse earthquakes, the GR relationship (Gutenberg and Richter, 1944) and Ishimoto–Iida's formula (Ishimoto and Iida, 1939), which link magnitude of earthquakes to their frequency of occurrence, have also been applied to explosive volcanic events (e.g. Deligne et al., 2010; Nishimura et al., 2016; Sheldrake and Caricchi, 2017; Rougier et al., 2018). Over the four-year recording period at Santiaguito, the energy magnitude of explosions varied over several orders of magnitude. We find a power-law dependency in our datasets between the magnitude of explosions and their rate of occurrence (Figure 3.5), similar to the GR. In the logarithmic-logarithmic space (Figure 3.5) the linear fit to a power law relationship follows:

$$\log_{10}(f) = a - b(M_e) \qquad (3.1)$$

where f is the frequency of explosion occurrence, M_e is the energy of an event, b is a parameter akin to the traditional b-value in the GR and a is a constant describing event productivity; the linear fit is performed only in the region above the magnitude of completeness of the catalogue.

Over the entire four-year observation period the b-value is found to be 1.55 ± 0.06 (Figure 3.6A). We investigated the variability of the magnitude-frequency relationship over the four phases of activity. We find that the b-value decreased from 1.84 ± 0.11 in phase 1 to 0.94 ± 0.06 in phase 2 (Figure 3.6), reflecting the transition from small-to-moderate explosions in the effusive regime to large explosions in the explosive regime. In phase 3 the b-value increased to 2.28 ± 0.69 and remained high in phase 4 with a b-value of 2.40 ± 0.58 as the eruption regime produced fewer events during stable effusive behaviour. For all calculations only events over the magnitude of completeness are included, which we constrain as 0.73, 0.76, 0.90 and 0.77 M_e for phases 1 to 4, respectively.

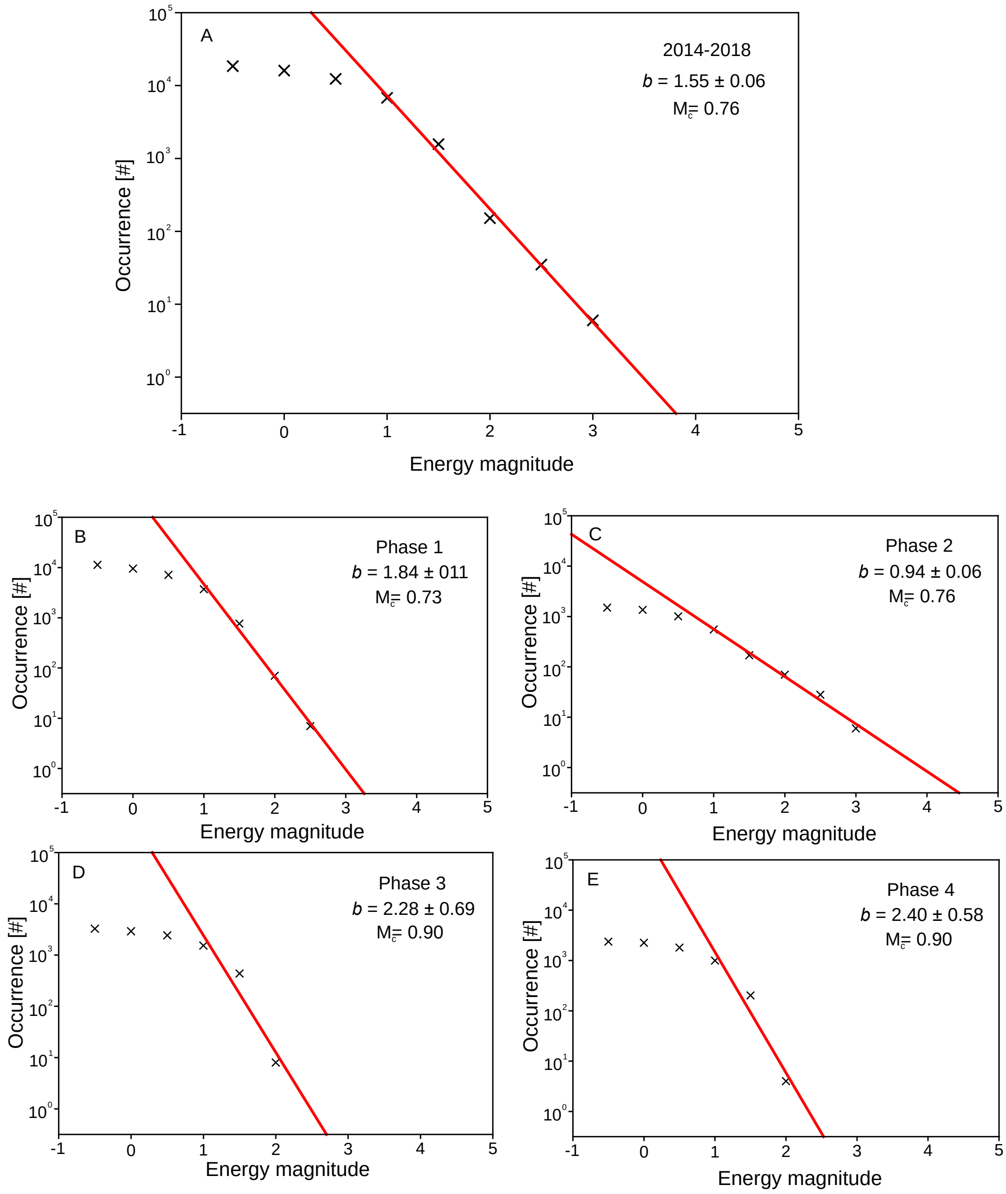

Figure 3.6. *Magnitude-frequency plots of the explosions occurring at Santiaguito. A) Full catalogue, B) Phase 1, C) Phase 2, D) Phase 3, E) Phase 4. A linear trend in log-log space shows that the explosions follow a power-law relationship. For all times, the b-value (gradient) and its standard error is displayed, fit through all points above the magnitude of completeness, which is indicated in each panel.*

3.6.3. Repose Times

Inter-explosion repose times indicate the occurrence and regularity of the explosions and are commonly used to determine the statistical models which describe the probabilistic estimates which form the basis for eruption forecasting models (e.g., Connor et al., 2003; Watt et al., 2007; Lamb et al., 2014; Varley at at., 2018). We find that for the whole catalogue and for all phases of activity at Santiaguito repose times follow exponential distributions (Figure 3.7). The linear slope of the repose time against the logarithm of occurrence for each repose time represents the rate parameter for the phase, that is the inverse of the mean repose time. The best fit to the repose times was made using an automatic piecewise regression function which tested the fit of two regression slopes at different breakpoints with a single regression line to find the best fitting slopes. The function compared the best fit with two regression lines with the best fitting single regression, if the regression of two slopes provided a significant improvement over a single slope, they were selected. We observe different rate parameters in each eruptive phase at Santiaguito, with phase 1 displaying two different rate parameters, indicated by a break in slope at a repose time of 0.17 days (i.e., 4 hours). A break in slope is also observed over the whole catalogue, showing two dominant rate parameters over the four-year recording period (Figure 3.7A). The rate parameters vary between 1.80 and 11.58, which occur in phases 4 and 1, respectively. The colour bar in Figure 3.6A shows that the repose times in phases 1 and 3 have a time dependency, and do not exhibit a randomness of repose intervals, as observed in phases 2 and 4. The repose times in the overall catalogue also shows a time dependency.

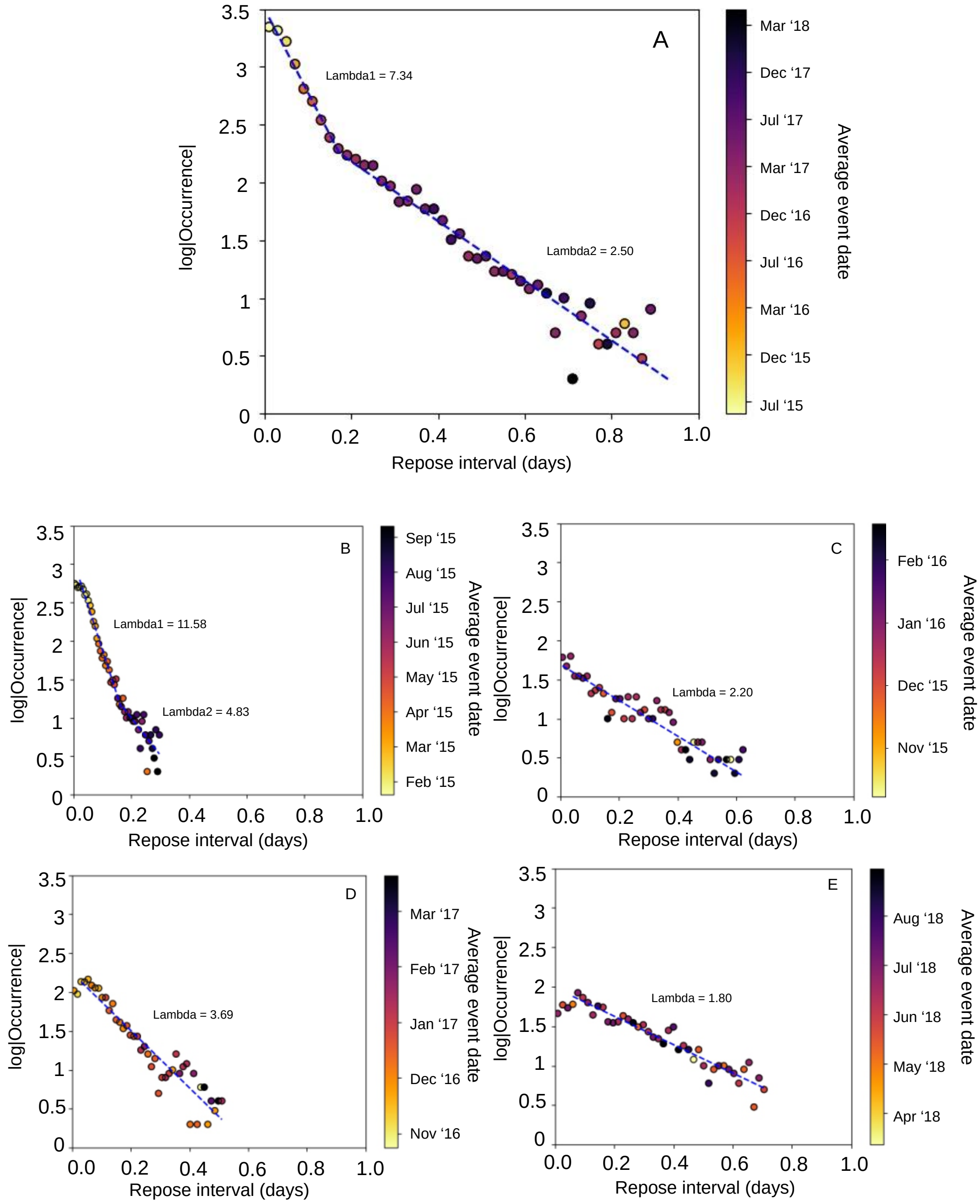

Figure 3.7: *Exponential distributions of inter-explosion repose times. A) Full catalogue, B) Phase 1, C) Phase 2, D) Phase 3, E) Phase 4. The colour scale displays the average date-time of the events contributing to each point. For phase 1 and the whole catalogue, more than one rate parameter is observed, indicating multiple controlling processes. Only events above the magnitude of completeness are included in the analysis of each phase.*

3.7. Discussion

Eruption phases and styles

Our observations agree with Harris et al. (2003) that the behaviour of Santiaguito is commonly characterised by effusion of blocky lava flows from Caliente lava dome, punctuated by small-to-moderate sized explosions reaching up to 1.5 km above the vent (GVP, 2016b), as seen in phases 1, 3 and 4. Previous studies at Santiaguito have stated that the explosions are regular in their occurrence with a repeatable source, generating explosions between 0.5 and 2 times per hour (e.g. Harris et al., 2003; Bluth and Rose, 2004; Sahetapy-Engel et al., 2004; Yamamoto et al., 2008). Over the four years of this study, we see that the repose times are not so consistent, with event rates which varied between 500 times a week (3 times per hour) in January 2015 to less than 5 times a week (0.03 times per hour) in May 2016.

The combination of visual and seismic observations at Santiaguito revealed four eruptive phases; this builds on previous studies by Lamb et al. (2019) and Wallace et al. (2020), as we present for the first time a description of phase 4.

Eruptive phase 1 is characterised by the effusive eruption regime observed between November 2014 and September 2015, with high occurrence rates of small-to-moderate explosions. We attribute the progressive increase in energy observed in this phase, along with the decrease in explosion occurrence to the system preparing to transition into the explosive phase 2.

Phase 2 began in September 2015 with the emergence of larger magnitude explosions, which resulted in increased hazard to the surrounding population. These explosions were characterised by plumes which rose to heights of up to 7 km above the vent, and collapsed to generate pyroclastic density currents, while also ejecting pyroclasts of size up to 3 m diameter to distances of 3 km from the vent (GVP, 2016a). The large explosions excavated a deep crater in the Caliente lava dome. Wallace et al., (2020) split phase 2 into two phases, before and after March 2016, based on the componentry of collected volcanic ash which showed a progression from the dominance of dense brown clasts to porous and transparent glassy particles. For the purposes of this study, based on the lack of distinction in geophysical signals, these brief phases are simply combined in our analysis of explosion energy vs repose time (Figures 3.5 and 3.7C).

Phase 3 saw the occurrence of effusive activity, interspersed with up to 200 small-to-moderate explosions per week, beginning in October 2016. SRE is observed to gradually increase during phase 3, which we associate with lava extrusion and dome growth throughout this phase (Figure 3.5).

Phase 4 began after the lava dome had filled the excavated vent of Caliente in April 2017 and was characterised by attainment of a stable effusive regime. Throughout phase 4 the number and magnitude of explosions remained consistent at approximately 50 explosions per week with magnitudes up to 1.5 M_e, which is reflected in the SRE trends. We note however, that statistically phase 3 and phase 4 are almost identical, as observed by their comparable *b*-values. We separate these phases through the observations of dome growth and upward trending weekly energy in phase 3, and continued effusion with an established dome and slowly decreasing weekly energy produced by a more consistent eruption rate in phase 4.

Phases 1 - 3 largely align with the phases outlined by Lamb et al. (2019), describing the same activity styles in each of the three phases. The differences between the phases here and those described by Lamb et al (2019) are the boundaries between each phase. These differences are likely due to the methodology used to select the boundary times. In Lamb et al. (2019) the phase boundaries were chosen based on visual observations of the activity alone, whereas here, we use the SRE trends as a primary indicator, with visual observations used to corroborate the boundary choices.

From the observed trends in explosion rates and SRE, as well as the temporal distribution of repose times, we see that transitions between eruptive phases have occurred over different timescales, with gradual transitions occurring between phases 1 and 2 and phases 3 and 4, as well as a more abrupt transition between phases 2 and 3. The visual observations made throughout the four years again helped constrain these transitions and their timescales.

The duration of the explosions, automatically calculated as the time between 2.5% and 90% of the cumulative seismic energy of the associated waveform, increased during the explosive behaviour in phase 2 to have a mean length of 25.8 seconds, compared to a mean of 18.9 seconds during the dominantly effusive regime of phases 1, 3 and 4. The duration of the explosions measured from the seismic waveforms matches closely with the visual observations of 30 – 60 s made by Bluth and Rose (2004) of the momentum-driven phase of gas release at Caliente. We speculate therefore, that it is likely that the seismic waveforms are a record of the vigorous gas venting phase while the fracture pathways remain open. The increased duration of the explosive events in phase 2 is possibly caused in-part by signal overprint from pyroclastic density current activity, and by larger gas overpressure developed over longer timescales in deeper parts of the magmatic column (cf. Wallace et al., 2020). Larger overpressures would enhance fragmentation efficiency (e.g., Kueppers et al., 2006), and deepen fragmentation, lengthening the travel distance in the conduit for gas and ash to erupt.

At the time of writing this paper, the activity at Santiaguito appears to be entering a new phase, with explosions becoming visibly larger, rising up to 1.3 km above the vent, occurring at increased rates of 35-40 explosions per day (GVP, 2019d). This suggests that a transition into a fifth eruptive phase may have occurred since the end of our monitoring period in December 2018. Visual observations report that the size of the dome is currently larger than before the May 2014 dome collapse episode. From these visual observations, it is thought that the possibility of a dome collapse presents a significant risk, and such an episode could be hazardous should one occur at Santiaguito in the near future.

Source stability

We have noted through magnitude-frequency analysis that the explosions at Santiaguito obey a power-law relationship similar to the Gutenberg-Richter relationship used in earthquake seismology (Figure 3.6). The power-law relationship depends on the *b*-value, which describes the magnitude of faulting events (i.e., ratio of small to large magnitude seismicity; Aki, 1967). In this paper we use the energy magnitude M_e to describe the magnitude of explosion. We infer that the observed *b*-values reflect, in part, the state of the magma in the conduit system, which has controls on fragmentation. However, we argue that magma properties can vary both spatially and temporally, which makes it difficult to relate changes in *b*-values to specific properties and thermo-kinetic conditions within the system (Roberts et al., 2015). Despite energy magnitudes spanning over 5 orders of magnitude, the power-law relationship indicates self-similarity between explosions at a mechanistic level (cf. Nishimura et al., 2016; Papale, 2018). Over the four-year period, Santiaguito expressed a *b*-value of 1.55 ± 0.06. However, across the four different eruptive phases we observed variations in the *b*-value. The variations represent the evolution of spacing and size of events between phases; in other words, each phase may be considered as a discrete "experiment" with the sum of events defining its mechanistic character. The evolution from high *b*-value during phases 1, 3 & 4 (with frequent small events) to low *b*-value during phase 2 (with less frequent and larger events) suggests that the properties of the explosion source mechanism varied through time. Changes in source properties can involve differences in both the applied stress accumulation within the system as well as the scale and architecture of rupture, in part dictated by material properties.

The rupture and "strength" of magmas is controlled by several factors, including the fraction of heterogeneities (i.e., crystallinity and porosity), the viscosity of the silicate melt phase, and strain rate (Lavallée et al., 2019). As magmas are viscoelastic bodies (e.g., Dingwell and Webb, 1989), understanding magmatic fragmentation and resultant seismicity requires careful consideration of thermo-kinetic conditions (e.g., Papale, 1999; Zhang, 1999; Lavallée et al., 2012). The rupture of silicate melts results from an inability of the melt structure to relax an applied stress, provoking structural breakdown. The rate of structural relaxation of silicate melts is proportional to their viscosity, regulated by its chemistry and temperature (Dingwell and Webb, 1989); i.e., at low temperature, a melt's viscosity is higher and requires lower strain rate to rupture. So, understanding the rupture of silicate melts, or magmas (additionally hosting pores and crystals), requires knowledge of both viscosity and strain rates (e.g., Lavallée et al., 2008; 2013; Cordonnier et al., 2009; Kendrick et al., 2013; Hornby et al., 2019). Material rupture results from the nucleation of micro-cracks, which propagate and coalesce in the build-up to system-size failure (Voight 1989; Kilburn, 2003; 2012), and magma rupture ensues accordingly (Lavallée et al., 2013). Heterogeneities, commonly present in magmas, act as stress concentrators that focus the nucleation of micro-fractures (Sammis and Ashby, 1986); thus, their presence lowers the strength of silicate melts (Vasseur et al., 2013; Cordonnier et al., 2012) and facilitates failure via characteristic acceleration in microseismic events that may be monitored to forecast rupture with increasing accuracy (Vasseur et al., 2015; 2017).

Zobin et al. (2014) speculated that a change in *b*-value associated with volcanic activity at different volcanoes may result from differences in magma crystallinity, which affected the viscosity of magmas and the stress required to failure. Whilst an increase in crystallinity may provoke changes in *b*-values of magma rupture, such a generalisation may be tenuous as the physico-chemical properties and stress conditions of magmas can vary widely between volcanic systems. As porosity generally has a greater impact on material strength than crystallinity (e.g., Coats et al., 2018), we anticipate that it would likely provide stronger controls on the development of material rupture and resultant seismic *b*-value, if other considerations (i.e., the viscosity of the melt phase and strain rate experienced) remained the same; this is supported by laboratory observations that single-phase melts rupture rapidly through localised fractures with large stress drops, whereas porous melts break slowly via multiple distributed small fractures with small associated stress drops (e.g., Vasseur et al., 2013). Likewise, a complementary study showed that the *b*-value resulting from magma rupture (under equivalent strain rates) generally increases with porosity (Vasseur et al., 2015). The development of porosity (Mueller et al., 2011) and pore pressure (e.g., Castro and Gardner, 2008) have previously been linked to changes in explosivity. Considering a single volcanic centre, as in our study, it is common to note a wide range of porosity in eruptive products (e.g., Lavallée et al., 2012; Mueller et al., 2011), yet only moderate changes in crystallinity within a given eruptive period (e.g., Bain et al., 2019), although magma viscosity may evolve regardless due to interstitial melt sensitivity to changes in temperature (e.g., Mastin 2005; Blundy et al., 2006; Lavallée et al., 2015) and dissolved volatile content (e.g., Hess and Dingwell 1996; Castro and Dingwell, 2009; Castro et al., 2005; Edmonds and Herd, 2007), and changes in ascent rate. Discharge rate and ascent rates can vary widely during volcanic eruptions; as a result, and crucial for the present seismic analysis, this implies that shear rates can vary by several orders of magnitude during explosions at lava dome eruptions (e.g., Quane and Russell, 2005). At Santiaguito, magma fragmentation has previously been linked to the rate of shear traction experienced in the magmatic column leading to explosions (Lavallée et al., 2015). Complementarily, laboratory testing has shown that shear rate plays a key role in the development of damage and associated *b*-value (Lavallée et al., 2013). In particular, laboratory experiments have shown that an increase in applied strain rate results in an increased localisation of fracture propagation during material rupture, which results in a decrease in *b*-value (Lavallée et al., 2013).

Thus, one needs to exert caution in inferring reasons for fluctuations in seismic *b*-values as many factors compete and in-situ magma properties and local thermo-kinetic conditions vary both spatially and temporally. Wallace et al. (2020) showed that changes in crystal textures, silica content and temperature (and thus viscosities) took place in the eruptive period studied here at Santiaguito. Hornby et al. (2019) demonstrated that magma porosity, temperature and applied strain rates were key controls on the tensile strength of Santiaguito magma, thus it is likely that some or all of these controlling factors have conspired to generate the *b*-values we resolved during the 4-year eruptive period studied at Santiaguito. Yet, it remains that the small explosions which cause little-to-no damage to the lava dome result from small pressure releases, whilst large explosions on the other hand, release larger stresses in the system and tend to have ruptures with increased length-scales (Lavallee et al., 2013). If we return to our analogy that an eruptive phase represents an experiment, involving a material deformed within a bounding set of conditions (as identified by the seismic signatures and event spacing that define each phase) then the shifts in *b*-value between different eruptive phases demonstrate that explosions evolved from small, frequent events (high *b*-value) akin to the slow accumulation of damage during material deformation, to periods of larger scale, less frequent events which caused significant damage (low *b*-value), akin to wholesale failure during material deformation, driven by greater pressure accumulation. Thus, we must also stress that for meaningful interpretation, *b*-value must be considered over restricted and constrained time-periods, rather than considered as a stable, system-specific value.

Secondary explosions

The data highlighted the occurrence of explosion duets. We define secondary explosions as explosions which occur within 10 minutes of an initial explosion, where the infrasound waveforms for both explosions are near identical yet separated by a period at a background level of activity. We observe that secondary explosions account for 24% of the explosion catalogue, making up a significant proportion of the explosive activity at Santiaguito. However, during the period of heightened explosivity in phase 2, the secondary explosions made up only 8% of explosions, predominantly following the smaller magnitude events during this phase, indicating that secondary explosions are a common feature of lava dome effusion at Caliente, occurring when the explosion fractures are more restricted. We also observe that over 85% of the secondary events radiate less than 25% of the energy compared to the primary event (Figure 3.4B). We compared the infrasound signals of the primary and secondary explosions to investigate the relationship between the two events and show that the infrasound signals associated with primary and secondary explosions show a high degree of similarity (Figures 3.4C and 3.4D). T-tests on the time domain cross-correlations between all explosion's infrasound waveforms show that the similarity between primary explosions and their secondary explosions is significantly higher than the cross-correlation between any randomly chosen pair of explosions to a significance level of 0.1%. Example waveforms are shown in Figure 3.5C and 3.5D, where the waveforms of the 2 primary events show different shapes, yet the secondary events show high similarity to the primary events they follow. These observations indicate that the secondary events are somehow linked to the primary event, with a time dependence which cuts off at approximately 10 minutes. We speculate that the high correlation between primary and secondary explosions requires magmatic fragmentation under the same conditions, i.e., magma would likely fragment at the same depth, and the gas-and-ash products would be released via the same vent (geometry and size). We advance that this may be the case if the gas-and-ash are erupted from the same fracture pathways, as occasionally observed. Therefore, the repose interval may reflect the state of the fractures present in the lava dome. Due to the limitations in our observations however, we cannot validate these assertions.

Assessing future eruptive potential

The frequency of the inter-explosion repose times follows exponential distributions (Figure 3.7), where the fit to the exponential distributions represents the rate parameter, which is the inverse of the mean return time. The rate parameters described by the exponential distributions are observed to change between eruptive phases as a result of the changes in source conditions and mechanisms between phases. Across the whole catalogue, two robust rate parameters are observed which relate to the mechanisms producing frequent low magnitude events during the effusive eruption regime, and infrequent large events in the explosive regime in phase 2 (Figure 3.7A). The occurrence rate of different repose times is shown to correlate with time (colour bar - Figure 3.7), which is a consequence of the explosion mechanisms and source conditions transitioning through time. During phases 1 and 3, there is also a transition from low to high repose duration through time, suggesting that the source behaviour is gradually transitioning (Figure 3.7B and 3.7D). In contrast, phases 2 and 4 displays no correlation between repose duration and time, indicating that the source is more stable (Figure 3.7C and 3.7E).

Above the cut-off magnitude (set at the magnitude of completeness), the stochastic explosion process can be represented by a Poisson distribution. Poissonian processes in explosion repose times are seen on both a global scale (De la Cruz-Reyna, 1991; Papale, 2018) and at specific volcanoes (e.g., at Volcán de Colima, Mexico; De la Cruz-Reyna, 1993). Marzocchi and Papale (2019) used the Poisson relationship for volcanic events of different sizes worldwide to determine the probability of events across varying magnitudes occurring within different time periods. However, on local scales at different volcanoes, inter-explosion repose times are commonly described by different statistical models such as Weibull and log-logistic, as well as Poissonian, which show variability in how explosions evolve within a system (Watt et al., 2007). Watt et al. (2007) showed that over time the statistical model describing the inter-explosion repose times can also change as the system evolves. On a global scale, only one exponential relationship is observed (Papale, 2018), however, we show that different phases are characterised by distinct frequency scaling of explosivity, which is likely caused by different source parameters and perhaps triggering mechanisms, which leads to the different rate parameters observed. Due to the nature of Poissonian processes, when an explosion has occurred, it is impossible to predict when the next event will occur, although probabilistic estimates can be given for the expected return time. Yet, probabilistic estimates of the expected return time are phase dependent (as each phase displayed different activity) and therefore change frequently on the timescale of several months. Other proxies may thus be necessary to enable the development of tools to ensure long-term assessments of eruptive behaviour at Santiaguito.

The maximum explosion magnitude expected within an eruptive phase can be estimated by extrapolating the linear fit of the magnitude-frequency distribution to a value of 1 event occurrence within the phase. For the entire catalogue, we obtain an estimate for the largest explosion to have an energy magnitude of 3.49, where the largest event recorded had an energy magnitude of 3.46. As with the overall catalogue, the estimates for each of the individual phases are overestimates. We calculated the largest events as 3.00, 3.92, 2.48, and 2.32 M_e for phases 1 to 4, respectively, while the largest events observed had energy magnitudes of 2.82, 3.46, 2.11, 2.12 for phases 1 to 4, respectively. The level of caution in these estimates can easily be adapted; decreasing the event occurrence rate at which the estimation is taken increases the likelihood that the estimate of the largest possible event magnitude will be an overestimate. A caveat to this method is that the estimation assumes that the volcano will remain in the same eruptive regime, whereas the system has been shown to evolve rapidly, as observed between the dominantly explosive and effusive regimes in phase 2 and phase 3, respectively. Furthermore, the estimates made here are performed in hindsight; in real time, it may not be possible to determine which phase of activity is being exhibited, and for this reason we do not give errors in these calculations. Finally, changes in a volcano's eruptive behaviour affect the upper estimates of explosion magnitude, thus caution must be exerted when using it as a predictive tool.

3.8. Conclusions

Long-term seismic and acoustic monitoring at Santiaguito has revealed details on the changing nature of the explosivity at the active Caliente vent and revealed relationships between explosion energy and recurrences. Explosions occur at different intervals, ranging from a few minutes up to ~6 days. On the shorter end of the scale, many explosions are followed within 10 minutes by secondary explosions (accounting for 24% of the total recorded explosions) with near identical acoustic signals to their primary explosion, and lower energy release. On the longer end of the scale, repose times between explosions however lead to contrasting signals and behaviour. Trends in the seismically radiated energy have provided an effective indicator of eruptive phase changes at Santiaguito, enabling the discrimination between one phase and the next. Magnitude-frequency analysis has shown that the *b*-value changes between eruptive phases. While the source mechanism of the explosions shows a level of self-similarity, the changes in *b*-value suggest that the properties which control magma fracturing vary, thus local conditions cannot easily be reconciled. Yet, we infer that the phases characterised by small, frequent events, resulting from small stress drops, have high *b*-values and more restricted damage, whilst phases characterised by large events, representing larger stress drops, resulted in lower *b*-values and more wholesale damage. Changes in the source properties between phases also influence the characteristic magnitudes and repose times, restricting extrapolation of behaviour to within a single phase and limiting the potential for long-term assessments of future trends in eruptive activity at Santiaguito

Chapter 4. Characterisation of Open-Vent Activity at Volcán de Fuego

4.1. Summary

Following the work at Santiaguito, this third manuscript, entitled "Characterisation of open-vent activity at Volcán de Fuego from seismo-acoustic network observations and energy partitioning", takes the algorithm building methods developed and applies them to a new volcano, namely Volcán de Fuego.

Following the June 2018 paroxysmal eruption of Volcán de Fuego which devastated the local region, taking the lives of many in the communities nearby, a new network of permanent remote sensing stations was deployed. This provided an opportunity to test out the method of using automatic detection and classification algorithms in a new setting and provide information which could aid in mitigating the hazards posed by future eruptions at the volcano.

The method of cataloguing events using a detection and classification algorithm is further developed in this study and is explained in detail in the supplementary material (Appendix A1.1), with the primary focus of the manuscript being primarily on the analysis on the catalogued data. At Fuego, in contrast to Santiaguito, the network of acoustic infrasound microphones was more established than the network of seismometers. It was decided therefore that the acoustic data streams would be used for the detection and classification of volcanic events, with seismics used to support the results. The methods presented here demonstrate automatic detection and classification of seismic and acoustic tremor, as well as both ash- and gas-rich explosions. In this manuscript we describe the different event types, outlining the key parameters that make them identifiable from one another, in order to implement an automatic classification scheme. The catalogues produced are provided in the supplementary materials (Appendix A3.2 – A3.4), which logged 99,618 explosions, 6,048 seismic tremor events and 2,200 acoustic tremor events over the 3 years of recording. We provide the start time, and the duration for all events in the catalogue.

Following the development of the new detection algorithm, we analysed the events extracted to show how the background activity at Fuego, much like at Santiaguito, can be split into distinct phases. We demonstrate how the activity changes in style, with changes

to the occurrence of the different event types, and energy released through time, linking them to observations of activity at the summit. We show how the combination of seismic and acoustic measurements, alongside visual observations of the activity can help identify these phases, as well as be used in the assessment of different event types.

During the recording period of this study, a paroxysmal eruption occurred. We show how the paroxysm disturbed the baseline activity and discuss the different models suggested for the triggering mechanisms of these large hazardous events based on the inferences made from our recordings and observations.

By taking advantage of both ground-based and satellite observations to support the geophysical results, we holistically track the state of the volcano and develop a conceptual model for the evolution of the activity. This model aims to show how multi-parameter studies can link different observations and their interpretations together to understand how the internal properties of the volcano temporally evolve to produce the observed activity.

Finally, in this manuscript we show that the recording of acoustic tremor can be linked to the observations of continual gas release that have been made by many studies over the past few decades. We show that the acoustic tremor is an important feature to monitor to track the changes in the activity observed at the vent.

4.2. Abstract

Volcán de Fuego (Guatemala) exhibits open-vent activity, with regular lava effusion, strombolian explosions, and occasional paroxysms (VEI ≤ 4). Following the deadly June 2018 paroxysm, we established a permanent network of seismometers and acoustic (infrasound) sensors to monitor eruptive activity at Fuego. Using the data collected by this network between October 2018 and October 2020, we applied a detection and classification algorithm which automatically catalogued explosions and seismic and acoustic tremor. We obtained a catalogue of 99,618 explosions, 6,048 seismic tremor events and 2,200 acoustic tremor events. We analysed the seismic and acoustic records jointly with ground- and satellite-based observations of crater fill and lava flow activity at Fuego. Our analyses suggest that baseline activity at Fuego consists of the occurrence of two statistically distinct populations of small-to-moderate explosions (gas-rich and ash-

rich), periods of sustained surface gas release, and episodic lava flow activity. This style of activity is periodically interrupted by paroxysmal events, such as during 18th - 20th November 2018 when elevated explosive activity caused the summit crater to empty. Here, we show how the November 2018 paroxysm disrupted background activity, and discuss how long-term geophysical observations can link to models on the triggering mechanisms of paroxysmal events. In particular, we observe that the ratio of acoustic to seismic energy release helps identify shifts in activity at Fuego and may be used to shed light on the source mechanisms of explosions and tremor. Our observations suggest that activity at Fuego during the period of this study can be divided into six separate stages. Finally, we present a conceptual model of the evolution of the activity that best represents the six phases of activity that are observed.

4.3. Background

Volcán de Fuego (14.47°N, 90.88°W), located in southern Guatemala (Figure 4.1), is one of the most active volcanoes in Central America and has been in a period of open-vent eruptive activity since 1999 (Lyons et al., 2010). The activity at Volcán de Fuego is defined by long periods of persistent lava effusion interspersed with mild Strombolian explosions, and occasionally (every few months to years) activity is disrupted by large paroxysmal eruptions, which range between VEI 2-4 (Lyons and Waite, 2011; Escobar-Wolf, 2013; Naismith et al., 2019). In 2015, Fuego entered a new phase of activity characterised by an increased frequency of paroxysmal eruptions (Naismith et al., 2019), with the most notable event occurring on 3 June 2018 (GVP, 2018f), which destroyed several local villages, taking the lives of 169 people, leaving 256 people missing, and displaced nearly 13,000 people from their homes (GVP, 2018f). In 2018, two other paroxysms occurred, in February and November (GVP, 2018e; 2018g). The large paroxysmal events at Fuego occurring over the past 2 decades have been discussed by Naismith et al, (2019) and Lyons et al, (2010) to likely be triggered through mechanisms described by models including the collapsing foam model of Jaupart and Vergniolle (1998), rise-speed dependent model of Parfitt and Wilson (1995) and for certain cases could be triggered by gravity-driven shedding of material from an ephemeral summit cone (Naismith et al., 2019). Other triggers for paroxysms proposed for similar volcanoes worldwide include deep volatile rich magma slowing magma recycling in the upper conduit, leading to rapid decompression of the deeper reservoir (Ripepe et al., 2017), and CO_2 influx through the system at Stromboli (Allard, 2010), as well as both gas-burst and gas-rich magma recharge at Mt Etna (Viccaro et al., 2014). Fuego typically recovers between paroxysms to a background level of open-vent activity (Castro-Escobar, 2017). The importance of characterizing low-level background activity has been highlighted (Brill et al., 2018) in order to resolve processes within the plumbing system and identify signs leading up to the large paroxysmal phases (Berlo et al., 2012). Although Fuego has been in a state of open-vent activity for over two decades, and caused devastation to the local region, key questions remain open as limited work has been done to quantify the level of activity leading to, during, and following paroxysms, and to understand these dramatic shifts in activity through time (cf. Lyons et al., 2010), as they are likely to recur.

Here, we aim to demonstrate through long-term observations of a permanent seismo-acoustic network, supported by visual and satellite observations, that we can obtain a better understanding of the paroxysms at Fuego, and of the low-level activity that occurs between them. We further aim to resolve the changes in activity and use the key findings to inform a conceptual model of how the system evolves through time and how paroxysms disrupt background activity.

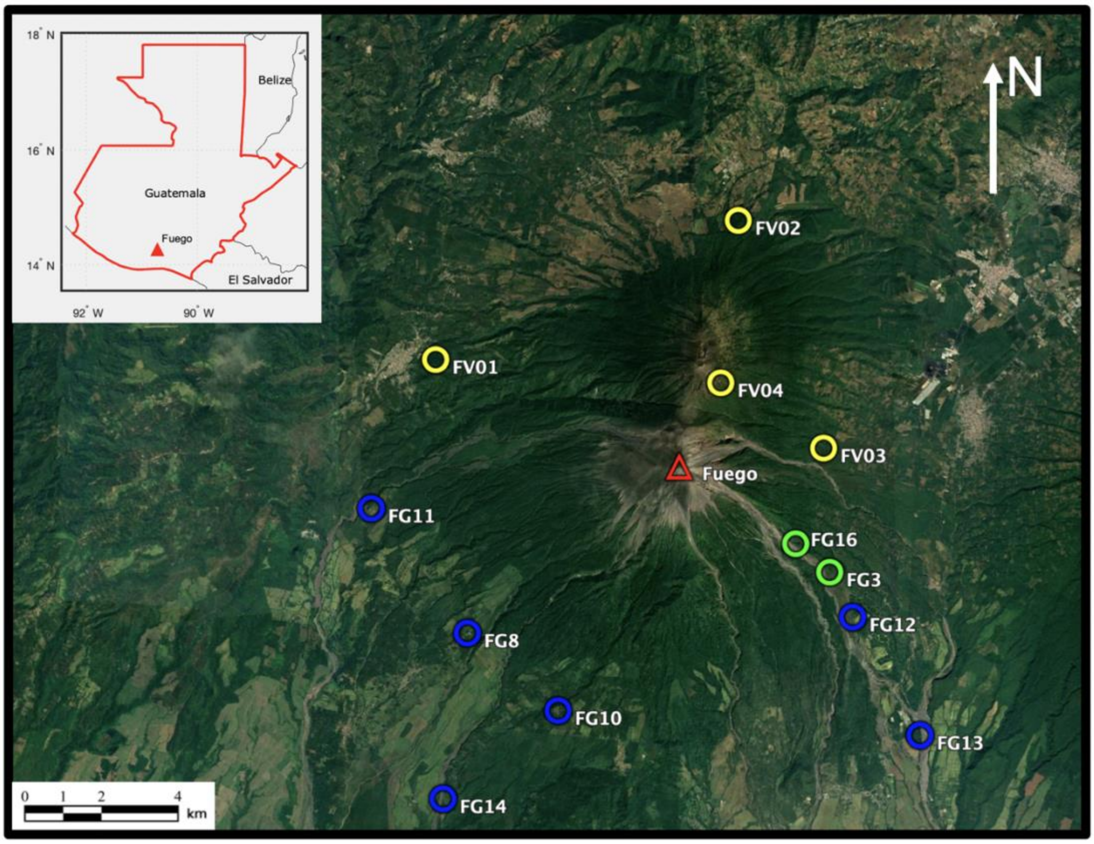

Figure 4.1. *Volcán de Fuego seismo-acoustic network. Blue circles indicate permanent seismo-acoustic stations, green circles indicate permanent seismic only stations, yellow circles indicate temporary acoustic only stations from a short-term survey in November 2018. Inset: Location of Volcán de Fuego (red triangle) in Guatemala. Map data: Google Earth V 7.3.3.7786 (2021).*

4.3.1. Activity at Volcán de Fuego

During low-level "background" open-vent activity (i.e., between paroxysmal eruptions), Fuego commonly exhibits almost continuous effusion, generating lava flows, as well as occasional gas emission events and small to moderate explosions (Martin and Rose, 1981; Rodríguez et al., 2004; Castro-Escobar, 2017; Brill et al., 2018; Diaz-Moreno et al., 2020; GVP 2019a; 2019b; 2019c). Gas release episodes are seen to occur (Lyons at al., 2010; Brill et al., 2018; De Angelis et al., 2019; Naismith et al., 2019; Diaz-Moreno et al., 2020), and volcanic tremor is also commonly detected in both the seismic (Waite and Lyons, 2009; Lyons et al., 2010; Lyons and Waite, 2011, Nadeau et al., 2011; Brill et al., 2018) and acoustic records (Lyons at al., 2013; De Angelis et al., 2019; Diaz-Moreno et al., 2020).

Strombolian explosions dominate the background activity at Fuego and can occur between 2 and 32 times per hour (e.g. GVP, 2019a; 2020b), commonly producing either gas-rich or ash-rich plumes (Waite et al., 2013; Diaz-Moreno et al., 2020; GVP, 2020a; 2020b). Explosions often eject incandescent material to heights of several hundred meters (e.g. GVP, 2018e; 2019a; 2019c), with plumes typically rising to 1,100 m above the vent (e.g. GVP, 2019b; 2019c; 2019e). These events eject variable quantities of ash which is deposited downwind as distally as 23 km (GVP, 2019e). During the rainy season, the remobilisation of deposited ash can cause lahars in established drainage channels (e.g. GVP, 2018f; 2019b). The conduit and underlying magma plumbing system has been modelled as an inclined sill at 300 m depth below the summit vents and centred 300 m to the west (Lyons and Waite, 2011). Explosions appear to result from a cyclic pattern of magma pressurisation within the sill, followed by depressurisation when overpressure exceeds the tensile strength of the capping viscous magma plug, releasing gases and ash in the explosive event; then, as gas pressure is lost, fractures close, shutting the permeable network and enabling a new cycle of pressurisation and explosion (Lyons and Waite, 2011). As the explosions are repetitive, they are likely non-destructive to the source mechanism (cf. Arciniega-Ceballos et al., 1999; Chouet et al., 1999).

Volcanic activity at Fuego has traditionally been monitored using seismometers; in particular, seismic tremor has commonly been observed in recent decades (e.g. Lyons et al., 2010; Lyons and Waite, 2011; Nadeau et al., 2011; Brill et al., 2018). Seismic tremor has been commonly linked to different processes including conduit resonance caused by the flow of fluids (either gas or magma) through cracks causing oscillations (Chouet, 1988; 1996; Julian, 1994; 2000; Balmforth et al., 2005; Lipovsky & Dunham, 2015), and the coalescence of bubbles in the conduit (Ripepe and Gordeev, 1999). At Fuego, Lyons et al. (2010) observed a correlation between seismic tremor, thermal output (as measured by the MODIS thermal satellite data) and lava flow lengths; they recorded much higher seismic tremor energy during paroxysmal events with peaks 10-50 times that of tremor during background, inter-paroxysm phases. Lyons and Waite (2011) described tremor episodes on the order of minutes which occurred directly following an explosion, and that later explosions would briefly disrupt the tremor before it would return 10's of seconds after these later explosions ended. Nadeau et al. (2011) showed that the tremor at Fuego is also correlated with the release of SO_2 gas and suggested that these two observations share a common source; they postulated that degassing would lead to progressive stiffening of the shallow magma, causing a potential deepening of the tremor source through time. Brill et al. (2018) noted that tremor is the largest contributor to the real-time seismic amplitude measurements during the inter-paroxysm phases and made visual observations of white, ash-poor emissions occurring during tremor events.

At Fuego, persistent gas emission has been visually observed to be a common feature of background activity during the open-vent periods of eruptive behaviour (Lyons et al., 2010). During these times acoustic tremor has been recorded with both harmonic and non-harmonic frequency spectra (Lyons et al., 2013; Diaz-Moreno et al., 2020). Acoustic tremor is caused by the continual vibration of the atmosphere, and commonly lasts at Fuego between minutes and hours (Diaz-Moreno et al., 2020). The sources to acoustic tremor have been suggested to range from the excitation of the lava-gas mixture inside lava tubes, such as at Kīlauea (Garcés et al., 2003), the release of gas from unsteady shallow degassing of magma leading to resonance with good atmospheric coupling (Garcés et al., 1999; Fee et al., 2010), fluid flow instabilities (Garcés et al., 2003), magma resonance inside the conduit (Hagerty et al., 2000), the shallow, regular bursting of small gas bubbles (Ripepe et al., 1996; Hagerty et al, 2000; Jolly et al., 2016), a Helmholtz resonator (Goto and Johnson, 2011), or flow of high-pressure gas passing through an opening (Hagerty et al, 2000). Harmonic tremor is distinguished from non-harmonic tremor by the presence of regularly spaced peaks (i.e., harmonics) in its frequency spectrum at integer multiples of the fundamental frequency. Harmonic tremor typically exhibits amplitude modulated waveforms compared to the more erratic appearance of non-harmonic tremor (Figure 4.2). These differences have been attributed to differences in gas dynamics within the shallow conduit, ranging between random gas supply for non-harmonic tremor and periodic supply for harmonic tremor (Girona et al., 2019). The determination factors for the different flow rates which produce either harmonic or non-harmonic tremor are not known, however it is plausible that the likely factors are due to the geometry of the vents, the composition of the gas and ash mix being released, and the changes occurring to the forces within the system. Diaz-Moreno et al. (2020) have described the seismic and acoustic tremor observed at Fuego during May 2018, only weeks before the June 2018 paroxysm, reporting events lasting up to an hour in duration with both harmonic and non-harmonic character. They also recorded chugging, a quasi-periodic form of harmonic acoustic tremor, which occurs as a series of short repose repeating explosions, emitting a noise similar to that of a steam train. Lyons et al. (2013) proposed an interpretation of the switching between seismic tremor and seismo-acoustic tremor at Fuego based on analogue experiments. They noted that the viscosity of magma is a key factor in controlling whether tremor is expressed seismically or seismo-acoustically, as higher viscosities allow for the establishment of stable pathways through which gas can escape. They proposed that the occurrence of different tremor styles at Fuego is an indicator of changing magma properties and could be controlled by the stiffness of the magma due to the amount it has degassed.

Lava flows are also a common feature of background level activity at Fuego (Lyons et al., 2010; Naismith et al., 2019; Aldeghi et al., 2019). Individual lava flows can last on the order of days to weeks (e.g., GVP, 2019c; 2020a), whereas periods in which lava flows are active can last for several months. Increased lava flow activity is an indicator of higher extrusion rates and occurs when the crater has been filled by the building of an ephemeral cone, leading to overspill. It has been thought that the presence of lava flows has links to paroxysmal eruptions, often preceding these larger events (Naismith et al., 2019).

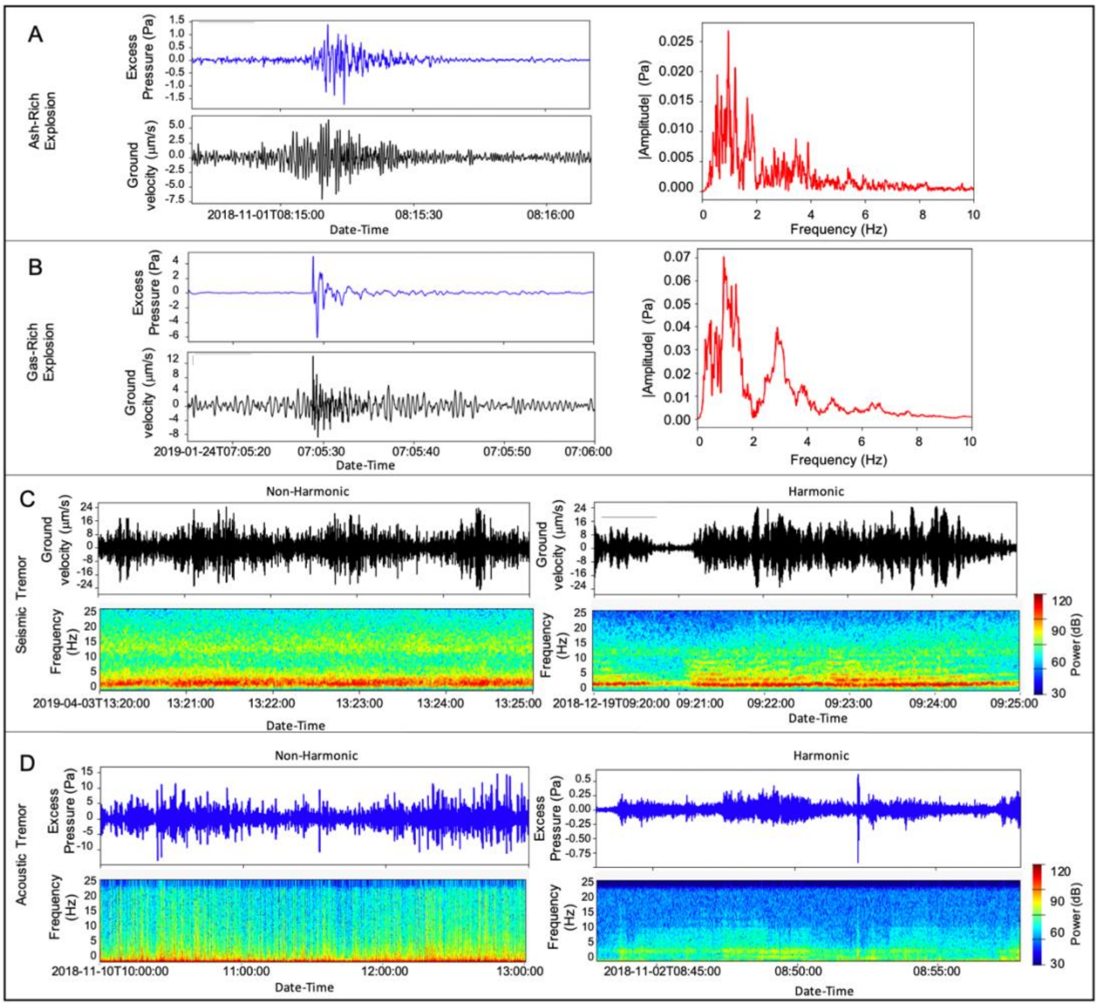

Figure 4.2. *Example waveforms and spectral information for common volcanic events. A) Ash-rich explosion: acoustic waveform (blue, top left), seismic waveform (black, bottom left), frequency spectrum for acoustic signal (red, right). B) Gas-rich explosion: acoustic waveform (blue, top left), seismic waveform with ground coupled-airwave (black, bottom left), frequency spectrum for acoustic signal (red, right). C) Seismic tremor: Seismic waveforms (black, top) and spectrograms (bottom), non-harmonic tremor variant on the left, and harmonic variant on the right. D) Acoustic tremor: Acoustic waveforms (blue, top) and spectrograms (bottom), non-harmonic tremor variant on the left, and harmonic variant on the right.*

4.3.2. Multi-Parameter Observations

Geophysical and field data collected over long periods of time have been used at volcanoes worldwide to identify and evaluate cycles and phases of activity, including seismic (e.g. Hagerty et al., 2000; Lyons et al., 2010; Rivet et al., 2014; Richardson et al., 2014; Carter et al., 2020), acoustic infrasound (e.g. Hagerty et al., 2000; Richardson et al., 2014), gas measurements (e.g., Symonds et al., 1996; Chiodini et al., 2010), ground deformation (e.g. Poland et al., 2006; Parker et al., 2014; Rivet et al., 2014; Chen et al., 2017), thermal infrared (e.g. Wooster, 2001) and petrological studies (e.g. Beard and Borgia, 1989; Reubi et al., 2019; Liu et al., 2020). These data allow investigations into the background activity as well as providing a record of larger eruptive events. The analysis of these data can help to unravel the complex dynamics of processes occurring within the shallow volcano plumbing, and to identify key parameters, which can assist risk mitigation efforts and testing new eruption forecasting algorithms.

The joint use of seismo-acoustic data is becoming ever more common within the volcano monitoring community as a way to continually track the state of activity (e.g., De Angelis et al., 2012; Fee et al., 2020; Carter et al., 2020). Seismo-acoustic networks can improve the reliability of the recordings compared to single station monitoring, enabling events to be located, increase the signal-to-noise ratio of event signals, and filter out non-volcanic sources of seismic and acoustic energy. As well as for monitoring purposes, networks have been used to characterise and model eruption plumes (e.g., Prejean and Brodsky, 2011; De Angelis et al., 2016), characterise source mechanisms (e.g., Neuberg et al., 1998; Chouet et al., 2005; Kim et al., 2014), and map the internal plumbing system (e.g., Lyons and Waite, 2011; Brengruier et al., 2014). Continuous records from dense networks of seismo-acoustic sensors produce large quantities of data, pose a challenge for manual analysis aimed at detecting and classifying events of interest, including explosions, tremor, rockfalls, volcano-tectonic earthquakes and lahars. In recent years it has become increasing commonplace that catalogues of seismic and acoustic data are constructed through automatic detection and classification algorithms (e.g., Stephens and Chouet, 2001; Scarpetta et al. 2005; Green and Neuberg, 2006; Langer et al. 2006; Umakoshi et al., 2008; Hammer et al. 2013; Carter et al., 2020).

Satellite data are also becoming an ever-growing resource for volcanologists, in particular for the study of volcanoes in remote regions and where access is difficult owing to their harsh environment. Although satellite data can often have poor temporal resolution, they can give clarification to ground-based measurements and show with high spatial resolution the impact of events. Common uses of satellite data to track the activity at volcanoes includes visual, and banded optical images (e.g. Dean et al., 2002; Aldeghi et al., 2019); ground deformation (e.g. Lanari et al., 1998; Wadge et al., 2011; Ebmeier et al. 2012); gas release (e.g. Pardini et al., 2019); thermal monitoring (e.g. Dehn et al., 2000; Ganci et al., 2012; Coppola et al., 2016); and plume monitoring (e.g. Dean et al., 1994;

Grainger et al., 2013). As satellites record data with every overpass, long-term datasets can be obtained to recognise trends and patterns in the activity, as well as identify significant events occurring at the vent.

Between 1st October 2018 and 29th October 2020, The Instituto Nacional de Sismologia, Vulcanologia, Meteorologia e Hidrologia (INSIVUMEH) deployed, with the assistance of numerous international partners, a network of seismic and acoustic instruments to monitor activity at Fuego (displayed in Figure 4.1 and detailed in Appendix A2.2). The new equipment recorded the occurrence of a paroxysmal event in November 2018. Throughout 2018-2020, activity followed the characteristic patterns described in previous studies (e.g., Nadeau et al., 2011; Brill et al., 2013; Brill et al., 2018; Naismith et al., 2019). Ground-based visual observations suggest between 2 and 32 explosions occurring per hour (e.g., GVP, 2019a; 2020b). During this time, we used satellite images in conjunction with seismo-acoustic data and ground based observations to obtain information about the levels of crater infill, as well as to confirm and monitor the presence of lava flows in the barrancas along the flanks of Fuego.

In this manuscript, we report on the waveform types recognized in the seismo-acoustic data, and analyse the catalogue of 99,618 explosions, 6,048 seismic tremor events and 2,200 acoustic tremor events detected by an automatic detection algorithm. We will discuss 6 separate phases of activity observed over the 2 years of data. We will demonstrate that the use of multi-parameter data, complemented by visual observations, can improve the identification of separate phases of activity, and that the joint analysis of seismic and acoustic data offers a unique insight into shallow conduit processes at open-vent volcanoes such as Volcán de Fuego.

4.3.3. Energy Release From Volcanic Events

Not all energy released from volcanic events is radiated through the ground or atmosphere, as several processes occur at the source of the explosion including the fractionation of magma, ejection of pyroclasts, and frictional heating between moving particles (Alatorre-Ibargüengoitia et al., 2010). Furthermore, unknown amounts of energy can also be contained within the conduit via reflection with the conduit walls (Garcés et al., 1998; Garcés and Hansen, 1998; Rowe et al., 2000; Johnson and Aster, 2005), limiting the amount of energy which is radiated out and recorded at stations a further distances away. The remaining energy which is radiated to the surroundings is split between acoustic and seismic wave propagation.

Acoustic propagation of energy is caused by perturbations of the atmosphere causing changes in atmospheric pressure. This can be caused by a range of sources, but in the case of volcanic acoustic emission is generated by an accelerating multiphase fluid (Johnson and Aster, 2005) which is caused by the fragmentation of magma (Palacios et al., 2016) during explosions, or sustained gas release through cracks during tremor. The amount of energy propagated into the atmosphere during an explosion is a function of the total energy release at the source during the event, and the coupling of this source with the atmosphere. The source of acoustic waves can be modelled as a monopole (mass flux variations), dipole (solid-fluid interactions) or a quadrupole (fluid-fluid interactions) source (Woulff and McGetchin, 1976). For simplicity, the source of acoustic wave propagation is often assumed to be a monopole for energy calculations (e.g., Johnson and Aster, 2005).

Seismic radiation of energy is attributed to the transfer of elastic energy through the ground (Johnson and Aster, 2005), which in volcanic settings can be initiated by pressure or shear sources (Green and Neuberg, 2006). In volcanic settings, the source of seismic radiated energy has been attributed to sources including the stick slip motion of magmatic plugs in a conduit (Green and Neuberg, 2006; Dmitrieva et al., 2013; Hotovec et al., 2013), the resonance of fluid filled cracks causing oscillation of the cracks during the upward migration of the fluids (Chouet, 1988; 1996, Balmforth et al., 2005; Julian, 1994; Lipovsky & Dunham, 2015), the coalescence of bubbles (Ripepe & Gordeev, 1999), and the fragmentation of magma when gas bubbles burst (Palacios et al., 2016). The amount of seismically radiated energy depends on several factors including the energy stored before release at the source of the event, efficiency of the source, and the coupling of the source with the surrounding rock.

For volcanic explosions, the common source for both acoustic and seismic radiation of energy is typically attributed to the fragmentation of magma (Palacios et al., 2016). For tremor events, although they can be restrained to just seismic or acoustic radiation by the range of different sources mentioned above, for the investigation of energy splitting, we only consider tremor events which occurred simultaneously on both the acoustic and seismic records. Seismo-acoustic tremor must be produced by a source which both causes a resonance of the ground, while sustaining an emission of gases into the atmosphere. This could be explained by fissures opening and releasing gas which has built up at depth from under a plug, which resonate as the gases flow through, or from acoustic tremor which has a strong ground coupled airwave (Ichihara et al., 2012; Matoza and Fee, 2014).

The partition of energy between acoustic and seismic radiation has been observed to vary at several volcanoes, such as at Stromboli (Ripepe et al., 1993), Etna (Sciotto et al., 2011); Karymsky (Johnson and Lees, 2000; Johnson and Aster, 2005) and Erebus (Rowe et al., 2000; Aster at al., 2003; Johnson, 2003; Johnson and Aster, 2005). Although there is usually a positive correlation between seismic and acoustic energy (e.g., Johnson and Aster, 2005; Palacios et al., 2016) the volcano acoustic-seismic ratio (VASR) can differ over several orders of magnitude (e.g., Johnson and Aster, 2005). Johnson and Aster (2005) argue that the changes in VASR can be attributed to the source conditions, including the geometry of the conduit and vent, the dimensions of the source, the magma characteristics, and the amount of disruption caused to the system during an event. They claim that an increase in VASR (therefore a relative increase in the acoustic energy compared to the seismic energy) could occur if there is a decrease in the density of the plume due to a density-dependency on the transfer of kinetic energy or a high impedance contrast between the magma with the conduit walls which increases the reflection of seismic energy (cf. Garcés et al., 1998; Rowe et al., 2000). They also claim an increase in VASR could occur from a shorter/wider conduit which loses less acoustic energy to viscous flow than a longer/thinner conduit which can more effectively transmit seismic energy, and that a smaller source region would increase the VASR by increasing the pressure contrast at the onset of the event. Lab experiments by Lyons et al. (2013), investigating the switching between seismo-acoustic and purely seismic tremor, concluded that the stability of the gas pathways due to the magma viscosities was the main factor in determining if tremor would be purely seismic or seismo-acoustic. The magma viscosities therefore will contribute to the changes in VASR as the proportion of the acoustic signal will vary depending on the stability of the pathways to the atmosphere. When the conditions at a volcano remain constant, the VASR remains stable, however variable conditions or processes at the source will cause the VASR to alter in response.

In this study, we will use the VASR to investigate the different seismo-acoustic events at Fuego, as well as how the style of eruption changes through time due to the energy split changes that occur at the source of the events and infer how the changes in the VASR relate to the source properties at Fuego.

4.4. Multi-Parameter Data

4.4.1. Ground-Based Visual Observations

Visual observations are routinely performed by the observatory at Fuego, which is managed by INSIVUMEH, and published in bulletins accessible from the Global Volcanism Program website (www.volcano.si.edu). The observers document the frequency of explosions, estimates of the plume heights and description of the plume, presence and height of any incandescent material ejected, ash-fall locations, if shockwaves have been produced, lava flow lengths and locations when active, and drainage channels which have had lahars flow (e.g., GVP, 2018e; 2019a; 2019b; 2019c; 2020a). Although these reports can vary in detail, they provide valuable information about surface activity that complements the instrumental records. The reports are limited to times when the activity is visible. The use of these visual observations allows for the link between different event types and their geophysical signals, so that with only the signals, it is possible to determine what events are occurring (Figure 4.3).

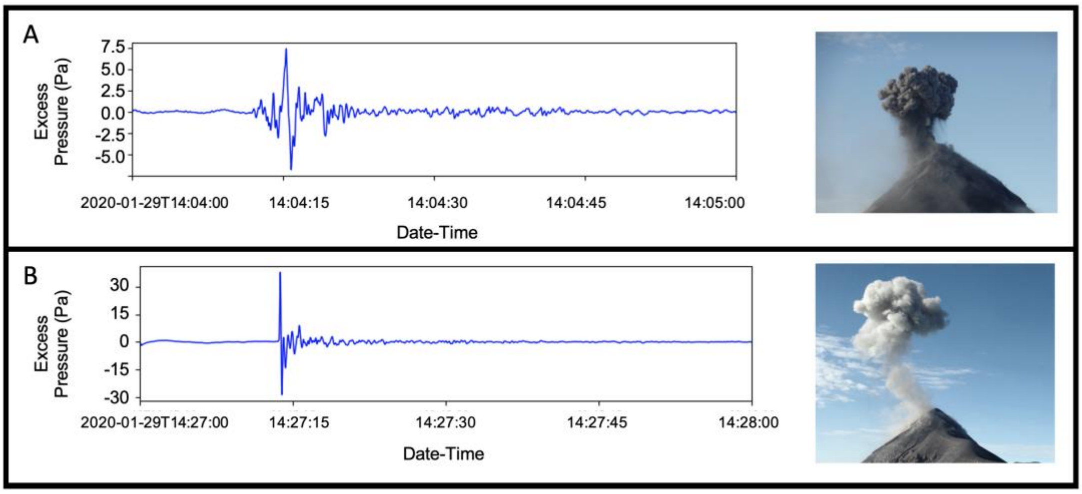

Figure 4.3. *Explosion acoustic waveforms and visual observations. A) Ash-rich explosion from January 2020. B) gas-rich explosion from 2020. Both events occurred within the same day with acoustic recordings taken from the same station.*

4.4.2. Seismo-Acoustic Network

Between 1st October 2018 and 29th October 2020, a network of seismo-acoustic arrays was deployed around Volcán de Fuego. Combined, they provide a long-term record of the activity at the volcano. In total, 22 infrasound sensors and 8 seismometers were deployed across 8 sites (Figure 4.1; FG3, FG8, FG10, FG11, FG12, FG13, FG14, FG16).

The infrasound sensors are Chaparral M64 (sensitivity of 9 mV/Pa) and iTem prs100 (sensitivity of 0.4 V/Pa) microphones, located at distances between 3 and 12 km from the vent. Data are recorded at 50 Hz with 24-bit resolution. All seismometers are Nanometrics Trillium T120 compact broadband instruments (T =120 s, sensitivity of 750 V/ms^{-1}), also recorded at 50 Hz using either CENTAURUS or EDR209 digitizers.

Four additional acoustic stations were deployed during the week of November 27th – December 3rd 2018, shortly following the paroxysm in November 2018. The sensors at these stations used Chaparral M60 (sensitivity of 9 mV/Pa) and IST2018 (sensitivity of 20 mV/Pa) microphones. The sampling rate was set at 100 Hz with 24-bit resolution using DiGOS DATA-CUBE digitizers.

4.4.3. Satellite Observations

In this study, we take advantage of data from the Sentinel 2 satellite, accessible through the sentinel hub online browser (www.sentinel-hub.com), to track lava flows and assess the level of crater infill by the ephemeral cone. Satellite imagery, using optical and short-wave infrared (SWIR) bands were used to confirm lava flow observations made on the ground, and allow for observations of the crater to be made which are not possible from the ground (Figure 4.4). Images are taken at each overpass, which occurs every five days. We used images clear of cloud cover, which reduced the temporal resolution of images, leading to large gaps in data, especially during the rainy season. The high spatial resolution of images, however, allowed for the observation of crater infill to be made in the optical range, and activity and lengths of lava flows to be measured in SWIR.

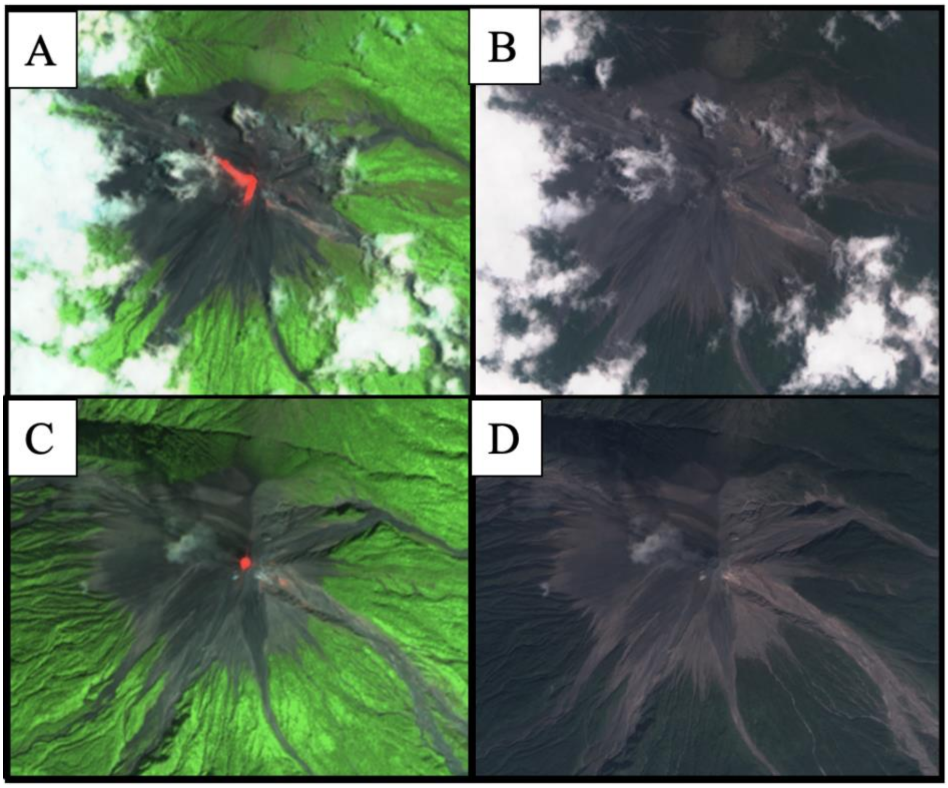

Figure 4.4. *Satellite images of Volcán de Fuego. A and B are images from 24-04-2020 (Modified Copernicus Sentinel data [2020], Sentinel Hub), and C and D are images from 16-12-2018 (Modified Copernicus Sentinel data [2018], Sentinel Hub). A and C are short-wave infrared images, highlighting magma close to the surface and lava flows. B and D are true colour images which are useful to view crater fill*

4.5. Seismo-Acoustic Signals

Fuego produces different types of activity with a clear seismic and/or infrasound signature. These signals include vent activity such as explosions, rockfalls, pyroclastic flows, and internal activity such as tremor and volcano-tectonic earthquakes. In this section we outline and describe the activity that will be the focus of this study, giving details on the signals which are recorded by the seismic and acoustic sensors.

Explosions

Explosive Strombolian-type activity commonly occurs at Fuego at rates between 2 and 32 per hour (e.g., GVP, 2019a; 2020b). These discrete explosions release plumes with variable proportions of ash and gas, commonly to heights of 500-1,000 m above the vent, and eject incandescent material to heights of 300 m (e.g., GVP, 2018e; 2019a; 2019c; 2020a; 2020b). The explosions typically fall into two categories, ash-rich and gas-rich, based on the relative amounts of tephra and gas in the plume. The two explosion types are clearly identified in seismic and acoustic data through appropriate waveform parameterization (Brill et al., 2018).

Ash-rich explosions produce plumes that are usually dark grey owing to a higher volume of tephra. Ash-rich explosions typically have longer durations lasting between 7 and 15 s before amplitudes return to background noise levels (Figure 4.2A). These signals tend to have emergent onsets, although typically occur with a compressive first arrival, and peak amplitudes occurring approximately 2 to 5 seconds after the onset of the explosion. The energy of the ash-rich explosions is generally concentrated in the 0-2Hz band, peaking at 1Hz. (Figure 4.2A).

Gas-rich explosions are short-lived events (durations < 7 s) associated with plumes that are typically light grey, sometimes with a blue hue to them. These explosions create acoustic signals displaying high amplitude, impulsive and compressive onsets followed by a low amplitude coda that returns quickly to background levels (Figure 4.2B). It is common for gas-rich explosions to also generate shock waves (e.g., GVP, 2019a; 2019c; 2020a) caused by large overpressure build-up within the shallow conduit, with a wavefront that travels at supersonic speeds. Shockwaves are observed to have a much larger amplitude acoustic onset than a typical gas-rich event, showing a characteristic 'N' shape wavelet. Shockwaves have been observed to produce excess pressures of up to 100 Pa at distances up to 7.5 km from the vent. In the frequency domain it can be seen that most of the energy of a gas-rich explosion is contained between 0 and 2 Hz, peaking at ~1 Hz. A key feature that separates gas-rich explosions from ash-rich is a second peak of energy observed at 3 Hz, after a drop in the energy at 2 Hz. There is very little energy above 4 Hz (Figure 4.2B).

The seismic signals associated with ash-rich explosions have longer durations than their acoustic counterparts (Figure 4.2A), usually lasting between 30 and 60 s. The waveforms are emergent and tend to be symmetric, where the increase to the maximum amplitude is reflected in the following waning of the signal back to baseline levels. The energy of these waveforms is concentrated within a narrow band in the frequency domain, peaking near 2 Hz; there is little-to-no energy above 4 Hz.

The seismic record for both gas- and ash-rich explosions shows the presence of ground coupled airwaves (GCA) (Figure 4.2B). A GCA is an acoustic wave that has travelled along the boundary layer between the ground and atmosphere, often in the form of a Rayleigh or Stoneley wave and has sufficient energy to be observed in the seismic record (Edwards et al., 2007; Ichihara et al., 2012).

The explosions are sometimes divided with a third class, namely extended explosions. These are explosions which are produced with multiple pulses of either gas- or ash-rich explosions, lasting longer than an explosion with a single pulse. We have not separated this class in this study but have kept them classified as either gas- or ash-rich explosions.

Tremor

Tremor at Fuego is detected in both the seismic (Lyons et al., 2010; Lyons and Waite, 2011, Nadeau et al., 2011; Brill et al., 2018) and acoustic data (e.g., Lyons et al., 2013; De Angelis et al., 2019; Diaz-Moreno et al., 2020).

Seismic tremor at Fuego can be either harmonic or non-harmonic, with non-harmonic tremor being more commonly observed. Most tremor episodes range in duration between a few minutes and a day. Tremor is traditionally defined as a period of sustained increase in seismic amplitude. It is not uncommon for explosions to occur during a tremor episode. At Fuego, non-harmonic seismic tremor is restricted to frequencies between 1 and 4 Hz, peaking at 2 Hz, whereas harmonic tremor typically displays a fundamental frequency between 1.5 and 3 Hz and up to 4 overtones (Figure 4.2C). The fundamental frequency is generally stable, although spectral gliding is observed at times.

Acoustic tremor has been documented at Fuego (Lyons et al., 2013; Diaz-Moreno et al., 2020), and similarly to seismic tremor can be either harmonic or non-harmonic. Non-harmonic acoustic tremor occurs more regularly than harmonic tremor, and episodes can range in duration from ~10 mins to over a day in length. The frequency of acoustic non-harmonic tremor mostly peaks at 1 Hz, with limited energy radiated above 4 Hz. The fundamental frequency of harmonic acoustic tremor is in the range between 1.5 – 2 Hz and is typically consistent through time (Figure 4.2D). It is noticeable that when explosions occur during a tremor episode, the fundamental frequency glides in the build-up, decreasing in frequency. Due to attenuation in the atmosphere, we typically only observe one or two overtones.

4.6. Catalogued Data

4.6.1. Vent Observations

Based on observations from the weekly bulletin reports and the sentinel satellite images, we compiled a chronology of the status of the summit crater at Fuego, including times when the crater was emptying or empty and periods when the crater was filling, full or over-spilling through lava flow activity (Figure 4.5). This time-history of the state of the vent helps to correlate the characteristics of geophysical signals with the observed surface activity at the volcano. As there is limited information on lava flow lengths, we could not make inferences on effusion rates or lava flow volumes, and so do not attempt to extrapolate this information from the observations.

4.6.2. Seismo-Acoustic Network Catalogues

The seismo-acoustic data were processed by an automatic detection and classification algorithm to produce catalogues of events. The details of the algorithm production and application to the network data at Fuego can be found in the supplementary material (A1.1). The automatic detection and classification algorithm produced an extensive catalogue of explosions and tremor events, including 99,618 explosions, 6,048 seismic tremor episodes and 2,200 acoustic tremor episodes. The full catalogues of explosion and tremor events can also be found in the supplementary records (A3.2 – A3.4). Here, we describe the results of the automatic detection and classification algorithm.

Explosions

Figure 4.4C shows the number of weekly detected explosions and the cumulative weekly acoustic energy released. We observe that over the course of the recording period the number of explosions varies although without following a regular pattern. The weekly energy output stays relatively constant, with the exception of the high energy output following the paroxysm in November 2018. Given that the overall energy remains largely constant, yet the number of weekly events varies between 700 and 2000, the data suggests that the mean explosion energy changes through time, with periods of many low energy explosions, and periods of fewer high energy explosions.

The explosions at Fuego were classified into two categories: ash-rich and gas-rich. We plot the number of ash-rich and gas-rich events per week in Figure 4.5D to show how the dominance of each explosion type changes through time. Over the course of the recording period, the classification algorithm catalogued 42,468 gas-rich events and 57,150 ash-rich events. It can be seen that the ash-rich events are commonly more present throughout the study, however there are several periods in which the gas-rich events are either produced at a similar rate to the ash-rich or become the dominant type for several weeks. As with the total number of explosions, there does not appear to be any identifiable trend or pattern to the changes observed in the number of gas- or ash-rich explosions.

Tremor

Our detections show that both acoustic and seismic tremor occur regularly at Fuego. Seismic and acoustic tremor can be observed to occur either at the same time, or separately, with the latter being most common. As tremor can range in duration from the order of minutes to hours or days, we plot the weekly duration of the tremor, rather than the number of individual events (Figure 4.5E and 4.5F for acoustic and seismic tremor, respectively). We also show the cumulative weekly energy radiated by tremor.

Acoustic tremor durations vary between 30 and 120 hours per week. We observe slow increases in duration over the course of several months up to maximums in December 2018, December 2019, and June 2020, with drops in the duration shortly after these maximums occur. The energy propagated through acoustic tremor is mostly constant through time, with the exception of a period of ~4 months following the November 2018 paroxysm. This shows that the acoustic tremor cycles through times of highly energetic, but reduced occurrence, activity, and periods of higher activity with reduced energy.

For seismic tremor, durations vary between 10 and 80 hours per week. It can be noticed that the general trend in the seismic tremor appears to have a quasi-sinusoidal pattern (Figure 4.5F), transitioning slowly between the peaks in May 2019 and July 2020 and a minimum in September 2019. The energy release pattern for seismic tremor mirrors that of its duration, indicating that the average energy of seismic tremor is consistent through time, unlike the energy of explosions and acoustic tremor.

4.6.3. Energy Calculations

For each event, explosion or tremor, we calculated the energy at all stations which made a detection. The energy of an explosion is split between energy radiated in the atmosphere and through the ground. For simplicity, the seismically radiated energy can be described by the elastic energy produced by an isotropic source, at the surface of a homogeneous half-space (Boatwright, 1980; Johnson and Aster, 2005), and the acoustically radiated energy can be defined as being proportional to the square of the excess pressure, divided by the air density and acoustic wave speed (Pierce, 1981) assuming isotropic radiation from a monopole point source (e.g. Firstov and Kravchenko, 1996; Johnson, 2003; Vergniolle et al., 2004; Johnson and Aster, 2005). The seismic energy, E_s, is given in Equation 2.1, and the acoustic energy, E_a, is given by:

$$E_a = \frac{2\pi r^2}{\rho_{atmos} c_{atmos}} \int \Delta P(t)^2 dt \qquad (4.1)$$

where ρ_{atmos} is the density of the atmosphere, C_{atmos} is the acoustic wave velocity and ΔP is the excess pressure in the atmosphere, compared to base-level atmospheric pressure.

The data were filtered before calculating seismic and acoustic energies in order to minimize the effect of noise. We used a bandpass filter between 0.2 Hz and 6 Hz for the acoustic data, and between 0.2 Hz and 10 Hz for the seismic data. To account for unknown site effects and attenuation, we calculated a network energy by using the median of all energy calculated at individual sensors.

4.6.4. Energy Partitioning and Acoustic-Seismic Ratio

When volcanic activity occurs, the energy released is radiated through both the atmosphere and the ground (Hagerty et al., 2000; Rowe et al., 2000; Aster et al., 2003; Johnson et al., 2003; Johnson and Aster, 2005; Palacios et al., 2016). The partitioning of the energy can vary, through time as well as for different event types, depending on source characteristics, including source depth and conduit geometry, reflective index of the conduit walls, energy consumed during fractionation, and the coupling between the source and the atmosphere (Johnson and Aster, 2005). Calculating the volcano acoustic-seismic ratio (VASR) time over time can shed light on changes to these parameters, while comparing the VASR for different event types can indicate differences in the source mechanisms.

Seismic and acoustic indices, rather than energies, can be used to determine how intense the signal is averaged over a period of time. Therefore, the intensity of a short duration event can be easily compared to that of a long duration event, despite differences in the overall energies. The seismic and acoustic intensities are time-dependent (Palacios et al., 2016). Thus, the seismic intensity is given as:

$$I_s(t) = \frac{E_s}{\Delta T} = \frac{2\pi r^2 \rho_{earth} c_{earth}\, S^2}{A\, \Delta T} \int U(t)^2 dt \tag{4.2}$$

Where I_s is the seismic intensity and ΔT is the window length, and the acoustic intensity is given as:

$$I_a(t) = \frac{E_a}{\Delta T} = \frac{2\pi r^2}{\rho_{atmos} c_{atmos}\, \Delta T} \int \Delta P(t)^2 dt \tag{4.3}$$

Where I_a is the acoustic intensity. The acoustic and seismic intensities can be compared to obtain the time independent volcanic acoustic-seismic ratio through the equation:

$$\eta(t) = \frac{I_a(t)}{I_s(t)} \tag{4.4}$$

Where η is the VASR. We used the VASR on a rolling window to see how the split between seismic and acoustic intensities changes through time. For our calculations, we used co-located seismic and acoustic sensors at station FG12, allowing us to cancel out the terms relating to the distance, and used the same length window for both seismic and acoustic indices to cancel out the window length terms from the calculation and therefore also show the energy split between the atmosphere and ground. Higher VASR values refer to a higher proportion of energy propagated through the atmosphere, while lower VASR values relate to increased proportion of energy propagation through the ground.

Event VASR

The seismic and acoustic energies for each event detected in the explosion and tremor catalogues were calculated and plotted against one another in Figure 4.6. It can be seen that the partitioning of seismic and acoustic energy varies depending on the event type. For explosions, we observe a clear difference between clusters of gas-rich and ash-rich events, with gas-rich events mostly clustering between a VASR of 0.1 and 10, with a median VASR of 1.08, while ash-rich events cluster mostly between a VASR 0.1 and 1, with a median VASR of 0.46. These VASR clusters indicate that gas-rich events tend to radiate energy with roughly an even split in the atmosphere and ground, whereas the ash-rich events usually have between an even split of energy and ten times the energy transmitted through the ground than the atmosphere. The two clusters are statistically independent of one another, with a p-value of 0.047 obtained through an independent t-test, showing that the two event types are independent to a significance level of 5%.

Volcanic seismo-acoustic tremor (VSAT), which are tremor events which occur both seismically and acoustically, simultaneously, are clearly separated from explosions (Figure 4.5). The VSAT does not cluster as tightly as the explosion events, but rather is spread over several orders of VASR, ranging as low as 0.1, and as high as 100, with a median VASR of 3.69, showing that the energy output from tremor can range between having a seismic signal 10 times more energetic than the acoustic signal, and acoustic signals with 100 times the energy than seismic in different events.

Moving Time-Averaged VASR

We calculated the VASR at station FG12 over the study period when both seismic and acoustic stations were active. The resulting moving time-averaged VASR is shown in Figure 4.5B The VASR typically varies between values on the order of 10^1 and 10^3, and clearly shows periods of higher and lower VASR, and periods in which there is a transition from high to low, or vice versa. The VASR is typically ranges between 10^1 and 10^3 which shows that the acoustic intensity is predominantly larger than the seismic intensity.

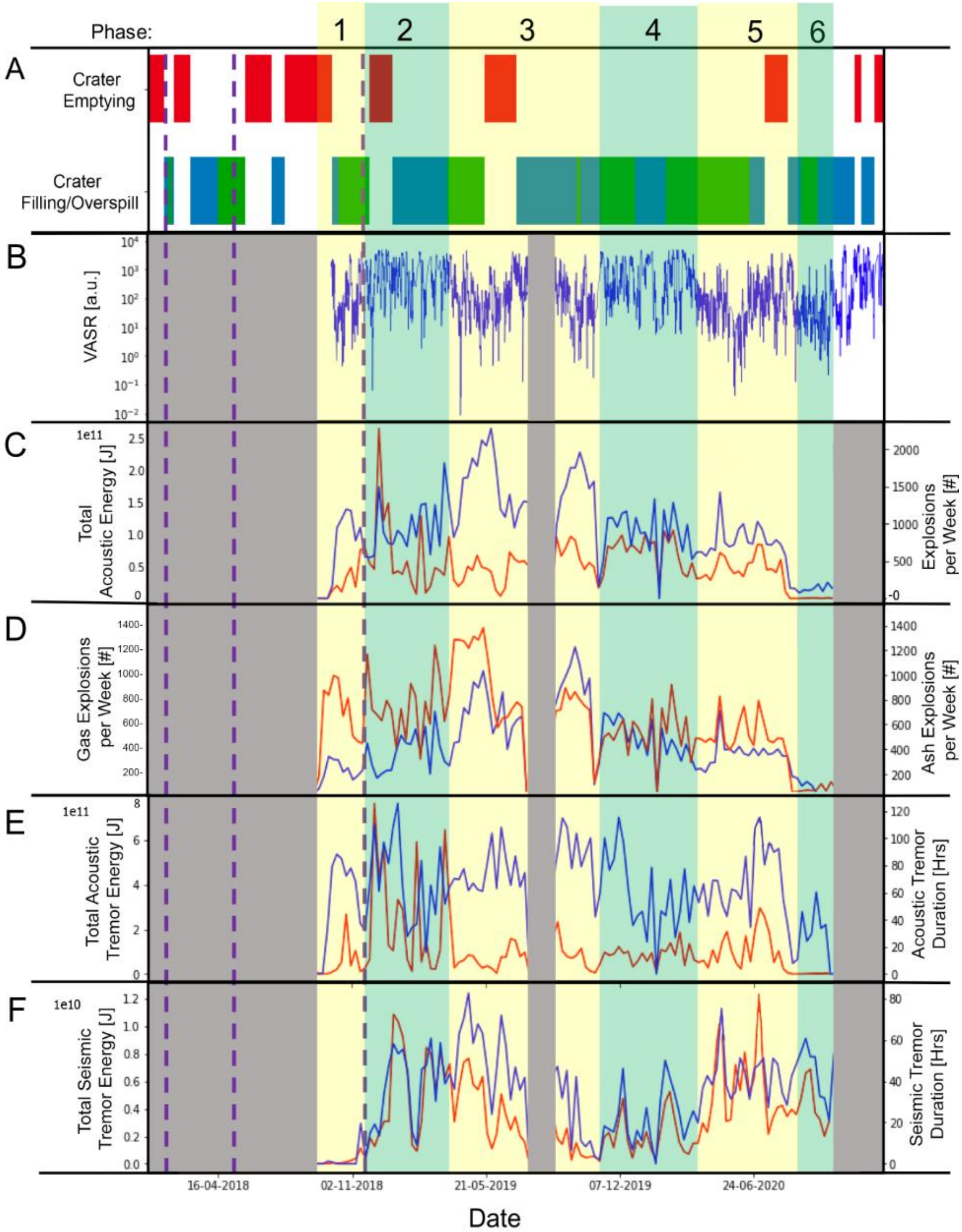

Figure 4.5. *Long-term multiparameter activity at Volcán de Fuego. A) Crater fill and lava flow activity. Periods in which the crater is being emptied through ejection of material from rockfalls and explosions highlighted by red bars, periods in which the crater is being filled highlighted by blue bars or over spilling via lava flow activity highlighted by green bars when the crater is completely filled. B) Moving time-averaged volcanic acoustic-seismic ratio calculated at station FG12 with a window length of 1 hour. C) Number of explosions per week (blue) and the total acoustic energy output per week from the same explosions (red). D) Number of gas-rich explosions (blue) compared to the number of ash-rich explosions (red) as determined by the automatic classification algorithm. E) Weekly duration of acoustic tremor (blue) and the weekly acoustic energy associated with the tremor events (red). F) Weekly duration of seismic tremor (blue) and the weekly acoustic energy associated with the tremor events (red).*

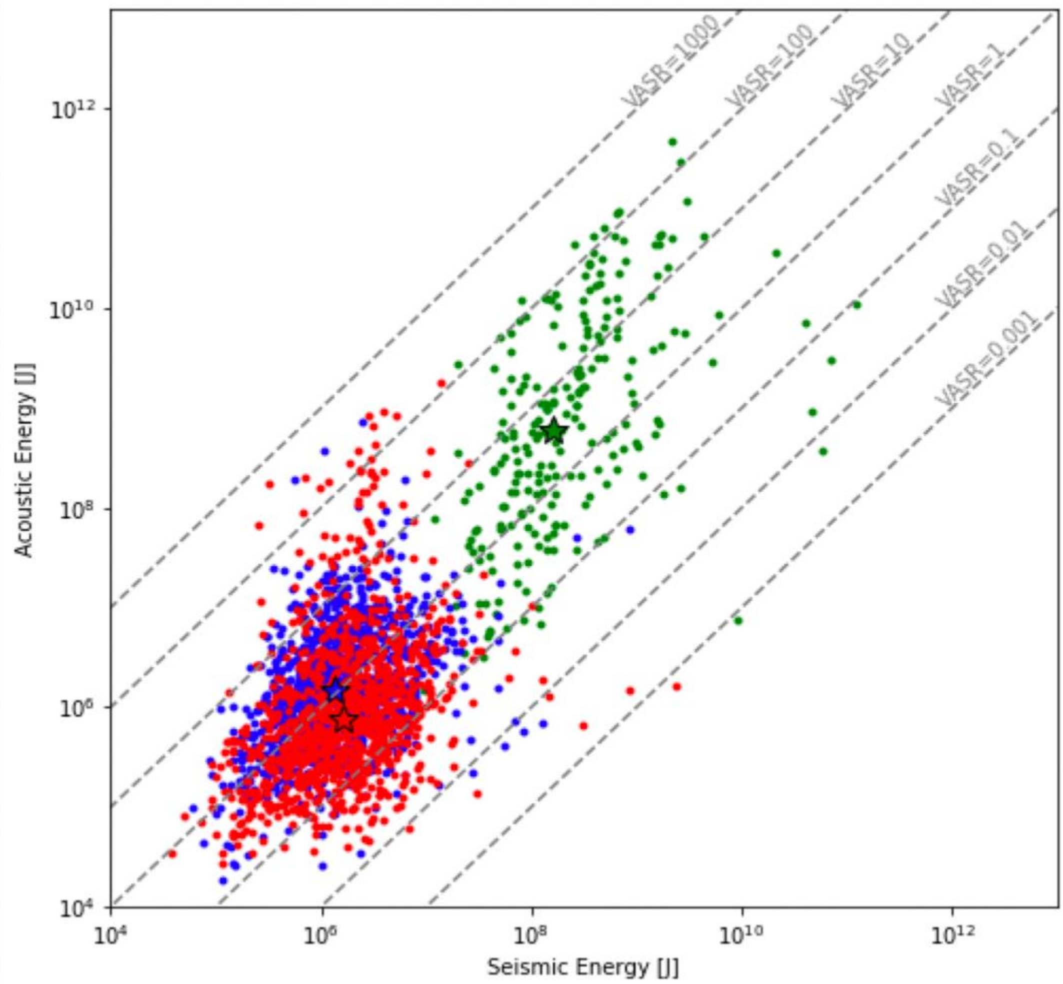

Figure 4.6. *Seismic vs acoustic energy for individual events. Red points show the ash-rich explosions, blue points show the gas-rich explosions, and green points show seismo-acoustic tremor. Red, blue and green stars show the median points for the ash-rich explosions, gas-rich explosions and seismo-acoustic tremor, respectively. Diagonal grey dashed lines show the lines of equal volcanic acoustic-seismic ratio, where the ratios are labelled in the top right.*

4.7. Discussion

4.7.1. Paroxysm Disruption to Baseline Activity

The paroxysmal events that occur at Fuego are the most important events to understand and monitor, given their associated hazards. By focusing on changes that occurred during phases 1 (pre-paroxysm build-up) and 2 (post-paroxysm restoring) (both highlighted in Figure 4.5), we may gain a better understanding of how the paroxysms disrupt the persistent, low-level, open-vent activity at Fuego.

Phase 1 represents the build-up to the paroxysm in November 2018, and phase 2 is related to the system returning to a stable baseline activity. The timing of the start of phase 1 could not be assessed as the seismic and acoustic data record starts in October 2018, when this phase was already ongoing. There are several models which describe possible mechanisms that cause the triggering of the paroxysms; these models suggest that the triggering mechanism can be either due to influx of magma, increased gases flushing through the system, or from pressure changes within the system. We focus here on three models suggested to be potential candidates to the triggering of the paroxysms at Fuego and link them to the geophysical observation reported in our study.

The first model is the collapsing foam model (Jaupart and Vergniolle, 1998), which suggests that a foam layer accumulates within the conduit and is the driving force for repeating Strombolian activity. The foam layer is unstable and causes paroxysmal activity when it collapses into an underlying gas slug, driving the fountaining of material in a high-energy event. This foam layer is thought to be required to reach a certain critical thickness in order for it to collapse (Vergniolle and Jaupart, 1986), which would put constraints on the time between paroxysmal events. The model also suggests that the evacuation of the foam layer from a paroxysmal event provides a volume which can consequently be filled in the following period. The observations we made following the November 2018 paroxysm show that the paroxysm caused an excavation of the dome, removing the ephemeral cone and providing space for effusion of magma to fill in the following phase of activity. Although it was suggested that this would lead to a decrease in activity while this refilling occurs, we observe the opposite; after the paroxysm we observe increased activity as magma from below replenishes the system, indicated by seismic tremor, as it migrates through the system and rebuilds the ephemeral cone, emitting high levels of acoustic tremor and producing explosions as exsolved gases are released. The model proposes that sufficient viscosity or gas flux through the system can allow a cycle of growth and collapse of the foam layer, consequently driving cyclic activity, which has been suggested could fit the observed cycles at Fuego (Diaz-Moreno et al., 2020). Liu et al., (2020) suggested that gas accumulation could have occurred in a process of gas-holdup in which the volume of the magma increases while the mass stays constant, and that the gas accumulation before the June 2018 paroxysmal eruption occurred beneath a low permeability plug which eventually failed. We observed that there was a drop in the rate of events for 2 weeks prior to the paroxysm in November 2018, which could be linked to a choking process linked to gas-holdup below a plug in the build-up to the eruption. A petrological study of eruption products at Volcán de Fuego by Liu et al., (2020) also proposes that the paroxysms have been predominantly gas-driven by gases exsolved from magmas deeper within the plumbing system; this is in agreement with the collapsing foam model of Jaupart and Vergniolle (1998). They attribute the degradation and collapse of a plug to a rise in paroxysmal energy mid-way through the June 2018 paroxysm. Liu et al., (2020) acknowledge however, that this gas could in part be due to fresh, volatile rich magma at depth which degasses as it rises, invoking the suggestion that a magma-driven model may also be occurring.

The second model we discuss is the magma driven, rise-speed dependent model by Parfitt and Wilson (1995) which proposes that the rise speed of material through the conduit is the controlling factor for the eruptive style. They propose that lower rise speeds allow for the coalescence of bubbles. When these bubbles reach the surface, they are able to burst, producing Strombolian activity. Higher rise speeds do not allow for as much coalescence due to a lower differential ascent rate between the magma and bubbles, which leads to the 75% volume threshold for fragmentation to be reached for run-away coalescence at depth, producing lava fountaining. This has been linked to previous observations at Fuego (Parfitt, 2004), as an increase in rise speed causes the Strombolian explosions to become more frequent and with larger energies, as observed in the build-up to the paroxysms at Fuego. The observations of cycles in which Strombolian activity is dominant between paroxysmal eruptions strongly support this model. Diaz-Moreno et al. (2020) state that as with the collapsing foam model, the rise-speed dependant model is capable of producing the cycles observed, and that both models are likely to cause magma stiffening and plug formation under which gases can accumulate before periodic release (cf. Johnson and Lees, 2000; Lyons and Waite, 2011).

Finally, Naismith et al., (2019) propose that for some paroxysms, a gravity-driven shedding model is applicable, with material removed from the ephemeral summit cone causing unloading and depressurisation of the conduit. During baseline activity, an ephemeral cone slowly accumulates through lava fountaining. With lava filling the crater and overflowing after the crater has been filled, the flow could destroy the cone when avalanches occur, removing enough volume to trigger a paroxysm via decompression of the magmatic system. For the November 2018 paroxysm, as well as the June 2018 event, lava flow activity is observed in the months leading up to the event. This model is in line with the decompression model proposed by Ripepe et al., (2017) for eruptions at Stromboli, which states that during pre-paroxysmal activity, magma-static effusive discharge leads to decompression within the magmatic system and ultimately a change in the equilibrium between shallow and deep magma sources, driving paroxysms as the magma undergoes exsolution of gases. Furthermore, Pardini et al. (2019) have attributed the trigger mechanism of the 1974 paroxysm to the shedding of material, which they infer led to the influx of deeper, fresh melt which caused the eruptive episode to occur. They also stated that this mechanism could also explain many other paroxysms at Fuego where the removal of mass occurs before the paroxysm.

Based on our observations and interpretations of the geophysical signals from before and after the November 2018 paroxysm discussed here, we suggest that the paroxysms are likely to have been triggered by a source that most closely resembles the collapsing foam layer model. This model seems to provide the simplest explanation to the observations of the effusion and the seismic and acoustic expression of activity, and most closely matched with the model of activity through the recording period which we provide in Figure 4.6.

Fuego is undergoing a period of high-frequency paroxysmal events, which started in 2015 (Naismith et al., 2019). However, from November 2018 to the time of writing this paper (Nov 2021), there has been an extended repose in the occurrence of paroxysms (cf. Liu et al., 2020). This pause in the paroxysmal activity could signal the end of this period of elevated activity, similar to between 2007 and 2012. It is also possible that the large June 2018 paroxysm (as the 2^{nd} most recent event) caused changes within the system (either a disruption to the repetitive cycle or a depletion of the triggering material or gases within the plumbing system), or that the volcano is currently building towards another large paroxysmal event. Our knowledge of how to project the current observations to give an indication of what will occur is limited, and only through continued monitoring will we be able to increase the ability to interpret the observations in relation to forecasting.

4.7.2. Seismo-Acoustic Energy Partition

A positive correlation can be observed between seismic and acoustic energy released by volcanic events (Figure 4.6), similar to the observations of Johnson and Aster (2005). This correlation allows us to make the assumption that the sources of both the seismic and acoustic energy are one common source. We have shown that the energy radiated by tremor, gas-rich and ash-rich explosions produce significantly different clusters of seismic vs acoustic energy. The statistical significant difference between ash-rich and gas-rich events shows that these two types of explosions can be viewed as separate event types, likely produced with differing mechanisms within the conduit, however, the overlap between the two clusters supports the argument that they are end members of a spectrum with varying amounts of ash entrained with in the plume due to the level of fractionation occurring at the source at the onset of the explosion. The different ratios observed for different event types (Figure 4.6), all which can occur within a short time frame, points to variations in the source processes as the factors which determine the VASR variations. These variations include the source dimension variability and the density-dependant energy transfer from the plume, which is likely a result of the amount of fragmentation within the source, controlling the volume of ash entrained within the plume. However, we also observed long-term variations in VASR (Figure 4.5B) between eruptive phases, which are most likely caused by systematic changes in the conduit and vent geometry including the presence or lack of an ephemeral cone, changes to the magma properties which will affect the impedance contrasts with the conduit walls, or the fragmentation efficiency.

4.7.3. Acoustic Tremor and Gas Release

The catalogue of events shows that acoustic tremor is a common feature at Fuego, occurring on a weekly basis with total weekly durations occurring no less than 20 hours per week, and peaking at 120 hours per week. Observations of gas release episodes seem to suggest that the tremor recorded by the seismo-acoustic networks is related to these episodes. Along with explosions (particularly gas-rich explosions) the presence of acoustic tremor therefore indicates that sustained gas release from the vent is occurring in fluxes large enough to cause atmospheric disturbances that can be recorded at stations over 12 km from the vent, and the durations act as a first order proxy to the amount of gas being released from the vent. High levels of gas release, occurring as a regular feature of vent activity at Fuego, has been observed and noted in many studies (e.g. Lyons et al., 2007; Lyons et al., 2010; Brill et al., 2018; Diaz-Moreno et al., 2020). It is only now through the long-term assessment of background activity with the addition of acoustic instrumentation that we have a measure of how common these episodes are, which now enables a more complete understanding of vent activity.

We see through time that the level of acoustic tremor varies, from high weekly duration with low average energy outputs, to low weekly duration with higher average energy outputs. These observations occur alongside the observations of smaller, but more frequent explosions vs less frequent but larger energy explosions, respectively. This suggests that the release of gas can occur on a scale between weak, slow release and a more vigorous release. The cause for the range in strength of gas release is likely due to the relation of several properties within the vent system. These could include porosity, permeability, magma viscosity, overpressure and effusion rate. It is not possible through the geophysical observations alone to determine which factors cause the varying energetics of acoustic tremor and explosions. Inclusion of data which can give inferences to the magma properties in phases which experience different styles of acoustic tremor could allow for a better picture of how the internal properties link directly to the surface activity to be obtained.

4.7.4. Conceptual Model for the Evolution of Activity

Our observations suggest that activity at Fuego during 2018-2020 can be divided into 6 different phases (Figure 4.5). Here, we identify each phase based on the dominant style of activity observed and report the key observations for each of these periods.

Phase 1 - Pre-paroxysm build-up (October 2018 - November 2018):
The VASR increases through phase 1, indicating a switch from releasing a higher share of energy seismically to acoustically (Figure 4.5). Lava overflows from the full crater through lava flows down the flanks. Two weeks prior to the paroxysm, during the first week of November, there was a drop in the level of activity of tremor and explosions, before the high-level activity observed during the paroxysm from the 18th to 20th of November.

The higher share of acoustic signals suggests that an increased level of gas release may be occurring throughout this phase, which in turn affects the magma viscosity and leads to the stalling of events in the 2 weeks prior to the paroxysm due to a choking of the conduit by the build-up of a plug causing increased overpressures (Sparks, 1997; Melnik and Sparks, 1999; Massol and Jaupart, 1999), which will have in turn led to the paroxysm in mid-November.

Phase 2 - Post-paroxysm restoring (December 2018 - April 2019):
This is the only phase where both the explosions and tremor have high amplitudes on both seismic and acoustic records. VASR remains high as acoustic output continues to be at a high level despite the high seismic energy during explosion and tremor events. After the emptying of the crater during the paroxysm, effusion slowly rebuilds the ephemeral cone. There is a larger proportion of gas-rich explosions within this phase.

The excavation of the crater during the paroxysm, followed by increased acoustic and seismic energy indicates that during this phase we may be observing signals from a greater depth. This is implied by the increased seismic tremor which indicates increased magma migration (Chouet, 1988), and increased acoustic energy indicates high levels of gas release (Garcés et al., 1999; Fee et al., 2010), which is possibly from a fresh volume of volatile rich magma ascending after the removal of high overpressures when the crater emptied during the paroxysm.

Phase 3 - Return to baseline behaviour (May 2019 - November 2019):
The moving time averaged VASR drops as the acoustic signal from events subsides and the energy is radiated from events with a higher seismic share. This is mirrored in the increased number of ash-rich explosions during the start of this phase. After the filling of the crater in phase 2, lava flow activity initiates at the start of this phase.

Throughout the phase, there is a slow transition towards an increased proportion of acoustic energy, as more gas-rich explosions occur, and seismic tremor reduces. There is a reduction in seismic tremor through this phase which suggests that the rate of magma migration at depth may be reducing. A reduction in acoustic tremor energy implies that less gas is being released from the system, either due to a reduction in degassing, or the system is becoming less efficient at releasing the gases.

Phase 4 - Crater-full activity (December 2019 - March 2020):
Acoustic amplitudes and VASR increase in a short time span and remain high for the whole phase. Lava overspill of the crater is also observed at the onset of this phase and is active for the most part, with the exception of the month of January 2020. During this

phase, seismic tremor duration and the associated energy is at the lowest recorded over the whole study.

The ongoing lava flow activity shows that there is still an upward migration of material, however the rate of this seems to be slowing, indicated by the reduction in seismic tremor. This slowed effusion may be due to the increased overpressures from the full crater. The high acoustic energy suggests that there is high gas release occurring from the magma in the conduit and summit cone (Garcés et al., 1999; Fee et al., 2010). Due to degassed magma typically having increased viscosities (Sparks, 2003), this could have also caused the lower rate of seismic tremor due to reduced magma migration velocities.

Phase 5 - Quasi-Stable Baseline (March 2020 - August 2020):
The rate of explosions and level of acoustic amplitude remain steady in this phase. The split between ash- and gas-rich explosions remains consistent too, with ash-rich explosions slightly more frequent than gas-rich. VASR drops as seismic tremor becomes more active at the onset of this phase, although it slowly increases as acoustic tremor also slowly increases in both duration and its cumulative energy output.

During this phase the increase of seismic tremor, reducing the VASR, suggests that migration of magma may have increased (Chouet, 1988). This is soon followed by the increase of acoustic tremor durations, signifying that the material that is being moved up through the system may be undergoing increased degassing (Garcés et al., 1999; Fee et al., 2010).

Phase 6 - Activity reduction (September 2020 - October 2020):
The number of explosions and acoustic tremor both decrease to low levels while seismic tremor is initially high but is soon also reduced. These changes caused a low VASR during phase 6.

There are two possible explanations of the observed low-level acoustic activity in the 6th phase: either the system has been mostly depleted of gas or that it is being blocked or choked, such that any gas within the system is trapped and unable to be released. The reduction in the seismic tremor would most likely be explained by the reduction in the migration of magma within the system (Chouet, 1988).

Linking the different key observations and their interpretations from each phase, we build a conceptual model to represent each phase and illustrate the evolution of the system through time, shown in Figure 4.7. Although this is a first-order representation of the complex processes that take place within the volcanic system, it allows a rapid, albeit qualitative, interpretation of the large amount of data and trends that are shown in Figure 4.5.

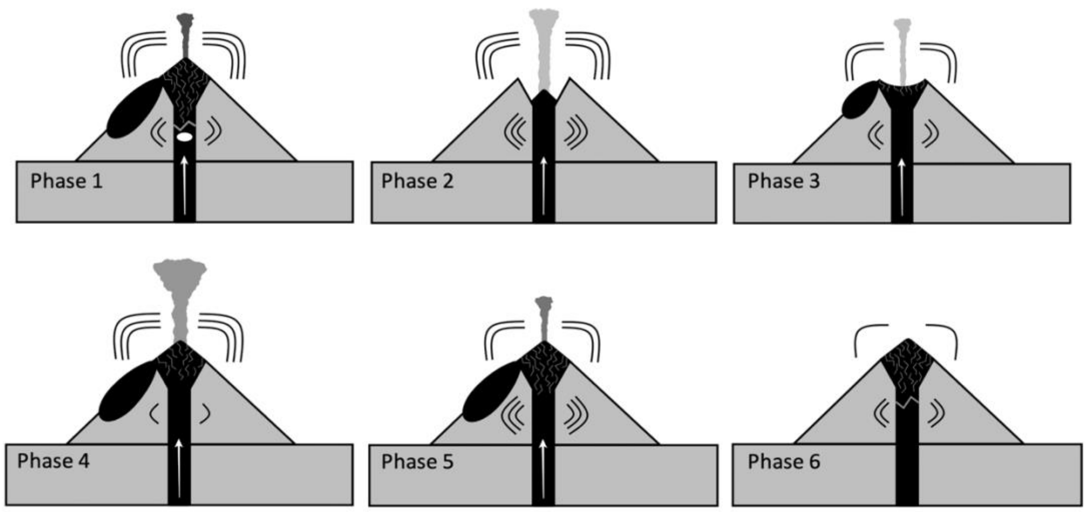

Figure 4.7. *Conceptual model for the evolution of the phases in activity observed. Phases described are between October 2018 and October 2020. Illustrations showing the 6 phases illustrate the key internal and external parameters which define the phases labelled. Tremor is shown by curved lines, with more lines indicating increased tremor activity. Acoustic tremor is shown by the curved lines above the vent while seismic tremor is shown by the curved lines within the vent. Lava flow activity is indicated by the lobe on the flank. Migration of magma is indicated by the white arrow. Average explosion energy is indicated by plume size and the darker the plume indicates the higher proportion of ash-rich explosions, with lighter plumes indicating a higher proportion of gas-rich explosions. Grey lines in the dome indicate the level of degassing and the thick grey line in phase 1 and 6 indicates the formation of a plug which restricts the conduit. White oval in phase 1 indicates a bubble from gas accumulation under the plug.*

Different styles of activity at Fuego have previously been observed and described to occur between the paroxysms in previous studies. Lyons et al. (2010) describe activity at Fuego based on seismic data collected between 2005 and 2007. They report the cyclic occurrence of 3 main phases of activity: passive lava effusion is generally followed by an increase in strombolian explosions leading to paroxysmal events. These paroxysms had produced large eruption columns, long lava flows, and block and ash flows before the system returned to background levels of activity characterized by discrete gas-rich explosions with no lava effusion. This type of activity resembles similarities to phase 1 and 2 in our study, where phase 1 encompasses both the build-up and paroxysm observed by Lyons et al. (2010), in which we identify ash-laden explosions and lava effusion leading up to a paroxysmal eruption, followed by gas-rich explosions with a pause in the emplacement of lava flows. During the 2-year study, Lyons et al. (2010) observed 5 paroxysmal events, and consequently observed a repeated cycle of these 3 phases. In our study, however, we did not observe repeated cycles, but observed a prolonged period without paroxysmal events. Brill et al. (2018) also describe the background activity at Volcán de Fuego. Although only for a short period in January 2012, their study used a network of seismic stations accompanied by infrasound microphones and cameras to build up an accurate description of the activity between paroxysms. They report activity including harmonic and non-harmonic seismic tremor, both gas-rich degassing episodes and ash-rich explosions and no lava flow emplacement. The baseline behaviour described closely matches the description of phase 2, and parts of phase 3 in our study however, as at that time Fuego had not produced a paroxysm since late 2007, it is likely that the study by Brill et al. (2018) describes activity which is consistent with our observations during phase 3, when no lava flows were active. As their study was limited to a short period of time, there is no further information to determine if the activity between the paroxysms of December 2007 and mid 2012 underwent a similar pattern to our study with prolonged repose after a paroxysm.

4.8. Conclusions

Using data collected by the long-term seismo-acoustic network, we have characterised the evolution of activity at Volcán de Fuego during the period October 2018- October 2020. The volcanic acoustic-seismic ratio parameter has been shown to be highly effective in the assessment of phase development at Fuego and we infer that it has potential to be an important tool to detect and confirm changes to the state of the system shortly after the shifts in eruptive behaviour have begun. The first two phases detected between October 2018 and October 2020 are phases that have previously been described at Fuego, relating to the cycle of paroxysms, however, the addition of further background phases of activity detected here raise the importance of understanding how the activity evolves. Additional assessment of the background behaviour and continued phase shifts could be important for forecasting future shifts, especially towards more hazardous activity and future paroxysmal eruptions. We also have noted that Fuego is currently undergoing an extended period of repose between paroxysmal events, raising the question of if it is still in the same period of activity of frequent paroxysmal activity which began in 2015, as assessed by Naismith et al., (2019).

We have shown that volcanic acoustic tremor is a prominent event at Fuego, occurring commonly with weekly durations up to 120 hours. As a proxy to vent-centred gas release, the detection of acoustic tremor in this study shows for the first time that gas release is occurring at rates that are potentially significant for the understanding of the magma processes occurring within the conduit. The range of durations and energies detected and calculated for acoustic tremor show that gas is released with varying degrees of force from a slow leak style to a more vigorous and forceful ejection of gases in sustained events.

Finally, we have addressed the splitting of energy during individual seismo-acoustic events and shown that the explosions at Fuego have two statistically distinct types, ash-rich and gas-rich, which likely endmembers of a spectrum determined by the level of fractionation occurring within the explosion source, the coupling of the source mechanism with the atmosphere and conduit walls, and volume of gas which has accumulated prior to release.

Chapter 5. Discussions and Conclusions

The work completed in this thesis had three distinct tasks. The first of these was the collection of long-term data using networks of seismic and acoustic sensors at Guatemalan volcanoes to remotely record their activity. The second was the building and application of automatic detection and classification algorithms to produce catalogues of the events produced by the volcanoes, including explosions and tremor. The final task of the work was to use the catalogued events for investigations into the long-term behaviour of the volcanic systems and to determine information on the mechanisms, processes and magma properties which led to the observed activity. Each of these tasks required decisions to be made due to the advantages and limitations of the different methods and approaches undertaken to obtain the results desired to answer the questions in each of the investigations. Here, I will discuss these further, and how they differed for the cases of Santiaguito and Fuego.

5.1. Long-Term Seismo-Acoustic Network Recording

The long-term investigations in this thesis required continuous recording of seismic and acoustic data over the span of several years, collected by networks of stations around the volcanoes. Long-term recording is essential for the studies carried out at Fuego and Santiaguito which aimed to look at the longer-term trends in the activity, the processes which occur over several months to years, as well as to record the build-up to paroxysm and the different phases of base-line activity. During the fieldwork and data handling of the network recordings, it became apparent that there are several limitations when carrying out long-term network recordings, as well as many advantages to the method to obtain data which can be used for the purposes required for these investigation.

Open-vent volcanoes produce activity which spans several orders of magnitude (Vergnolle and Métrich, 2021). For events to be detected by seismic and acoustic sensors, the seismic and acoustic waves radiated by the volcano must be strong enough so that after the attenuation, geometrical spreading, and site effects which alter the initial source waveform, the signal still has sufficiently high amplitudes to be detected above the background noise. Depending on the noise level and distance from the sensor to the vent, these factors introduce a magnitude cut-off for the events that can be detected. The location of the installation of any sensors is therefore a critical consideration depending on how low this cut-off is required. Sensors which were deployed closer to the volcanoes (therefore detecting higher amplitudes at the receiver), and stations which were deployed further away from sources of local noise, achieved better signal-to-noise ratios and had better detection rates than those further away from the vent or closer to noise sources. For the studies carried out at Santiaguito and Fuego, several sensors were deployed in remote areas which can be hard to access in order for them to be away from loud noise sources such as roads, towns and farms. At Santiaguito we showed how different station locations recorded with different levels of background noise, and how this affected the detection capabilities of the automatic algorithm. We showed that site locations which were more remote typically had lower levels of background noise, and how the noise level from the stations closer to human activity had a daily cycle of high and low background noise relating to the daytime and night-time, respectively.

We found that having sensors deployed in remote locations can run into difficulties in maintenance due to difficulty for gaining access, and for sensors that are deployed close to the vent, they can often be destroyed by the activity (e.g. lava flows, pyroclastic flows or lahars). Due to poorer infrastructure, the remote locations were not always able to facilitate real-time data telemetry. These issues were apparent with the data collection at Santiaguito. During times when there were issues with stations which recorded data on site, the issues went unnoticed for weeks until the next data retrieval which led to gaps in the record. The issue of data dropouts at single stations was mitigated by having the network of sensors. For both the Santiaguito and Fuego studies, with seismics and acoustic infrasound as the main methodologies to record vent activity, respectively, the number of stations active at any one time varied over the span of the studies, yet with the networks, almost continual recording was achieved.

These advantages and limitations of different site locations highlighted the importance of having a mix of remote and easily accessible stations to have a combination of high-quality data and reliable coverage. After completing the work in this thesis, I believe that the benefits of collecting long-term data through networks vastly outweighed the difficulties, and with a well-thought-out approach to data collection and site locations, the best quality datasets can be obtained.

5.2. Automatic Detection and Classification Schemes

The seismic and acoustic data used in the studies at Fuego and Santiaguito were catalogued after the collection, rather than in real-time, which introduced the issue of having large quantities of data to process which contained many events of interest. The work I have presented in this thesis shows how automatic detection and classification algorithms can be used to process large datasets which span several years over multiple stations. With the large datasets obtained from the networks at Santiaguito and Fuego, the ability to study the eruptive events is dependent on having a catalogue of events that have been accurately identified from the raw data streams. As my work shows, automatic detection and classification schemes are capable of doing this work in place of manual detection. The choice to use automatic algorithms over manual detection was based on the time that it would take to complete the detection and classification of the events in the whole dataset, to remove human bias from these steps, and to investigate how these algorithms can improve the investigations of long-term data. For short datasets, manual detection is a much quicker method than building an automatic algorithm from scratch, as the algorithms require parameterisation of the events and tests to determine the unique identifiers which adequately separate the different event types from each other as well as background noise. However, as the length of recording and number of stations increase, the time for manual detection increases, while the time for production of an automatic system remains the same, and eventually, the use of automatic schemes becomes more time efficient. Furthermore, assuming the critical event parameters for detection and classification remain the same through time, automatic detection schemes can be used for future datasets, enabling quick processing with pre-built algorithms for both short-term datasets as well as long-term data. For the datasets at Fuego and Santiaguito, the length of recording, combined with the number of stations made using automatic systems a much quicker and efficient method of producing the catalogues, making it the preferred option for producing the catalogues of events studied.

Before an algorithm is constructed it is important to ensure that the purpose of the catalogue is first considered, so that the level of completeness and the cleanness of the catalogue required can be met, and that the details of the events required to be included in the catalogue can be calculated. These factors have a knock-on effect on the number of algorithm steps required, and the testing required to ensure that the level at which the parameter thresholds are set produce the desired catalogue. Depending on the number of steps and checks required to develop an algorithm, the time taken for the algorithm to be developed can vary.

The purpose for the catalogue at Santiaguito was to aid in the investigation of the explosive volcanic and magmatic processes leading to shifts in styles of eruption, being of a high enough quality to allow for statistical measures to be taken to determine differences in the phases of activity. A catalogue which was fit for this purpose would need to have a low magnitude of completeness and be clean of false positives that give false representation to the state of the volcano, especially in the periods in which there were only a few events occurring per week. Therefore, the algorithm required to produce such a catalogue needed a high detection rate at the lowest possible magnitude and to have enough checks and tests to correctly remove noise from being detected. The algorithm for Santiaguito used only seismic data to detect, classify and catalogue the explosions, from a mix of broadband and short-period sensors.

At Fuego however, both seismic and acoustic data were available. The aims of the study were to obtain a better understanding of both the paroxysms and background activity between them, as well as to infer details of the transitions between the phases in activity. With the high number of explosions which occurred at the vent of Fuego, the inclusion of a small number of false positive detections in the catalogue was less impactful on the analysis compared to at Santiaguito, which had periods of much lower explosion rates. Furthermore, building an algorithm to produce a completely clean catalogue would have taken a significantly longer time compared to an algorithm which included a low number of false positives with an insignificant impact on the results.

Following the differences in requirements for the catalogues at Santiaguito and Fuego, as well as the use of different types of data for the algorithm to use (seismics and acoustic infrasound), the automatic algorithms we developed to catalogue the data were therefore also different. There were several steps that were required to produce the automatic algorithms so that they were appropriate for the data collected, and which would produce a catalogue appropriate for the analysis that would be later undertaken. The steps for producing the automatic algorithms each required checks and improvements in an iterative process to ensure the resulting catalogues met the requirements set out. These were the waveform detection step, event classification step, and network coherence and cleaning steps.

The first step of waveform detection was critical as only events which pass this initial check could be included in the final catalogue. Although a detection method could have a low threshold and pass through many waveforms to ensure all events are included, the inclusion of too many noise waveforms could have dramatically slowed down the run time of the algorithms and increased the chances of false triggers being included. We carried out tests on the detection schemes used to ensure that the maximum number of events were detected while keeping the number of false events to an appropriate level for the following steps in the algorithm to handle.

Different methods were used for the seismic data at Santiaguito and acoustic data at Fuego for detecting explosions. At Fuego the detection algorithm we produced relied on an STA/LTA. For the acoustic data at Fuego, the explosion waveforms were impulsive and generally had a high signal to noise ratio, which made this method very effective at picking incoming waveforms. The seismic waveforms of explosions at Santiaguito however, were less impulsive and as the algorithm was aimed to detect low amplitude and low signal to noise ratio events to compile a more complete catalogue, we found that the STA/LTA method was inconsistent and missed many true events, even when optimised. We therefore decided that although a computationally slower method, a simple amplitude threshold detection was more appropriate, which would analyse all waveforms which were above the given amplitude.

The second step carried out in the algorithm was feature selection for event classification, in which the event waveforms were parameterised to determine which features, or combination of features uniquely identified them compared to other event types and background noise. To identify these features, we first had to test a large range of features in both the time and frequency domains to determine if they had a typical threshold or range of values which differed from other events and background noise, making them adequate for use in the final algorithm. In most instances, individual parameters which showed a difference between the mean value for an event compared to noise still had an overlap with more extreme cases, such that no single parameter could separate the events alone. However, an event that overlapped with noise for one parameter did not always overlap for others, so we used multiple parameters with carefully chosen thresholds so that most events could be detected while most noise would be filtered out. The process of finding which features could be used to separate events from noise, and the best combination of these with the best thresholds to produce the desired catalogue was the most time-consuming step in the algorithm development due to the checks and improvements which occurred until the algorithm was optimised.

As well as having different detection methods, the two algorithms we produced to catalogue explosions at Santiaguito and Fuego relied on different features to classify events. This is because the parameters which provided a good threshold to discriminate between the explosions at Santiaguito with background noise and other seismic events were not able to discriminate between the different event types and noise at Fuego using acoustic data. The seismic waveforms at Santiaguito were found to have distinct central frequencies, dominant frequencies, and bandwidth at 50% of the dominant frequency's amplitude, as the waveforms had a frequency spectrum with a simple, single peak, where the location and width of the peak did not vary greatly between events. Following the frequency attribute checks, a cross correlation was used to compare the waveforms with a synthetic waveform, produced by a stack of real, manually detected waveforms. For the algorithm used for the acoustic data at Fuego, the detection STA/LTA sufficiently separated the explosions from the background noise without the need of further classification steps, however, the classification steps were required to distinguish between the gas-rich and ash-rich classes of explosions. The classification between the two explosion types was not as simple as classifying between noise and explosions at Santiaguito, as many of the simple features were the same for both classes. This highlighted the importance of understanding the signals of all events present in the data streams, as well as the background noise, as a preliminary step before building an algorithm. The features used to classify between the two explosion types also relied upon both time domain and frequency domain attributes. The features we used were the event duration, amplitude ratio between maximum and median amplitude, and the identification of a second frequency peak between 3 and 4.5 Hz.

The final step of network coherence and cleaning was used after the initial steps had been carried out on each station's data. For both Santiaguito and Fuego the network coherence step was the same. Events produced by the volcano were expected to originate from within the network and therefore expected to be detected at multiple stations. Local noise, however, would only occur at one station, while tectonic sources which could be detected across the network would 'sweep' across from one side to the other. Therefore, using the network of stations to only allow events into the catalogue which occur at multiple sensors and be located from the centre of the network efficiently ruled out noise waveforms which were initially incorrectly identified as an event. For the algorithms used for the data at Santiaguito and Fuego, the timing of the events at the different stations were compared, and only if they occurred within a given move-out time, were they considered to be produced by the same event and included in the catalogues. At Santiaguito, as the catalogue was required to be fully clean of noise, we also added the step of cross-correlation between detected events with one another to produce families of similar explosions, from which ungrouped waveforms were manually inspected to remove all remaining noise. This step was not carried out at Fuego as it was not necessary for all the noise to be removed. Furthermore, the catalogue at Fuego was too large for cross-correlations to be made between all events due to the computational power and memory required for this to be carried out.

Due to the differences not only in the requirements of the algorithms, but in the features that can be used to identify and classify events, it is likely therefore that if similar algorithms were to be developed for other volcanoes globally, the combination of features used and the thresholds to produce the catalogues would each be unique. The uniqueness has the effect that no single algorithm would be appropriate for use at multiple volcanoes, however we have shown by the ability to adapt the algorithms to take advantage of different features of the seismic and acoustic signals, the general methodology is very much transferable. Although the algorithms that are produced for any volcano need to be tailor-made, the results of these algorithms will be of a higher standard and more fit for purpose than any general algorithm could produce.

There are limitations to this method of algorithm development. Firstly, there needs to be a large enough number of events occurring within the whole dataset so that an initial training dataset can be obtained and used in the trials and tests to develop the algorithm. Datasets with low numbers of events may not have a sufficient training dataset to produce an accurate algorithm. Secondly, the data within the test datasets can introduce biases if the events are not representative, or where manual selection has been involved. If not careful, biases in the training datasets will lead to catalogues which share these biases and lead to analyses which have inaccurate results. Finally, as highlighted by the inability to run a cross correlation between all events at Fuego, the algorithms analysing large datasets are limited by the computational power available. Many steps in the algorithms are iterative and the computational power required, and total algorithm run time, is defined by the most computationally intensive and slowest processing step. Therefore, as the algorithm produced must be appropriate for the computers available, which may be a key consideration for many institutions with limited resources. The more powerful computers available, the more complex the algorithm can be for the datasets.

For both the Santiaguito and Fuego datasets, the training datasets were compiled from events manually detected at times across the whole recording period to mitigate biases that could occur if there were systematic changes which occurred to the waveforms through time. All events that were used in the training datasets did not have interference from noise sources to ensure that only features of the event sources were parametrised. The events selected spanned a wide range of magnitudes, durations and waveform shapes to ensure that the widest span of events were included in the training set in order to get the best representation of the possible events that could occur, reducing the chances of any events being omitted by the algorithm. Although the algorithm development relied upon a high level of manual selection and testing, the algorithms that were developed had no 'black box' elements, with every step from initial waveform detections to the final catalogue being known and understood. This level of understanding of the waveforms and algorithm increases the confidence that the catalogue that has been produced has the desired features for analysis. Furthermore, following the automatic steps, only minor post-production checks are needed to confirm that the included/excluded waveforms have been done so correctly.

5.3. Future Development of the Algorithms and Catalogues

The algorithms at Fuego and Santiaguito that we developed have produced high quality catalogues of events using seismic and acoustic data. Going forward, it may be possible for them to be adapted to assess the recordings in real-time. This would ensure that manual detection of events would not be needed, and the only manual steps required would be to check that the algorithms are still operating as expected, with no changes having occurred to the event signals that would require edits to the thresholds and classifying parameters.

One of the aims of the studies at Santiaguito and Fuego was to produce the catalogues such that they can be used to train more intelligent systems such as neural networks. Neural networks require large enough datasets to train the machine learning algorithms (e.g., Falsaperla et al., 1996; Scarpetta et al., 2005; Esposito et al., 2013; Shoji et al., 2018), which would be amply provided by the catalogues at Fuego and Santiaguito, which each contain thousands of events. Investigations using neural networks could be able to study the different features of the waveforms and infer more information about the events such as including how the events change through time, and the state of the volcanoes through in-depth classifications of the events (e.g., Scarpetta et al., 2005). The catalogue of explosions at Santiaguito is already being used as a training data set for a neural network by a study at INSIVUMEH, with the aim of using the catalogue to train a neural network to detect events in real-time and build towards an early warning system for hazardous events.

Finally, although the algorithms are tailored to the volcano for which they are initially produced to analyse the data of, it may be possible to adapt the structure of the algorithms to produce a generic algorithm that can be easily adapted with a range of features that can be added or removed depending on a manual assessment of the waveforms. This could enable the production of such algorithms in a much shorter time frame, making the method more suitable for smaller datasets, or for circumstances which have time pressures for quick results.

5.4. New Catalogues at Guatemalan Volcanoes

Following the development and application of the detection and classification schemes at Fuego and Santiaguito, we produced new catalogues of volcanic activity at the two volcanoes. These long-term catalogues were the first of their kind to be produced in Guatemala, paving the way for future investigations to be made. The production of catalogues show that automated algorithms can be used with both seismic and acoustic data to catalogue explosions, seismic tremor and acoustic tremor. With these new catalogues, we were able to carry out investigations into the long-term trends and phases of activity as well as the volcanic mechanisms and processes linked to the events.

Uses of the Long-Term Catalogues

Following the production of the catalogues from the automatic detection and classification algorithms, we analysed the ongoing activity at both Santiaguito and Fuego. Long-term catalogues have many advantages over short-term investigations, in that they can monitor the changes which occur to the volcano through time, identifying different behavioural phases and track the evolution of the activity to identify trends and signals which could be useful for forecasting future events. They can identify processes which occur over longer time periods, which often relate to deeper volcanic processes, and that short-term geophysical observations are not sensitive to. In the work carried out at both Santiaguito and Fuego, the catalogues we produced were used to provide insights into the mechanisms, processes and source properties which produce the ongoing activity. By monitoring how the signals of the volcanic events varied in time, we showed how the changes observed can be used to indicate changes to both the source mechanisms as well as parameters that relate to the state of the volcano. In these multiparameter studies using both seismic and acoustic infrasound, the different signals were compared and contrasted for the same events and phases to produce a more rounded understanding of the activity. The long-term observations are also able to be better compared to other long-term datasets, such as petrology or gas recordings, which are generally only sensitive to longer-term changes to the system, allowing for a better integration between different methods.

5.5. Phases of Open-Vent Activity

The trends in the catalogues at both Santiaguito and Fuego showed that there were multiple phases of activity which occurred during the 2-3 years of recordings from large paroxysmal phases to different styles of background activity. These phases could be defined either by the main style of activity occurring at the vent or by the energy output. The identification of the different phases relied upon assessment of key parameters and observing how these changed through time. These parameters included the rate/duration of event occurrence, the magnitude of events, the energy output of the volcano, or the VASR, showing the split of energy between ground and atmospheric radiation, and therefore changes in the volcanic processes (Johnson and Aster, 2005). During an individual phase, we showed that the features can either be static until the next phase occurs, at which point a sudden change occurs, or that there can be a trend in the feature as the volcano transitions between two states. At Santiaguito and Fuego, we observed both static and transitioning types of phases. At Santiaguito, the number of explosions in the first phase shifted from high occurrence to low occurrence before the transition to phase 2, in which the number of explosions occurring per week was generally more consistent between weeks during the paroxysmal activity of 2016. During 2018 at Santiaguito, we observed that there was a gradual reduction of energy output while the number of explosions remained more constant, showing that in a single phase, some features can remain constant while others transition. At Fuego, we found that the best identifier for the different phases was the VASR. Phases 2, 4 and 6 had VASR's which were stable for several months, while in phases 1, 3 and 5 there was a pseudo-linear trend occurring. As the VASR was calculated from the ratio between the acoustic and seismic energy release, there were several different combinations of trends that these two features could display to result in these observations (for example: an increase in VASR could be the result of a stable acoustic energy output and a decreasing seismic output, an increasing acoustic output and a stable seismic output, or an increasing acoustic and decreasing seismic output). Other features that commonly changed from one phase to the next at Fuego were the number of explosions per week and the difference between the number of gas-rich or ash-rich explosions which occurred each week.

We found that although two neighbouring phases of activity could both be easily identifiable by their characteristic traits, the boundary between them could be either sudden and distinct, easy to observe in all features measured, or span a wider time interval and be less clear in some features than in others, making it difficult to define the transition from one phase to the next. At Fuego, we observed that the changes in the VASR were typically abrupt and therefore easily defined due to the breaks in the trends over a short period of time. However, for the phase shifts at Santiaguito, we found that not all transitions were quite as clear. The phase change between phases 2 and 3 at Santiaguito was very clear due to the dramatic and abrupt change from a few explosions occurring per week (< 10), to nearly 200 explosions per week, while the cumulative weekly energy changed from being inconsistent week to week, to falling into a well-fitting rising trend. The phase change between phase 1 and phase 2, on the other hand, was less well defined, with the number of explosions per week continuing to fall, and the trend in the energy output slowly becoming more scattered. It is possible that this transition took place over the course of several weeks as the style of activity changed from weak and frequent explosions to strong but infrequent explosions which defined the paroxysmal phase. Investigating these phases and the transitions was important for the comparison between the observations and the models which have been outlined for the evolution of volcanic behaviour. The comparisons we made were able to help with the understanding of these systems and aided with the interpretations of the activity for forecasting and hazard assessments.

5.6. Mechanism and Models of Volcanic Activity

At both Fuego and Santiaguito, we investigated the mechanisms of the volcanic events and the models which describe the occurrence of paroxysmal phases. With the aid of models which explain the generation of paroxysms, investigations of the background levels of activity and the changes which occurred leading up to paroxysmal phases were able to assist with the assessment of the potential hazards that could occur in the future. Investigations of the individual event types enabled further insights into the mechanisms of the explosions and tremor and helped gain information on the source parameters and processes within the volcano during different phases of eruptive behaviour. We achieved this through the assessment of the occurrence, repose intervals, energy output, and seismo-acoustic energy split of the explosion and tremor waveforms to statistically infer information on the sources of these events. By assessing how these features changed through time between phases, we inferred details on how the source properties and mechanisms evolved to track the state of the volcanoes over the course of the studies. We also identified the changes which occurred in the lead up to paroxysms, showing how they disrupted the baseline activity.

In both the studies at Santiaguito and Fuego, we investigated the regular explosions. The sources of the explosions at open-vent volcanoes are described as non-destructive, that is, that the source can restore and repeat such that further explosions can occur (cf. Arciniega-Ceballos et al., 1999; Chouet et al., 1999). For the explosions at Santiaguito, we statistically analysed the explosions across the catalogues with magnitude-frequency analysis to show that the explosions followed a power-law relationship, which reflected a self-similarity between the explosions across the range of magnitudes produced. We inferred that the relationship is a reflection of the magma properties, which varied from phase to phase, where phases which had a lower *b*-value had higher viscosities and rupture strength. The assessment of the *b*-value from magnitude-frequency analysis provided a good assessment of the largest event type possible in a given phase, although this was done retrospectively. Using this analysis in the future, it could be possible to obtain an estimate of the largest possible eruption size during a phase in real-time, and therefore the hazards associated with it. For this to occur, real-time detections would be required, and the start of the current phase would need to be correctly identified, so that the *b*-value could be accurately calculated.

The frequency of different repose times highlighted at Santiaguito that explosion duets were common, with the secondary explosion having a high statistical similarity to the initial explosion it followed. The presence of these explosions suggested that there is a healing time after the explosions occur, of about 10 minutes, before which the strength of the magma is sufficiently low for lower-pressure build-ups to re-fracture the existing gas fracture pathways. These duets show how the explosions occur in a cycle of mechanisms which involve pressure build-up, fracturing and subsequent healing. The number of events with different repose times was also used to show that the explosions at Santiaguito obey a Poissonian relationship in their occurrence rate, making the timing of the next explosion probabilistic, and not something that can be predicted.

For the explosions at Fuego, it has commonly been observed that two styles of explosions occur, ash-rich and gas-rich. We investigated the difference between these two explosion types through the assessment of the event VASR. We showed that the two different classes of explosions clustered broadly in both seismic and acoustic energy release, ranging across VASR's of several orders of magnitude difference. Although the two explosion types had a high degree of overlap, the mean VASR for the two types of explosions were statistically independent. The statistical difference between the two classes likely points towards two separate mechanisms which occur to produce these different events. However, the overlap between the two clusters also suggests that they may be endmembers on a spectrum that are defined by the level of fragmentation that has occurred at the source of the explosion, causing varying levels of ash to be ejected by the eruption plume.

We also detected and investigated the seismic and acoustic tremor signals at Fuego. Seismic tremor is well understood and is commonly believed to be the result of fluids such as magma moving through the bedrock and causing resonance in the cracks through which they flow (Chouet, 1988). Acoustic tremor at open-vent volcanoes has been less commonly investigated, and by detecting this feature across the whole study, we showed that the signal is common at Fuego, and that it is likely linked to the long duration gas-release events which have been observed to occur (e.g. Lyons at al., 2010; Brill et al., 2018; De Angelis et al., 2019; Naismith et al., 2019; Diaz-Moreno et al., 2020). Although the long-term study was not necessary to make the link between the signal and the source of acoustic tremor, the study was able to show how important it is to understand the entire system, given the role that gases and other volatiles play in the build-up of pressure, magma viscosity, and eruption style from effusive to explosive (Sparks, 2003). We showed that both seismic and acoustic tremor events occur at varying levels, which indicated that there were times with higher and lower magma transport through the system, as well as varying levels of gas release from the vent which could have been due to either different levels of magma degassing, or varying efficiency of gas release.

Combining the observations and mechanical interpretations of the events at Fuego, we produced a model which describes the evolution of activity in each phase. Using this model, it may be possible for future observations of activity to be compared with the different phases in the model to identify the current state of the volcano, as well as assessing the likely changes in activity over the following few months, under the assumption that the stages in the model will evolve in the same way.

Paroxysms occurred at both Santiaguito and Fuego and are important features of a volcano's activity to understand, given that they are commonly the periods of activity which cause the most destruction and devastation to infrastructure, communities, and life. The two volcanoes displayed different styles of paroxysmal activity during the investigations, where the paroxysm observed at Fuego was a short lived, several day period of continual high powered eruption, causing large plumes and pyroclastic flows during the ejection of material, typical for paroxysms at Fuego (e.g. Lyons et al., 2010; Naismith et al., 2019), while the paroxysmal phase at Santiaguito lasted several months, with infrequent (<5 per week) large isolated explosions which each had large plumes and produced pyroclastic flows. Both paroxysms at Fuego and Santiaguito disrupted the regular background level of open-vent activity which for both vents are described by the effusion of lava flows and emission of regular small to moderate sized explosions.

At Santiaguito, the statistical analysis of the paroxysm in 2016 showed that the explosions had a low rate parameter of 2.20, compared to 3.69 in the following phase. We showed that the paroxysmal phase had no correlation between repose duration and time, indicating that the source mechanisms of the large explosions in the paroxysmal phase were stable. The *b*-value during the paroxysm was low at 0.94 ± 0.06, compared to 2.28 ± 0.69 in the following phase, showing the high contribution of large magnitude events compared to the low magnitude events. The changes that occurred to the activity from the base-level phases to the paroxysmal phase were likely linked to changes in the magma porosity, temperature and applied strain rates, which have been shown to be controlling factors of the tensile strength, and therefore explosion magnitudes at Santiaguito (Hornby et al., 2019). The paroxysm had been stated to have been triggered by an influx of new magma (Wallace et al., 2020). This influx of fresh material likely caused magma mixing at depth which would have in turn caused changes to the properties of the magma which led to a deepening of the source, and greater build-up of pressure between explosions to produce the large explosions observed.

At Fuego, there have been several models proposed which describe the mechanisms which occur to produce the paroxysms. Using the catalogued events before and after the paroxysmal event in November 2018, we compared the properties of the events with the proposed models to see which model best fit the observed activity. The observation of a drop in the rate of explosions prior to the paroxysm suggested that choking was occurring in the conduit below a plug, allowing a build-up of pressure. We also observed an evacuation of material in the conduit producing a volume which was later filled during the following period. These are both features of the collapsing foam model by Jaupart and Vergniolle (1998), which has been regularly cited as a potential model for Fuego's paroxysms (e.g., Lyons et al., 2010; Naismith et al., 2019), and which we have proposed as the best fitting model to the observations. Unlike the magma-driven paroxysm at Santiaguito, the paroxysm observed at Fuego was likely gas-driven.

With observations that both Fuego and Santiaguito display phases in their activity, determining if there were any trends, patterns or signals that could be used to indicate how the phases are likely to change would be beneficial for forecasting efforts. This would be most beneficial for improving the forecasting time of the paroxysms which are most likely to have large impacts on the local communities. By understanding the signals produced through the transition from the background activity to the paroxysms, how they relate to the magma properties, and how the signals link to the models, we were able to achieve a better understanding of the state of the volcano during the different phases. At Fuego, we were able to produce a model describing the evolution of the internal and external activity during each phase. This model shows the internal magma processes and properties that are linked to the activity, and how they must have changed to produce the evolving activity. In future studies that aim to evaluate the state of the volcano and the possible future changes in the activity, comparisons to the model could be made to assess the current magma properties based on the observed activity, and how they could change based on how they have previously changed when the system displayed similar activity. During the studies at each volcano however, only one paroxysm was observed. It is not possible to determine if any signal or trend that occurred before these paroxysms is a reliable feature that could be used to indicate the changes in activity towards the paroxysms. Only after the signals leading up to several paroxysms have been compared can any statistical proof be made to show that the signals are indeed indicating that a paroxysm will occur. Despite the lack of evidence in the studies at Fuego and Santiaguito to suggest that the paroxysm can be accurately forecasted with the data provided in the catalogues, we do not rule out the possibility that the assessment of phases of activity from long-term recording of volcanic activity could allow this to occur in the future, or at other volcanoes. If more paroxysms are recorded through long-term assessments at Fuego and Santiaguito, it may be possible to find notable features that could be used. Even without the ability to directly forecast the potential for paroxysmal eruptions from the assessment of the baseline activity in the studies undertaken, the improved knowledge of the internal mechanisms and the inferences on the state of the volcano and the magma properties can be used to better understand the volcano as a whole, and in conjunction with other datasets, could provide further insights that unlock the forecasting problem.

5.7. Open Questions and Future Development

During the work completed at Santiaguito and Fuego, we showed that automatic algorithms can be developed to successfully detect, classify, and catalogue events at open-vent volcanoes from the recording of seismic and acoustic data by networks of stations. The catalogues that we produced can be used to answer many questions on the ongoing activity at the vents, including the statistical properties of the explosions, insights into the mechanisms of the explosions and tremor events, as well as the models that explain the occurrence of paroxysms and the phases that occur between them. However, following the conclusion of the work done in the studies that make up this thesis, and considering the initial aims and objectives of the work, there are several questions that remain on the topic that could be investigated to build upon this work.

The method of producing automatic algorithms to detect and classify the explosions and tremor at Fuego and Santiaguito required unique algorithms, tailored to the waveforms of the events at each location. For these algorithms to be produced, time is required to go through all the tests and checks to find appropriate features to discriminate between different event signals and noise. To reduce the time for these algorithms to be produced, a generic algorithm could by written, which could be easily adapted for different datasets with their unique identifying parameters.

The algorithms that have been produced for use at Santiaguito and Fuego could also undergo further development. If the networks were updated to have all stations relay the recorded data in real-time to a central server, the algorithms could be adapted to work in real-time, detecting and classifying events as they happen, producing a continually up-to-date catalogue of events, allowing for investigations into current activity to be carried out without delay.

Although the investigations in this study did not find any unique parameter or trend which could be used to aid forecasting efforts of the large paroxysms, it does not mean that there is no potential for long-term recordings to identify any metrics that could be used for this purpose. The two investigations here each only recorded one paroxysmal phase. To identify key features or trends in the data which accurately indicate a future paroxysm, multiple paroxysms would be required for comparisons. Increasing the duration of the catalogues at these open-vent systems to record multiple paroxysms would allow for this to occur. Furthermore, a dedicated study to investigate a wide range of parameters for different volcanic events to track how each of these parameters change through time could provide further details on the evolving source mechanisms of these events and may also be able to discover features which better forecast the paroxysms. It is also possible, that the current study at INSIVUMEH using our catalogue of explosions at Santiaguito to train a neural network for real-time detection could identify key parameters for forecasting and increase the temporal range that forecasting can be made before large events.

Finally, future long-term studies at Santiaguito and Fuego could incorporate a wider range of methods, including petrology, thermal or gas recordings to aid in the investigation of magma properties and the state of the volcano during different phases of the activity at these open-vent systems. These data would help improve the models produced and provide further insights into the volcanic systems to give a more complete description of the activity.

5.8. Concluding Remarks

The aims of this thesis were to investigate the use of networks of seismic and acoustic sensors deployed around the flanks of the open-vent volcanoes in Guatemala to detect and investigate the activity from background levels to paroxysms. I have shown in the studies carried out at Volcán de Fuego and the Santiaguito lava dome complex that automatic algorithms are an effective tool to detect, classify and catalogue both explosions and tremor events from the long-term recordings using networks. These algorithms can be tailored to produce catalogues of the activity at different volcanoes using both seismic and acoustic data, which are fit for purpose in different studies depending on their aims. I also produced high-quality catalogues which could be used in the development of more intelligent systems for the improvement of monitoring and forecasting efforts in Guatemala.

In this thesis, I produced new catalogues of activity for Fuego and Santiaguito, the first of their kind for volcanoes in Guatemala. I have also shown that both these volcanoes produce several different phases of activity during background open-vent behaviour. These phases can be identified by tracking the rate of occurrence of different events, energy released, and the split of energy radiated through the ground and atmosphere. Finally, I showed that the analysis of these long-term catalogues can provide insights into the mechanisms of the volcanic events and models which describe the paroxysms, as well as giving insights to the changes to the volcanic systems which produce them. This study has enabled a better understanding of the processes of the protracted eruptions that occur at open-vent volcanoes in Guatemala and provides important datasets from which to develop future volcano monitoring strategies.

Bibliography

Aki, K., 1967. Scaling law of seismic spectrum. J. Geophys. Res. 72, 1217-1231. https://doi.org/10.1029/jz072i004p01217

Aki, K., Ferrazzini, V., 2000. Seismic monitoring and modeling of an active volcano for prediction. J. Geophys. Res. Solid Earth 105, 16617–16640. https://doi.org/10.1029/2000JB900033

Alatorre-Ibargüengoitia, M.A., Scheu, B., Dingwell, D.B., Delgado-Granados, H., Taddeucci, J., 2010. Energy consumption by magmatic fragmentation and pyroclast ejection during Vulcanian eruptions. Earth Planet. Sci. Lett. 291, 60–69. https://doi.org/10.1016/j.epsl.2009.12.051

Aldeghi, Carn, Escobar-Wolf, Groppelli, 2019. Volcano Monitoring from Space Using High-Cadence Planet CubeSat Images Applied to Fuego Volcano, Guatemala. Remote Sens. 11, 2151. https://doi.org/10.3390/rs11182151

Allard, P., 2010. A CO2-rich gas trigger of explosive paroxysms at Stromboli basaltic volcano, Italy. J. Volcanol. Geotherm. Res. 189, 363–374. https://doi.org/10.1016/j.jvolgeores.2009.11.018

Allen, R., 1982. Automatic phase pickers: Their present use and future prospects. Bull. Seismol. Soc. Am. 72, S225–S242. https://doi.org/10.1785/BSSA07206B0225

Andres, R., Rose, W., Stoiber, R., Williams, S., Matías, O., Morales, R., 1993. A summary of sulfur dioxide emission rate measurements from Guatemalan volcanoes. Bull. Volcanol. 55, 379–388. https://doi.org/10.1007/BF00301150

Arciniega-Ceballos, A., Chouet, B.A., Dawson, P., 1999. Very long-period signals associated with Vulcanian Explosions at Popocatepetl Volcano, Mexico. Geophys. Res. Lett. 26, 3013–3016. https://doi.org/10.1029/1999GL005390

Aster, R., 2003. Very long period oscillations of Mount Erebus Volcano. J. Geophys.

Res. 108, 2522. https://doi.org/10.1029/2002JB002101

Ball, J.L., Calder, E.S., Hubbard, B.E., Bernstein, M.L., 2013. An assessment of hydrothermal alteration in the Santiaguito lava dome complex, Guatemala: implications for dome collapse hazards. Bull. Volcanol. 75, 676. https://doi.org/10.1007/s00445-012-0676-z

Bain, A.A., Lamur, A., Kendrick, J.E., Lavallée, Y., Calder, E.S., Cortés, J.A., Butler, I.B., Cortés, G.P., 2019. Constraints on the porosity, permeability and porous micro-structure of highly-crystalline andesitic magma during plug formation. J. Volcanol. Geotherm. Res. 379, 72–89. https://doi.org/10.1016/j.jvolgeores.2019.05.001

Balmforth, N.J., Craster, R.V., Rust, A.C., 2005. Instability in flow through elastic conduits and volcanic tremor. J. Fluid Mech. 527, 353–377. https://doi.org/10.1017/S0022112004002800

Barrière, J., d'Oreye, N., Oth, A., Theys, N., Mashagiro, N., Subira, J., Kervyn, F., Smets, B., 2019. Seismicity and outgassing dynamics of Nyiragongo volcano. Earth Planet. Sci. Lett. 528, 115821. https://doi.org/10.1016/j.epsl.2019.115821

Barrière, J., Oth, A., Theys, N., d'Oreye, N., Kervyn, F., 2017. Long-term monitoring of long-period seismicity and space-based SO_2 observations at African lava lake volcanoes Nyiragongo and Nyamulagira (DR Congo). Geophys. Res. Lett. 44, 6020–6029. https://doi.org/10.1002/2017GL073348

Basuki, A., Nugraha, A.D., Hidayati, S., Triastuty, H., 2019. Determination of Hypocentre and Seismic Velocity Structure in Guntur Volcano Using Seismic Data from 2010 to 2014. Indones. J. Geosci. 6, 279–289. https://doi.org/10.17014/ijog.6.3.279-289

Beard, J.S., Borgia, A., 1989. Temporal variation of mineralogy and petrology in cognate gabbroic enclaves at Arenal volcano, Costa Rica. Contrib. Mineral. Petrol. 103, 110–122. https://doi.org/10.1007/BF00371368

Bell, A.F., Hernandez, S., Gaunt, H.E., Mothes, P., Ruiz, M., Sierra, D., Aguaiza, S., 2017. The rise and fall of periodic 'drumbeat' seismicity at Tungurahua volcano, Ecuador. Earth Planet. Sci. Lett. 475, 58–70. https://doi.org/10.1016/j.epsl.2017.07.030

Bennett, E.H.S., Conway, F.M., Rose, W.I., 1992. Santa María, Guatemala: A decade volcano. Eos Trans. Am. Geophys. Union 73, 521–521. https://doi.org/10.1029/91EO00387

Berlo, K., Stix, J., Roggensack, K., Ghaleb, B., 2012. A tale of two magmas, Fuego, Guatemala. Bull. Volcanol. 74, 377–390. https://doi.org/10.1007/s00445-011-0530-8

Blackburn, E.A., Wilson, L., Sparks, R.S.J., 1976. Mechanisms and dynamics of strombolian activity. J. Geol. Soc. 132, 429–440. https://doi.org/10.1144/gsjgs.132.4.0429

Blundy, J., Cashman, K., Humphreys, M., 2006. Magma heating by decompression-driven crystallization beneath andesite volcanoes. Nature. 443, 78-80. https://doi.org/10.1038/nature05100

Bluth, G.J.S., Rose, W.I., 2004. Observations of eruptive activity at Santiaguito volcano, Guatemala. J. Volcanol. Geotherm. Res. 136, 297–302. https://doi.org/10.1016/j.jvolgeores.2004.06.001

Boatwright, J., 1980. A spectral theory for circular seismic sources; simple estimates of source dimension, dynamic stress drop, and radiated seismic energy. Bull. Seismol. Soc. Am. 70, 1–27. https://doi.org/10.1785/BSSA0700010001

Bonis, S., Salazar, O., 1973. The 1971 and 1973 eruptions of Volcán Fuego, Guatemala, and some socio-economic considerations for the volcanologist. Bull. Volcanol. 37, 394–400. https://doi.org/10.1007/BF02597636

Braun, T., Ripepe, M., 1993. Interaction of seismic and air waves recorded at Stromboli Volcano. Geophys. Res. Lett. 20, 65–68. https://doi.org/10.1029/92GL02543

Brenguier, F., Campillo, M., Takeda, T., Aoki, Y., Shapiro, N.M., Briand, X., Emoto, K., Miyake, H., 2014. Mapping pressurized volcanic fluids from induced crustal seismic velocity drops. Science 345, 80–82. https://doi.org/10.1126/science.1254073

Brill, K.A., Waite, G.P., Chigna, G., 2018. Foundations for Forecasting: Defining Baseline Seismicity at Fuego Volcano, Guatemala. Front. Earth Sci. 6, 87. https://doi.org/10.3389/feart.2018.00087

Brill, K.A., Waite, G.P., Rodriguez, K., 2013. Seismic event classification and precursor identification at Fuego Volcano, Guatemala. American Geophysical Union, Fall Meeting 2013, abstract id. V43D-04

Cannata, A., Di Grazia, G., Aliotta, M., Cassisi, C., Montalto, P., Patanè, D., 2013. Monitoring Seismo-volcanic and Infrasonic Signals at Volcanoes: Mt. Etna Case Study. Pure Appl. Geophys. 170, 1751–1771. https://doi.org/10.1007/s00024-012-0634-x

Cardaci, C., Falsaperla, S., Gasperini, P., Lombardo, G., Marzocchi, W., Mulargia, F., 1993. Cross-correlation analysis of seismic and volcanic data at Mt Etna volcano, Italy. Bull. Volcanol. 55, 596–603. https://doi.org/10.1007/BF00301812

Carter, W., Rietbrock, A., Lavallée, Y., Gottschämmer, E., Moreno, A.D., Kendrick, J.E., Lamb, O.D., Wallace, P.A., Chigna, G., De Angelis, S., 2020. Statistical evidence of transitioning open-vent activity towards a paroxysmal period at Volcán Santiaguito (Guatemala) during 2014–2018. J. Volcanol. Geotherm. Res. 398, 106891. https://doi.org/10.1016/j.jvolgeores.2020.106891

Castro, J.M., Dingwell, D.B., 2009. Rapid ascent of rhyolitic magma at Chaitén volcano, Chile. Nature. 461, 780-783. https://doi.org/10.1038/nature08458

Castro, J.M., Gardner, J.E., 2008. Did magma ascent rate control the explosive-effusive transition at the Inyo volcanic chain, California? Geology. 36(4), 279–282. https://doi.org/10.1130/G24453A.1

Castro, J.M., Manga, M., Martin, M.C., 2005. Vesiculation rates of obsidian domes inferred from H2O concentration profiles. Geophys. Res. Lett. 32, L21307. https://doi.org/10.1029/2005GL024029

Castro-Escobar, M., 2017. Patterns in eruptions at Fuego from statistical analysis of video surveillance, (PhD thesis). Retrieved from: https://digitalcommons.mtu.edu/etdr/414/(2017), Accessed 27 April 2021

Celso., Thompson, G., West, M., Usfseismiclab., Ketner, D., Tape, C., 2018. Geoscience-Community-Codes/Gismo: Version 1.20 Beta. Zenodo. https://doi.org/10.5281/ZENODO.1404723

Chen, C.C., Wang, W.C., Chang, Y.F., Wu, Y.M., Lee, Y.H., 2006. A correlation between the b-value and the fractal dimension from the aftershock sequence of the 1999 Chi-Chi, Taiwan, earthquake. Geophys. J. Int. 167(3), 1215-1219. https://doi.org/10.1111/j.1365-246X.2006.03230.x

Chen, Y., Remy, D., Froger, J.-L., Peltier, A., Villeneuve, N., Darrozes, J., Perfettini, H., Bonvalot, S., 2017. Long-term ground displacement observations using InSAR and GNSS at Piton de la Fournaise volcano between 2009 and 2014. Remote Sens. Environ. 194, 230–247. https://doi.org/10.1016/j.rse.2017.03.038

Chesner, C.A., Rose, W.I., 1984. Geochemistry and evolution of the fuego volcanic complex, Guatemala. J. Volcanol. Geotherm. Res. 21, 25–44. https://doi.org/10.1016/0377-0273(84)90014-3

Chiodini, G., Caliro, S., Cardellini, C., Granieri, D., Avino, R., Baldini, A., Donnini, M., Minopoli, C., 2010. Long-term variations of the Campi Flegrei, Italy, volcanic system as revealed by the monitoring of hydrothermal activity. J. Geophys. Res. 115, B03205. https://doi.org/10.1029/2008JB006258

Chouet, B., 2005. Source mechanism of Vulcanian degassing at Popocatépetl Volcano, Mexico, determined from waveform inversions of very long period signals. J. Geophys. Res. 110, B07301. https://doi.org/10.1029/2004JB003524

Chouet, B., 1988. Resonance of a fluid-driven crack: Radiation properties and implications for the source of long-period events and harmonic tremor. J. Geophys. Res. Solid Earth 93, 4375–4400. https://doi.org/10.1029/JB093iB05p04375

Chouet, B., Saccorotti, G., Dawson, P., Martini, M., Scarpa, R., De Luca, G., Milana, G., Cattaneo, M., 1999. Broadband measurements of the sources of explosions at Stromboli Volcano, Italy. Geophys. Res. Lett. 26, 1937–1940. https://doi.org/10.1029/1999GL900400

Chouet, B.A., 1996. Long-period volcano seismicity: its source and use in eruption forecasting. Nature 380, 309–316. https://doi.org/10.1038/380309a0

Choy, G.L., Boatwright, J.L., 1995. Global patterns of radiated seismic energy and apparent stress. J. Geophys. Res. Solid Earth 100, 18205–18228. https://doi.org/10.1029/95JB01969

Coats, R., Kendrick, J.E., Wallace, P.A., Miwa, T., Hornby, A.J., Ashworth, J.D., Matsushima, T., Lavallée, Y., 2018. Failure criteria for porous dome rocks and lavas: A study of Mt. Unzen, Japan. Solid Earth. 9, 1299–1328. https://doi.org/10.5194/se-9-1299-2018

Connor, C.B., Sparks, R.S.J., Mason, R.M., Bonadonna, C., Young, S.R., 2003. Exploring links between physical and probabilistic models of volcanic eruptions: The Soufrière Hills Volcano, Montserrat. Geophys. Res. Lett. 30, 1701. https://doi.org/10.1029/2003GL017384

Conway, F.M., Diehl, J.F., Rose, W.I., Matías, O., 1994. Age and Magma Flux of Santa María Volcano, Guatemala: Correlation of Paleomagnetic Waveforms with the 28,000 to 25,000 yr B.P. Mono Lake Excursion. J. Geol. 102, 11–24. https://doi.org/10.1086/629645

Coombs, M.L., Wech, A.G., Haney, M.M., Lyons, J.J., Schneider, D.J., Schwaiger, H.F., Wallace, K.L., Fee, D., Freymueller, J.T., Schaefer, J.R., Tepp, G., 2018. Short-Term

Forecasting and Detection of Explosions During the 2016–2017 Eruption of Bogoslof Volcano, Alaska. Front. Earth Sci. 6, 122. https://doi.org/10.3389/feart.2018.00122

Coppola, D., Laiolo, M., Massimetti, F., Cigolini, C., 2019. Monitoring endogenous growth of open-vent volcanoes by balancing thermal and SO2 emissions data derived from space. Sci. Rep. 9, 9394. https://doi.org/10.1038/s41598-019-45753-4

Cordonnier, B., Hess, K.U., Lavallee, Y., Dingwell, D.B., 2009. Rheological properties of dome lavas: Case study of Unzen volcano. Earth Planet. Sci. Lett. 279, 263–272. https://doi.org/10.1016/j.epsl.2009.01.014

Cordonnier, B., Caricchi, L., Pistone, M., Castro, J., Hess, K.U., Gottschaller, S., Manga, M., Dingwell, D.B., Burlini, L., 2012. The viscous-brittle transition of crystal-bearing silicic melt: Direct observation of magma rupture and healing. Geology 40, 611–614. https://doi.org/10.1130/G3914.1

Cruz, F.G., Chouet, B.A., 1997. Long-period events, the most characteristic seismicity accompanying the emplacement and extrusion of a lava dome in Galeras Volcano, Colombia, in 1991. J. Volcanol. Geotherm. Res. 77, 121–158. https://doi.org/10.1016/S0377-0273(96)00091-1

De Angelis, S., Diaz-Moreno, A., Zuccarello, L., 2019. Recent Developments and Applications of Acoustic Infrasound to Monitor Volcanic Emissions. Remote Sens. 11, 1302. https://doi.org/10.3390/rs11111302

De Angelis, S., Fee, D., Haney, M., Schneider, D., 2012. Detecting hidden volcanic explosions from Mt. Cleveland Volcano, Alaska with infrasound and ground-coupled airwaves: REGIONAL DETECTION OF VOLCANIC ERUPTIONS. Geophys. Res. Lett. 39, n/a-n/a. https://doi.org/10.1029/2012GL053635

De Angelis, S., Henton, S.M., 2011. On the feasibility of magma fracture within volcanic conduits: Constraints from earthquake data and empirical modelling of magma viscosity: ON THE FEASIBILITY OF MAGMA FRACTURE. Geophys. Res. Lett. 38, n/a-n/a. https://doi.org/10.1029/2011GL049297

De Angelis, S., Lamb, O.D., Lamur, A., Hornby, A.J., von Aulock, F.W., Chigna, G., Lavallée, Y., Rietbrock, A., 2016. Characterization of moderate ash-and-gas explosions at Santiaguito volcano, Guatemala, from infrasound waveform inversion and thermal infrared measurements: EXPLOSIONS AT SANTIAGUITO. Geophys. Res. Lett. 43, 6220–6227. https://doi.org/10.1002/2016GL069098

Dean, K., Bowling, S.A., Shaw, G., Tanaka, H., 1994. Satellite analyses of movement and characteristics of the Redoubt Volcano plume, January 8, 1990. J. Volcanol. Geotherm. Res. 62, 339–352. https://doi.org/10.1016/0377-0273(94)90040-X

Dean, K., Dehn, J., McNutt, S., Neal, C., Moore, R., Schneider, D., 2002. Satellite imagery proves essential for monitoring erupting Aleutian Volcano. Eos Trans. Am. Geophys. Union 83, 241. https://doi.org/10.1029/2002EO000168

Dehn, J., Dean, K., Engle, K., 2000. Thermal monitoring of North Pacific volcanoes from space. Geology 28. https://doi.org/10.1130/0091-7613(2000)28<755:TMONPV>2.0.CO;2

De la Cruz-Reyna, S., 1993. Random patterns of occurrence of explosive eruptions at Colima Volcano, Mexico. J. Volcanol. Geotherm. Res. 55, 51-68. https://doi.org/10.1016/0377-0273(93)90089-A

De la Cruz-Reyna, S., 1991. Poisson-distributed patterns of explosive eruptive activity. Bull. Volcanol. 54, 57-67. https://doi.org/10.1007/BF00278206

Deligne, N.I., Coles, S.G., Sparks, R.S.J., 2010. Recurrence rates of large explosive volcanic eruptions. J. Geophys. Res. Solid Earth. 115, B06203. https://doi.org/10.1029/2009JB006554

De Luca, G., Scarpa, R., Del Pezzo, E., Simini, M., 1997. Shallow structure of Mt. Vesuvius Volcano, Italy, from seismic array analysis. Geophys. Res. Lett. 24, 481–484. https://doi.org/10.1029/97GL00169

Diaz-Moreno, A., Iezzi, A.M., Lamb, O.D., Fee, D., Kim, K., Zuccarello, L., De

Angelis, S., 2019. Volume Flow Rate Estimation for Small Explosions at Mt. Etna, Italy, From Acoustic Waveform Inversion. Geophys. Res. Lett. 46, 11071–11079. https://doi.org/10.1029/2019GL084598

Diaz-Moreno, A., Roca, A., Lamur, A., Munkli, B.H., Ilanko, T., Pering, T.D., Pineda, A., De Angelis, S., 2020. Characterization of Acoustic Infrasound Signals at Volcán de Fuego, Guatemala: A Baseline for Volcano Monitoring. Front. Earth Sci. 8, 549774. https://doi.org/10.3389/feart.2020.549774

Dingwell, D.B., Webb, S.L., 1989. Structural relaxation in silicate melts and non-Newtonian melt rheology in geologic processes. Phys. Chem. Miner. 16, 508-516. https://doi.org/10.1007/BF00197020

Dmitrieva, K., Hotovec-Ellis, A.J., Prejean, S., Dunham, E.M., 2013. Frictional-faulting model for harmonic tremor before Redoubt Volcano eruptions. Nat. Geosci. 6, 652–656. https://doi.org/10.1038/ngeo1879

Durst, K.S., 2008. Erupted magma volume estimates at Santiaguito and Pacaya Volcanoes, Guatemala using digital elevation models (Master of Science in Geology). Michigan Technological University, Houghton, Michigan. https://doi.org/10.37099/mtu.dc.etds/318

Ebmeier, S.K., Biggs, J., Mather, T.A., Elliott, J.R., Wadge, G., Amelung, F., 2012. Measuring large topographic change with InSAR: Lava thicknesses, extrusion rate and subsidence rate at Santiaguito volcano, Guatemala. Earth Planet. Sci. Lett. 335–336, 216–225. https://doi.org/10.1016/j.epsl.2012.04.027

Edmonds, M., Herd, R.A., 2007. A volcanic degassing event at the explosive-effusive transition. Geophys. Res. Lett. 34, L21310. https://doi.org/10.1029/2007GL031379

Edwards, W.N., Eaton, D.W., McCausland, P.J., ReVelle, D.O., Brown, P.G., 2007. Calibrating infrasonic to seismic coupling using the Stardust sample return capsule shockwave: Implications for seismic observations of meteors. J. Geophys. Res. 112, B10306. https://doi.org/10.1029/2006JB004621

El-Isa, Z.H., Eaton, D.W., 2014. Spatiotemporal variations in the b-value of earthquake magnitude-frequency distributions: Classification and causes. Tectonophysics. 615, 1-11. https://doi.org/10.1016/j.tecto.2013.12.001

Escobar-Wolf, R.P., Diehl, J.F., Singer, B.S., Rose, W.I., 2010. 40Ar/39Ar and paleomagnetic constraints on the evolution of Volcan de Santa Maria, Guatemala. Geol. Soc. Am. Bull. 122, 757–771. https://doi.org/10.1130/B26569.1

Escobar-Wolf, R., 2013. Volcanic Processes and Human Exposure as Elements to Build a Risk Model for Volcan de Fuego, Guatemala, (PhD thesis). Retrieved from: https://digitalcommons.mtu.edu/etds/638 (2013), Accessed 27 April 2021

Esposito, A.M., D'Auria, L., Giudicepietro, F., Peluso, R., Martini, M., 2013. Automatic Recognition of Landslides Based on Neural Network Analysis of Seismic Signals: An Application to the Monitoring of Stromboli Volcano (Southern Italy). Pure Appl. Geophys. 170, 1821–1832. https://doi.org/10.1007/s00024-012-0614-1

Esse, B., Burton, M., Varnam, M., Kazahaya, R., Wallace, P.A., Von-Aulock, F., Lavallée, Y., Salerno, G., Scollo, S., Coe, H., 2018. Quantification of ash sedimentation dynamics through depolarisation imaging with AshCam. Sci. Rep. 8, 15680. https://doi.org/10.1038/s41598-018-34110-6

Falsaperla, S., Graziani, S., Nunnari, G., Spampinato, S., 1996. Automatic classification of volcanic earthquakes by using Multi-Layered neural networks. Nat. Hazards 13. https://doi.org/10.1007/BF00215816

Farrell, J., Husen, S., Smith, R.B., 2009. Earthquake swarm and b-value characterization of the Yellowstone volcano-tectonic system. J. Volcanol. Geotherm. Res. 188, 260-176. https://doi.org/10.1016/j.jvolgeores.2009.08.008

Fee, D., Garcés, M., 2007. Infrasonic tremor in the diffraction zone: INFRASONIC TREMOR IN THE DIFFRACTION ZONE. Geophys. Res. Lett. 34. https://doi.org/10.1029/2007GL030616

Fee, D., Garcés, M., Patrick, M., Chouet, B., Dawson, P., Swanson, D., 2010. Infrasonic harmonic tremor and degassing bursts from Halema'uma'u Crater, Kilauea Volcano, Hawaii. J. Geophys. Res. 115, B11316. https://doi.org/10.1029/2010JB007642

Fee, D., Izbekov, P., Kim, K., Yokoo, A., Lopez, T., Prata, F., Kazahaya, R., Nakamichi, H., Iguchi, M., 2017. Eruption mass estimation using infrasound waveform inversion and ash and gas measurements: Evaluation at Sakurajima Volcano, Japan. Earth Planet. Sci. Lett. 480, 42–52. https://doi.org/10.1016/j.epsl.2017.09.043

Fee, D., Lyons, J., Haney, M., Wech, A., Waythomas, C., Diefenbach, A.K., Lopez, T., Van Eaton, A., Schneider, D., 2020. Seismo-acoustic evidence for vent drying during shallow submarine eruptions at Bogoslof volcano, Alaska. Bull. Volcanol. 82, 2. https://doi.org/10.1007/s00445-019-1326-5

Fee, D., Matoza, R.S., 2013. An overview of volcano infrasound: From hawaiian to plinian, local to global. J. Volcanol. Geotherm. Res. 249, 123–139. https://doi.org/10.1016/j.jvolgeores.2012.09.002

Fehler, M., Chouet, B., 1982. Operation of a Digital Seismic Network on Mount St. Helens Volcano and observations of long period seismic events that originate under the volcano. Geophys. Res. Lett. 9, 1017–1020. https://doi.org/10.1029/GL009i009p01017

Feldman, L., 1993. Mountains of fire, lands that shake : Earthquakes and volcanic eruptions in the historicmnpast of Central America (1505-1899). Labyrinthos, Culver City, California (1993). p.295.

Firstov, P.P., Kravchenko, N.M., 1996. Estimation of the amount of explosive gas released in volcanic eruptions using air waves. Volcanol. Seismol. 17.

Ganci, G., Vicari, A., Cappello, A., Del Negro, C., 2012. An emergent strategy for volcano hazard assessment: From thermal satellite monitoring to lava flow modeling. Remote Sens. Environ. 119, 197–207. https://doi.org/10.1016/j.rse.2011.12.021

Garcés, M., Harris, A., Hetzer, C., Johnson, J., Rowland, S., Marchetti, E., Okubo, P., 2003. Infrasonic tremor observed at Kīlauea Volcano, Hawai'i. Geophys. Res. Lett. 30, 2003GL018038. https://doi.org/10.1029/2003GL018038

Garcés, M., Iguchi, M., Ishihara, K., Morrissey, M., Sudo, Y., Tsutsui, T., 1999. Infrasonic precursors to a Vulcanian Eruption at Sakurajima Volcano, Japan. Geophys. Res. Lett. 26, 2537–2540. https://doi.org/10.1029/1998GL005327

Garcés, M.A., Hagerty, M.T., Schwartz, S.Y., 1998. Magma acoustics and time-varying melt properties at Arenal Volcano, Costa Rica. Geophys. Res. Lett. 25, 2293–2296. https://doi.org/10.1029/98GL01511

Garcés, M.A., Hansen, R.A., 1998. Waveform analysis of seismoacoustic signals radiated during the fall 1996 eruption of Pavlof Volcano, Alaska. Geophys. Res. Lett. 25, 1051–1054. https://doi.org/10.1029/98GL00543

Gaudin, D., Taddeucci, J., Scarlato, P., Harris, A., Bombrun, M., Del Bello, E., Ricci, T., 2017. Characteristics of puffing activity revealed by ground-based, thermal infrared imaging: the example of Stromboli Volcano (Italy). Bull. Volcanol. 79, 24. https://doi.org/10.1007/s00445-017-1108-x

Gibbons, S.J., Ringdal, F., 2006. The detection of low magnitude seismic events using array-based waveform correlation. Geophys. J. Int. 165, 149–166. https://doi.org/10.1111/j.1365-246X.2006.02865.x

Girona, T., Caudron, C., Huber, C., 2019. Origin of Shallow Volcanic Tremor: The Dynamics of Gas Pockets Trapped Beneath Thin Permeable Media. J. Geophys. Res. Solid Earth 124, 4831–4861. https://doi.org/10.1029/2019JB017482

Giudicepietro, F., Calvari, S., Alparone, S., Bianco, F., Bonaccorso, A., Bruno, V., Caputo, T., Cristaldi, A., D'Auria, L., De Cesare, W., Di Lieto, B., Esposito, A.M., Gambino, S., Inguaggiato, S., Macedonio, G., Martini, M., Mattia, M., Orazi, M., Paonita, A., Peluso, R., Privitera, E., Romano, P., Scarpato, G., Tramelli, A., Vita, F., 2019. Integration of Ground-Based Remote-Sensing and In Situ Multidisciplinary

Monitoring Data to Analyze the Eruptive Activity of Stromboli Volcano in 2017–2018. Remote Sens. 11, 1813. https://doi.org/10.3390/rs11151813

Global Volcanism Program, 1980. Report on Santa Maria (Guatemala) (Squires, D., ed.). Scientific Event Alert Network Bulletin, 5:12. Smithsonian Institution. https://doi.org/10.5479/si.GVP.SEAN198012-342030.

Global Volcanism Program, 1985. Report on Santa Maria (Guatemala) (McClelland, L., ed.). Scientific Event Alert Network Bulletin, 10:2. Smithsonian Institution. https://doi.org/10.5479/si.GVP.SEAN198502-342030.

Global Volcanism Program, 1990. Report on Santa Maria (Guatemala) (McClelland, L., ed.). Bulletin of the Global Volcanism Network, 15:6. Smithsonian Institution. https://doi.org/10.5479/si.GVP.BGVN199006-342030.

Global Volcanism Program, 1996. Report on Santa Maria (Guatemala) (Wunderman, R., ed.). Bulletin of the Global Volcanism Network, 21:12. Smithsonian Institution. https://doi.org/10.5479/si.GVP.BGVN199612-342030.

Global Volcanism Program, 2003. Report on Santa Maria (Guatemala) (Venzke, E., ed.). Bulletin of the Global Volcanism Network, 28:5. Smithsonian Institution. https://doi.org/10.5479/si.GVP.BGVN200305-342030.

Global Volcanism Program, 2007. Report on Santa Maria (Guatemala) (Wunderman, R., ed.). Bulletin of the Global Volcanism Network, 32:10. Smithsonian Institution. https://doi.org/10.5479/si.GVP.BGVN200710-342030.

Global Volcanism Program, 2012. Report on Fuego (Guatemala). In: Sennert, S K (ed.), Weekly Volcanic Activity Report, 12 September-18 September 2012. Smithsonian Institution and US Geological Survey.

Global Volcanism Program, 2015. Report on Santa Maria (Guatemala). In: Sennert, S K (ed.), Weekly Volcanic Activity Report, 20 May-26 May 2015. Smithsonian Institution and US Geological Survey

Global Volcanism Program, 2016a. Report on Santa Maria (Guatemala). In: Venzke, E (ed.), Bulletin of the Global Volcanism Network, 41:9. Smithsonian Institution

Global Volcanism Program, 2016b. Report on Santa Maria (Guatemala). In: Sennert, S K (ed.), Weekly Volcanic Activity Report, 2 March-8 March 2016. Smithsonian Institution and US Geological Survey

Global Volcanism Program, 2017a. Report on Santa Maria (Guatemala). In: Venzke, E (ed.), Bulletin of the Global Volcanism Network, 42:7. Smithsonian Institution.

Global Volcanism Program, 2017b. Report on Santa Maria (Guatemala). In: Venzke, E (ed.), Bulletin of the Global Volcanism Network, 42:12. Smithsonian Institution.

Global Volcanism Program, 2018a. Report on Krakatau (Indonesia) (Crafford, A.E., and Venzke, E., eds.). Bulletin of the Global Volcanism Network, 43:10. Smithsonian Institution. https://doi.org/10.5479/si.GVP.BGVN201810-262000

Global Volcanism Program, 2018b. Report on Fuego (Guatemala) (Crafford, A.E., and Venzke, E., eds.). Bulletin of the Global Volcanism Network, 43:8. Smithsonian Institution. https://doi.org/10.5479/si.GVP.BGVN201808-342090

Global Volcanism Program, 2018c. Report on Santa Maria (Guatemala). In: Venzke, E (ed.), Bulletin of the Global Volcanism Network, 43:05. Smithsonian Institution.

Global Volcanism Program, 2018d. Report on Santa Maria (Guatemala). In: Venzke, E (ed.), Bulletin of the Global Volcanism Network, 43:12. Smithsonian Institution.

Global Volcanism Program, 2018e. Report on Fuego (Guatemala), 31 January-6 February. Editor S K Sennert, Weekly Volcanic Activity Report. Smithsonian Institution and US Geological Survey.

Global Volcanism Program, 2018f. Report on Fuego (Guatemala), 30 May-5 June 2018. Editor S K Sennert, Weekly Volcanic Activity Report. Smithsonian Institution and US

Geological Survey.

Global Volcanism Program, 2018g. Report on Fuego (Guatemala), 14 November-20 November 2018. Editor S K Sennert, Weekly Volcanic Activity Report. Smithsonian Institution and US Geological Survey.

Global Volcanism Program, 2019a. Report on Fuego (Guatemala), 20 March-26 March. Editor S K Sennert, Weekly Volcanic Activity Report. Smithsonian Institution and US Geological Survey.

Global Volcanism Program, 2019b. Report on Fuego (Guatemala), 27 March-2 April. Editor S K Sennert, Weekly Volcanic Activity Report. Smithsonian Institution and US Geological Survey.

Global Volcanism Program, 2019c. Report on Fuego (Guatemala), 15 May-21 May. Editor S K Sennert, Weekly Volcanic Activity Report. Smithsonian Institution and US Geological Survey.

Global Volcanism Program, 2019d. Report on Santa Maria (Guatemala). In: Sennert, S K (ed.), Weekly Volcanic Activity Report, 26 June-2 July 2019. Smithsonian Institution and US Geological Survey.

Global Volcanism Program, 2019e. Report on Fuego (Guatemala), 28 August-3 September. Editor S K Sennert, Weekly Volcanic Activity Report. Smithsonian Institution and US Geological Survey.

Global Volcanism Program, 2020a. Report on Fuego (Guatemala), 18 March-24 March. Editor S K Sennert, Weekly Volcanic Activity Report. Smithsonian Institution and US Geological Survey.

Global Volcanism Program, 2020b. Report on Fuego (Guatemala), 28 October-3 November. Editor S K Sennert, Weekly Volcanic Activity Report. Smithsonian Institution and US Geological Survey.

Gonnermann, H.M., Manga, M., 2003. Explosive volcanism may not be an inevitable consequence of magma fragmentation. Nature 426, 432–435. https://doi.org/10.1038/nature02138

Google Earth V 7.3.3.7786, (January 29, 2021). Volcán de Fuego, Guatemala, 14˚28'39.90"N, 90˚52'55.03"W, eye alt 25.68 km. Digital Globe 2020 (July 21, 2020). Accessed 27 April 2021. http://www.earth.google.com

Goto, A., 1999. A new model for volcanic earthquake at Unzen Volcano: Melt Rupture Model. Geophys. Res. Lett. 26, 2541–2544. https://doi.org/10.1029/1999GL900569

Goto, A., Johnson, J.B., 2011. Monotonic infrasound and Helmholtz resonance at Volcan Villarrica (Chile): MONOTONIC INFRASOUND AT VILLARRICA. Geophys. Res. Lett. 38, n/a-n/a. https://doi.org/10.1029/2011GL046858

Gottschämmer, E., Rohnacher, A., Carter, W., Nüsse, A., Drach, K., De Angelis, S., Lavallée, Y., Kendrick, J.E., Roca, A., Castellanos, P., Chigna, G., Rietbrock, A., 2021. Volcanic emission and seismic tremor at Santiaguito, Guatemala: New insights from long-term seismic, infrasound and thermal measurements in 2018–2020. J. Volcanol. Geotherm. Res. 411, 107154. https://doi.org/10.1016/j.jvolgeores.2020.107154

Grainger, R.G., Peters, D.M., Thomas, G.E., Smith, A.J.A., Siddans, R., Carboni, E., Dudhia, A., 2013. Measuring volcanic plume and ash properties from space. Geol. Soc. Lond. Spec. Publ. 380, 293–320. https://doi.org/10.1144/SP380.7

Green, D.N., Neuberg, J., 2006. Waveform classification of volcanic low-frequency earthquake swarms and its implication at Soufrière Hills Volcano, Montserrat. J. Volcanol. Geotherm. Res. 153, 51–63. https://doi.org/10.1016/j.jvolgeores.2005.08.003

Green, D.N., Neuberg, J., Cayol, V., 2006. Shear stress along the conduit wall as a plausible source of tilt at Soufrière Hills volcano, Montserrat: SOUFRIÈRE HILLS VOLCANO, MONTSERRAT. Geophys. Res. Lett. 33, n/a-n/a. https://doi.org/10.1029/2006GL025890

Greenfield, T., Keir, D., Kendall, J.-M., Ayele, A., 2019. Low-frequency earthquakes beneath Tullu Moye volcano, Ethiopia, reveal fluid pulses from shallow magma chamber. Earth Planet. Sci. Lett. 526, 115782. https://doi.org/10.1016/j.epsl.2019.115782

Greenfield, T., White, R.S., Roecker, S., 2016. The magmatic plumbing system of the Askja central volcano, Iceland, as imaged by seismic tomography: THE MAGMATIC PLUMBING SYSTEM OF ASKJA. J. Geophys. Res. Solid Earth 121, 7211–7229. https://doi.org/10.1002/2016JB013163

Gutenberg, B., Richter, C.F., 1944. Frequency of earthquakes in California. Bull. Seismol. Soc. Am. 34, 185–188

Hagerty, M.T., Schwartz, S.Y., Garcés, M.A., Protti, M., 2000. Analysis of seismic and acoustic observations at Arenal Volcano, Costa Rica, 1995–1997. J. Volcanol. Geotherm. Res. 101, 27–65. https://doi.org/10.1016/S0377-0273(00)00162-1

Hammer, C., Beyreuther, M., Ohrnberger, M., 2012. A Seismic-Event Spotting System for Volcano Fast-Response Systems. Bull. Seismol. Soc. Am. 102, 948–960. https://doi.org/10.1785/0120110167

Hammer, C., Ohrnberger, M., Fäh, D., 2013. Classifying seismic waveforms from scratch: a case study in the alpine environment. Geophys. J. Int. 192, 425–439. https://doi.org/10.1093/gji/ggs036

Hanagan, C., La Femina, P.C., Rodgers, M., 2020. Changes in Crater Morphology Associated With Volcanic Activity at Telica Volcano, Nicaragua. Geochem. Geophys. Geosystems 21. https://doi.org/10.1029/2019GC008889

Harris, A.J., Rose, W.I., Flynn, L.P., 2003. Temporal trends in lava dome extrusion at Santiaguito 1922–2000. Bull. Volcanol. 65, 77–89. https://doi.org/10.1007/s00445-002-0243-0

Harris, A.J.L., Flynn, L.P., Matías, O., Rose, W.I., 2002. The thermal stealth flows of Santiaguito dome, Guatemala: Implications for the cooling and emplacement of dacitic block-lava flows. GSA Bull. 114, 533–546. https://doi.org/10.1130/0016-7606(2002)114<0533:TTSFOS>2.0.CO;2

Harris, A.J.L., Vallance, J.W., Kimberly, P., Rose, W.I., Matías, O., Bunzendahl, E., Flynn, L.P., Garbeil, H., 2006. Downstream aggradation owing to lava dome extrusion and rainfall runoff at Volcán Santiaguito, Guatemala, in: Volcanic Hazards in Central America. Geological Society of America. https://doi.org/10.1130/2006.2412(05)

Hess, K.-U., Dingwell, D.B., 1996. Viscosities of hydrous leucogranitic melts: a non-Arrhenian model. Am. Mineral. 81, 1297-1300.

Hibert, C., Provost, F., Malet, J.-P., Maggi, A., Stumpf, A., Ferrazzini, V., 2017. Automatic identification of rockfalls and volcano-tectonic earthquakes at the Piton de la Fournaise volcano using a Random Forest algorithm. J. Volcanol. Geotherm. Res. 340, 130–142. https://doi.org/10.1016/j.jvolgeores.2017.04.015

Holland, A.S.P., Watson, I.M., Phillips, J.C., Caricchi, L., Dalton, M.P., 2011. Degassing processes during lava dome growth: Insights from Santiaguito lava dome, Guatemala. J. Volcanol. Geotherm. Res. 202, 153–166. https://doi.org/10.1016/j.jvolgeores.2011.02.004

Hornby, A.J., Lavallée, Y., Kendrick, J.E., De Angelis, S., Lamur, A., Lamb, O.D., Rietbrock, A., Chigna, G., 2019. Brittle-Ductile Deformation and Tensile Rupture of Dome Lava During Inflation at Santiaguito, Guatemala. J. Geophys. Res. Solid Earth 124, 10107–10131. https://doi.org/10.1029/2018JB017253

Hotovec, A.J., Prejean, S.G., Vidale, J.E., Gomberg, J., 2013. Strongly gliding harmonic tremor during the 2009 eruption of Redoubt Volcano. J. Volcanol. Geotherm. Res. 259, 89–99. https://doi.org/10.1016/j.jvolgeores.2012.01.001

Huang, Y., Beroza, G.C., 2015. Temporal variation in the magnitude-frequency distribution during the Guy-Greenbrier earthquake sequence. Geophys. Res. Lett.

42(16), 6639-6646 https://doi.org/10.1002/2015GL065170

Huang, R., Song, W.-Z., Xu, M., Peterson, N., Shirazi, B., LaHusen, R., 2012. Real-World Sensor Network for Long-Term Volcano Monitoring: Design and Findings. IEEE Trans. Parallel Distrib. Syst. 23, 321–329. https://doi.org/10.1109/TPDS.2011.170

Hutchison, A.A., Cashman, K.V., Williams, C.A., Rust, A.C., 2016. The 1717 eruption of Volcán de Fuego, Guatemala: Cascading hazards and societal response. Quat. Int. 394, 69–78. https://doi.org/10.1016/j.quaint.2014.09.050

Ibs-von Seht, M., 2008. Detection and identification of seismic signals recorded at Krakatau volcano (Indonesia) using artificial neural networks. J. Volcanol. Geotherm. Res. 176, 448–456. https://doi.org/10.1016/j.jvolgeores.2008.04.015

Ichihara, M., Takeo, M., Yokoo, A., Oikawa, J., Ohminato, T., 2012. Monitoring volcanic activity using correlation patterns between infrasound and ground motion: INFRASONIC-SEISMIC CORRELATION METHOD. Geophys. Res. Lett. 39, n/a-n/a. https://doi.org/10.1029/2011GL050542

Iezzi, A.M., Fee, D., Kim, K., Jolly, A.D., Matoza, R.S., 2019. Three‐Dimensional Acoustic Multipole Waveform Inversion at Yasur Volcano, Vanuatu. J. Geophys. Res. Solid Earth 124, 8679–8703. https://doi.org/10.1029/2018JB017073

Ilanko, T., Pering, T., Wilkes, T., Apaza Choquehuayta, F., Kern, C., Díaz Moreno, A., De Angelis, S., Layana, S., Rojas, F., Aguilera, F., Vasconez, F., McGonigle, A., 2019. Degassing at Sabancaya volcano measured by UV cameras and the NOVAC network. Volcanica 2, 239–252. https://doi.org/10.30909/vol.02.02.239252

Ishimoto, M., Iida, I., 1939. Observations of earthquakes registered with the microseismograph constructed recently. Bull. Earthq. Res. Inst.

Iverson, R.M., Dzurisin, D., Gardner, C.A., Gerlach, T.M., LaHusen, R.G., Lisowski, M., Major, J.J., Malone, S.D., Messerich, J.A., Moran, S.C., Pallister, J.S., Qamar, A.I., Schilling, S.P., Vallance, J.W., 2006. Dynamics of seismogenic volcanic extrusion at Mount St Helens in 2004–05. Nature 444, 439–443. https://doi.org/10.1038/nature05322

Jaupart, C., Vergniolle, S., 1988. Laboratory models of Hawaiian and Strombolian eruptions. Nature 331, 58–60. https://doi.org/10.1038/331058a0

Jeddi, Z., Tryggvason, A., Gudmundsson, Ó., 2016. The Katla volcanic system imaged using local earthquakes recorded with a temporary seismic network: Three-Dimensional Velocity Structure of Katla Volcano. J. Geophys. Res. Solid Earth 121, 7230–7251. https://doi.org/10.1002/2016JB013044

Johnson, J.B., 2003. Generation and propagation of infrasonic airwaves from volcanic explosions. J. Volcanol. Geotherm. Res. 121, 1–14. https://doi.org/10.1016/S0377-0273(02)00408-0

Johnson, J.B., Aster, R.C., 2005. Relative partitioning of acoustic and seismic energy during Strombolian eruptions. J. Volcanol. Geotherm. Res. 148, 334–354. https://doi.org/10.1016/j.jvolgeores.2005.05.002

Johnson, J.B., Lees, J.M., 2000. Plugs and chugs—seismic and acoustic observations of degassing explosions at Karymsky, Russia and Sangay, Ecuador. J. Volcanol. Geotherm. Res. 101, 67–82. https://doi.org/10.1016/S0377-0273(00)00164-5

Johnson, J.B., Harris, A.J.L., Sahetapy-Engel, S.T.M., Wolf, R., Rose, W.I., 2004. Explosion dynamics of pyroclastic eruptions at Santiaguito Volcano. Geophys. Res. Lett. 31, L06610. https://doi.org/10.1029/2003GL019079

Johnson, J.B., Lees, J., Varley, N., 2011. Characterizing complex eruptive activity at Santiaguito, Guatemala using infrasound semblance in networked arrays. J. Volcanol. Geotherm. Res. 199, 1–14. https://doi.org/10.1016/j.jvolgeores.2010.08.005

Johnson, J.B., Lees, J.M., 2010. Sound produced by the rapidly inflating Santiaguito lava dome, Guatemala: SOUND FROM THE SANTIAGUITO LAVA DOME. Geophys.

Res. Lett. 37, n/a-n/a. https://doi.org/10.1029/2010GL045217

Johnson, J.B., Lees, J.M., Gerst, A., Sahagian, D., Varley, N., 2008. Long-period earthquakes and co-eruptive dome inflation seen with particle image velocimetry. Nature 456, 377–381. https://doi.org/10.1038/nature07429

Johnson, J.B., Lees, J.M., Gordeev, E.I., 1998. Degassing explosions at Karymsky Volcano, Kamchatka. Geophys. Res. Lett. 25, 3999–4002. https://doi.org/10.1029/1998GL900102

Johnson, J.B., Lyons, J.J., Andrews, B.J., Lees, J.M., 2014. Explosive dome eruptions modulated by periodic gas-driven inflation: Dome eruptions and periodic inflation. Geophys. Res. Lett. 41, 6689–6697. https://doi.org/10.1002/2014GL061310

Johnson, J.B., Ripepe, M., 2011. Volcano infrasound: A review. J. Volcanol. Geotherm. Res. 206, 61–69. https://doi.org/10.1016/j.jvolgeores.2011.06.006

Johnson, J.B., Watson, L.M., Palma, J.L., Dunham, E.M., Anderson, J.F., 2018. Forecasting the Eruption of an Open-Vent Volcano Using Resonant Infrasound Tones. Geophys. Res. Lett. 45, 2213–2220. https://doi.org/10.1002/2017GL076506

Jolly, A., Kennedy, B., Edwards, M., Jousset, P., Scheu, B., 2016. Infrasound tremor from bubble burst eruptions in the viscous shallow crater lake of White Island, New Zealand, and its implications for interpreting volcanic source processes. J. Volcanol. Geotherm. Res. 327, 585–603. https://doi.org/10.1016/j.jvolgeores.2016.08.010

Jones, K.R., Johnson, J.B., 2011. Mapping complex vent eruptive activity at Santiaguito, Guatemala using network infrasound semblance. J. Volcanol. Geotherm. Res. 199, 15–24. https://doi.org/10.1016/j.jvolgeores.2010.08.006

Julian, B.R., 2000. Period doubling and other nonlinear phenomena in volcanic earthquakes and tremor. J. Volcanol. Geotherm. Res. 101, 19–26. https://doi.org/10.1016/S0377-0273(00)00165-7

Julian, B.R., 1994. Volcanic tremor: Nonlinear excitation by fluid flow. J. Geophys. Res. Solid Earth 99, 11859–11877. https://doi.org/10.1029/93JB03129

Kanamori, H., Given, J.W., Lay, T., 1984. Analysis of seismic body waves excited by the Mount St. Helens eruption of May 18, 1980. J. Geophys. Res. Solid Earth 89, 1856–1866. https://doi.org/10.1029/JB089iB03p01856

Kendrick, J.E., Lavallée, Y., Hess, K.U., Heap, M.J., Gaunt, H.E., Meredith, P.G., Dingwell, D.B., 2013. Tracking the permeable porous network during strain-dependent magmatic flow. J. Volcanol. Geotherm. Res. 260, 117–126. https://doi.org/10.1016/j.jvolgeores.2013.05.012

Kendrick, J.E., Lavallée, Y., Varley, N.R., Wadsworth, F.B., Lamb, O.D., Vasseur, J., 2016. Blowing off steam: Tuffisite formation as a regulator for lava dome eruptions. Front. Earth Sci. https://doi.org/10.3389/feart.2016.00041

Kilburn, C., 2012. Precursory deformation and fracture before brittle rock failure and potential application to volcanic unrest. J. Geophys. Res. Solid Earth. 117, B02211. https://doi.org/10.1029/2011JB008703

Kilburn, C.R.J., 2003. Multiscale fracturing as a key to forecasting volcanic eruptions. J. Volcanol. Geotherm. Res. 125, 271-289. https://doi.org/10.1016/S0377-0273(03)00117-3

Kim, K., Lees, J.M., 2015. Imaging volcanic infrasound sources using time reversal mirror algorithm. Geophys. J. Int. 202, 1663–1676. https://doi.org/10.1093/gji/ggv237

Kim, K., Lees, J.M., Ruiz, M.C., 2014. Source mechanism of Vulcanian eruption at Tungurahua Volcano, Ecuador, derived from seismic moment tensor inversions. J. Geophys. Res. Solid Earth 119, 1145–1164. https://doi.org/10.1002/2013JB010590

Kueppers, U., Scheu, B., Spieler, O., Dingwell, D.B., 2006. Fragmentation efficiency of explosive volcanic eruptions: A study of experimentally generated pyroclasts. J. Volcanol. Geotherm. Res. 153, 125-135.

https://doi.org/10.1016/j.jvolgeores.2005.08.006

Kumagai, H., Palacios, P., Maeda, T., Castillo, D.B., Nakano, M., 2009. Seismic tracking of lahars using tremor signals. J. Volcanol. Geotherm. Res. 183, 112–121. https://doi.org/10.1016/j.jvolgeores.2009.03.010

Lamb, O.D., Lamur, A., Díaz-Moreno, A., De Angelis, S., Hornby, A.J., von Aulock, F.W., Kendrick, J.E., Wallace, P.A., Gottschämmer, E., Rietbrock, A., Alvarez, I., Chigna, G., Lavallée, Y., 2019. Disruption of Long-Term Effusive-Explosive Activity at Santiaguito, Guatemala. Front. Earth Sci. 6, 253. https://doi.org/10.3389/feart.2018.00253

Lamb, O.D., Varley, N.R., Mather, T.A., Pyle, D.M., Smith, P.J., Liu, E.J., 2014. Multiple timescales of cyclical behaviour observed at two dome-forming eruptions. J. Volcanol. Geotherm. Res. 284, 106-121. https://doi.org/10.1016/j.jvolgeores.2014.07.013

Lanari, R., Lundgren, P., Sansosti, E., 1998. Dynamic deformation of Etna Volcano observed by satellite radar interferometry. Geophys. Res. Lett. 25, 1541–1544. https://doi.org/10.1029/98GL00642

Langer, H., Falsaperla, S., Powell, T., Thompson, G., 2006. Automatic classification and a-posteriori analysis of seismic event identification at Soufrière Hills volcano, Montserrat. J. Volcanol. Geotherm. Res. 153, 1–10. https://doi.org/10.1016/j.jvolgeores.2005.08.012

Lanza, F., Waite, G.P., 2018. A nonlinear approach to assess network performance for moment-tensor studies of long-period signals in volcanic settings. Geophys. J. Int. 215, 1352–1367. https://doi.org/10.1093/gji/ggy338

Lavallée, Y., Benson, P.M., Heap, M.J., Hess, K.U., Flaws, A., Schillinger, B., Meredith, P.G., Dingwell, D.B., 2013. Reconstructing magma failure and the degassing network of domebuilding eruptions. Geology 41, 515–518. https://doi.org/10.1130/G33948.1

Lavallée, Y., Dingwell, D.B., Johnson, J.B., Cimarelli, C., Hornby, A.J., Kendrick, J.E., von Aulock, F.W., Kennedy, B.M., Andrews, B.J., Wadsworth, F.B., Rhodes, E., Chigna, G., 2015. Thermal vesiculation during volcanic eruptions. Nature 528, 544–547. https://doi.org/10.1038/nature16153

Lavallée, Y., Heap, M.J., Kendrick, J.E., Kueppers, U., Dingwell, D.B., 2019. The Fragility of Volcán de Colima—A Material Constraint. In: Varley N., Connor C., Komorowski JC. (eds) Volcán de Colima. Active Volcanoes of the World. Springer, Berlin, Heidelberg. 241-266. https://doi.org/10.1007/978-3-642-25911-1_7

Lavallée, Y., Meredith, P.G., Dingwell, D.B., Hess, K.-U., Wassermann, J., Cordonnier, B., Gerik, A., Kruhl, J.H., 2008. Seismogenic lavas and explosive eruption forecasting. Nature 453, 507–510. https://doi.org/10.1038/nature06980

Lavallée, Y., Varley, N.R., Alatorre-Ibargüengoitia, M.A., Hess, K.U., Kueppers, U., Mueller, S., Richard, D., Scheu, B., Spieler, O., Dingwell, D.B., 2012. Magmatic architecture of dome-building eruptions at Volcán de Colima, Mexico. Bull. Volcanol. 74, 249–260. https://doi.org/10.1007/s00445-011-0518-4

Lipovsky, B.P., Dunham, E.M., 2015. Vibrational modes of hydraulic fractures: Inference of fracture geometry from resonant frequencies and attenuation. J. Geophys. Res. Solid Earth 120, 1080–1107. https://doi.org/10.1002/2014JB011286

Liu, E.J., Cashman, K.V., Miller, E., Moore, H., Edmonds, M., Kunz, B.E., Jenner, F., Chigna, G., 2020. Petrologic monitoring at Volcán de Fuego, Guatemala. J. Volcanol. Geotherm. Res. 405, 107044. https://doi.org/10.1016/j.jvolgeores.2020.107044

Lyons, J.J., Ichihara, M., Kurokawa, A., Lees, J.M., 2013. Switching between seismic and seismo-acoustic harmonic tremor simulated in the laboratory: Insights into the role of open degassing channels and magma viscosity: SHT - SAHT SWITCHING SIMULATED IN THE LAB. J. Geophys. Res. Solid Earth 118, 277–289. https://doi.org/10.1002/jgrb.50067

Lyons, J.J., Johnson, J.B., Waite, G.P., Rose, W.I., 2007. Observations of cyclic strombolian eruptive behavior at Fuego volcano, Guatemala reflected in the seismo-acoustic record. American Geophysical Union, Fall Meeting 2007, abstract id. V11C-0745

Lyons, J.J., Waite, G.P., 2011. Dynamics of explosive volcanism at Fuego volcano imaged with very long period seismicity. J. Geophys. Res. 116, B09303. https://doi.org/10.1029/2011JB008521

Lyons, J.J., Waite, G.P., Ichihara, M., Lees, J.M., 2012. Tilt prior to explosions and the effect of topography on ultra-long-period seismic records at Fuego volcano, Guatemala: TILT AND THE EFFECT OF TOPOGRAPHY. Geophys. Res. Lett. 39, n/a-n/a. https://doi.org/10.1029/2012GL051184

Lyons, J.J., Waite, G.P., Rose, W.I., Chigna, G., 2010. Patterns in open vent, strombolian behavior at Fuego volcano, Guatemala, 2005–2007. Bull. Volcanol. 72, 1–15. https://doi.org/10.1007/s00445-009-0305-7

Marchetti, E., Ripepe, M., Campus, P., Le Pichon, A., Brachet, N., Blanc, E., Gaillard, P., Mialle, P., Husson, P., Arnal, T., 2019. Infrasound Monitoring of Volcanic Eruptions and Contribution of ARISE to the Volcanic Ash Advisory Centers, in: Le Pichon, A., Blanc, E., Hauchecorne, A. (Eds.), Infrasound Monitoring for Atmospheric Studies. Springer International Publishing, Cham, pp. 1141–1162. https://doi.org/10.1007/978-3-319-75140-5_36

Marzocchi, W., Papale, P., 2019. Volcanic threats to global society. Science. 363, 1275-1276. https://doi.org/10.1126/science.aaw7201

Martin, D.P., Rose, W.I., 1981. Behavioral patterns of Fuego volcano, Guatemala. J. Volcanol. Geotherm. Res. 10, 67–81. https://doi.org/10.1016/0377-0273(81)90055-X

Massol, H., Jaupart, C., 1999. The generation of gas overpressure in volcanic eruptions. Earth Planet. Sci. Lett. 166, 57–70. https://doi.org/10.1016/S0012-821X(98)00277-5

Mastin, L.G., 2005. The controlling effect of viscous dissipation on magma flow in silicic conduits. J. Volcanol. Geotherm. Res. 143, 17-28. https://doi.org/10.1016/j.jvolgeores.2004.09.008

Matoza, R.S., Fee, D., 2014. Infrasonic component of volcano-seismic eruption tremor. Geophys. Res. Lett. 41, 1964–1970. https://doi.org/10.1002/2014GL059301

McNutt, S.R., 2005. VOLCANIC SEISMOLOGY. Annu. Rev. Earth Planet. Sci. 33, 461–491. https://doi.org/10.1146/annurev.earth.33.092203.122459

McNutt, S.R., Roman, D.C., 2015. Volcanic Seismicity, in: The Encyclopedia of Volcanoes. Elsevier, pp. 1011–1034. https://doi.org/10.1016/B978-0-12-385938-9.00059-6

Melnik, O., Sparks, R.S.J., 1999. Nonlinear dynamics of lava dome extrusion. Nature 402, 37–41. https://doi.org/10.1038/46950

Miller, A.D., Stewart, R.C., White, R.A., Luckett, R., Baptie, B.J., Aspinall, W.P., Latchman, J.L., Lynch, L.L., Voight, B., 1998. Seismicity associated with dome growth and collapse at the oufriere Hills Volcano, Montserrat. Geophys. Res. Lett. 25, 3401–3404. https://doi.org/10.1029/98GL01778

Mueller, S., Scheu, B., Kueppers, U., Spieler, O., Richard, D., Dingwell, D.B., 2011. The porosity of pyroclasts as an indicator of volcanic explosivity. J. Volcanol. Geotherm. Res. 203, 168–174. https://doi.org/10.1016/j.jvolgeores.2011.04.006

Nadeau, P.A., Palma, J.L., Waite, G.P., 2011. Linking volcanic tremor, degassing, and eruption dynamics via SO $_2$ imaging: LINKING VOLCANIC TREMOR AND DEGASSING. Geophys. Res. Lett. 38, n/a-n/a. https://doi.org/10.1029/2010GL045820

Naismith, A.K., Matthew Watson, I., Escobar-Wolf, R., Chigna, G., Thomas, H., Coppola, D., Chun, C., 2019. Eruption frequency patterns through time for the current (1999–2018) activity cycle at Volcán de Fuego derived from remote sensing data: Evidence for an accelerating cycle of explosive paroxysms and potential implications of eruptive activity. J. Volcanol. Geotherm. Res. 371, 206–219. https://doi.org/10.1016/j.jvolgeores.2019.01.001

Nakano, M., Kumagai, H., Chouet, B.A., 2003. Source mechanism of long-period events at Kusatsu–Shirane Volcano, Japan, inferred from waveform inversion of the effective excitation functions. J. Volcanol. Geotherm. Res. 122, 149–164. https://doi.org/10.1016/S0377-0273(02)00499-7

Neuberg, J., Baptie, B., Luckett, R., Stewart, R., 1998. Results from the Broadband Seismic Network on Montserrat. Geophys. Res. Lett. 25, 3661–3664. https://doi.org/10.1029/98GL01441

Neuberg, J.W., Collinson, A.S.D., Mothes, P.A., C. Ruiz, M., Aguaiza, S., 2018. Understanding cyclic seismicity and ground deformation patterns at volcanoes: Intriguing lessons from Tungurahua volcano, Ecuador. Earth Planet. Sci. Lett. 482, 193–200. https://doi.org/10.1016/j.epsl.2017.10.050

Neuberg, J.W., Tuffen, H., Collier, L., Green, D., Powell, T., Dingwell, D., 2006. The trigger mechanism of low-frequency earthquakes on Montserrat. J. Volcanol. Geotherm. Res. 153, 37–50. https://doi.org/10.1016/j.jvolgeores.2005.08.008

Nishimura, T., 1998. Source mechanisms of volcanic explosion earthquakes: single force and implosive sources. J. Volcanol. Geotherm. Res. 86, 97–106. https://doi.org/10.1016/S0377-0273(98)00088-2

Nishimura, T., Iguchi, M., Hendrasto, M., Aoyama, H., Yamada, T., Ripepe, M., Genco, R., 2016. Magnitude-frequency distribution of volcanic explosion earthquakes 5. Volcanology. Earth, Planets Sp. 68, 125. https://doi.org/10.1186/s40623-016-0505-2

Nugraha, A.D., Indrastuti, N., Kusnandar, R., Gunawan, H., McCausland, W., Aulia, A.N., Harlianti, U., 2019. Joint 3-D tomographic imaging of Vp, Vs and Vp/Vs and hypocenter relocation at Sinabung volcano, Indonesia from November to December 2013. J. Volcanol. Geotherm. Res. 382, 210–223. https://doi.org/10.1016/j.jvolgeores.2017.09.018

Obermann, A., Molinari, I., Métaxian, J.-P., Grigoli, F., Strauch, W., Wiemer, S., 2019. Structure of Masaya and Momotombo volcano, Nicaragua, investigated with a temporary seismic network. J. Volcanol. Geotherm. Res. 379, 1–11. https://doi.org/10.1016/j.jvolgeores.2019.04.013

Oikawa, G., Aso, N., Nakajima, J., 2019. Focal Mechanisms of Deep Low-Frequency Earthquakes Beneath Zao Volcano, Northeast Japan, and Relationship to the 2011 Tohoku Earthquake. Geophys. Res. Lett. 46, 7361–7370. https://doi.org/10.1029/2019GL082577

Oliva, S.J., Ebinger, C.J., Wauthier, C., Muirhead, J.D., Roecker, S.W., Rivalta, E., Heimann, S., 2019. Insights Into Fault-Magma Interactions in an Early-Stage Continental Rift From Source Mechanisms and Correlated Volcano-Tectonic Earthquakes. Geophys. Res. Lett. 46, 2065–2074. https://doi.org/10.1029/2018GL080866

Ortiz, R., 2003. Villarrica volcano (Chile): characteristics of the volcanic tremor and forecasting of small explosions by means of a material failure method. J. Volcanol. Geotherm. Res. 128, 247–259. https://doi.org/10.1016/S0377-0273(03)00258-0

Palacios, P.B., Díez, M., Kendall, J.-M., Mader, H.M., 2016. Seismic-acoustic energy partitioning during a paroxysmal eruptive phase of Tungurahua volcano, Ecuador. Geophys. J. Int. 205, 1900–1915. https://doi.org/10.1093/gji/ggw136

Papale, P., 1999. Strain-induced magma fragmentation in explosive eruptions. Nature 397, 425–428. https://doi.org/10.1038/17109

Papale, P., 2018. Global time-size distribution of volcanic eruptions on Earth. Sci. Rep. 8, 6838. https://doi.org/10.1038/s41598-018-25286-y

Pardini, F., Queißer, M., Naismith, A., Watson, I.M., Clarisse, L., Burton, M.R., 2019. Initial constraints on triggering mechanisms of the eruption of Fuego volcano (Guatemala) from 3 June 2018 using IASI satellite data. J. Volcanol. Geotherm. Res.

376, 54–61. https://doi.org/10.1016/j.jvolgeores.2019.03.014

Parfitt, E.A., 2004. A discussion of the mechanisms of explosive basaltic eruptions. J. Volcanol. Geotherm. Res. 134, 77–107. https://doi.org/10.1016/j.jvolgeores.2004.01.002

Parfitt, E.A., Wilson, L., 1995. Explosive volcanic eruptions-IX. The transition between Hawaiian-style lava fountaining and Strombolian explosive activity. Geophys. J. Int. 121, 226–232. https://doi.org/10.1111/j.1365-246X.1995.tb03523.x

Parker, A.L., Biggs, J., Lu, Z., 2014. Investigating long-term subsidence at Medicine Lake Volcano, CA, using multitemporal InSAR. Geophys. J. Int. 199, 844–859. https://doi.org/10.1093/gji/ggu304

Pierce, A.D., Smith, P.W., 1981. Acoustics: An Introduction to Its Physical Principles and Applications. Phys. Today 34, 56–57. https://doi.org/10.1063/1.2914388

Poland, M., Bürgmann, R., Dzurisin, D., Lisowski, M., Masterlark, T., Owen, S., Fink, J., 2006. Constraints on the mechanism of long-term, steady subsidence at Medicine Lake volcano, northern California, from GPS, leveling, and InSAR. J. Volcanol. Geotherm. Res. 150, 55–78. https://doi.org/10.1016/j.jvolgeores.2005.07.007

Power, J.A., Haney, M.M., Botnick, S.M., Dixon, J.P., Fee, D., Kaufman, A.M., Ketner, D.M., Lyons, J.J., Parker, T., Paskievitch, J.F., Read, C.W., Searcy, C., Stihler, S.D., Tepp, G., Wech, A.G., 2020. Goals and Development of the Alaska Volcano Observatory Seismic Network and Application to Forecasting and Detecting Volcanic Eruptions. Seismol. Res. Lett. 91, 647–659. https://doi.org/10.1785/0220190216

Prejean, S.G., Brodsky, E.E., 2011. Volcanic plume height measured by seismic waves based on a mechanical model. J. Geophys. Res. 116, B01306. https://doi.org/10.1029/2010JB007620

Quane, S.L., Russell, J.K., 2005. Welding: Insights from high-temperature analogue experiments. J. Volcanol. Geotherm. Res. 142, 67-87.

https://doi.org/10.1016/j.jvolgeores.2004.10.014

Reubi, O., Blundy, J., Pickles, J., 2019. Petrological Monitoring of Volcán de Colima Magmatic System: The 1998 to 2011 Activity, in: Varley, N., Connor, C.B., Komorowski, J.-C. (Eds.), Volcán de Colima, Active Volcanoes of the World. Springer Berlin Heidelberg, Berlin, Heidelberg, pp. 219–240. https://doi.org/10.1007/978-3-642-25911-1_9

Rhodes, E., Kennedy, B.M., Lavallée, Y., Hornby, A., Edwards, M., Chigna, G., 2018. Textural Insights Into the Evolving Lava Dome Cycles at Santiaguito Lava Dome, Guatemala. Front. Earth Sci. 6, 30. https://doi.org/10.3389/feart.2018.00030

Richardson, J.P., Waite, G.P., Palma, J.L., 2014. Varying seismic-acoustic properties of the fluctuating lava lake at Villarrica volcano, Chile: Lava Lake Seismic-Acoustic Properties. J. Geophys. Res. Solid Earth 119, 5560–5573. https://doi.org/10.1002/2014JB011002

Ripepe, M., Coltelli, M., Privitera, E., Gresta, S., Moretti, M., Piccinini, D., 2001. Seismic and infrasonic evidences for an impulsive source of the shallow volcanic tremor at Mt. Etna, Italy. Geophys. Res. Lett. 28, 1071–1074. https://doi.org/10.1029/2000GL011391

Ripepe, M., Gordeev, E., 1999. Gas bubble dynamics model for shallow volcanic tremor at Stromboli. J. Geophys. Res. Solid Earth 104, 10639–10654. https://doi.org/10.1029/98JB02734

Ripepe, M., Pistolesi, M., Coppola, D., Delle Donne, D., Genco, R., Lacanna, G., Laiolo, M., Marchetti, E., Ulivieri, G., Valade, S., 2017. Forecasting Effusive Dynamics and Decompression Rates by Magmastatic Model at Open-vent Volcanoes. Sci. Rep. 7, 3885. https://doi.org/10.1038/s41598-017-03833-3

Ripepe, M., Poggi, P., Braun, T., Gordeev, E., 1996. Infrasonic waves and volcanic tremor at Stromboli. Geophys. Res. Lett. 23, 181–184. https://doi.org/10.1029/95GL03662

Ripepe, M., Rossi, M., Saccorotti, G., 1993. Image processing of explosive activity at Stromboli. J. Volcanol. Geotherm. Res. 54, 335–351. https://doi.org/10.1016/0377-0273(93)90071-X

Rivet, D., Brenguier, F., Clarke, D., Shapiro, N.M., Peltier, A., 2014. Long-term dynamics of Piton de la Fournaise volcano from 13 years of seismic velocity change measurements and GPS observations. J. Geophys. Res. Solid Earth 119, 7654–7666. https://doi.org/10.1002/2014JB011307

Roberts, N., Bell, A., Main, I., 2015. Are volcanic seismic b-values high, and if so when? J. Volcanol. Geotherm. Res. 308. https://dio.org/10.1016/j.jvolgeores.2015.10.021

Rodríguez, L.A., Watson, I.M., Rose, W.I., Branan, Y.K., Bluth, G.J.S., Chigna, G., Matías, O., Escobar, D., Carn, S.A., Fischer, T.P., 2004. SO2 emissions to the atmosphere from active volcanoes in Guatemala and El Salvador, 1999–2002. J. Volcanol. Geotherm. Res. 138, 325–344. https://doi.org/10.1016/j.jvolgeores.2004.07.008

Roggensack, K., 2001. Unraveling the 1974 eruption of Fuego volcano (Guatemala) with small crystals and their young melt inclusions. Geology 29, 911–914. https://doi.org/10.1130/0091-7613(2001)029<0911:UTEOFV>2.0.CO;2

Rohnacher, A., Rietbrock, A., Gottschämmer, E., Carter, W., Lavallée, Y., De Angelis, S., Kendrick, J.E., Chigna, G., 2021. Source Mechanism of Seismic Explosion Signals at Santiaguito Volcano, Guatemala: New Insights From Seismic Analysis and Numerical Modeling. Front. Earth Sci. 8, 603441. https://doi.org/10.3389/feart.2020.603441

Roman, D.C., Cashman, K.V., 2006. The origin of volcano-tectonic earthquake swarms. Geology 34, 457. https://doi.org/10.1130/G22269.1

Rose, K.M., Matoza, R.S., 2021. Remote hydroacoustic-infrasonic detection and characterization of Anak Krakatau eruptive activity leading to, during, and following the December 2018 flank collapse and tsunami. Bull Volcanol. 83, 50. https://doi.org/10.1007/s00445-021-01468-x

Rose, W.I., 1987. Volcanic activity at Santiaguito volcano, 1976–1984, in: Geological Society of America Special Papers. Geological Society of America, pp. 17–28. https://doi.org/10.1130/SPE212-p17

Rose, W.I., 1972. Santiaguito Volcanic Dome, Guatemala. Geol. Soc. Am. Bull. 83, 1413. https://doi.org/10.1130/0016-7606(1972)83[1413:SVDG]2.0.CO;2

Rose, W.I., Anderson, A.T., Woodruff, L.G., Bonis, S.B., 1978. The October 1974 basaltic tephra from Fuego volcano: Description and history of the magma body. J. Volcanol. Geotherm. Res. 4, 3–53. https://doi.org/10.1016/0377-0273(78)90027-6

Rose, W.I., 1973. Pattern and mechanism of volcanic activity at the Santiaguito Volcanic Dome, Guatemala. Bull. Volcanol. 37, 73. https://doi.org/10.1007/BF02596881

Rose, W.I., Grant, N.K., Hahn, G.A., Lange, I.M., Powell, J.L., Easter, J., Degraff, J.M., 1977. The Evolution of Santa María Volcano, Guatemala. J. Geol. 85, 63–87. https://doi.org/10.1086/628269

Rose, W.I., Self, S., Murrow, P.J., Bonadonna, C., Durant, A.J., Ernst, G.G.J., 2008. Nature and significance of small volume fall deposits at composite volcanoes: Insights from the October 14, 1974 Fuego eruption, Guatemala. Bull. Volcanol. 70, 1043–1067. https://doi.org/10.1007/s00445-007-0187-5

Rougier, J., Sparks, R.S.J., Cashman, K. V., Brown, S.K., 2018. The global magnitude–frequency relationship for large explosive volcanic eruptions. Earth Planet. Sci. Lett. 482, 621-629. https://doi.org/10.1016/j.epsl.2017.11.015

Rowe, C.A., Aster, R.C., Kyle, P.R., Dibble, R.R., Schlue, J.W., 2000. Seismic and acoustic observations at Mount Erebus Volcano, Ross Island, Antarctica, 1994–1998. J. Volcanol. Geotherm. Res. 101, 105–128. https://doi.org/10.1016/S0377-0273(00)00170-0

Rubin, A.M., Gillard, D., 1998. Dike-induced earthquakes: Theoretical considerations. J.

Geophys. Res. Solid Earth 103, 10017–10030. https://doi.org/10.1029/97JB03514

Russell, D.A., Titlow, J.P., Bemmen, Y.-J., 1999. Acoustic monopoles, dipoles, and quadrupoles: An experiment revisited. Am. J. Phys. 67, 660–664. https://doi.org/10.1119/1.19349

Sahetapy-Engel, S.T., Harris, A.J.L., 2009. Thermal-image-derived dynamics of vertical ash plumes at Santiaguito volcano, Guatemala. Bull. Volcanol. 71, 827–830. https://doi.org/10.1007/s00445-009-0284-8

Sahetapy-Engel, S.T., Harris, A.J.L., Marchetti, E., 2008. Thermal, seismic and infrasound observations of persistent explosive activity and conduit dynamics at Santiaguito lava dome, Guatemala. J. Volcanol. Geotherm. Res. 173, 1–14. https://doi.org/10.1016/j.jvolgeores.2007.11.026

Sahetapy-Engel, S.T.M., Flynn, L.P., Harris, A.J.L., Bluth, G.J., Rose, W.I., Matias, O., 2004. Surface temperature and spectral measurements at Santiaguito lava dome, Guatemala. Geophys. Res. Lett. 31, L19610. https://doi.org/10.1029/2004GL020683

Sammis, C.G., Ashby, M.F., 1986. The failure of brittle porous solids under compressive stress states. Acta Metall. 34, 511-526. https://doi.org/10.1016/0001-6160(86)90087-8

Sanderson, R.W., Johnson, J.B., Lees, J.M., 2010. Ultra-long period seismic signals and cyclic deflation coincident with eruptions at Santiaguito volcano, Guatemala. J. Volcanol. Geotherm. Res. 198, 35–44. https://doi.org/10.1016/j.jvolgeores.2010.08.007

Sanderson, R.W., Matoza, R.S., Haymon, R.M., Steidl, J.H., 2021. A Pilot Experiment on Infrasonic Lahar Detection at Mount Adams, Cascades: Ambient Infrasound and Wind-Noise Characterization at a Quiescent Stratovolcano. Seismol. Res. Lett. https://doi.org/10.1785/0220200361

Scarpetta, S., Giudicepietro, F., Ezin, E.C., Petrosino, S., Del Pezzo, E., Martini, M., Marinaro, M., 2005. Automatic Classification of Seismic Signals at Mt. Vesuvius

Volcano, Italy, Using Neural Networks. Bull. Seismol. Soc. Am. 95, 185–196. https://doi.org/10.1785/0120030075

Scharff, L., Hort, M., Gerst, A., 2014. The dynamics of the dome at Santiaguito volcano, Guatemala. Geophys. J. Int. 197, 926–942. https://doi.org/10.1093/gji/ggu069

Schorlemmer, D., Wiemer, S., Wyss, M., 2005. Variations in earthquake-size distribution across different stress regimes. Nature. 437, 539-542. https://doi.org/10.1038/nature04094

Sciotto, M., Cannata, A., Di Grazia, G., Gresta, S., Privitera, E., Spina, L., 2011. Seismoacoustic investigations of paroxysmal activity at Mt. Etna volcano: New insights into the 16 November 2006 eruption. J. Geophys. Res. 116, B09301. https://doi.org/10.1029/2010JB008138

Scott, J.A.J., Mather, T.A., Pyle, D.M., Rose, W.I., Chigna, G., 2012. The magmatic plumbing system beneath Santiaguito Volcano, Guatemala. J. Volcanol. Geotherm. Res. 237–238, 54–68. https://doi.org/10.1016/j.jvolgeores.2012.05.014

Sentinel Hub, https://www.sentinel-hub.com/, Sinergise Ltd

Sentinel Hub, 2018, Sinergise Ltd.

Sentinel Hub, 2020, Sinergise Ltd.

Sheldrake, T., Caricchi, L., 2017. Regional variability in the frequency and magnitude of large explosive volcanic eruptions. Geology. 45(2), 111–114. https://doi.org/10.1130/G38372.1

Sherburn, S., Scott, B.J., Nishi, Y., Sugihara, M., 1998. Seismicity at White Island volcano, New Zealand: a revised classification and inferences about source mechanism. J. Volcanol. Geotherm. Res. 83, 287–312. https://doi.org/10.1016/S0377-0273(98)00022-5

Shinohara, M., Ichihara, M., Sakai, S., Yamada, T., Takeo, M., Sugioka, H., Nagaoka, Y., Takagi, A., Morishita, T., Ono, T., Nishizawa, A., 2017. Continuous seismic monitoring of Nishinoshima volcano, Izu-Ogasawara, by using long-term ocean bottom seismometers. Earth Planets Space 69, 159. https://doi.org/10.1186/s40623-017-0747-7

Shoji, D., Noguchi, R., Otsuki, S., Hino, H., 2018. Classification of volcanic ash particles using a convolutional neural network and probability. Sci. Rep. 8, 8111. https://doi.org/10.1038/s41598-018-26200-2

Sisson, T.W., Layne, G.D., 1993. H2O in basalt and basaltic andesite glass inclusions from four subduction-related volcanoes. Earth Planet. Sci. Lett. 117, 619–635. https://doi.org/10.1016/0012-821X(93)90107-K

Soubestre, J., Seydoux, L., Shapiro, N.M., Rosny, J., Droznin, D.V., Droznina, S.Ya., Senyukov, S.L., Gordeev, E.I., 2019. Depth Migration of Seismovolcanic Tremor Sources Below the Klyuchevskoy Volcanic Group (Kamchatka) Determined From a Network-Based Analysis. Geophys. Res. Lett. 46, 8018–8030. https://doi.org/10.1029/2019GL083465

Sparks, R.S.J., 2003. Forecasting volcanic eruptions. Earth Planet. Sci. Lett. 210, 1–15. https://doi.org/10.1016/S0012-821X(03)00124-9

Sparks, R.S.J., 1997. Causes and consequences of pressurisation in lava dome eruptions. Earth Planet. Sci. Lett. 150, 177–189. https://doi.org/10.1016/S0012-821X(97)00109-X

Stephens, C.D., Chouet, B.A., 2001. Evolution of the December 14, 1989 precursory long-period event swarm at Redoubt Volcano, Alaska. J. Volcanol. Geotherm. Res. 109, 133–148. https://doi.org/10.1016/S0377-0273(00)00308-5

Stoiber, R.E., Carr, M.J., 1973. Quaternary volcanic and tectonic segmentation of Central America. Bull. Volcanol. 37, 304–325. https://doi.org/10.1007/BF02597631

Stoiber, R.E., Rose, W.I., 1974. Fumarole incrustations at active central american volcanoes. Geochim. Cosmochim. Acta 38, 495–516. https://doi.org/10.1016/0016-7037(74)90037-4

Symonds, R.B., Mizutani, Y., Briggs, P.H., 1996. Long-term geochemical surveillance of fumaroles at Showa-Shinzan dome, Usu volcano, Japan. J. Volcanol. Geotherm. Res. 73, 177–211. https://doi.org/10.1016/0377-0273(96)00029-7

Tilling, R.I., 2008. The critical role of volcano monitoring in risk reduction. Adv. Geosci. 14, 3–11. https://doi.org/10.5194/adgeo-14-3-2008

Tsukakoshi, Y., Shimazaki, K., 2008. Decreased b-value prior to the M 6.2 Northern Miyagi, Japan, earthquake of 26 July 2003. Earth, Planets Sp. 60, 915-924. https://doi.org/10.1186/BF03352847

Turner, S.J., Izbekov, P., Langmuir, C., 2013. The magma plumbing system of Bezymianny Volcano: Insights from a 54year time series of trace element whole-rock geochemistry and amphibole compositions. J. Volcanol. Geotherm. Res. 263, 108–121. https://doi.org/10.1016/j.jvolgeores.2012.12.014

Umakoshi, K., Takamura, N., Shinzato, N., Uchida, K., Matsuwo, N., Shimizu, H., 2008. Seismicity associated with the 1991–1995 dome growth at Unzen Volcano, Japan. J. Volcanol. Geotherm. Res. 175, 91–99. https://doi.org/10.1016/j.jvolgeores.2008.03.030

University of Liverpool., Karlsruhe Institute of Technology., 2020. Santiaguito Volcano 2014-2018 explosion catalogue. British Geological Survey. https://doi.org/10.5285/466263b1-06bb-4824-a805-534486be0bfd

University of Liverpool., Karlsruhe Institute of Technology., 2019. A multiparameter geophysical experiment at Santiaguito volcano, Guatemala, following a marked increase in explosive activity. British Geological Survey. https://doi.org/10.5285/b25b3800-21b8-4396-ac77-a1d504519001

Vallance, J.W., Siebert, L., Rose, W.I., Girón, J.R., Banks, N.G., 1995. Edifice collapse and related hazards in Guatemala. J. Volcanol. Geotherm. Res. 66, 337–355. https://doi.org/10.1016/0377-0273(94)00076-S

Vallance, J.W., Schilling, S.P., Matías, O., Rose, W.I., and Howell, M.M, 2001, Volcano Hazards at Fuego and Acatenango, Guatemala: U.S. Geological Survey Open-File Report 01-431, 24 pp. 4 plates, https://pubs.usgs.gov/of/2001/0431/.

Varley, N., Johnson, J., Ruiz, M., Reyes, G., Martin, K., 2018. Applying statistical analysis to understanding the dynamics of volcanic explosions, in: Statistics in Volcanology. H. M. Mader, S. G. Coles, C. B. Connor, L. J. Connor. https://doi.org/10.1144/iavcei001.6

Vasseur, J., Wadsworth, F.B., Heap, M.J., Main, I.G., Lavallée, Y., Dingwell, D.B., 2017. Does an inter-flaw length control the accuracy of rupture forecasting in geological materials? Earth Planet. Sci. Lett. 475, 181–189. https://doi.org/10.1016/j.epsl.2017.07.011

Vasseur, J., Wadsworth, F.B., Lavallée, Y., Bell, A.F., Main, I.G., Dingwell, D.B., 2015. Heterogeneity: The key to failure forecasting. Sci. Rep. 5, 13259. https://doi.org/10.1038/srep13259

Vasseur, J., Wadsworth, F.B., Lavallée, Y., Hess, K.U., Dingwell, D.B., 2013. Volcanic sintering: Timescales of viscous densification and strength recovery. Geophys. Res. Lett. 40, 5658–5664. https://doi.org/10.1002/2013GL058105

Vergniolle, S., Boichu, M., Caplan-Auerbach, J., 2004. Acoustic measurements of the 1999 basaltic eruption of Shishaldin volcano, Alaska. J. Volcanol. Geotherm. Res. 137, 109–134. https://doi.org/10.1016/j.jvolgeores.2004.05.003

Vergniolle, S., Jaupart, C., 1986. Separated two-phase flow and basaltic eruptions. J. Geophys. Res. Solid Earth 91, 12842-12860. https://doi.org/10.1029/JB091iB12p12842

Vergniolle, S., Métrich, N., 2021. Open-vent volcanoes: a preface to the special issue.

Bull. Volcanol. 83, 29, s00445-021-01454–3. https://doi.org/10.1007/s00445-021-01454-3

Viccaro, M., Garozzo, I., Cannata, A., Di Grazia, G., Gresta, S., 2014. Gas burst vs. gas-rich magma recharge: A multidisciplinary study to reveal factors controlling triggering of the recent paroxysmal eruptions at Mt. Etna. J. Volcanol. Geotherm. Res. 278–279, 1–13. https://doi.org/10.1016/j.jvolgeores.2014.04.001

Voight, B., 1989. A relation to describe rate-dependent material failure. Science. 243, 200-203. https://doi.org/10.1126/science.243.4888.200

Voight, B., Hoblitt, R.P., Clarke, A.B., Lockhart, A.B., Miller, A.D., Lynch, L., McMahon, J., 1998. Remarkable cyclic ground deformation monitored in real-time on Montserrat, and its use in eruption forecasting. Geophys. Res. Lett. 25, 3405–3408. https://doi.org/10.1029/98GL01160

Wadge, G., Cole, P., Stinton, A., Komorowski, J.-C., Stewart, R., Toombs, A.C., Legendre, Y., 2011. Rapid topographic change measured by high-resolution satellite radar at Soufriere Hills Volcano, Montserrat, 2008–2010. J. Volcanol. Geotherm. Res. 199, 142–152. https://doi.org/10.1016/j.jvolgeores.2010.10.011

Waite, G.P., and Lyons, J.J., 2009. Relative Slowness Estimates for Locations of Repeating Low-Frequency Earthquakes and Narrow-Band Tremor at Fuego Volcano, Guatemala. American Geophysical Union, Fall Meeting 2009, abstract id. V31G-08

Waite, G.P., Lanza, F., 2016. Nonlinear inversion of tilt-affected very long period records of explosive eruptions at Fuego volcano: INVERSION OF TILT-AFFECTED VLP EVENTS. J. Geophys. Res. Solid Earth 121, 7284–7297. https://doi.org/10.1002/2016JB013287

Waite, G.P., Nadeau, P.A., Lyons, J.J., 2013. Variability in eruption style and associated very long period events at Fuego volcano, Guatemala: VLP EVENTS AND ERUPTION VARIABILITY. J. Geophys. Res. Solid Earth 118, 1526–1533. https://doi.org/10.1002/jgrb.50075

Walker, F., Schofield, N., Millett, J., Jolley, D., Holford, S., Planke, S., Jerram, D.A., Myklebust, R., 2021. Inside the volcano: Three-dimensional magmatic architecture of a buried shield volcano. Geology 49, 243–247. https://doi.org/10.1130/G47941.1

Wallace, P.A., Lamb, O.D., De Angelis, S., Kendrick, J.E., Hornby, A.J., Díaz-Moreno, A., González, P.J., von Aulock, F.W., Lamur, A., Utley, J.E.P., Rietbrock, A., Chigna, G., Lavallée, Y., 2020. Integrated constraints on explosive eruption intensification at Santiaguito dome complex, Guatemala. Earth Planet. Sci. Lett. 536, 116139. https://doi.org/10.1016/j.epsl.2020.116139

Watt, S.F.L., Mather, T.A., Pyle, D.M., 2007. Vulcanian explosive cycles: Patterns and predictability. Geology. 35(9), 839–842. https://doi.org/10.1130/G23562A.1

Webley, P.W., Wooster, M.J., Strauch, W., Saballos, J.A., Dill, K., Stephenson, P., Stephenson, J., Escobar Wolf, R., Matias, O., 2008. Experiences from near-real-time satellite-based volcano monitoring in Central America: case studies at Fuego, Guatemala. Int. J. Remote Sens. 29, 6621–6646. https://doi.org/10.1080/01431160802168301

Werner, C., Bergfeld, D., Farrar, C.D., Doukas, M.P., Kelly, P.J., Kern, C., 2014. Decadal-scale variability of diffuse CO2 emissions and seismicity revealed from long-term monitoring (1995–2013) at Mammoth Mountain, California, USA. J. Volcanol. Geotherm. Res. 289, 51–63. https://doi.org/10.1016/j.jvolgeores.2014.10.020

Williams, S.N., Self, S., 1983. The October 1902 plinian eruption of Santa Maria volcano, Guatemala. J. Volcanol. Geotherm. Res. 16, 33–56. https://doi.org/10.1016/0377-0273(83)90083-5

Witham, C.S., 2005. Volcanic disasters and incidents: A new database. J. Volcanol. Geotherm. Res. 148, 191–233. https://doi.org/10.1016/j.jvolgeores.2005.04.017

Woitischek, J., Woods, A.W., Edmonds, M., Oppenheimer, C., Aiuppa, A., Pering, T.D., Ilanko, T., D'Aleo, R., Garaebiti, E., 2020. Strombolian eruptions and dynamics of magma degassing at Yasur Volcano (Vanuatu). J. Volcanol. Geotherm. Res. 398, 106869. https://doi.org/10.1016/j.jvolgeores.2020.106869

Wooster, M.J., 2001. Long-term infrared surveillance of Lascar Volcano: Contrasting activity cycles and cooling pyroclastics. Geophys. Res. Lett. 28, 847–850. https://doi.org/10.1029/2000GL011904

Woulff, G., McGetchin, T.R., 1976. Acoustic Noise from Volcanoes: Theory and Experiment. Geophys. J. Int. 45, 601–616. https://doi.org/10.1111/j.1365-246X.1976.tb06913.x

Yamamoto, H., Watson, I.M., Phillips, J.C., Bluth, G.J., 2008. Rise dynamics and relative ash distribution in vulcanian eruption plumes at Santiaguito Volcano, Guatemala, revealed using an ultraviolet imaging camera. Geophys. Res. Lett. 35, L08314. https://doi.org/10.1029/2007GL032008

Yamaoka, K., Oikawa, J., Ida, Y., 1991. An isotropic source of volcanic tremor-observation with a dense seismic network at Izu-Oshima volcano, Japan. J. Volcanol. Geotherm. Res. 47, 329–336. https://doi.org/10.1016/0377-0273(91)90007-M

Zhang, Y., 1999. A criterion for the fragmentation of bubbly magma based on brittle failure theory. Nature. 402, 648-650. https://doi.org/10.1038/45210

Zobin, V.M., Bretón, M., Navarro, C., 2014. Similarity in seismic source scaling relations for tectonic and volcanic processes. Phys. Earth Planet. Inter. 231, 65-73. https://doi.org/10.1016/j.pepi.2014.03.007

Zobin, V.M., Sudo, Y., 2017. Source properties of Strombolian explosions at Aso volcano, Japan, derived from seismic signals. Phys. Earth Planet. Inter. 268, 1–10. https://doi.org/10.1016/j.pepi.2017.05.002

Appendix 1: Supplementary Material

A1.1. Fuego Data Processing Steps: Explosion and Tremor Detection, and Data Classification Algorithm

We developed an algorithm to detect, classify, and catalogue seismic and acoustic events at Fuego. The types of events of concern for detection were explosions, both ash- and gas-rich, and both seismic and acoustic tremor.

Activity at Fuego occurs at a high rate (up to 32 explosions/hour) and so the algorithm was built with the aim of producing a clean catalogue, clear of noise, while detecting as many events as possible to give a high-quality and accurate indication of the state and behaviour of the volcano across the recording period.

The algorithm follows a workflow that includes six steps:

1. Detection of explosions from acoustic data
2. Detection of explosions from seismic data
3. Detection of tremor from acoustic data
4. Detection of tremor from seismic data
5. Network coherence checks
6. Classification of confirmed explosions

Below, we describe the details of each step of the algorithm. The application of these procedures produced a catalogue of 99,618 explosions, 6,048 seismic tremor events and 2,200 acoustic tremor events. The steps of the algorithm are also outlined by the flow charts in Figure A1.1.

Through initial manual inspection and testing of different detection parameters in the datasets, we observed that infrasound signals at Fuego have better signal-to-noise ratio and more distinctive features than seismic signals making them a better candidate for detection and classification of events than seismic data. Furthermore, the number of infrasound stations deployed during the study period was higher than seismic stations.

Based on these considerations, the detection and classification algorithm was implemented to give priority to acoustic detections.

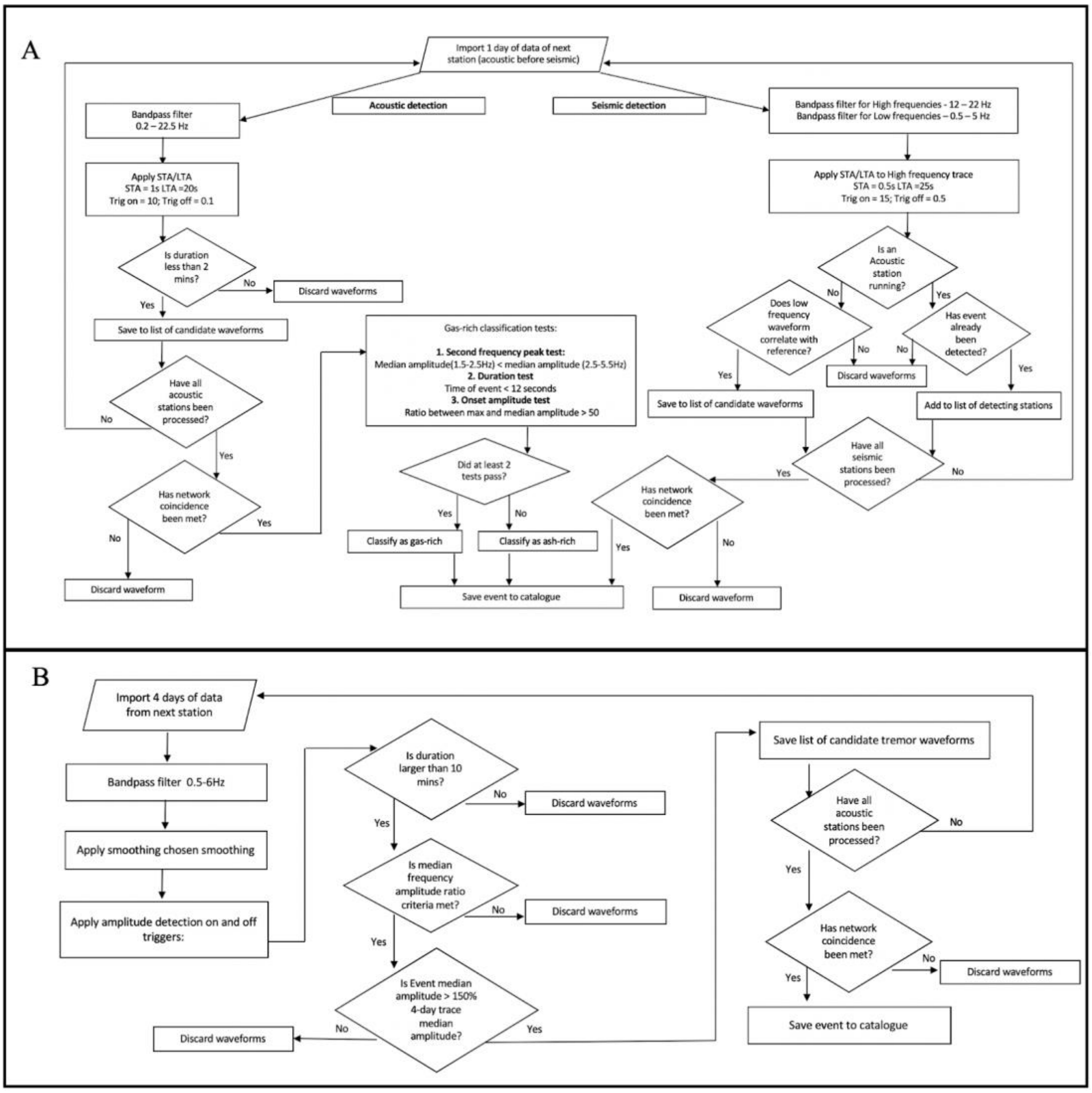

Figure A1.1. *Decision flow charts for the Fuego detection and classification algorithm. A. Algorithm flow charts for explosion detection and classification between gas-rich and ash-rich. B. Algorithm flow charts for tremor detections. Flow chart B is used for both seismic and acoustic tremor, but with different smoothing lengths, detection triggers and frequency ratio criteria used.*

Explosion detection – Infrasound

Explosion detection was performed by analysing one day at a time with a 10-minute overlap to avoid missing events that occurred at the boundary between days. Each data channel was processed individually, before combining the results in the network coherence stage to confirm the detections. Data were pre-processed with a bandpass filter between 0.2 and 22.5 Hz (90% of the Nyquist frequency) to remove unwanted noise, while preserving the frequencies of interest for event detection.

A short-term average to long-term average ratio method (STA/LTA) was applied with a short-term average window of 1 second, and long-term average window of 20 seconds. A detection was triggered for STA/LTA values greater than 10 and the end was triggered when it fell below 0.1, in order to capture the whole waveform. To avoid including tremor in the detections of explosions, the duration of the event (time between trigger on and off) was required to be less than 2 minutes.

The parameters used in the detection phase were calibrated with sensitivity tests performed on data collected during the week commencing on the 1st September 2019. The tests investigated filters used, STA/LTA triggers and lengths. Testing found that the detection process was not sensitive to the filter used, whereas the length of the LTA and trigger ratio had a large effect on the number of events detected and of false triggers. Manual inspection of the test catalogues guided the choice of the parameters for the final algorithm.

Explosion detection - Seismic

Seismic data for the detection of explosions were also analysed one day at a time with a 10-minute overlap. Explosions commonly generate a high-frequency ground-coupled airwave, which can be detected by the seismometers. This feature is easily identifiable on a seismic trace and can be used to identify explosion events. The seismic trace was split into a high-frequency trace (12-22 Hz) and a low-frequency (0.5-5 Hz) trace. An STA/LTA was applied to the high-frequency trace to detect the GCA, with a short-term average of 0.5 seconds and long-term average set to 25 seconds. The trigger for a detection was set at a ratio of 15, with the end of the event triggered by a ratio of 0.5.

When infrasound stations were running, GCA detection times were compared with confirmed explosions and added to the list of detecting stations when there was a correlation between the two. However, when infrasound stations were not operational, in order to increase the accuracy of the seismic detections, the low-frequency trace associated with the ground waves were compared with an example waveform through a low threshold cross correlation to verify the detection.

Appendix 1: Supplementary Material

Acoustic Tremor

Tremor events can last between several minutes to over a day. In order to account for this, acoustic tremor detection data were analysed in segments of four days, with an overlap of one day.

The four-day trace was filtered between 0.5 and 6 Hz to remove noise. The data were then smoothed with a 3-minute running average. An amplitude trigger was used on the smoothed trace to detect the tremor. The trigger for a detection was set to when the amplitude exceeded the 85th percentile of the 4-day window and the end trigger was declared when it fell below the 45th percentile. A detection was only confirmed when the duration of the event was greater than 10 minutes.

The detected waveforms were then checked to remove possible false triggers in two steps:

1) The median absolute amplitude of the unsmoothed event waveform was compared to the median absolute value of the unsmoothed, four days of data. If the median event value was over 150% the median value of the four days, then the detection was sent for the second check.

2) The second check compared the shape of the frequency spectra of the waveforms. Tremor events contain a noticeable proportion of energy in the frequency range above 2 Hz. A ratio of the energy in the frequency range between 3 and 4 Hz was compared to frequencies between 0.5 and 1.5 Hz. If the ratio of low to high frequency content was less than 2.5, then the event was deemed to be tremor.

Similar to explosion detection, sensitivity tests were carried out to determine the optimal parameters for the tremor detection algorithm using data recorded during the week beginning on the 1st September 2019. We tested the filters, smoothing length, on and off trigger thresholds, and the frequency amplitude ratio. Manual inspections were made on the detections to ensure the algorithm correctly identified the start and end of tremor episodes. The tests found that if the filter was too broad, events would be missed due to high-frequency noise. The tests also found that the algorithm were highly sensitive to the trigger thresholds, especially for the off trigger to correctly identify the end of an event, as these are often ambiguous due to the decay in the signal back to background noise levels. The algorithm had low sensitivity to the length of smoothing over the data, and the frequency attribute ratio, which both had wide ranges in which the detections remained accurate.

Seismic Tremor

Following a similar procedure to acoustic tremor, the seismic data were imported in window lengths of 4 days, with a one-day overlap. The seismic trace was also filtered between 0.5 and 6 Hz and smoothed with a 2-minute rolling average. The detection trigger was set at the 65th percentile of amplitude, and the end was triggered when the amplitude fell below the 25th percentile. The duration of the detections was required to last for a minimum of 10 minutes.

In the same way that the acoustic tremor detections were checked, the unsmoothed seismic waveforms were then tested to confirm the detection was a continuous high amplitude event by ensuring the median absolute amplitude was above 150% of the median absolute amplitude of the 4-day unsmoothed data.

Waveforms which passed the amplitude check then had a frequency ratio check. The seismic signals of tremor typically have a peak at 2 Hz, with reduced contributions from both higher and lower frequencies. Therefore, the ratio of the energy between 1.5 and 2.5 Hz was made with the mean energy between 0.5 - 1.5 Hz and 2.5 - 3.5 Hz. If the ratio exceeded 2.2, then the event was confirmed as tremor.

The parameters used were also tested in the sensitivity tests over the week beginning 1st September 2019. Similarly to the infrasound tremor, the filter, smoothing length, detection triggers and frequency attribute threshold were all tested. Seismic tremor events were found to have little sensitivity to the filter, provided the corner was below 10 Hz. Detections were also insensitive to the length of the smoothing, with shorter lengths being slightly more responsive to shorter waveforms and longer smoothing lengths occasionally having issues detecting the end of an event.

The on-trigger for a detection was stable due to the high energy compared to background noise, yet as the tremor slowly returns to background levels, the off-trigger was highly unstable, cutting events short if set too high, or continuing for hours after the event had ended if set too low. The ratio of energy in the frequency domain, set at 2.2, which checked for the frequency peak at 2 Hz, was found to be stable between 2 and 2.5.

Network coherence

Explosions and tremor episodes are expected to be detected across the instrument network by multiple stations. Therefore, when data from multiple channels were available, a threshold for the minimum number of detecting stations needed to confirm a detection was set.

Explosion detections from each of the individual stations were first combined considering the largest expected signal move-out across the network (assuming a source located at the summit vent of Fuego). If explosions detected at different stations occurred within a 30-second window, they were considered to be the same event. For tremor, events detected at different stations which had overlapping time windows were considered to be the same event.

For infrasound detections of explosions and acoustic tremor, when there were 4 or more infrasound instruments available, an event was required to be detected at a minimum of 3 microphones, over a minimum of 2 different station arrays. If there were only 3 available instruments, 2 detections were required, irrespective of the station arrays. If fewer than 3 instruments were active, then only 1 detection was required, and when there were no infrasound stations active, any seismic stations active was used to make the explosion detections, however, this final case was never met as there were no periods in which only seismic stations were active. For seismic tremor, when there were 3 or more instruments available, 2 stations were required to make a detection, but if less than 3 were online, only one detection was required.

Explosion Classification

The detected explosions were run through a classification algorithm, to separate gas-rich from ash-rich explosions. 3 tests were used to make this classification based on the characteristic attributes of the acoustic signals, outlined in chapter 4.5. A classification was assigned once at least two of the three tests produced the same result.
First, the duration of the explosion was checked. A duration of less than 12 seconds indicated a gas-rich explosion.

Second, the ratio between maximum and median acoustic amplitudes were compared. Gas-rich explosions typically have a high amplitude onset, and so if the ratio was above 50, the test indicated a gas-rich event.

In the case where the first two tests disagreed, a frequency-based check was made. Gas-rich explosions are observed to have a second peak between 3 and 4.5 Hz which ash-rich do not. Therefore, a check was made to identify if the second peak was present. If the ratio of the energy between 1.5 and 3 Hz, compared to 3 to 4.5 Hz was greater than 1, than the explosion was deemed to have a second frequency peak and classed as gas-rich, whereas if the ratio was equal to or less than 1, then the explosion was classed as being ash-rich.

Event Duration

The durations of the explosions were calculated as the time difference between the STA/LTA on trigger and off trigger in the acoustic record. Tremor durations for both seismic and acoustic tremor were calculated as the time between the on and off triggers for the amplitude thresholds on the smoothed traces.

Validation

Following the application of the three algorithms to produce the catalogues of seismic tremor, acoustic tremor, and explosions, tests were carried out to compare the automatic detections against manual catalogues made with a single station, which had not been used during the development of the algorithms. For these tests, manual catalogues from the week of 1st June 2019 were used. We found that the explosion catalogue detected 90 % of the events that were manually detected, but also found a further 16 % which were not noticed by manual inspections due to high noise. The events that were not detected all were of low magnitude. No false triggers were found. For the acoustic tremor, we found that the algorithm detected 80 % of the events that were manually detected, where the missed events were typically of shorter duration and lower average magnitude. Less than 5% of the events were false triggers. Finally, for the seismic tremor catalogue, the algorithm detected 84 % of the manually detected events, and also detected an additional 8 % which were not manually detected. The seismic tremor catalogue was also found to contain less than 5 % false triggers.

Appendix 2: Supplementary Tables

Table A2.1. *Site correction factors used to remove the difference in energy calculations between sites in the Santiaguito network, relative to station LB03. Factors change from before the 1st of January 2016 and after, due to some stations being redeployed, and their correction factors changing. Future studies will require new correction factors.*

Station	Pre 2016 site correction factor	2016 - 2018 site correction factor
LB01	0.4394913	0.3087270
LB02	0.1751500	0.1361163
LB03	1.0000000	1.0000000
LB04	0.0413037	0.0413037
LB05	0.3399529	0.3399529
LB06	0.0025446	0.0025446
LS01	0.1072035	0.1072035
LS02	1.2210946	1.2210946
LS03	0.0336349	0.0336349
LS04	0.0537372	0.0510069
LS05	0.6900589	1.7875000
LS06	0.1891340	1.3013100

Table A2.2. *Station deployment information at Volcán de Fuego.*

Station	Sensor location ID	Latitude	Longitude	Sensor type	Digitizer
FG3	01	14.44783	-90.842	Trillium 120 Compact	CENTAURUS
FG8	00	14.4325	-90.9359	Trillium 120 Compact	CENTAURUS
FG8	01	14.43287	-90.93532	Chaparral M64	CENTAURUS
FG8	02	14.43238	-90.93583	ITEM PRS100	CENTAURUS
FG8	03	14.43207	-90.93515	Chaparral M64	CENTAURUS
FG10	00	14.413	-90.91239	Trillium 120 Compact	EDR209
FG10	01	14.41286	-90.91197	ITEM PRS100	EDR210
FG10	02	14.41298	-90.91252	ITEM PRS100	EDR210
FG10	03	14.413	-90.91239	ITEM PRS100	EDR210
FG11	00	14.4639	-90.9608	Trillium 120 Compact	EDR209
FG11	01	14.4639	-90.9608	ITEM PRS100	EDR210
FG11	02	14.4601	-90.9578	ITEM PRS100	EDR210
FG11	03	14.4605	-90.9636	ITEM PRS100	EDR210
FG11	04	14.4662	-90.9570	ITEM PRS100	EDR210
FG12	00	14.43651	-90.83606	Trillium 120 Compact	CENTAURUS
FG12	01	14.43695	-90.83608	Chaparral M64	CENTAURUS
FG12	02	14.43646	-90.8361	Chaparral M64	CENTAURUS
FG12	03	14.43629	-90.83601	Chaparral M64	CENTAURUS
FG13	00	14.40677	-90.81859	Trillium 120 Compact	EDR209
FG13	01	14.40625	-90.81834	Chaparral M64	CENTAURUS
FG13	02	14.40677	-90.81841	Chaparral M64	CENTAURUS
FG13	03	14.40627	-90.81846	Chaparral M64	CENTAURUS
FG14	00	14.3908	-90.9422	Trillium 120 Compact	CENTAURUS
FG14	01	14.39051	-90.94219	Chaparral M64	CENTAURUS
FG14	02	14.39083	-90.94218	Chaparral M64	CENTAURUS
FG14	03	14.39121	-90.94192	Chaparral M64	CENTAURUS
FG14	04	14.39102	-90.94144	Chaparral M64	CENTAURUS
FG14	05	14.39054	-90.94151	Chaparral M64	CENTAURUS
FG14	06	14.39021	-90.94183	Chaparral M64	CENTAURUS
FG16	00	14.455	-90.8508	Trillium 120 Compact	EDR209
FV01	01	14.50135	-90.94413	Chaparral M60	DATACUBE
FV02	02	14.53636	-90.88634	Chaparral M60	DATACUBE
FV03	03	14.47906	-90.84358	Chaparral M60	DATACUBE
FV04	04	14.4955	-90.87022	IST2018	DATACUBE

Appendix 3: Supplementary Records

The supplementary records can all be found as .csv spreadsheets within the adjoining zip files for electronic copies, and on the memory sticks for hard copies of this thesis.

A.3.1. Santiaguito Explosion Catalogue

List of dates and times of the detection time for all explosions detected by the automatic detection algorithm. Event durations, seismic energy release, energy magnitude, number of broadband and short-period detecting stations, and the automatic trust values are also given.

A3.2. Fuego Explosion Catalogue

List of dates and times of the detection time for all explosions detected by the automatic detection algorithm. Event durations are also given.

A3.3. Fuego Seismic Tremor Catalogue

List of dates and times of the detection time for all seismic tremor events detected by the automatic detection algorithm. Event durations are also given.

A3.4. Fuego Acoustic Tremor Catalogue.

List of dates and times of the detection time for all acoustic tremor events detected by the automatic detection algorithm. Event durations are also given.